Robert Gaul, B.Eng.

Fundamental Insights into Arterial Remodelling; Strain-Mediated Degradation of Arterial Collagen

---

Trinity College Dublin, 2019

A thesis submitted to the University of Dublin in partial fulfilment of the requirements for the degree of

Doctor in Philosophy

Supervisor: Prof. Caitríona Lally

Internal Examiner: Prof. Ciaran Simms

External Examiner: Prof. Frank Gijsen

Declaration

I declare that this thesis has not been submitted as an exercise for a degree at this or any other university and it is entirely my own work.

I agree to deposit this thesis in the University's open access institutional repository or allow the library to do so on my behalf, subject to Irish Copyright Legislation and Trinity College Library conditions of use and acknowledgement.

Robert Gaul

_____

Summary

Maladaptive remodelling of structurally significant collagen fibres in the arterial wall is believed to play a critical role in the development and progression of degenerative arterial disease. A greater understanding of this strain-mediated process may pave the way for improved patient screening, as well as the development of novel medical devices capable of halting or even reversing maladaptive arterial remodelling. The aim of this thesis is to investigate, for the first time, the strain-dependent reorientation and degradation behaviour of arterial collagen, using a combined experimental and numerical approach.

To achieve this, structural analysis was first carried out with an optimised, purpose-built small angle light scattering system, to identify the collagen fibre response to strain-dependent degradation. Next, strain dependent degradation rates were determined from stress relaxation experiments in the presence of crude and purified collagenase. This allowed for determination of the tissue level degradation response in arterial dogbone specimens. A complementary computational model was developed, incorporating matrix stiffness and a gradient of collagen fibre crimp to decouple the mechanism behind the strain-dependent degradation data. This model was then used to predict the degradation response of full intact vessels, subjected to physiologically relevant pressures. Finally, the model was applied to an idealised vessel geometry to investigate the role of strain-dependent degradation in the development of degenerative arterial disease.

Structural analysis identified a statistically significant difference in collagen fibre alignment due to strain-dependent degradation. Subsequent mechanical testing identified a unique stress degradation response occurring at the tissue scale, which was not seen in other collagenous tissues. The model was capable of accurately predicting the experimental findings, but only in the presence of three critical components. Namely, the load bearing matrix, its degradation response and the gradient of collagen fibre crimp across the arterial wall. The model also predicted the increased rate of degradation-induced vessel expansion with increasing pressure, which was previously identified experimentally, despite elevated rates of degradation at low pressure. Finally, the model also identified accelerated degradation and subsequent aneurysm growth occurring at a location of initial vessel weakness. These findings highlight the critical role of strain in arterial degradation, particularly in the case of progressive degenerative disease whereby structural integrity may be compromised.

Acknowledgements

First and foremost, I would like to express my sincere gratitude to my supervisor Prof. Caitríona Lally for her knowledge, support and guidance over the past 4 years. Her enthusiasm and knowledge have been invaluable throughout. I would like to thank the Irish Research Council, Science Foundation Ireland and the European Research Council, without which none of this work would have been possible. I would also like to thank my examiners Prof. Ciaran Simms and Prof. Frank Gijsen for taking their time to read my thesis.

I have been lucky enough to work alongside many great researchers during my PhD both in DCU and in TCD. I have made some great friends, particularly in TCBE who I've shared many great nights out with. Particularly, I would like to thank Milad who has shared much of this journey with me. A special mention goes to my mentor and friend, Dave, who's knowledge, advice and many coffee breaks were invaluable. A special mention also goes to Peter O'Reilly who was always on hand to offer advice or assistance during the many hours in the lab. Outside of the lab, I would like to express my gratitude to Gilbert and Alan who were always available to express my frustrations to or listen to a presentation.

I would like to thank my parents, Geraldine and Vincent, my brothers Vinnie and Dave and my sister, Caroline for all their support and advice during my many years of research. Finally, I would like to thank Alix for her love and support, her advice and understanding, and without whom, I would have spent many more weekends in work. She has been a constant source of motivation throughout.

List of Publications, Conference Proceedings and Prizes

First-author journal publications

Gaul, R.T., Nolan, D.R., Lally, C., 2017. Collagen fibre characterisation in arterial tissue under load using SALS. J. Mech. Behav. Biomed. Mater. 75, 359–368. doi:10.1016/j.jmbbm.2017.07.036

Gaul, R.T., Nolan, D.R., Lally, C., 2018. The use of small angle light scattering in assessing strain induced collagen degradation in arterial tissue ex vivo. J. Biomech. 81, 155-160. doi:10.1016/j.jbiomech.2018.10.006

Gaul, R.T., Nolan, D.R., Ristori, T., Bouten, C.V.C., Loerakker, S., Lally, C., 2018. Strain mediated Enzymatic Degradation of arterial tissue: Insights into the role of the non-collagenous tissue matrix and collagen crimp. Acta Biomater. 77, 301-310. doi:10.1016/J.ACTBIO.2018.06.037

Gaul, R.T., Nolan, D.R., Ristori, T., Bouten, C.V.C., Loerakker, S., Lally, C., Pressure induced degradation in arterial tissue: Experimental and computational investigation. [In preparation]

Publications not included in this thesis

Shahid, S.S., Gaul, R.T., Kerskens, C.M., Flamini, V., Lally, C., 2017. Quantifying the ultrastructure of carotid artery using high-resolution micro-diffusion tensor imaging – comparison of intact vs. open cut tissue. Phys. Med. Biol. 62, 8850–8868. doi:10.1088/1361-6560/aa9159.

Whelan, A., Duffy, J., Gaul, R.T., O'Reilly, D., Nolan, D.R., Gunning, P., Lally, C., Murphy, B., 2018. Collagen Fibre Orientation and Dispersion Govern Ultimate Tensile Strength, Stiffness and the Fatigue Performance of Bovine Pericardium. J. Mech. Behav. Biomed. Mater. 10.1016/j.jmbbm.2018.09.038

Whelan, A., Williams, E., Duffy, J., Gaul, R.T., O'Reilly, D., Nolan, D.R., Gunning, P., Murphy, B., Lally, C., Collagen fibre architecture is more mechanically dominant than glutaraldehyde fixation technique in commercial-grade bovine pericardium. [Submitted]

Fitzpatrick E., Meehan B., Dunphy S.E., Gaul R.T., Smekens C., Lally C., Decellularised Porcine Carotid Arterial Graft: a short-term technique that preserves arterial structure and mechanical properties. [Submitted]

Carroll, L., Merle, F., Macmanus, D., Gaul, R., Lally, C., Gilchrist, M.D., Pierrat, B., n.d. Mechanical properties of the cerebral dura mater. [In preparation]

Conference Proceedings

Gaul, R.T., Nolan, D.R., Ristori, T., Bouten, C.V.C., Loerakker, S., Lally, C., (2019) 'Pressure Induced Degradation in Porcine Carotid Arteries: Experimental and Computational Investigation', in Proceedings of the 25th Annual Conference of the Section of Bioengineering of the Royal Academy of Medicine in Ireland. Limerick, Ireland.

Gaul, R.T., Nolan, D.R., Ristori, T., Bouten, C.V.C., Loerakker, S., Lally, C., (2018) 'Degradation of Arterial Collagen with Applied Strain: Critical Influence of Matrix Content and Collagen Crimp', in *8th World Congress of Biomechanics*. Dublin, Ireland.

Gaul, R.T., Nolan, D.R., Ristori, T., Bouten, C.V.C., Loerakker, S., Lally, C., (2018) 'Strain Mediated Arterial Degradation is Critically Influenced by Matrix Content and Collagen Crimp', in *Proceedings of the 24th Annual Conference of the Section of Bioengineering of the Royal Academy of Medicine in Ireland*. Meath, Ireland.

Gaul, R. and Lally, C. (2017) 'Strain Mediated Enzyme Degradation of Arterial Tissue; Implications in Disease and Medical Device Design', in *Summer Biomechanics, Bioengineering and Biotransport Conference 2017*. Tucson, USA.

Gaul, R.T., T., Lally, C., (2017) 'Strain Mediated Enzyme Degradation of Arterial Tissue Characterised by Small Angle Light Scattering', in *Proceedings of the 23rd*

Annual Conference of the Section of Bioengineering of the Royal Academy of Medicine in Ireland. Belfast, Ireland.

Gaul, R.T., T., Lally, C., (2016) 'Load Induced Changes in Collagen Fibre Architecture in Arteries Characterised by Small Angle Light Scattering', in *Proceedings of the 22nd Annual Conference of the Section of Bioengineering of the Royal Academy of Medicine in Ireland*. Galway, Ireland.

Gaul, R.T., Sinnott, T., Lally, C., (2015) 'The Automated Characterisation of Collagen Fibre Orientation in Arteries using Small Angle Light Scattering', in *UK Society of Biomaterials*. Belfast, United Kingdom.

Gaul, R.T., T., Lally, C., (2015). 'The use of Small Angle Light Scattering for the Characterisation of Collagen Fibre Orientation in Arteries', in *Proceedings of the 21st Annual Conference of the Section of Bioengineering of the Royal Academy of Medicine in Ireland*. Kildare, Ireland.

Prizes

Engineers Ireland Biomedical Research Medal (2018). This medal is awarded annually by Engineers Ireland at the annual *Bioengineering in Ireland* conference to a PhD student deemed to be making the most significant contribution to the field of biomedical engineering research in Ireland.

8th World Congress of Biomechanics ASME 2018 PhD Student Paper Competition 1st prize in the Cardiovascular Mechanics and Cell Biomechanics session.

Contents

List of Figures

List of Tables

Chapter 1 Introduction

1.1 Research Motivation

Cardiovascular disease (CVD) is the leading cause of mortality and morbidity worldwide and as such, carries a huge economic burden. CVDs were responsible for an estimated 17.5 million deaths in 2012 which corresponds to more than 30% of deaths globally (WHO, 2014). This figure is expected to rise to more than 22.2 million by 2030 such that CVDs will remain the number one cause of worldwide mortality (Mathers and Loncar, 2006; WHO, 2014). CVDs affect the vascular system within the body, including arteries, veins and the heart which are critical in the transport of nutrients and oxygen to the surrounding tissue (Martini, Nath and Bartholomew, 2011). Two of the most prevalent manifestations of CVD which effect arteries are atherosclerosis and aneurysm. If left untreated, these progressive degenerative diseases can progress to a major adverse clinical event including myocardial and cerebral infarctions as well as vessel dissection and rupture (Thompson, Geraghty and Lee, 2002; Chaikof *et al.*, 2009; Mozaffarian *et al.*, 2015).

A variety of treatments have been devised to treat CVDs which depend on the specific disease presenting as well as the severity, location and condition of the patient, among other factors (Colombo, Stankovic and Moses, 2002; Chaikof *et al.*, 2009; Bangalore *et al.*, 2011). In recent years, treatment of CVD has moved away from invasive surgical interventions such as carotid endarterectomy, where the plaque is surgically removed from the vessel wall, in favour of minimally invasive procedures, such as stenting (Chakhtoura *et al.*, 2001). The move toward minimally invasive procedures poses less risk to the patient while also reducing hospital costs during patient recovery. Although advances in stenting, particularly in the development of drug-eluting stents (DES) have greatly improved stenting outcomes, restenosis remains a common occurrence (Dangas *et al.*, 2010). In addition, the long-term consequences of using anti-proliferative cancer-fighting drugs as stent coatings remain unknown. These devices also

induce a remodelling response in the surrounding tissue which can dictate the long-term outcome of the device (Ghazanfari, Anita Driessen-Mol, *et al.*, 2016). A greater understanding of this response may motivate the design of novel medical devices which could stimulate healthy remodelling in diseased vessels, potentially slowing or even reversing vascular disease.

Arteries are composed of layers of fibre-reinforced tissue whereby collagen fibres provide structural strength to the vessel (Martini, Nath and Bartholomew, 2011). Arteries can adapt to their environment through instantaneous reorientation of collagen fibres as well as longer term remodelling in response to mechanical and chemical stimuli (Ghazanfari, Anita Driessen-Mol, *et al.*, 2016). Many techniques have been used to characterise the orientation of these important load-bearing constituents, including polarised light microscopy (PLM) (Canham *et al.*, 1989; Gasser *et al.*, 2012; Sáez *et al.*, 2016), confocal microscopy (O'Connell *et al.*, 2008; Rezakhaniha *et al.*, 2012), and multiphoton microscopy (Tsamis *et al.*, 2013; Krasny *et al.*, 2017). However, there are a number of limitations associated with each of these techniques; primarily, the requirement to excise the tissue from the body, as well as time-consuming and destructive tissue preparation steps (Sacks, Smith and Hiester, 1997). Many of these tools are also not suited to characterising fibre orientations across entire samples due to their highly localised nature. Developments in emerging imaging modalities such as diffusion tensor imaging (DTI) have shown great promise due to their ability to determine *in vivo* fibre directions, although further refinement is still required (Flamini *et al.*, 2010; Ghazanfari *et al.*, 2012, 2015; Opriessnig *et al.*, 2016). Alternative techniques, such as small angle light scattering (SALS), also show promise in its ability to determine fibre directions on a large scale, without the need for time-consuming preparation steps. SALS also offers the potential for determining structural changes of the tissue in response to load which may offer critical insights into vascular remodelling (Sacks, Smith and Hiester, 1997; Williams *et al.*, 2009; Robitaille *et al.*, 2011).

A greater understanding of the organisation, instantaneous reorientation and time-dependent remodelling of structurally important collagen fibres in healthy and diseased vessels is critical in the understanding and diagnosis of these

diseases, as well as in medical device design and development. PLM and multiphoton microscopy have previously been used to identify differences in collagen fibre organisation in aneurysmal tissue when compared to its healthy counterpart (Gasser *et al.*, 2012; Niestrawska *et al.*, 2016; Cavinato *et al.*, 2017). Accelerated collagen degradation which exceeds production has also been linked to late-stage aneurysm expansion and rupture (Thompson, Geraghty and Lee, 2002). Studies on other collagenous tissues have suggested that collagen degradation is a strain mediated process where the magnitude of strain experienced dictates the rate of collagen degradation (Huang and Yannas, 1977; Ghazanfari, A. Driessen-Mol, *et al.*, 2016; Yi *et al.*, 2016). If true for arterial tissue, structural and mechanical changes in aneurysmal and atherosclerotic tissue may help to explain disease progression and subsequent vessel and plaque rupture, however, this remains unknown.

In response to the rise in CVD deaths worldwide, computational modelling of CVD is becoming an increasingly important tool for understanding disease progression and treatment. Much time and effort has been spent on developing material models which are capable of predicting realistic vessel behaviour. Many of these models incorporate structural details of the vessels themselves including mean collagen fibre orientation (Holzapfel, Gasser and Ogden, 2000; Balzani, Schröder and Gross, 2006), dispersion (Gasser, Ogden and Holzapfel, 2006), remodelling (Driessen, Bouten and Baaijens, 2005; Hariton, DeBotton, T.C. Gasser, *et al.*, 2007; Creane *et al.*, 2011; Loerakker, Obbink-Huizer and Baaijens, 2013; Loerakker, Ristori and Baaijens, 2016) and damage (Simo and Ju, 1987; Miehe, 1995; Ghasemi, Nolan and Lally, 2018). However, the accuracy and predictive power of these models is limited by our understanding of biomechanics, including the role the mechanical environment plays in tissue reorganisation and degradation. Further development, informed by relevant experimental data may allow these models to be used as a predictive tool by clinicians to support their decisions to carry out medical interventions in patients suffering from CVD. Computational modelling has also regularly been used in the assessment and development of new medical devices including stents (Holzapfel, Stadler and Schulze-Bauer, 2002; Lally, Dolan and Prendergast, 2005), heart valves (Kunzelman *et al.*, 1993) and venous filters (Singer, Henshaw and Wang, 2009).

Finite element (FE) modelling of medical devices offers an inexpensive means of device development and analysis but requires reliable empirical data to inform the models. A greater understanding of the artery response to changes in its mechanical environment, allowing for experimentally informed models will undoubtedly lead to further advances in clinical patient screening and the design and development of more advanced medical devices.

1.2 Objectives

The overall aim of this thesis is to explore the mechanical stimuli which drive collagen fibre reorganisation and degradation in arterial tissue, with a view to gaining fundamental insights into vascular remodelling and to incorporate such insights into a computational model which can be used to investigate disease progression and as a design tool for next-generation medical devices. To achieve this aim, the following objectives must be met, an overview of which is shown in Figure 1.1:

1. Develop a system to non-destructively ascertain collagen fibre orientation and reorientation under load in arterial tissue.
2. Investigate structurally and mechanically whether a strain-dependent degradation response exists in arterial tissue.
3. Develop an experimentally informed numerical degradation model capable of predicting and explaining the experimentally determined degradation response of arterial tissue.
4. Investigate the degradation response of physiologically relevant vessel geometries experimentally and computationally, to gain insights into progressive degenerative diseases *in vivo*.

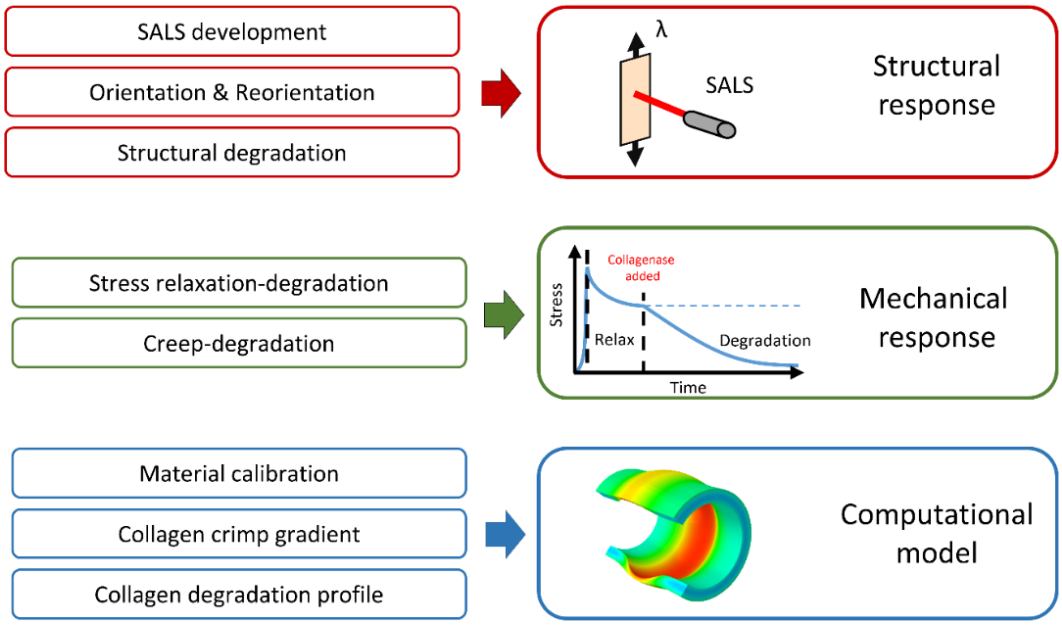

Figure 1.1 - Overview of the key research objectives.

1.3 Thesis Structure

This thesis consists of seven chapters centred around four studies, which emanate from four separate journal papers (three published, one in preparation). A brief description of each chapter can be found below:

Chapter 1: Outlines the motivation for the work completed as part of this thesis, highlighting the severity of CVDs, current treatment strategies, as well as current gaps in our understanding of vascular remodelling. The key objectives of this work are also outlined which will be addressed in Chapters 3-6.

Chapter 2: Begins with a general review of cardiovascular anatomy and physiology, providing a basis for the topics to follow. Next, an in-depth review of the current imaging modalities used to investigate arterial architecture is carried out, with emphasis on their ability to detect load-induced changes. The literature review concludes with a thorough analysis of the current understanding of load and strain-dependent degradation in collagen and collagenous tissues.

Chapter 3: Outlines the need for alternative, minimally destructive techniques for collagen fibre characterisation in arterial tissue. This study also investigates the ability of an optimised small angle light scattering (SALS) to determine collagen fibre orientation and reorientation in arterial tissue under load.

Chapter 4: Assesses the ability of the optimised SALS system to investigate changes in collagen fibre architecture in arterial tissue due to degradation. Additionally, this chapter establishes whether a strain-dependent degradation response exists in arterial tissue.

Chapter 5: Further explores the specific strain dependent degradation of arterial tissue through a series of stress relaxation experiments on dogbone specimens. A theoretical model of arterial degradation is also developed which is informed by structural and mechanical findings. The purpose of this model is to elucidate the role of non-collagenous matrix and collagen fibre crimp in the ultimate degradation response of the tissue.

Chapter 6: Investigates the physiological degradation response of arterial tissue established in Chapter 5, through a series of pressure-inflation creep experiments

on intact vessels. The existing numerical model is also implemented in a finite element framework to explain the new experimental findings. Finally, the model is expanded to investigate a case study of aneurysmal development in an idealised vessel geometry.

Chapter 7: Concludes with a final discussion to unify the key findings from Chapters 3-6 and highlight the contribution of this work to the field of arterial biomechanics. Recommendations for future work are also presented.

Chapter 2 Literature Review

2.1 Cardiovascular System

The cardiovascular system consists of the heart, blood vessels and circulating blood and is responsible for many important functions in the body. This circulating blood is tasked with supplying oxygen and nutrients to cells, removing waste products such as carbon dioxide, distributing heat, maintaining homeostasis, regulating pH levels and aiding the immune system. The cardiovascular system can be divided up into two circuits known as the pulmonary circuit and the systemic circuit with the heart located at the centre of each in an area known as the mediastinum. The heart is a four-chambered muscular organ which receives deoxygenated blood from the systemic circuit into the right atrium shown in Figure 2.1. From here the blood is passed on to the right ventricle which pumps this blood through the pulmonary circuit to become oxygenated by the lungs before returning to the left atrium. The left atrium passes blood into the left ventricle which pumps the now oxygenated blood through the aorta and around the body in what is known as the systemic circuit (Martini, Nath and Bartholomew, 2011).

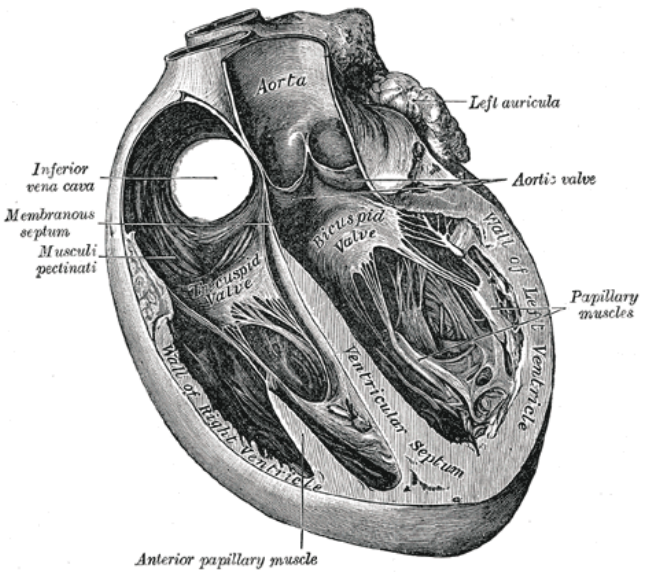

Figure 2.1 – Schematic of the heart showing the major components (Gray, 1858).

Although the basic structure and functions of the cardiovascular system are well understood and are explained in even the most basic of anatomy and physiology books, how the system adapts is still relatively poorly understood. Today's understanding has developed from research spanning centuries, beginning with the early work of physicians such as Hippocrates and Galen, who noted the cardiovascular system as comprising of two separate networks of blood vessels. Likewise, the relatively more recent work of William Harvey discovered many of the principles which still hold true today (Aird, 2011). Despite the extensive work carried out to-date, further research is required to gain a greater grasp of how this system functions, adapts and remodels itself in response to its environment. A more in-depth understanding of these areas may better equip patients and physicians in dealing with sickness and disease.

2.2 The Carotid Arteries

The carotid arteries are large and medium sized vessels located in the neck and head of mammals which are responsible for supplying oxygen-rich blood to the face and brain (Figure 2.2). The carotid arteries consist of a right and left common

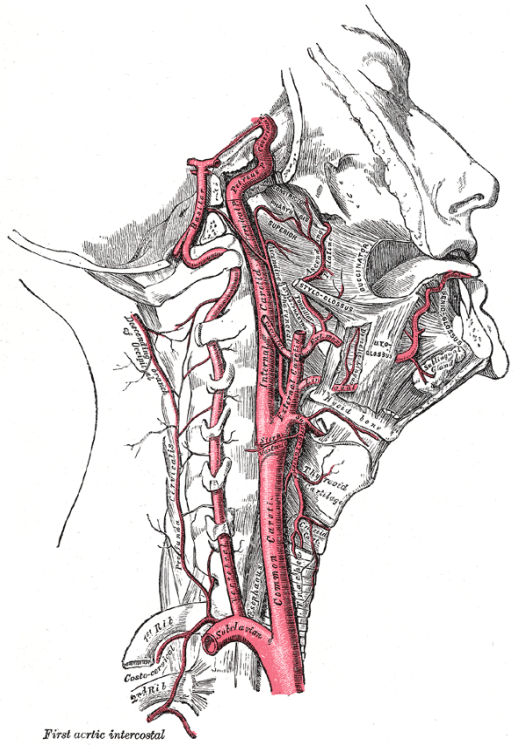

Figure 2.2 - Location of carotid vessels of the neck (Gray, 1853).

carotid artery, originating from the brachiocephalic trunk and aortic arch respectively. Both the right and left common carotid arteries branch to form an internal and external carotid artery. The internal carotid artery is responsible for supplying oxygenated blood to the brain and eyes; whereas, the external carotid artery is tasked with supplying oxygenated blood to the face, scalp and meninges. Unfortunately, this carotid bifurcation region commonly develops atherosclerotic plaque, a leading cause of stroke, marking its importance in the study of cardiovascular disease (Martini, Nath and Bartholomew, 2011).

2.3 Arterial Structure and Function

As mentioned previously, arteries are responsible for carrying oxygen and nutrient blood away from the heart and delivering it to areas of need. As these arteries move distally with reference to the heart they reduce in size and repeatedly branch to form a larger delivery network, eventually forming arterioles, the smallest type of artery. From these arterioles, blood enters smaller vessels known as capillaries which are responsible for exchanges that occur between the blood and the interstitial fluid. After the exchange of nutrients, the blood is collected in veins, known as venules before passing through larger veins on the blood's return to the heart.

In order to function efficiently and maintain performance, the structure and resulting mechanical properties of these vessels are extremely important. Arteries, for instance, can be subjected to high pressures as they pass up to 8000 litres of blood in a day and endure up to 40 million load cycles in a year (Holzapfel, 2008; Martini, Nath and Bartholomew, 2011). To deal with this high volume of blood, the wall of arteries and veins are made up of three layers known as the tunica intima, tunica media and tunica adventitia which predominantly consist of a matrix of elastin, smooth muscle cells (SMCs) and reinforcing collagen (Figure 2.3). Although both arteries and veins consist of this three-layer structure, the focus of the following section and this body of work as a whole will be on the arterial system.

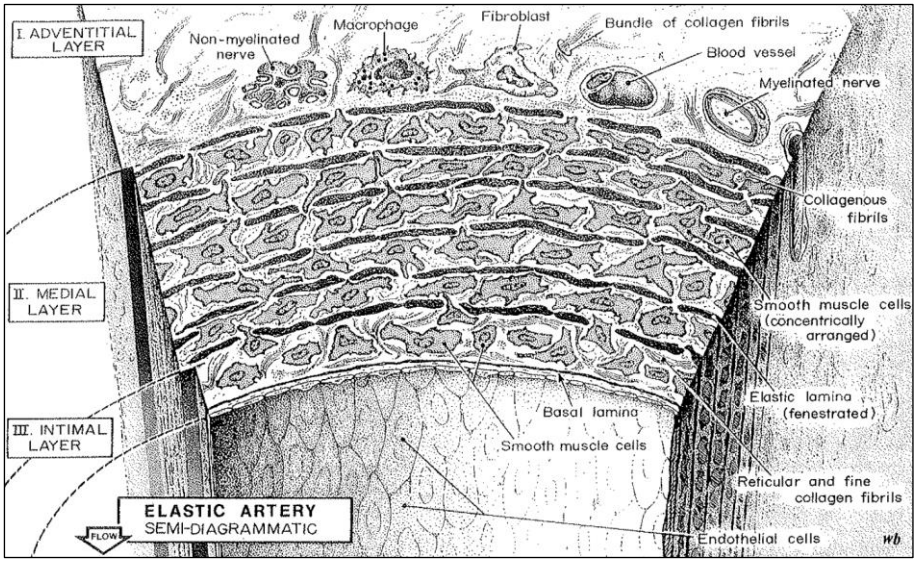

Figure 2.3 - Schematic of an elastic artery showing the three vessel layers; intima, media and adventitia and their main constituent components including collagen, elastin and SMCs (Rhodin, 1980).

2.3.1 Arterial layers

The tunica intima, also known as the tunica interna, is the innermost layer of a blood vessel. The structure of the intima can vary depending on the age and health of the artery as well as the type and function of the artery (Rhodin, 1980; Martini, Nath and Bartholomew, 2011). In small and immature arteries, this innermost layer is extremely thin consisting of a single layer of longitudinally orientated endothelial cells sitting on a thin basal lamina, together known as the endothelium. In larger elastic arteries, the intima also consists of a thin subendothelial layer containing myofibroblasts and SMCs interspersed with collagenous and elastic fibres (Rhodin, 1980). The intimal layer is considered to have negligible mechanical significance in young vessels. However, in aged and unhealthy arteries, a process known as arteriosclerosis results in a stiffening and thickening of the subendothelial layer. As this inner layer thickens and becomes more fibrous with age, the properties of this intimal layer become more mechanically relevant (Holzapfel, 2008).

The tunica media is generally the thickest of the three arterial layers and has the greatest mechanical influence on arterial walls. The media predominantly consists of SMCs, elastin and collagen fibres arranged helically within the wall of

the artery as shown in Figure 2.4. This helical structure is thought to offer the vessel resilience to both longitudinal and expansion forces *in vivo* (Rhodin, 1980). An early study by Wolinsky and Glagov (Wolinsky and Glagov, 1964) noted how these helically orientated SMCs align themselves with respect to forces experienced in the wall. An internal and external elastic lamina act as the inner and outer boundary to the media. Depending on the function and type of artery, additional concentric layers of laminae may be present through the media thickness with up to 60 laminae present in the human aorta (Rhodin, 1980). Consequently, these additional laminae can make the boundary more difficult to distinguish. This is particularly true in large elastic arteries as opposed to muscular arteries which present more distinct internal and external laminae with far fewer layers, many of which are incomplete. The laminar sheets are fenestrated allowing for transport of molecules through the wall of the vessel while a network of elastic fibres interconnects the concentric layers of the media. As vascular diseases such as atherosclerosis progress, this medial structure can become affected (Burke, 2002). The media of veins is much thinner than their arterial counterparts with much larger variations in structure and organisation depending on the age, location, size and presence of lumen valves in the vessel (Rhodin, 1980).

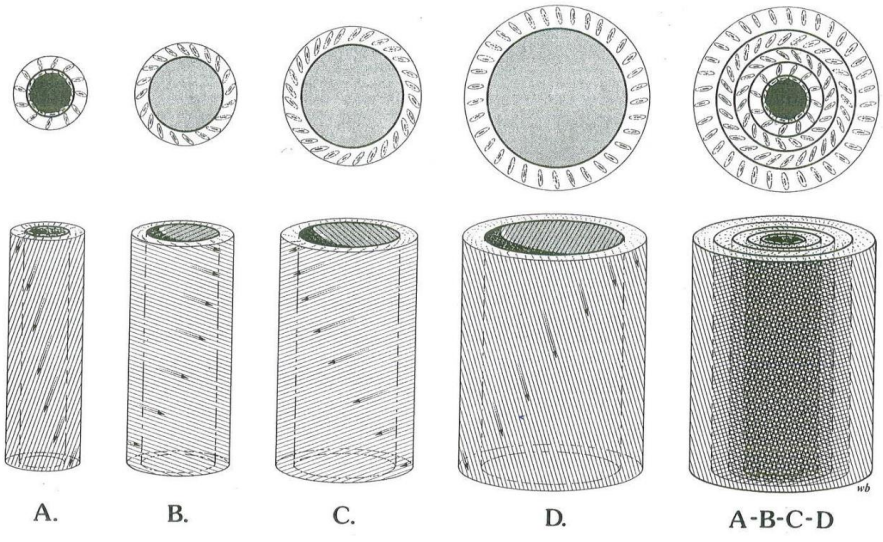

Figure 2.4 - Schematic showing a helical arrangement of circumferentially distributed SMCs and collagen fibres through the arterial wall. The pitch angle of these fibres is observed to increase as one moves radially outward shown in panels A-D (Rhodin, 1980).

The tunica adventitia or tunica externa is the outermost layer of a blood vessel although smaller vessels such as cerebral vessels in the brain may not exhibit a true adventitia. The adventitia is a loosely packed fibro-elastic layer predominantly consisting of collagen and lower levels of elastin in arteries while relatively more elastin, as well as SMCs, can be found in the venous system. The loose connective tissue of the adventitia helps to anchor blood vessels in surrounding tissue minimising movement and as a result, damage to the vessel wall. The adventitia also supports the vasa vasorum, a wide network of small arteries and capillaries which supply nutrients to the walls of large arteries and veins. Under high pressures, the adventitia also acts like a stiff 'jacket-like' structure to prevent over expansion of the blood vessel and subsequent damage. Moving radially outward from the vessel lumen, the 3D structure of collagen and elastin fibres can also be seen to increase in density (Rhodin, 1980).

Although there is a wealth of information available on the general structure of arteries, there is still much contrasting information regarding the specific arrangement of these vessel constituents across vessels and species. Arteries can generally be divided into three different classes of artery depending on their size, location and function within the cardiovascular system: elastic arteries, muscular arteries and arterioles also known as resistance vessels (Martini, Nath and Bartholomew, 2011).

2.3.2 Vessel types

Elastic arteries also known as conducting arteries, encompass the largest arteries in the body which are typically located proximally to the heart. The proximity of elastic arteries to the heart requires these vessels to conduct large volumes of blood at high pressures without loss of function over extended time. In order to facilitate this high pressure, the media of these vessels contain a relatively high level of elastin as compared to smaller muscular vessels (Figure 2.5) (Burton, 1962). This high proportion of elastin allows for the large expansion of the vessel wall in response to the high pressures attributed to ventricular systole. The ability to expand under the high-pressure conditions proximal to the heart allow the body to maintain a relatively uniform pressure further from the heart where vessels are more muscular and less distensible. This expansion and recovery of

these large vessels also serves to smooth the flow of blood through the vascular system during systole and diastole which would not be possible were there a constant stiffness throughout. This ability to maintain a relatively constant pressure throughout the cardiovascular system is known as the `windkessel" effect (Holzapfel, 2008). Examples of elastic arteries in the body include the major arteries of the body such as the aorta and pulmonary trunk as well as subsidiary vessels such as the pulmonary arteries, the subclavian artery and importantly, the common carotid artery. Moving distally, away from the heart, these vessels gradually transition to muscular arteries (Nowrozani and Zareiyan, 2011).

Muscular arteries or distributing arteries encompass most small and medium-sized arteries in the body. Thanks to the elastic properties of the preceding elastic vessels, muscular arteries are not subjected to the high pressures experienced closer to the heart. Consequently, muscular arteries have less elastic fibres and as their name suggests, contain a relatively high volume of smooth muscle cells within their media. The high proportion of SMCs aids in the active contraction of the vessel wall, ensuring that significantly high levels of pressure are found throughout the arterial system (Burton, 1962). The large network created through repeated branching of these vessels allows for the distribution of blood throughout the body. Some of the many examples of muscular arteries include the external carotid, brachial and femoral arteries.

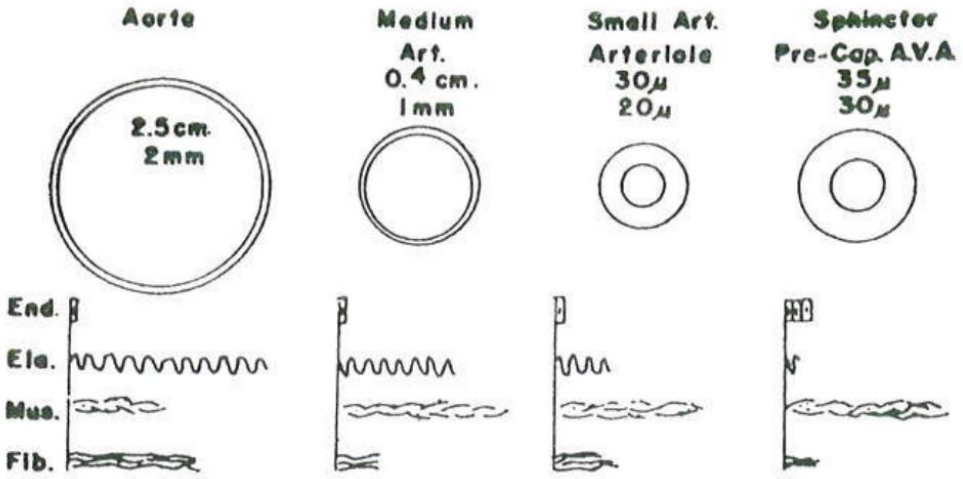

Figure 2.5 - Relative levels of endothelium, elastin, SMCs and collagen in different size arteries showing a reduction in elastin volume fraction, but increase in the collagen volume fraction as you move distally away from the heart (Burton, 1962).

The venous system is responsible for returning blood to the heart in both the pulmonary and systemic circuits. The walls of these vessels are much thinner than their arterial counterparts because of the lower blood pressure throughout the venous system. Due to this low pressure, the venous system relies on intimal valves throughout its vessels to help direct blood flow back toward the heart with the aid of skeletal muscle contraction. Damage and deterioration of these valves can lead to pooling of blood in veins leading to conditions such as varicose veins and even clotting. Although the level of elastin is seen to reduce with distance from the heart in the arterial system, elastin reappears in the larger vessels of the venous system. This reintroduction of elastin can be attributed to the high levels of tension required to maintain vessels of a larger radius. If this tension was to be provided by active contraction of SMCs, continuous energy expenditure would be required. Consequently, tension through elastic fibres allows for greater energy efficiency *in vivo* (Burton, 1962).

2.4 Mechanical Properties

The mechanical properties and subsequent performance of arteries and blood vessels as a whole rely heavily on the complex multi-component structure outlined in the previous sections. As we have seen, the walls of blood vessels are anisotropic in nature owing not only to constituent collagen fibres but also the elastic and cellular components. The comprehensive review of the physiological performance of arteries by Burton (Burton, 1962) provides a good starting point for those looking to understand the role of the elastic and muscular components of the cardiovascular system. Early work on the mechanical properties of artery dates back to the 1880s where the non-linear, anisotropic, elastic response of arterial tissue was analysed (Roy, 1881).

When subjected to uniaxial tensile testing, arterial tissue produces a characteristic 'J-shaped' curve as seen in many biological soft tissues where initially large levels of strain are observed at relatively low loads before a stiffening response is experienced (Figure 2.6) (Holzapfel, 2008). Elastin dominates the initial 'toe' region of this curve, where relatively low load results in large deformation. As deformation increases, successive recruitment,

straightening and alignment of previously undulated collagen fibres begin to bear the load, increasing the stiffness response of the vessel wall (Humphrey, 2002). To demonstrate the influence of both collagen and elastin in the mechanical response of artery, Roach and Burton (Roach and Burton, 1957) selectively digested away each constituent in human iliac artery (Figure 2.6). It was shown that with the selective digestion of collagen using formic acid, the initial arterial response in tension was dominated by the elastin in the tissue. Likewise, collagen was found to dominate the stiffer region of the curve and this was demonstrated through the selective digestion of elastin using crude trypsin.

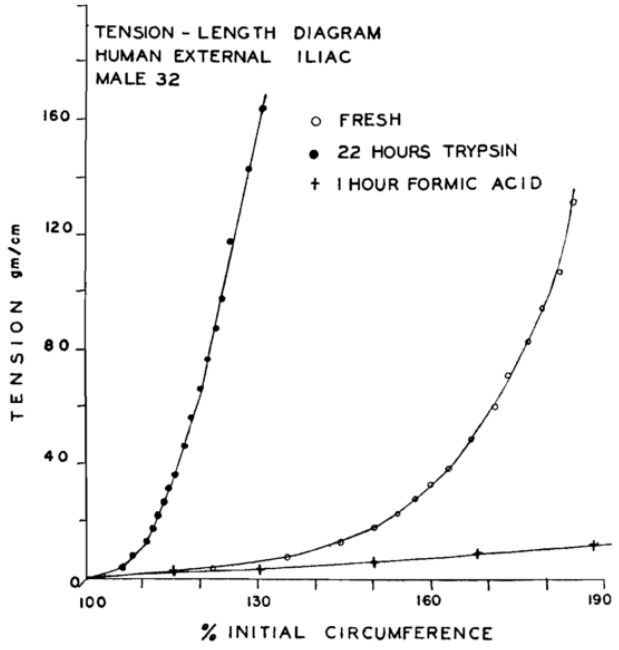

Figure 2.6 - Mechanical response of fresh human iliac artery in response to selective digestion of collagen and elastin showing the contribution of elastin at low strain and contribution of collagen at high strains (Roach and Burton, 1957).

It was previously noted that arteries exhibit an anisotropic response in loading owing to their complex anisotropic structure. Consequently, it is important to consider different deformation modes and in different directions to fully characterise the mechanical properties of artery. Not only does an artery demonstrate a different response to circumferential and longitudinal stretch, but the response has also been shown to be layer specific (Holzapfel *et al.*, 2005). This layer specific response to circumferential and longitudinal stretch is illustrated in Figure 2.7.

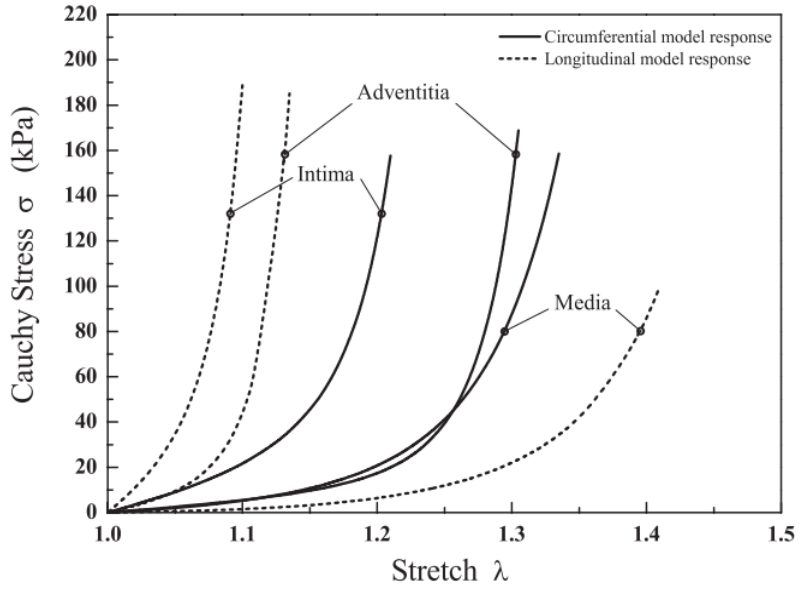

Figure 2.7 - Layer-specific stress-stretch curves for human coronary arteries highlighting the importance of investigating layer specific vessel structure and mechanics (Holzapfel *et al.*, 2005).

It is also important to note that both axial and circumferential residual stresses reside in arterial walls *in vivo* which are disturbed once the vessel is excised and dissected. As a result, sectioned vessels may show altered mean fibre orientations from those experienced *in vivo* (Schriefl *et al.*, 2012). Axial residual stresses can clearly be observed by monitoring the axial shortening of a vessel as it is excised from the body where it was once tethered. The extent to which tethering occurs has been found to depend on both the species and location of the vessel in question (Han and Fung, 1995) while axial strains up to 30% have been found in porcine carotid artery (García *et al.*, 2011). Similarly, circumferential residual stresses are clearly visualised by cutting a vessel open longitudinally and witnessing the vessel spring open rather than maintaining its cylindrical shape. The existence of these pre-existing stresses helps to ensure relatively even stress distributions throughout the vessel wall *in vivo* (Delfino *et al.*, 1997; Labrosse *et al.*, 2009). It is also worth noting that the individual vessel layers exhibit different residual stress levels to achieve an even stress distribution across the vessel wall. The individual residual stress response can be identified by delaminating the different vessel layers and measuring their response when cut open longitudinally (Figure 2.8). The layer-specific residual stresses may serve to minimise the stress across

the vessel at physiological pressures and allow the artery to respond to different axial and circumferential loading environments. The increased circumferential length observed in the intima in comparison to the media in Figure 2.8 may explain the spontaneous delamination that can occur at their interface at high pressure (Holzapfel, 2008). These stresses are both layer and location dependent in the vascular system and arise from growth and remodelling mechanisms in the tissue. These layer-specific responses also highlight the importance of considering individual structural and bio-mechanical response of each arterial layer. It is reasonable to assume that by excising these vessels from the body, effectively removing the *in vivo* loading conditions, both vessel structure and consequently the mechanical properties of the vessel will be altered. The effect of removing residual stresses in the vessel can be seen in Figure 2.8 below.

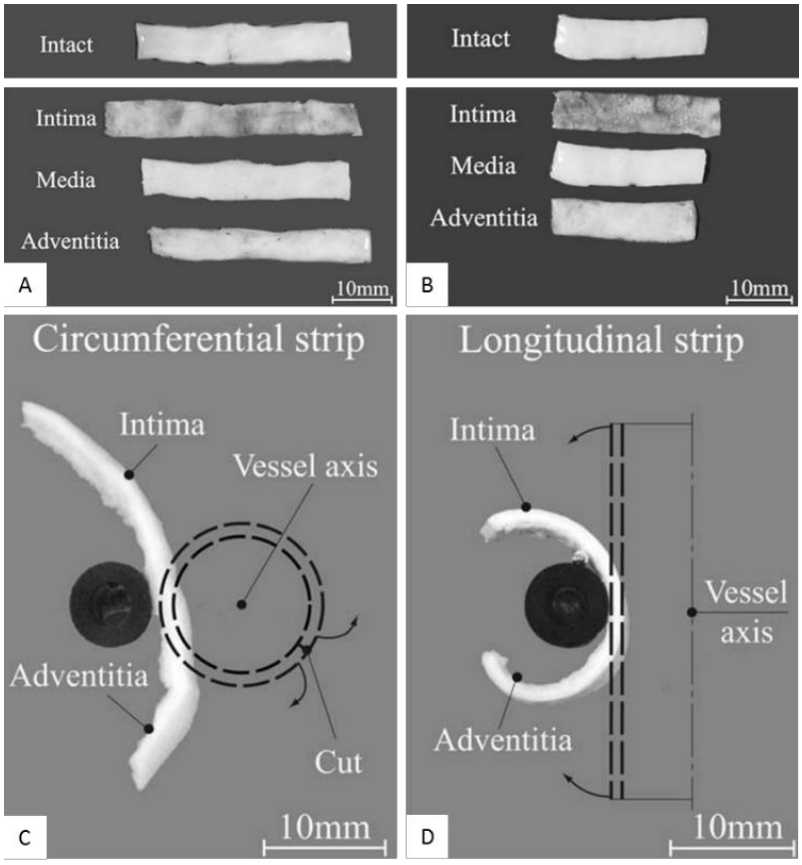

Figure 2.8 – Layer-specific response of anatomically separated A) circumferential and B) axial strips of human aortic tissue. The response of intact aortic tissue cut open to release residual stress is shown for C) circumferential and D) longitudinal strips (adapted from (Holzapfel *et al.*, 2007)*).*

Arteries also behave viscoelastically due to their inherent solid and fluid phase structure. This viscoelasticity manifests itself through creep at a constant load, stress relaxation under a constant strain and hysteresis in cyclic loading. While viscoelastic, arteries are also relatively insensitive to physiological strain rates and can be pre-conditioned in order to reduce hysteresis (Holzapfel, Gasser and Stadler, 2002). The exact mechanisms behind these processes are not completely understood, however macromolecule unfolding, fibre reorientation and physiological fluid distribution are considered to all play a role (Holzapfel, 2008). Consequently, prior to mechanical testing, samples are often preconditioned at lower stress/strain levels to ensure repeatability of measurements and to produce a more realistic *in vivo* tissue response (Figure 2.9). Failure responses are also exhibited by arteries in over distension which can occur due to interventional medical procedures such as balloon angioplasty (Steele *et al.*, 1985). These failure responses further complicate the mechanical response of vessels.

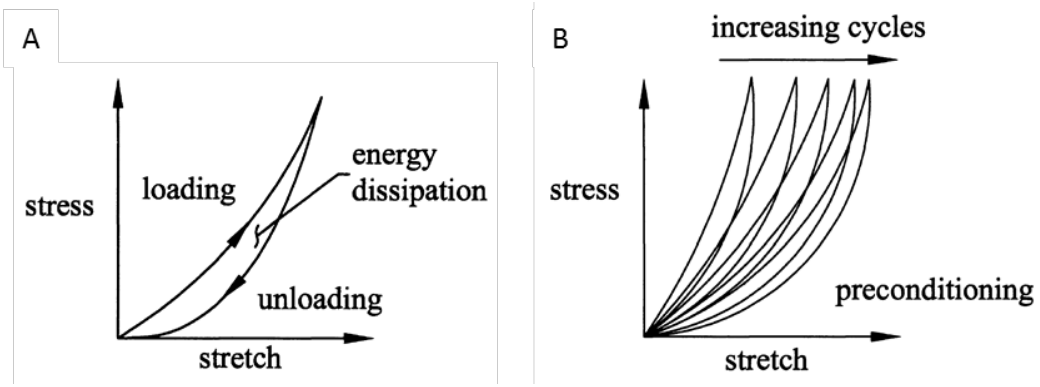

Figure 2.9 - A) Energy dissipation and B) preconditioning of soft tissues highlighting their complex structure-function response (Humphrey and Delange, 2004).

Mechanical testing has also been employed to link both vessel structure to the mechanical response of arterial tissue. Schriefl *et al.* (Schriefl *et al.*, 2012) carried out biaxial mechanical testing on human descending and abdominal aortic arteries as well as common iliac arteries to investigate the layer-specific collagen fibre orientations found in the arterial wall. Biaxial testing was conducted to simulate the loading experienced *in vivo*, with larger strains applied circumferentially to those axially as described in the literature (Learoyd and Taylor, 1966; Labrosse *et al.*, 2009). As mentioned previously, residual stresses are present in the vessel wall which are released upon cutting the vessel open.

Unfortunately, this process will influence both the native vessel structure and the subsequent mechanical response of the tissue. To circumvent this, pressure inflation experiments are often carried out to obtain more physiologically meaningful data (Macrae, Miller and Doyle, 2016). These studies are generally pressure controlled and strain is typically measured optically. Vessel inflation experiments have been utilised to determine vessel mechanical properties (Sommer and Holzapfel, 2012), identify adventitial fibre reorientation under load (Haskett *et al.*, 2013) and investigate fibre damage due to overdistension in ovine cerebral arteries (Converse *et al.*, 2018). Despite these studies, there is still a lack of understanding on how load influences the remodelling of arterial tissue, particularly through degradation.

The aforementioned mechanical characteristics are also dependent on many other factors including but not limited to; age, sex, health, lifestyle (Ozolanta *et al.*, 1998) and location along vascular tree (Silver, Snowhill and Foran, 2003).

2.5 Cardiovascular Disease

2.5.1 Atherosclerosis

As outlined at the onset, CVD is the leading cause of death worldwide, responsible for 17.5 million deaths in 2012 alone (WHO, 2014). Unfortunately, this is a position which it is expected to hold well into the future (Mathers and Loncar, 2006). CVD is a term which is used to describe diseases which affect the heart and vasculature of the body and can often lead to fatal clinical events such as cerebral infarctions (stroke) or myocardial infarctions (heart attack). Atherosclerosis is one such disease which affects arteries within the body and can culminate in a fatal event occurring.

Atherosclerosis is a complex immunoinflammatory disease which affects medium and large arteries in the body (Falk, 2006). It is a specific type of arteriosclerosis, the term used to classify a group of progressive conditions which result in a thickening and stiffening of the arterial wall. Atherosclerosis is characterised not only by this stiffening process but also the development of an atheromatous plaque in the arterial wall. It is widely believed that hemodynamic flow is a leading factor in the development of atherosclerosis and as such atherosclerotic

lesions typically develop in regions of complex vessel geometry such as the carotid bifurcations shown in Figure 2.10 (Friedman *et al.*, 1983; Slager *et al.*, 2005; Lee *et al.*, 2008). The proximity of the carotid bifurcation to the small vasculature of the brain and its susceptibility to atherosclerotic plaque development and rupture make it the leading cause of stroke. Ischemic stroke, where obstruction of blood flow occurs in the vasculature of the brain, often due to plaque debris or emboli blockage, accounts for 87% of cerebrovascular incidents (Mozaffarian *et al.*, 2015).

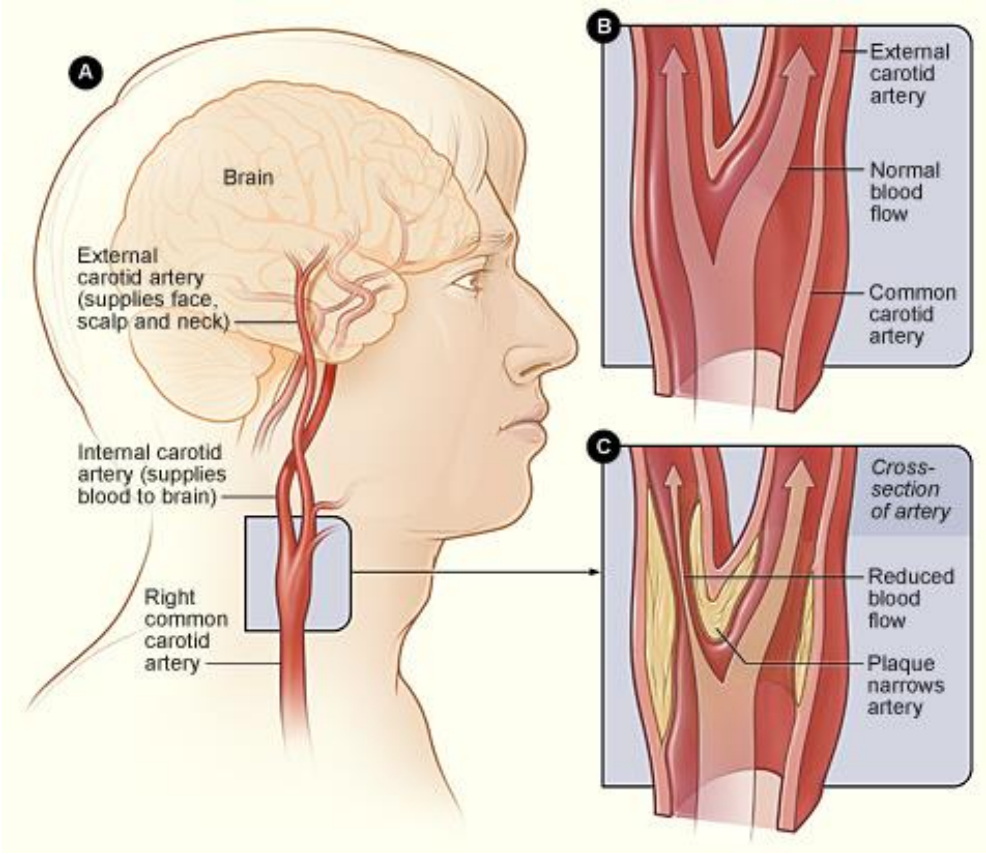

Figure 2.10 - Development of carotid artery disease at the carotid bifurcation (National Heart Lung and Blood Insitute (NIH), 2013c).

Although not fully understood, atherosclerosis develops in response to the infiltration of low-density lipoproteins (LDLs) through a dysfunctional endothelium into the subendothelial space. It is thought that endothelial injury may be a driving force in this initial developmental phase (Crowther, 2005). Once present, these LDLs become oxidised and pro-inflammatory, in turn recruiting

leukocytes such as monocytes present in the blood. As these monocytes migrate across the endothelium, they differentiate into macrophages to remove oxidised LDLs by ingestion. These white blood cells, termed 'foam cells' continue to successfully ingest atherogenic lipoproteins provided that suitably high levels of high-density lipoproteins (HDLs) are present. HDLs assist foam cells through the removal of ingested lipids, allowing the foam cell to continue to their ingestion of further lipids. If low levels of HDLs are present, continued ingestion of atherogenic lipoproteins culminates in apoptosis of the foam cell and deposition of previously ingested lipid material (Crowther, 2005; Falk, 2006). As the atherosclerotic lesion develops, this deposited material forms a soft lipid-rich plaque core. Many of the stages and products arising during this process are atherogenic themselves and can accelerate atherosclerotic development through positive feedback (Falk, 2006). There are numerous risk factors associated with increased risk of atherosclerosis including hypertension, smoking, blood cholesterol levels and being of male gender (Chambless *et al.*, 1997; Falk, 2006).

To better diagnose and treat patients suffering from atherosclerotic disease, a classification system has been put in place by the American Heart Association (AHA) which categorises plaques into one of eight categories (Stary *et al.*, 1994, 1995; Stary, 2000). Despite being developed for coronary artery disease, this scale which ranges from early plaque development to late progression is also used as a guide for carotid plaque development. This class system loosely relates to the increasing severity of the plaque progression with early onset of atherosclerosis seen in Type I lesions, where the first lipid-laden foam cells are seen in the intima to clinically significant Type V and VI lesions (Figure 2.11). These clinically significant lesions present severe intima disorganisation with the potential for destabilising fissure development. The lack of collagen and SMCs, coupled with macrophage infiltration, increase the risk associated with these lesion types.

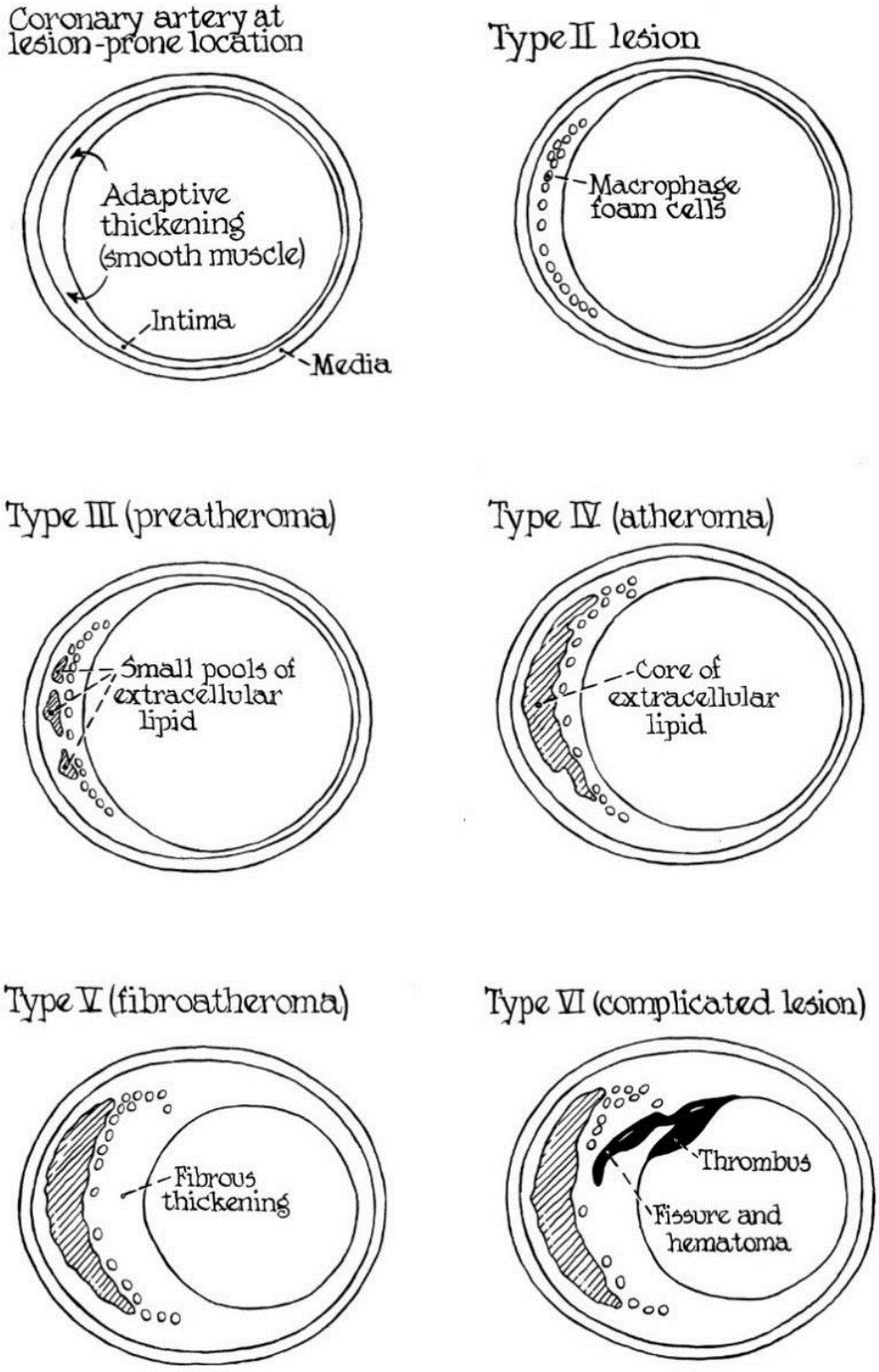

Figure 2.11 – Schematic of the anterior descending coronary artery showing plaque development and progression from early Type I plaques to clinically significant Type V and VI plaques (Stary *et al.*, 1995).

2.5.1.1 Vulnerable plaque/patient

In addition to the classification system published by the AHA (Stary *et al.*, 1994, 1995; Stary, 2000), work has been carried out attempting to more accurately identify plaques at risk of rupture (Varnava, 2002; Naghavi, 2003b; Aikawa, 2004; Falk, 2006; Peeters *et al.*, 2009). Insights into the factors driving plaque vulnerability could greatly aid in the identification and subsequent treatment of asymptomatic atherosclerotic arteries.

To achieve this, Varnava *et al.* (Varnava, 2002) looked to establish this link between inward and outward remodelling of the arterial wall and plaque vulnerability. Although outward or positive remodelling of an atheromatous artery is beneficial in reducing luminal stenosis, it was found to be associated with more complex, vulnerable plaques which were more at risk of rupture. A connection between outward arterial remodelling and increased lipid, macrophage and consequently matrix metalloproteinases (MMPs) content was found, all of which are indicators of rupture-prone plaque (Figure 2.12). MMP collagenases produced by this high macrophage content have been found to

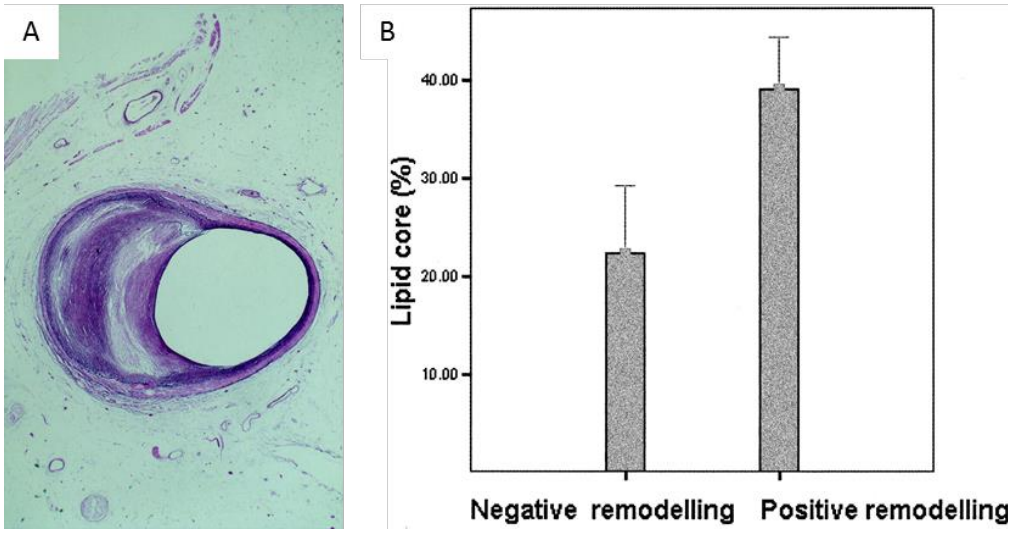

Figure 2.12 - Aa) Positive remodelling of a coronary artery and B) bar chart showing an increase in undesirable lipid material in outwardly remodelling vessels (Varnava, 2002).

potentially weaken the fibrous plaque cap increasing the likelihood of plaque fissuring or rupture (Aikawa, 2004; Daemen *et al.*, 2016). The performance of these MMP collagenases has also been found to be strain dependent (Flynn *et al.*, 2010; Adhikari, Chai and Dunn, 2011) which may influence the rate of degradation occurring in stiff atherosclerotic tissue. Additionally, regions of low cellular content which are associated with plaque progression, may decrease a tissue's healthy remodelling ability (Crisby *et al.*, 2001).

It has been suggested that vulnerable plaque is not the only consideration when attempting to predict plaque at risk of rupture. Naghavi *et al.* (Naghavi, 2003a, 2003b) looked to expand on the initial AHA classifications to consider what constitutes not only a vulnerable plaque but a 'vulnerable patient'. This new term encompasses the vulnerability of the plaque, blood and myocardium in order to diagnose patients. Potentially vulnerable plaque types are shown in Figure 2.13. Five major criteria were established in an aid to identifying plaque vulnerability including active inflammation, thin cap wall with a large lipid core and endothelial denudation with platelet aggregation. A closer look at plaque pathogenesis has identified structural, cellular and functional factors attributed to plaque stabilisation (Falk, 2006) which have also been seen to occur in non-fatal, ruptured plaques (Peeters *et al.*, 2009). Hemodynamic flow which is linked to initial plaque development has also been strongly linked to plaque vulnerability and may offer a means of early identification of vulnerable plaques and patients (Slager *et al.*, 2005; Groen *et al.*, 2008; Zahnd *et al.*, 2016). Despite the substantial volume of work investigating plaque development, progression and vulnerability, the mechanobiological cues driving atherosclerosis are still unclear.

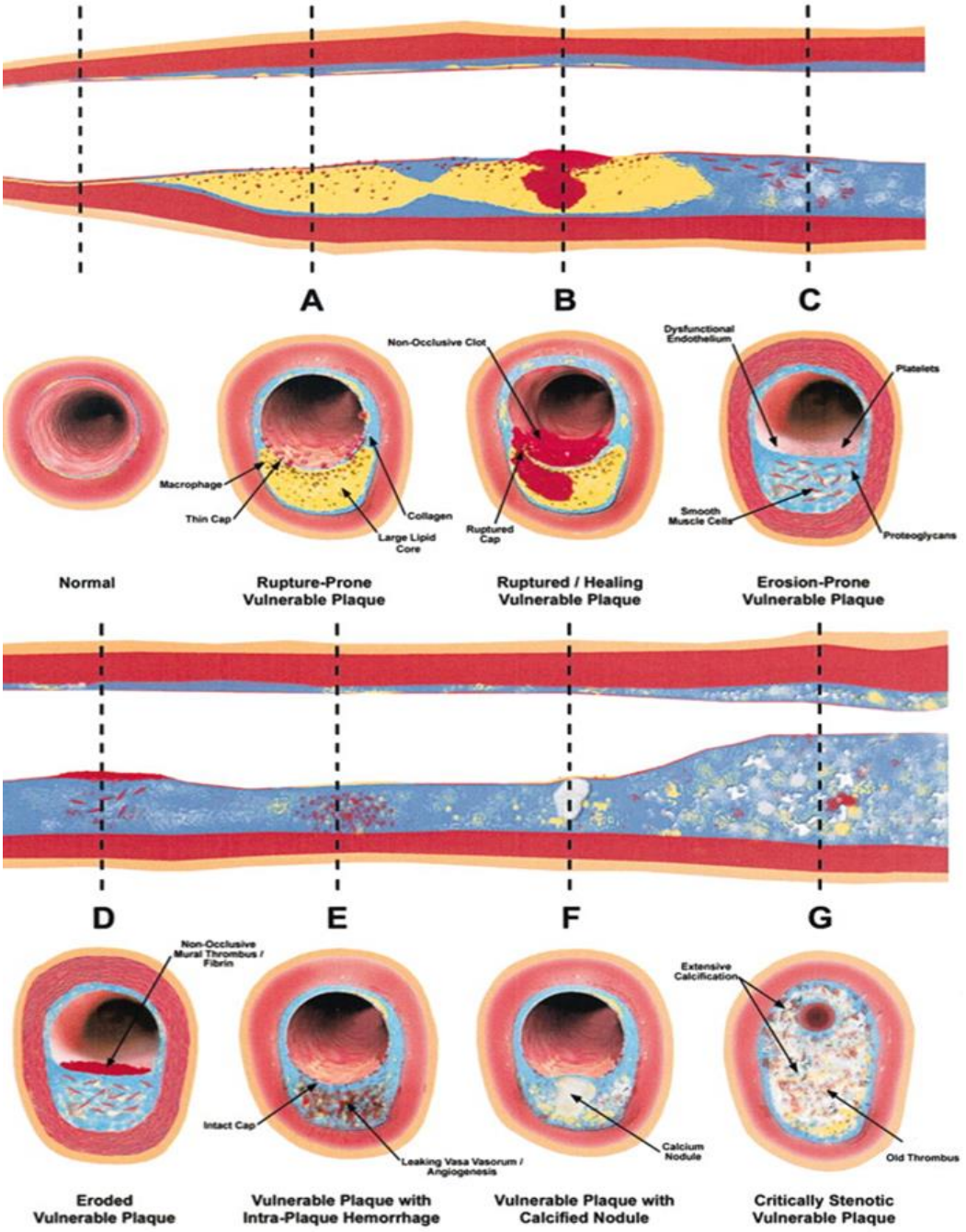

Figure 2.13 – Different forms of vulnerable plaques as set by Naghavi et al. (Adapted from (Naghavi, 2003a)*).*

2.5.1.2 Diagnosis and Treatment

Current strategies for diagnosing and measuring the degree of stenosis include duplex ultrasound (DU), intravascular ultrasound (IVUS), magnetic resonance imaging (MRI) and computerised tomography angiography (CTA) (Schaar *et al.*, 2007). Based on the imaging technique chosen, the severity of stenosis is compared to established guidelines arising from clinical trials ('MRC European Carotid Surgery Trial: interim results for symptomatic patients with severe (70-99%) or with mild (0-29%) carotid stenosis. European Carotid Surgery Trialists' Collaborative Group.', 1991; Moneta *et al.*, 1993). Unfortunately, these techniques often provide limited information on the structure and type of plaque present (Nair, 2002). Alternative techniques have been suggested for better identifying the various vulnerability criteria set out previously, such as thermography for identifying active inflammation (Naghavi, 2003a; Schaar *et al.*, 2007). Combining multiple techniques such as MRI with computational modelling may also offer a potential means of estimating plaque stresses and strains *in vivo* with the aim of identifying plaques at risk of rupture (Nieuwstadt *et al.*, 2015; Kok *et al.*, 2017). Unfortunately, time and resources can limit the use of multiple techniques for detailed identification of plaque vulnerability.

Once a vessel is identified as requiring medical intervention, carotid endarterectomy (CEA) or carotid artery stenting (CAS) is generally carried out. CEA is an invasive surgical procedure where a cervical neck incision is made to gain access to the carotid artery. The vessel is opened and shunted to redirect blood flow while the plaque is excised from the vessel wall (Figure 2.14). After plaque removal, the vessel and neck are sutured closed and healing can begin. CEA has been found to work significantly better than treatment with medicine alone in highly stenosed vessels (>70%) (Mozaffarian *et al.*, 2015). CEA is often recommended for those with high levels of stenosis. It has been found that CEA produces more favourable results than CAS in older patients (>70 years) where tortuous vasculature makes catheter-based procedures more challenging.

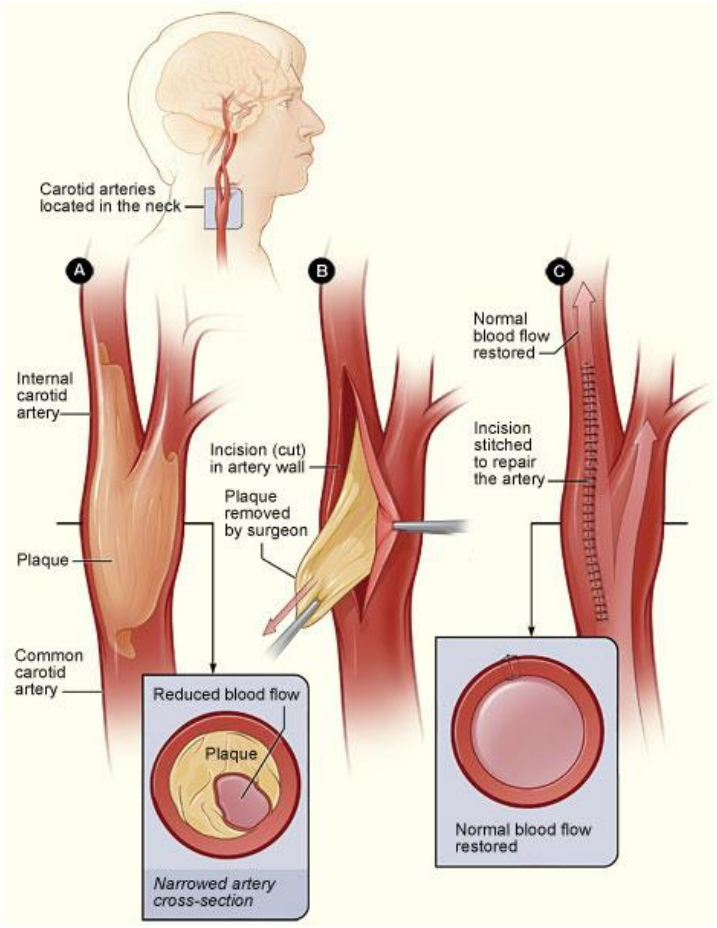

Figure 2.14 - Schematic showing a carotid endarterectomy procedure where plaque is surgically removed from the carotid artery using a forceps (National Heart Lung and Blood Insitute (NIH), 2013a).

CAS is a minimally invasive endovascular procedure where a self-expanding nitinol (NiTi) stent is guided to the stenosed region through the radial or femoral artery using a catheter. The stent is positioned at the site of plaque burden to restore lumen diameter once deployed (Figure 2.15). Correspondingly, CAS is recommended as a treatment for stenosed vessels where intravascular procedures pose minimal risk to the patient. There is much debate as to which technique produces more favourable results. Although CAS was found to reduce cranial nerve injuries and myocardial infarctions occurring during CEA, a significant increase has been found in the 30-day incidence of stroke (Bangalore *et al.*, 2011). Further studies have found similar short and long-term outcomes while noting an increase in stroke and heart attack incidence in CAS and CEA, respectively (Mantese *et al.*, 2010).

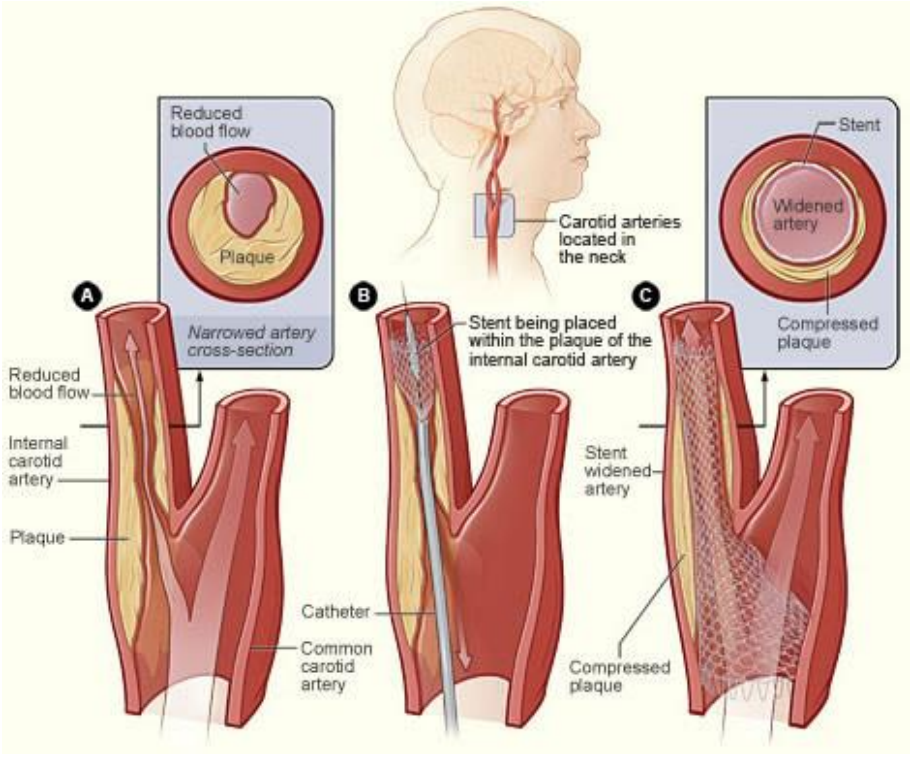

Figure 2.15 - Schematic showing the deployment of a minimally invasive self-expanding NiTi stent in the internal and common carotid artery as an alternative to a carotid endarterectomy (National Heart Lung and Blood Insitute (NIH), 2013b).

Early carotid stenting was carried out using stainless steel stents similar to those used in coronary stenting with limited success (Clair, 2008). Today, self-expanding NiTi rather than balloon-expandable stainless-steel stents are used in carotid stenting to take advantage of its superior elasticity and crush resistance (Figure 2.16). Major advances have been made since their initial introduction, with many designs available today (Clair, 2008). As with coronary stenting (Rutsch *et al.*, 2000; Lally, Dolan and Prendergast, 2005; Gijsen *et al.*, 2008; Dangas *et al.*, 2010), stent design has been found to influence the performance and outcome of carotid stents (Hart *et al.*, 2006; Clair, 2008). Stent performance has also been seen to be affected by plaque type present in the vessel prior to stenting.

Closed cell stents were found to be preferable to their open cell counterparts in the treatment of echolucent plaques in the carotid artery as identified by duplex ultrasound (Hart *et al.*, 2006). Stented vessels are also prone to in-stent restenosis (ISR), the process of neointima formation, attributed to stent deployment.

Thankfully, the advent of anti-proliferative drug coatings for stents has significantly reduced the rates of ISR, particularly in coronary stenting (Dangas *et al.*, 2010). Although low, in-stent restenosis (ISR) is also found to occur post carotid stenting. Follow up studies have found ISR (>80%) to have an occurrence rate of 5%, while lower restenosis levels (<80%) were found to have much higher incidence rates (Chakhtoura *et al.*, 2001; Lal *et al.*, 2003; Setacci *et al.*, 2005). Stent design has previously been found to affect ISR rates in coronary arteries, and as such, it is highly likely to be a factor in carotid ISR. Development of new and improved stents informed by experimental data on arterial remodelling may reduce these ISR rates further while also reducing the need for cytotoxic, cancer-fighting stent coatings. Further advances in carotid stent design and development will undoubtedly increase the popularity of CAS. A shift towards the use of minimally invasive stenting procedures will offer long-term cost savings thanks to reduced recuperation times and with improvement, less follow up procedures.

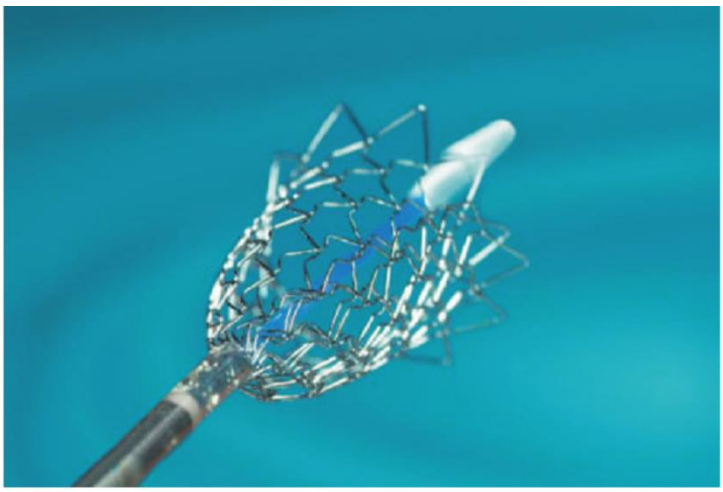

Figure 2.16 - Self-expanding NiTi stent for use in the carotid artery (Clair, 2008).

2.5.2 Aneurysm

Aneurysms are another histopathological manifestation of CVD which affect arteries in the body. Aneurysms present as a localised bulging or ballooning of the vessel wall (Figure 2.17), often forming along the aorta or in cerebral arteries. These aneurysms are categorised based on their morphology as either saccular or fusiform, as well as their size and location. If left untreated, aneurysm progression can compromise the structural integrity of the vessel, resulting in

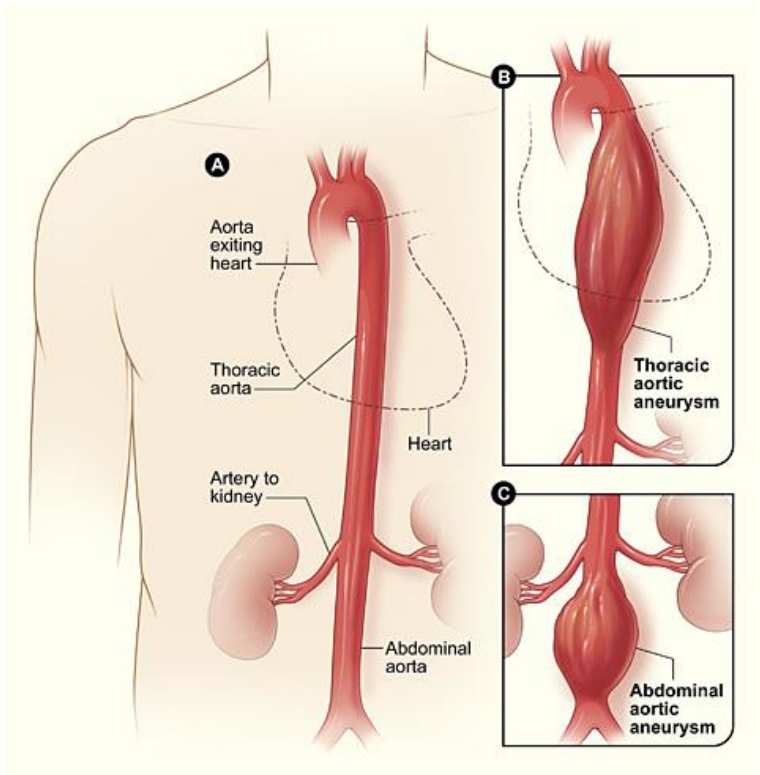

Figure 2.17 - Schematic showing A) a healthy aorta next to B) a thoracic aortic aneurysm and C) an abdominal aortic aneurysm. Aneurysmal tissue show significant vessel dilation.(National Heart Lung and Blood Insitute (NIH), 2010).

eventual rupture (Thompson, Geraghty and Lee, 2002). Unfortunately, aneurysm rupture is often fatal, with a 94% mortality rate in the case of thoracic aortic aneurysm rupture (Bickerstaff *et al.*, 1982). There are many risk factors associated with aneurysm development, progression and rupture including family history, gender, tobacco use, existing arterial disease, and hypertension (Chaikof *et al.*, 2009).

Aneurysm formation is linked to excessive degradation of the extracellular matrix by matrix metalloproteinases (MMPs) and other cysteine collagenases. These proteases are central to normal healthy arterial remodelling; however, they have been found to be upregulated in developing and ruptured aneurysmal tissue (Abdul-Hussien *et al.*, 2007). Increased macrophage and lymphocyte presence which contribute to inflammatory response associated with CVD are further hallmarks of aneurysm development (Xiong *et al.*, 2009). Numerous studies have

investigated structural changes in aneurysm progression with many reporting decreased elastin and collagen content (Tsamis, Krawiec and Vorp, 2013). A decrease in the relative ratio of elastin to collagen has also been noted which may be due to the inability of arteries to replace degraded mature elastin (Duca *et al.*, 2016). It is possible that degradation of elastin which is responsible for the low strain response in arterial tissue may play a role in early aneurysm formation. Correspondingly, collagen degradation may become more prominent during aneurysm progression as higher tissue strains are experienced. As mentioned previously, collagen degradation is known to be a strain-dependent process, potentially explaining the reduced collagen content observed in ruptured aneurysmal tissue (Thompson, Geraghty and Lee, 2002; Tsamis, Krawiec and Vorp, 2013) (Figure 2.18).

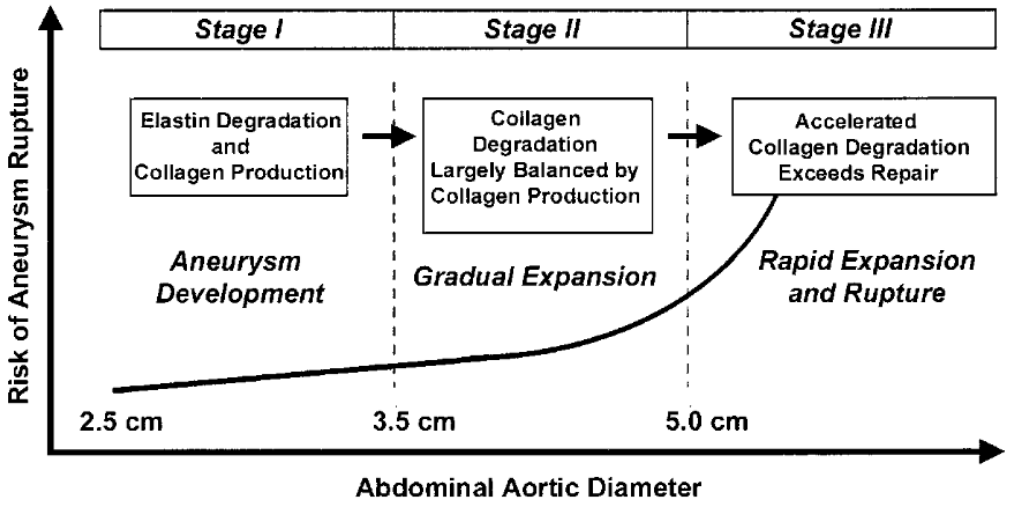

Figure 2.18 - Schematic showing the stages of aneurysmal development and progression. Collagen degradation exceeds production as an aneurysm develops until the vessel can no longer bear the load and rupture occurs (Thompson, Geraghty and Lee, 2002).

Currently, the decision to carry out aneurysm intervention is predominantly based on aneurysm diameter, with vessels above 5 cm considered at risk of rupture in the case of abdominal aortic aneurysm (AAA). Unfortunately, this criterion alone is not adequate for predicting vessel rupture, with rupture often found to occur below this threshold (Nicholls *et al.*, 1998). It is clear that further developments are required to provide more comprehensive clinical screening tools

which may assist clinicians in determining vessels requiring medical intervention. As discussed in Section 2.4 above, the underlying collagen fibre architecture governs the mechanical strength of arterial tissue, while, maladaptive remodelling of this architecture may alter the mechanical response of the vessel wall. Consequently, a greater understanding of the underlying structure of healthy and diseased arterial tissue may provide an alternate or additional means of identifying vessels at risk of rupture.

2.6 Structural Characterisation

There are a wide range of techniques regularly employed to investigate and characterise the structure of soft tissues. All of these techniques have their advantages and disadvantages and it often depends on time, money, access and the information sought as to which technique is chosen. Structural information acquired is often based on the technique chosen and can play an important role in understanding and predicting material behaviour. Experimentally obtained structural information can be used to improve material understanding, provide insights into tissue mechanical responses, validate theoretical and computational models and even inform future model development. Collagen fibres (predominantly types I and III) are known to be the most mechanically relevant component of the arterial wall and as such, numerous techniques have been used to identify the fibre architecture of the vessel wall (Holzapfel, 2008).

2.6.1 Bright-field Microscopy

Optical light microscopy has long been a popular method of viewing and characterising the structure of biological tissue samples. Bright-field microscopy is the simplest form of optical light microscopy and relies on the absorption of an illuminating white light to view a sample. Despite the simplicity of its setup, bright-field microscopy allows viewing of many different structures within biological tissues through the use of well-known histological stains such as H&E and elastic Van Gieson's stain (Figure 2.19). Resulting images provide a means of qualitatively analysing tissue structures while these images can often be further processed using image processing techniques to more quantitatively analyse the results.

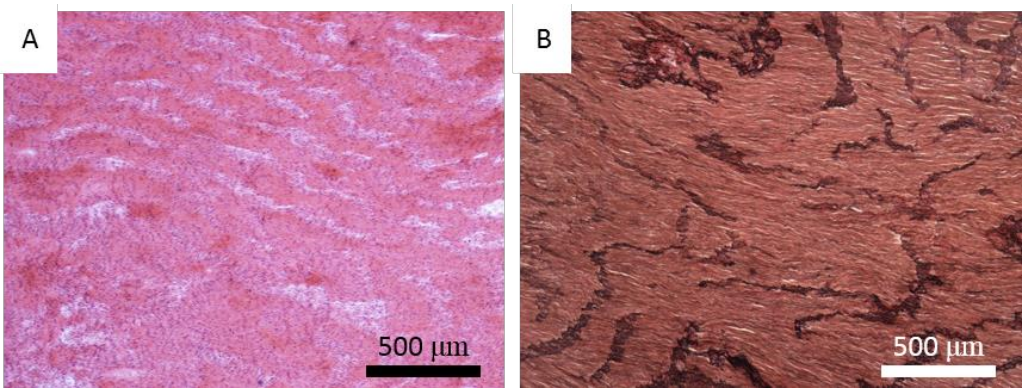

Figure 2.19 – Tangential sections of arterial wall stained with A) H&E and B) Elastic Van Gieson's showing structural details viewed under 4x magnification. H&E allows visualisation of cell nuclei in purple and other constituents depending on their pH while Elastic Van Gieson's stain shows elastin in black and collagen in brown.

Many early studies benefitted from the use of this simple microscopy method for characterising the structure of arteries including collagen content and orientation throughout the various arterial layers. The seminal work of Canham *et al.* (Canham *et al.*, 1989) used light and more advanced polarised light microscopy to determine the three-dimensional structure of coronary arteries fixed under pressure.

Although bright-field microscopy is still used today, more advanced imaging modalities have been developed and are actively used to better determine arterial structure including the response of these tissues to load. Adaptations of this imaging method have allowed for improved clarity and imaging depths while maintaining bright-field microscopy as a quick and cheap method of qualitatively characterising biological structures. Unfortunately, brightfield microscopy typically requires samples to be chemically fixed, histologically processed, and sectioned into thin slices prior to tissue staining and subsequent imaging. Although fixing aims to minimise tissue disruption during this process, changes in tissue architecture are likely to occur.

2.6.2 Polarised Light Microscopy

Polarised light microscopy (PLM) is a well-established characterisation technique which takes advantage of the birefringent properties of collagen within tissue samples. In PLM, antagonistic light is polarised by a polarising lens and passed through a sample before being fed through a second perpendicular polarising lens,

known as an analyser. Birefringent collagen fibres aligned with the polarising lenses will diffract the passing polarised light and pass through the analyser, while unaligned fibres will not be visible. Consequently, the polarising lenses or sample must be rotated and reimaged in order to capture a full picture of the sample. In the case of collagenous tissue, samples are stained to enhance the natural birefringence of the constituent collagen fibres before being viewed under polarised light. Through staining, collagen fibres can be identified and their azimuth (in-plane/circumferential) and elevation (out-of-plane/radial) angles determined with the use of a universal stage (Holzapfel, 2008). PLM has frequently been used to characterise collagen fibre orientation in many biological tissues such as heart valves (Cochran and Kunzelman, 1991; Hilbert *et al.*, 1996; Tower, Neidert and Tranquillo, 2002), coronary arteries (Canham *et al.*, 1989), and aortic and iliac arteries (Gasser *et al.*, 2012; Schriefl *et al.*, 2012). Some of the earliest work using PLM to characterise arterial tissue can be attributed to the work of Canham *et al.* (Canham *et al.*, 1989) in their investigations of coronary artery spasms. While many studies have considered the effect of loading on collagen orientation in biological tissue by fixing vessels or vessel sections in a loaded state (Canham *et al.*, 1989; Schriefl *et al.*, 2012), very few have looked at real-time dynamic reorientation during mechanical loading (Hilbert *et al.*, 1996; Tower, Neidert and Tranquillo, 2002), most likely due histological processing for thick samples. One of the first studies to actively look at collagen orientation during loading was performed on porcine aortic heart valves which are transparent enough not to require histological processing (Hilbert *et al.*, 1996). A custom uniaxial microtensile stage designed to be mounted on a standard microscope stage was used to stretch each sample while video images and micrographs were recorded. These images were subsequently analysed using fast Fourier transform to determine fibre orientation and alignment in the tissue. A similar subsequent study also considered porcine aortic heart valves as well as 'tissue equivalent' samples during uniaxial loading (Tower, Neidert and Tranquillo, 2002). Although PLM is considered a very useful and cost-effective method of tissue characterisation it also has a number of disadvantages associated with it. The ability to view many different components within a sample through the use of different staining protocols while an advantage, can also

present a disadvantage (Sacks, Smith and Hiester, 1997). Histological tissue processing techniques although well established, are time-consuming and may negatively impact tissue structure. The staining process can also introduce artefacts and lead to large variability in the resulting samples making future analysis difficult. PLM requires thin samples to allow for the transmittance of illuminating polarised light. Unfortunately, these processes can lead to increased variation between samples. Although real-time loading of tissue while using PLM has been carried out (Hilbert *et al.*, 1996; Tower, Neidert and Tranquillo, 2002), full tissue analysis is difficult as it requires thin, transparent samples.

Gasser *et al.* (Gasser *et al.*, 2012) used PLM and picrosirius red to identify structural differences in healthy and aneurysmal human aortic tissue. Using a universal stage, both the in-plane and out-of-plane fibre angles were measured through each vessel layer. Diseased tissue was identified as having large levels of fibre disorganisation identified by a high level of dispersion when compared to healthy tissue. These findings suggest that maladaptive remodelling occurs in diseased vessels which may potentially lead to a major adverse clinical event. Similarly, Schriefl *et al.* (Schriefl *et al.*, 2012) employed PLM in conjunction with picrosirius red to identify structural differences between the intima, media and adventitia of the human thoracic and abdominal aorta as well as common iliac arteries. PLM identified layer specific and location specific fibre architecture across each vessel. Two helically wound fibre families were present in the intima, media and adventitia in thoracic and abdominal aortic arteries with often a 3rd or

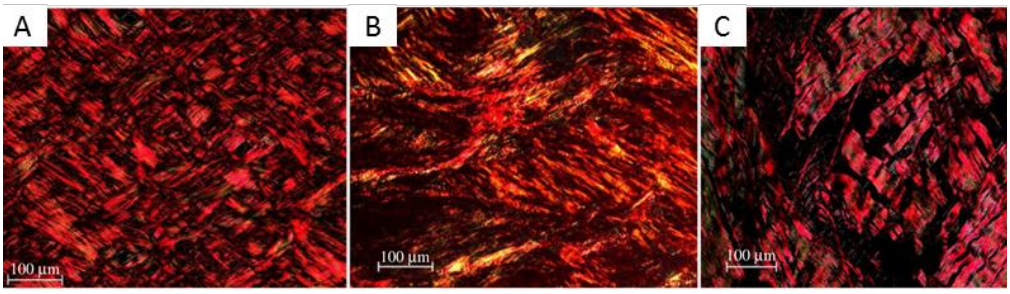

Figure 2.20 - Polarised light images of A) intima, B) media and C) adventitia showing multiple collagen fibre families crossing at slightly different mean fibre angles [Adapted from (Schriefl *et al.*, 2012)*]. Circumferential direction is left-right.*

even 4th presenting in the intima. Fibre orientation was found to be symmetrically arranged across each vessel layer with a more axial direction in the adventitia and circumferential direction in the media. The orientation of fibres in the intima were found to be in between that of the media and adventitia (Figure 2.20).

Surprisingly, the media of the iliac artery was found to present a single fibre family orientated circumferentially around the vessel wall. In an attempt to explain this change in vessel structure, Qi *et al.* (Qi *et al.*, 2015) used 3 different remodelling algorithms, all of which predicted this circumferential fibre alignment. The relatively low axial tethering of the common iliac artery was found to be the reason behind this single fibre family distribution. PLM analysis of the elevation (out-of-plane) angle, found very little variation across samples with no distinguishable difference between fibre families. This finding is in contrast to the results of Sáez *et al.* (Sáez *et al.*, 2016) who identified collagen fibre families based on their elevation angle as opposed to their azimuth (in-plane) angle. Instead, a single circumferential orientation of in-plane fibres was identified although layer specific fibre orientation (Schriefl *et al.*, 2012) was not considered. The mean angles and dispersion identified were incorporated into a structural constitutive model which was capable of capturing the mechanical response of the tissue to biaxial stretching. It is worth noting that experimental observations were made using porcine carotid arteries which further suggest the differences between layer, location and species in vessel architecture.

PLM typically carried out on histologically processed and stained sections of tissue, as is the case with brightfield microscopy. Consequently, PLM is quite labour intensive and slow for tissue characterisation while analysis of results can become subjective depending on the analysis method. PLM also only allows the user to see fibres which are not aligned in the direction of the two polarising lenses. As a result, a minimum of a second image is required at the same location with the polarisation axis rotated. These 2 images must then be combined in order to visualise the full fibrous structure of the tissue. If this process is not adhered to, it may lead the investigator to falsely conclude that a sample has 2 fibre families orientated approximately orthogonally to each other. It is possible that some studies in literature may have fallen susceptible to this oversight as appears

to be the case in Figure 2.20A. Additionally, due to the slow, labour intensive nature of the above the technique, it is difficult to gather large measurement numbers as capable with techniques such as small angle light scattering (SALS; Section 2.6.6 below) or diffusion tensor imaging (DTI; Section 2.6.8 below).

2.6.3 Confocal Microscopy

Confocal laser scanning microscopy (CLSM) improves on conventional brightfield microscopy by allowing the acquisition of high-resolution images through a sample's thickness (Pawley, 2006). A confocal microscope achieves this by raster scanning an excitation laser across a sample while only recording in focus excited light through the use of a pinhole aperture in the same focal plane as the sample. Consequently, out of focus light is removed from the resulting images, enabling the creation of a three-dimensional image through Z-stacking of multiple images through the thickness. The ability of CLSM to image high resolution discrete optical sections through a tissue has led confocal microscopy to become a popular technique for imaging biological tissue in the recent past (O'Connell *et al.*, 2008; Rezakhaniha *et al.*, 2012; Schrauwen *et al.*, 2012; Ghazanfari *et al.*, 2015). Confocal microscopy can be used to image many different biological structures as it depends on the excitable fluorescent probes chosen by the user. The fluorescent collagen marker, CNA35 is one such probe which has been used previously to visualise collagen fibres in arterial tissue (Rezakhaniha *et al.*, 2012; Schrauwen *et al.*, 2012). CNA35 enabled the orientation and undulation of adventitial collagen fibres of rabbit carotid arteries in their unloaded state to be analysed as seen in Figure 2.21. This study identified multiple fibre families with an associated degree of dispersion as has been found in other locations in the body using PLM (Schriefl *et al.*, 2012). These results contradict PLM results of porcine carotid artery which identified a single circumferentially arranged fibre family in the wall of the carotid artery. These differences may be explained by the different layers analysed (adventitia vs. full artery walls) as well as differences in species which the vessels were excised from (rabbit vs. pig) (Canham *et al.*, 1989; Schriefl *et al.*, 2012).

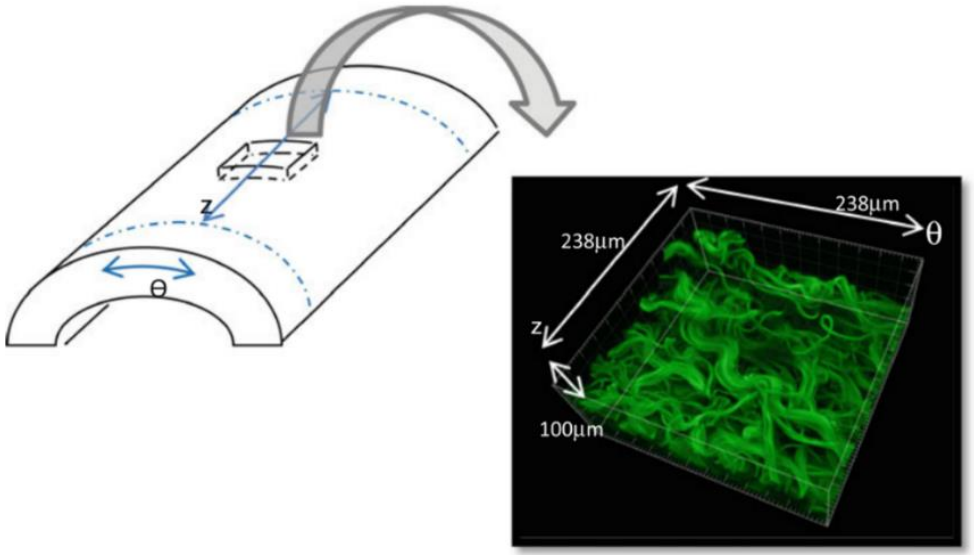

Figure 2.21 - Adventitial collagen fibres tagged with CNA35 probe seen by confocal microscopy (adapted from (Rezakhaniha *et al.*, 2012)*).*

A number of studies have also considered the orientation of collagen fibres within loaded and unloaded samples (Voytik-Harbin *et al.*, 2003; Schrauwen *et al.*, 2012). Voytik-Harbin *et al.* (Voytik-Harbin *et al.*, 2003) were one of the first groups to perform confocal microscopy in the form of confocal reflection and fluorescence microscopy in conjunction with uniaxial mechanical loading to determine microstructural changes in reconstituted collagen, three-dimensional tissue constructs and tissue-derived biomaterials. Schrauwen *et al.* (Schrauwen *et al.*, 2012) also used CLSM along with diffusion tensor imaging tractography techniques to identify the response of collagen fibres to loading in rabbit carotid arteries. This was achieved through incrementally pressurising the vessel from 0 to 140mmHg resulting in a gradual reorientation and straightening of the undulated collagen fibres, see Figure 2.22. Collagen fibres can be seen to begin load bearing between 80 mmHg and 120 mmHg. To compensate for the out of plane motion of the arterial wall during pressurisation, repositioning of the microscope stage was carried out between each step to ensure consistent imaging of a single plane. CLSM is often considered relatively slow for some applications and as a result, an alternative method known as spinning disk confocal microscopy can be used which allow multiple points within a sample to be imaged simultaneously. This technique, however, requires samples to be relatively thin

(< 20 μm) as opposed to CLSM which can image depths of 50-80 microns (Schrauwen *et al.*, 2012). As previously mentioned, samples must also be treated with a fluorescent probe prior to viewing. The ability to view different structures with different probes which fluoresce at different wavelengths along with the ability to build up a 3D structure makes confocal microscopy an attractive imaging method. However, as with many other imaging methods, confocal

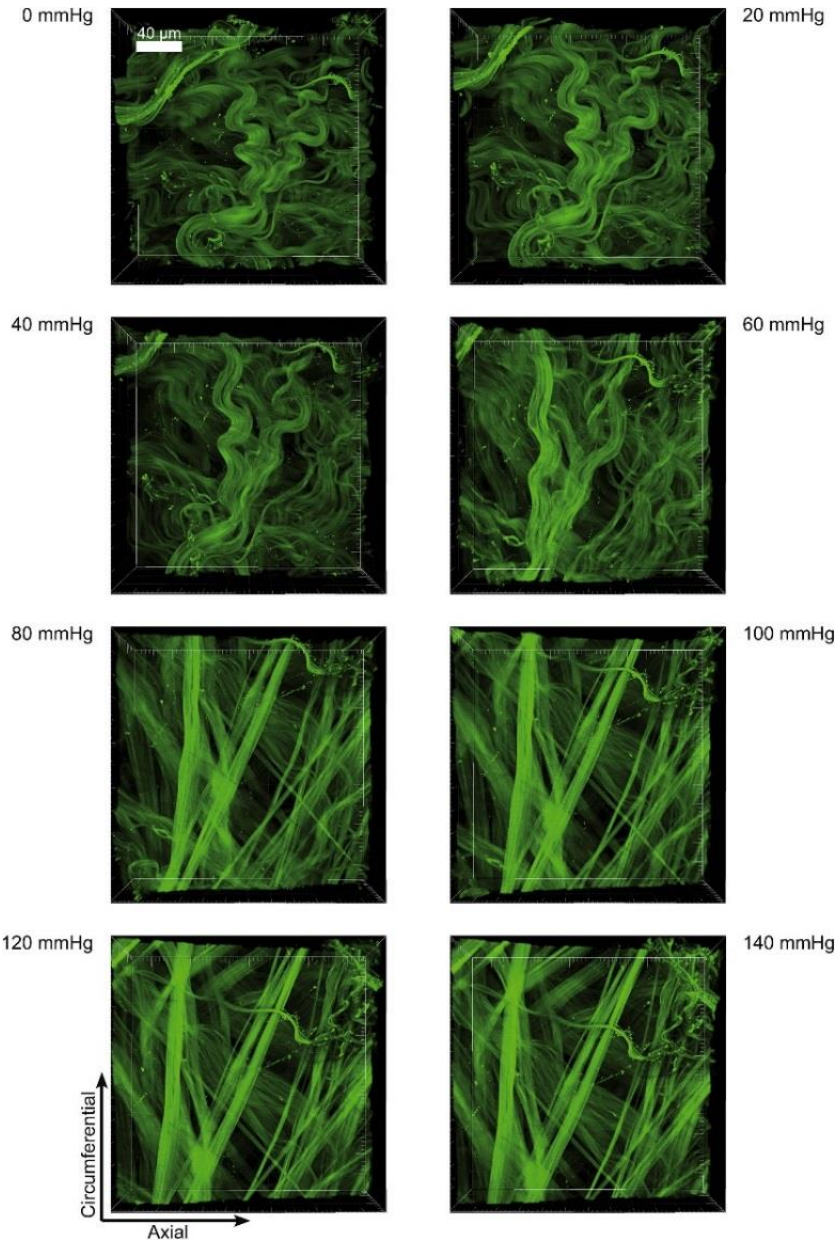

Figure 2.22 - Adventitial collagen fibres tagged with CNA35 showing reorientation and straightening with increasing luminal pressure (Schrauwen *et al.*, 2012).

microscopy requires time consuming and destructive tissue preparation steps while the high setup costs also reduce its desirability for characterising collagen. Unfortunately, the highly localised nature of confocal microscopy makes gross fibre mapping of a sample infeasible and alternative approaches are often required.

2.6.4 Multiphoton Microscopy

Multiphoton microscopy, often termed two-photon excitation microscopy, utilises a material's non-linear optics to excite fluorophores through the simultaneous absorption of energy from multiple photons (Raub *et al.*, 2007). Many studies (König *et al.*, 2005; Raub *et al.*, 2007; Cicchi *et al.*, 2010) have used this multiphoton fluorescence approach to look at collagen fibre orientation in tissue and tissue constructs. Using 2 excitation lasers at near-infrared wavelengths, multiphoton microscopy allows one to image samples at greater depths than similar techniques such as confocal microscopy. A second advantage of multiphoton microscopy is the ability to characterise a tissue's structure with minimal tissue processing. In fact, no staining or fluorescent probes are required to view elastin or collagen using multiphoton microscopy. Elastin can be viewed through two-photon excitation fluorescence (TPEF) while collagen can be imaged by taking advantage of its second harmonic generation (SHG) response. A number of anisotropic materials, including collagen, which have a non-centrosymmetric structure (Ghazanfari *et al.*, 2012) exhibit this SHG response whereby two photons of light can be absorbed by the collagen before a single photon of twice the frequency is emitted. The ability to keep a sample intact and unstained which may otherwise alter the vessel structure or mechanical response, makes multiphoton microscopy a promising technique for linking structural and mechanical properties of tissue. As previously outlined, this real-time information will not only aid in understanding the response of collagen during load but also in modelling the mechanical response of various biological tissues.

Although multiphoton microscopy is a relatively new technique, a number of studies have taken advantage of this promising feature by using multiphoton microscopy as a method of characterising collagen reorganisation (Hu, Humphrey and Yeh, 2009; Chen *et al.*, 2011; Keyes *et al.*, 2011; Tsamis *et al.*, 2013; Wang,

Brewster and Gleason, 2013; Nierenberger, Fargier, *et al.*, 2015; Krasny *et al.*, 2017). Using multiphoton microscopy, altered elastin and collagen have been identified in atherosclerotic (Watson *et al.*, 2016) and aneurysmal (Tsamis *et al.*, 2013; Niestrawska *et al.*, 2016; Cavinato *et al.*, 2017) tissue compared to healthy controls. Changes in fibre organisation due to load have also been investigated using multiphoton microscopy. Hu *et al.* (Hu, Humphrey and Yeh, 2009)

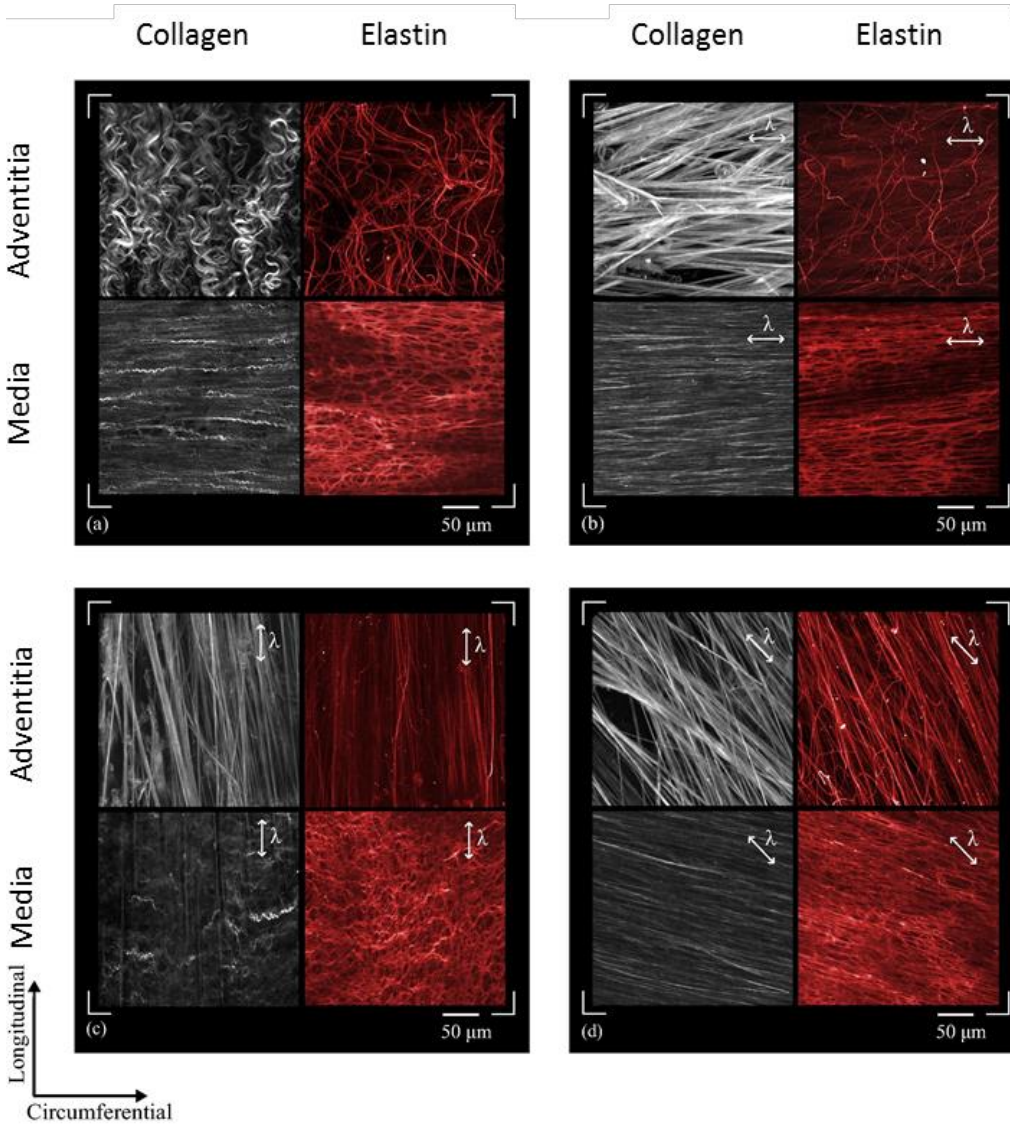

Figure 2.23 – Multiphoton images of adventitial (top panel) and medial (bottom panel) collagen (left panel) and elastin (right panel) in a) an unloaded state, b) circumferentially loaded, c) axially loaded and d) diagonally loaded state. Collagen is shown in grey and elastin in red [Adapted from] (Krasny *et al.*, 2017).

incorporated a biaxial stretching device with SHG to better understand the reorientation of collagen within fibroblast-seeded collagen gels. Krasny *et al.* also investigated changes in collagen and elastin architecture in rabbit carotid artery subject to uniaxial loading in multiple directions (Krasny *et al.*, 2017). Adventitial fibres were better able to adapt and reorientate in the direction of applied loading compared to medial fibres which can be seen in Figure 2.23.

SHG in conjunction with TPEF has also been employed to investigate changes in adventitial collagen and elastin fibres in intact vessels with increasing luminal pressure (Chen *et al.*, 2011; Keyes *et al.*, 2011). Both these studies identified reorientation and straightening of collagen fibres from a more longitudinal orientation to a more circumferential orientation with increasing pressure (Figure 2.24). More recently, analysis of the reorientation of collagen under load has been carried out using continuous monitoring by two-photon microscopy as opposed to at fixed time points (Nierenberger, Fargier, *et al.*, 2015).

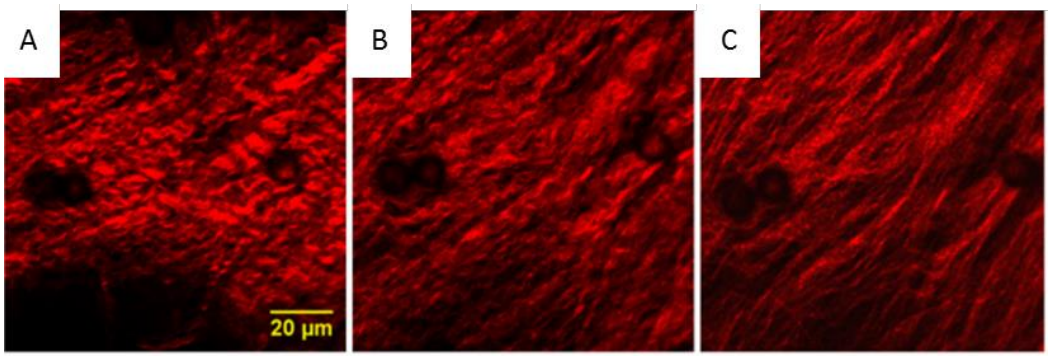

Figure 2.24 - Multiphoton images showing straightening of adventitial collagen of the coronary artery under increasing load from A to C (Adapted from [(Chen *et al.*, 2011)*]).*

Although multiphoton microscopy does not require the extensive tissue preparation steps of many other techniques, it does require the use of fluorescent dyes in order to view other structural constituents such as smooth muscle cells. SHG circumvents the need for collagen staining by utilising a materials second harmonic response to view structural information although it is not a viable method to view immature collagen fibres (Ghazanfari *et al.*, 2015). Although there are many advantages of multiphoton microscopy in the characterisation of collagen fibres in tissue, high set up costs often restrict its use. As with confocal microscopy, multiphoton microscopy does no lend itself to large-scale fibre

mapping. This inability to characterise full samples makes it an unsuitable technique for identifying gross structural changes which may occur in response to medical intervention such as stenting.

2.6.5 Electron Microscopy

Scanning electron microscopy (SEM) and transmission electron microscopy (TEM) are methods of electron microscopy which are commonly used to look at the micro and nanostructure of samples. The achievable high resolution of electron microscopy images has led SEM and TEM to become a popular method of analysing the structure of biological tissues including the orientation of collagen fibrils (Wolinsky and Glagov, 1964; Engelmayr *et al.*, 2006; Dahl, Vaughn and Niklason, 2007; O'Connell *et al.*, 2008; Robitaille *et al.*, 2011). O'Connell *et al.* (O'Connell *et al.*, 2008) used electron microscopy and confocal microscopy to analyse the three-dimensional micro and nanostructure of rat abdominal aortas finding a predominant circumferential collagen fibre orientation (Figure 2.25). SEM has also been used to look at changes in collagen fibres in healthy and aneurysmal vessels, identifying a reduction in collagen organisation but no change in mean orientation (Urabe *et al.*, 2016). SEM and

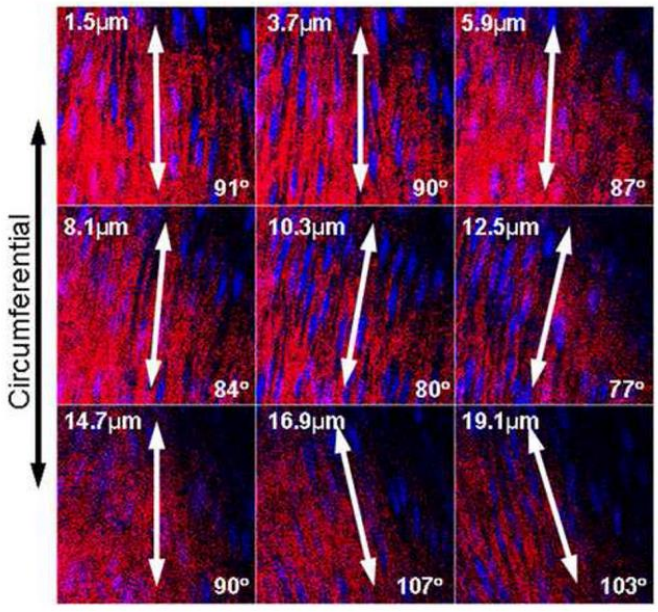

Figure 2.25 - SBF-SEM images showing circumferential collagen fibre organisation in media of rat abdominal aorta (O'Connell *et al.*, 2008).

TEM have also been used to investigate strain induced protection and degradation in collagen fibrils (Bhole *et al.*, 2009; Robitaille *et al.*, 2011; Flynn, Tilburey and Ruberti, 2013; Yi *et al.*, 2016). These studies suggested that strain induced a collagen protection mechanism, reducing their rate of degradation over time. TEM has also been used to compare the structure of tissue engineered arteries and native porcine common carotid arteries (Dahl, Vaughn and Niklason, 2007). Results found that the tissue-engineered arteries had thinner, more loosely packed fibres which were less circumferentially orientated than native arteries.

Unfortunately, SEM and TEM typically require considerable sample preparation and only provide information on a very limited sample region and consequently are not complementary to full tissue characterisation. The demanding preparation associated with electron microscopy restricts dynamic imaging of samples during mechanical testing. The destructive nature of SEM and TEM due to these preparation methods as well as the damage caused by electrons also reduce the attractiveness of this method as a means of identifying collagen reorganisation and remodelling.

2.6.6 Small Angle Light Scattering

Small angle light scattering (SALS) is an imaging technique which utilises light scattering principles to determine structural information of a sample. The premise of this technique is that photons of light will change direction as they encounter obstacles when passing through a medium. As a beam of radiation interacts with an interfering object, part of the incident beam is scattered, while the remaining beam is absorbed or transmitted through the object (Dahlgren, 2002). This beam maintains the same wavelength as the incident beam. In SALS analysis of fibrous soft tissues, the tissue is assumed to behave like a 2-dimensional assembly of slits and as such, single slit diffraction theory can be applied (Ferdman, 1987; Sacks, Smith and Hiester, 1997). Accordingly, incident light scatters orthogonally to the central axis of the constituent fibres. Single slit diffraction theory also permits the calculation of fibre diameters; however, this is only possible when both the fibre diameter and spacing between the fibres (slits) are equivalent and no multiple scattering occurs through the thickness. In order to achieve favourable results, these obstacles must have a diameter within an

order of magnitude of the antagonising light source wavelength (Sacks, Smith and Hiester, 1997). At these magnitudes, the resulting scatter has been shown to occur at angles less than 6° (Ferdman, 1987; Ferdman and Yannas, 1993). From the resulting scatter pattern, information relating to the structure of the sample can be postulated. Consequently, SALS is a useful method of quantifying a sample's microstructure through the orientation and size of its constituent parts. SALS' dependence on light transmission through a sample is however, its major limiting factor. As a sample's thickness increases or a sample becomes more opaque, light transmission reduces and so too does the signal-to-noise ratio. In addition, increasing thickness also leads to multiple scattering effects as light passes through a sample's thickness (Sacks, Smith and Hiester, 1997). This is a particular issue if a sample's structure is found to vary significantly through its thickness. SALS is also a relatively low-resolution technique which averages the acquired structural information across the diameter of beam chosen. Finally, SALS is an indirect measure of fibre architecture and relies on subsequent post processing to extract useful information. Despite these limitations, it will be shown that there are many benefits to using SALS which make it a useful technique for looking at fibre orientation and remodelling across tissues.

SALS emerged from the more general light scattering (LS) technique which was first developed to help in the characterisation of polymers in solution. Observations made about the intensity distribution of this scattered light allowed for the determination of the molecular weight of polymers (Debye, 1947). From LS other techniques emerged such as depolarised light scattering (DPLS) now commonly known as SALS which allowed for characterisation of optically anisotropic materials from analysis of the resulting small scatter angle. As the understanding of SALS increased, the use of an arc lamp as a light source was replaced with the inclusion of a laser. Further developments in technology allowed for the use of CCD and CMOS cameras instead of photographic film, improving the quality and ease of use of SALS (Nishida, Ogawa and Matsuba, 2008). SALS also falls under the heading of small angle scattering (SAS), which was coined to describe a number of other techniques which analyse a resulting scatter pattern to determine structural properties of a material. Included under this heading is small angle X-ray scattering (SAXS) and small angle neutron

scattering (SANS) which have been widely used in biology (Sasaki and Odajima, 1996; Daxer and Fratzl, 1997; Misof, Rapp and Fratzl, 1997; Liao *et al.*, 2005; Robitaille *et al.*, 2011).

The benefits of SALS in the study of biological tissue became apparent once researchers found that SALS could be used as a relatively fast and inexpensive means of quantitatively assessing fibre size and direction within soft tissues (Cochran and Kunzelman, 1991). Consequently, SALS popularity increased in a number of areas including the study of striated muscle spacing and size (Kawai and Kuntz, 1973; Baskin, Roos and Yeh, 1979; Rüdel and Zite-Ferenczy, 1980), the measurement of inhaled fibres within human lung tissue (Ferdman, 1987) and the anisotropic structure of canine diaphragm tissue (Wilkes and Wilkes, 1974). As the use of SALS evolved, more and more looked to use this technique as a means of specifically quantifying collagen fibre orientation, size and distribution within soft tissues. Some of the earliest studies were carried out by Kronick and Buechler (Kronick and Buechler, 1986) who used SALS in conjunction with SAXS as a means to quantitatively assess the structure of calfskin as well as Ferdman (Ferdman, 1987; Ferdman and Yannas, 1993) who looked at the anisotropic nature of scar tissue. Another of these early studies was carried out by Cochran *et al.* (Cochran and Kunzelman, 1991) in the analysis of mitral valve tissue. SALS results showed a close correlation with PLM results obtained from the same tissue samples. From these structural observations, it was hypothesised that collagen orientation within mitral valve tissue influences its mechanical properties and consequently its physiological function.

Although SALS benefits from being both a fast and inexpensive means of structural quantification of tissue, perhaps its most promising feature is its ability to dynamically test intact samples. Many studies have looked at changes in collagen fibre orientation due to loading using SALS (Chien and Chang, 1972; Billiar and Sacks, 1997, 2000; Sacks, Smith and Hiester, 1997; Dahlgren, 2002; Liao *et al.*, 2005; Robitaille *et al.*, 2011). While a number of these studies performed SALS before and after chemical fixation in a stressed state (Chien and Chang, 1972; Sacks, Smith and Hiester, 1997; Dahlgren, 2002), SALS has also been performed in real-time as the sample is stretched (Billiar and Sacks, 1997;

Liao *et al.*, 2005; Robitaille *et al.*, 2011). Billiar and Sacks (Billiar and Sacks, 1997) were one of the first to combine SALS with a custom-made stretching device to dynamically test porcine aortic valve leaflets and bovine pericardium. Biaxial tests were carried out where the samples were stretched along one direction while its orthogonal direction was held constant. Results from these experiments demonstrated a marked difference between the initial collagen orientation and the deformed collagen orientation after loading, particularly in bovine pericardium. Liao *et al.* also carried out dynamic SALS testing of bovine pericardium under similar biaxial stretch conditions (Liao *et al.*, 2005). Comparable results can be seen between Liao *et al.* (Robitaille *et al.*, 2011) and Billiar and Sacks (Billiar and Sacks, 1997) for bovine pericardium in which collagen shifts towards the primary load direction during testing. As with the above studies, large-scale fibre mapping has been carried out using SALS on porcine aortic valves fixed at 0 and 4 mmHg. Results show a distinct reorientation of collagen fibres even at low-pressure increases (Figure 2.26).

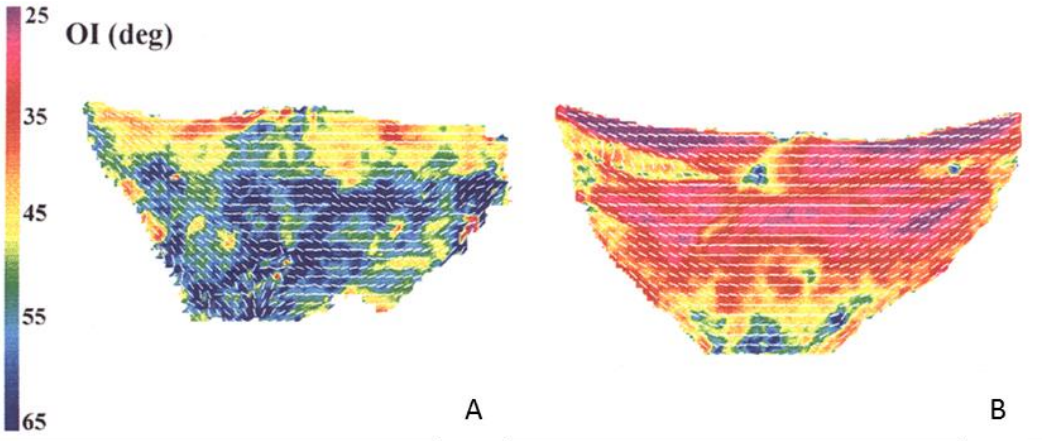

Figure 2.26 – Porcine aortic valves fixed at A) 0 mmHg and B) 4 mmHg showing overlaid fibre directions as measured by SALS. The superimposed colour map is representative of local fibre alignment and shows substantially increased alignment at 4 mmHg (adapted from (Sacks, Smith and Hiester, 1997)*).*

Limited testing has been carried out on vascular tissue using SALS with only two known studies looking at arterial structure (Williams *et al.*, 2009; Haskett *et al.*, 2010). SALS has traditionally been used on thin, highly organised and transparent soft tissues which may suggest why a lack of literature is available on relatively thick and opaque arteries. In order to circumvent the potential issue

of light transmission through the vessel wall, Haskett *et al.* (Haskett *et al.*, 2010) histologically sectioned human aortic tissue at 50 µm. These slices were interrogated using a similar SALS system to that described in the literature (Sacks, Smith and Hiester, 1997). As with existing PLM studies (Hariton, DeBotton, T.C. Gasser, *et al.*, 2007; Sáez *et al.*, 2016), a predominantly circumferential arrangement of collagen fibres was found through the vessel wall. Despite testing at different depths, no distinction was made between vessel layers as was carried out by Schriefl *et al.* (Schriefl *et al.*, 2012). Although fibre reorganisation and remodelling in response to load was not considered, vessels were found to become more anisotropic with age.

Williams *et al.* (Williams *et al.*, 2009) also utilised SALS to determine changes in fibre structure, this time arising from the decellularisation of rabbit carotid artery. SALS analysis identified greater reorientation of fibres in the circumferential loading direction in decellularised tissue (Figure 2.27 C-D) in comparison to native tissue (Figure 2.27 A-B). This increased reorientation as well as the increased alignment (Figure 2.27), determined by low OI (orientation index) values suggests that decellurisation partially compromises the vessel structure. Unlike the previous study (Haskett *et al.*, 2010), testing was carried out on intact planar samples of vessel wall, fixed and cleared chemically. The ability to conduct SALS on intact vessels minimised the potential alterations to vessel structure caused during the histological sectioning procedure. Although real-time structural changes were not considered, vessels were processed before and after pressurisation and an increase in fibre mobility was found in decellularised vessels. Although chemical clearing allowed intact vessel analysis, it requires fixed end timepoints, not permitting analysis of remodelling effects over time in the same sample. Keeping the vessel intact may also mask any layer specific fibre architecture which is known to occur (Schriefl *et al.*, 2012). While SALS has shown capabilities in identifying collagen reorganisation in response to loading, it remains to be seen whether changes in tissue structure can be identified without chemical clearing or histological processing.

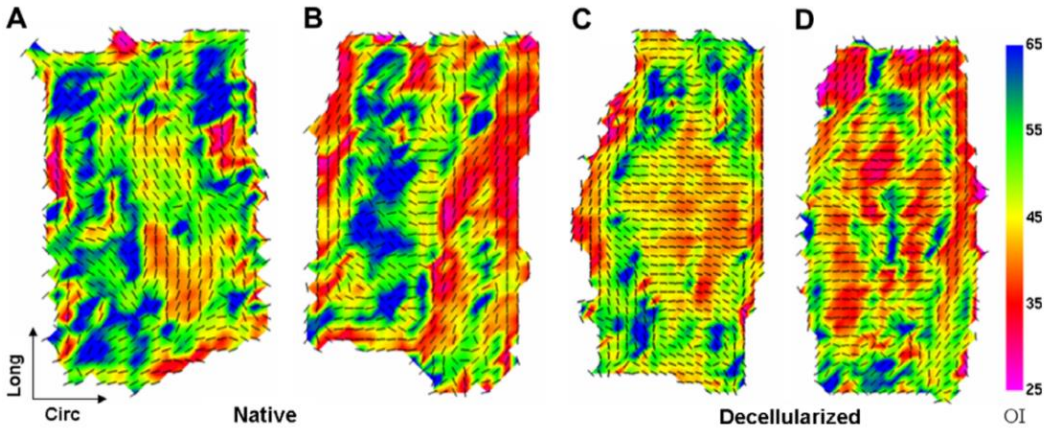

Figure 2.27 - Native (A, B) and decellularised (C, D) rabbit carotid artery stretched and fixed at 80 mmHg showing increased fibre reorientation in decellularised vessels (C,D) in the direction of loading (circumferentially – left to right). Vectors show the measured fibre orientation and the superimposed colour map is representative of local fibre alignment with warm colours indicating greater alignment (Williams *et al.*, 2009).

Robitaille *et al.* (Robitaille *et al.*, 2011) implemented a dynamic stretch based testing approach for biological tissue whilst assessing fibre alignment with SALS. To gain insight into tissue remodelling, the effect of loading on the preferential enzymatic degradation of collagen within bovine corneal tissue was investigated. Robitaille *et al.* concluded that SALS was capable of tracking real-time changes in tissue structure under load and provided invaluable information on tissue remodelling. Accordingly, SALS offers a potential method of identifying whether this remodelling process seen elsewhere (Ellsmere, Khanna and Michael Lee, 1999; Wyatt, Bourne and Torzilli, 2009; Robitaille *et al.*, 2011), presents itself in arterial tissue.

Although questions still remain over whether SALS is capable of identifying fibre orientations in larger, more opaque vessels, layer separation may offer a potential solution to this issue. While SALS does not offer the resolution of many alternative imaging methods, the quantitative nature of results obtained and ability to map gross fibre orientations of a sample make it an interesting technique for use in arterial tissue.

2.6.7 X-Ray Imaging

A number of techniques have also used X-rays to characterise collagen architecture in soft tissues, including small angle X-ray scattering (SAXS) (Sasaki and Odajima, 1996; Daxer and Fratzl, 1997; Misof, Rapp and Fratzl, 1997; Liao *et al.*, 2005) and X-ray computed microtomography (μCT) (Nierenberger, Rémond, *et al.*, 2015; Walton *et al.*, 2015; Helfenstein-Didier *et al.*, 2018).

Small Angle X-Ray Scattering (SAXS) is a SAS technique which has been widely used to determine ultrastructural information regarding collagen through the use of X-rays (Sasaki and Odajima, 1996; Daxer and Fratzl, 1997; Misof, Rapp and Fratzl, 1997; Liao *et al.*, 2005; Robitaille *et al.*, 2011). As with SALS, SAXS provides an X-ray scatter distribution which provides structural information about a sample. From this distribution, details of collagen fibril density, size and orientation can be determined to allow for a better understanding of the underlying nature of collagen fibres. Previous studies have used SAXS to explore collagen fibril behaviour in both statically fixed tissue samples (Daxer and Fratzl, 1997) as well as mechanically tested samples (Sasaki and Odajima, 1996; Misof, Rapp and Fratzl, 1997; Liao *et al.*, 2005). Daxer and Fratzl (Daxer and Fratzl, 1997) employed SAXS to study the orientation of collagen fibrils within corneal tissue and found two pronounced fibril orientations near orthogonal to each other in healthy tissue. Diseased tissue was found to exhibit variations in this orthogonal relationship which may be related to known diseased tissue instabilities that may also present in arterial tissue. SAXS in conjunction with uniaxial tensile tests has previously been used to better understand the response of collagen fibrils to load in bovine Achilles tendon (Sasaki and Odajima, 1996), rattail tendon (Misof, Rapp and Fratzl, 1997) and bovine pericardium (Liao *et al.*, 2005).

SAXS has the advantage of requiring very little sample preparation prior to tissue testing as with other light scattering techniques such as SALS. The absence of histological staining required by many other imaging techniques can help reduce the variability between test samples. The automation of SAXS is another desirable feature allowing for full tissue quantification. However, the high setup costs associated with SAXS development reduce the desirability of this technique.

Nevertheless, SAXS may be of use in determining ultrastructural information on arterial tissue structure and remodelling.

Unlike SAXS, whereby collagen fibre architecture is indirectly measured through X-ray scattering, μCT allows collagen visualisation, similar to that seen in many of the microscopy techniques discussed previously. Traditionally, μCT has been employed to characterise the 3-dimensional structure of hard calcified tissues such as bone or visualise soft tissue geometry using contrast agents (Bouxsein *et al.*, 2010; Campbell and Sophocleous, 2014). However, recent studies have developed techniques enabling high-resolution collagen visualisation in soft tissues, including vascular tissue (Nierenberger, Rémond, *et al.*, 2015; Walton *et al.*, 2015; Helfenstein-Didier *et al.*, 2018). Nierenberger *et al.* investigated the collagen fibre architecture of intact porcine iliac veins using a number of different contrast agents (Nierenberger, Rémond, *et al.*, 2015). The use of specific contrast agents allowed the authors to identify different fibre architectures across the vessel layers as shown in Figure 2.28. μCT has also been used to resolve different sub-structures in unpressurised and pressurised arterial tissue in the absence of contrast agents (Walton *et al.*, 2015).

μCT shows promise in bridging the gap between the collagen fibre response and tissue level response by combining micron-scale resolution with global 3-dimensional intact tissue analysis. The ability of μCT to resolve tissue components without the need for potentially mechanically altering contrast agents also increase its desirability as a characterisation tool. Unfortunately, like SAXS, the high associated setup costs potentially limit its use on a large scale.

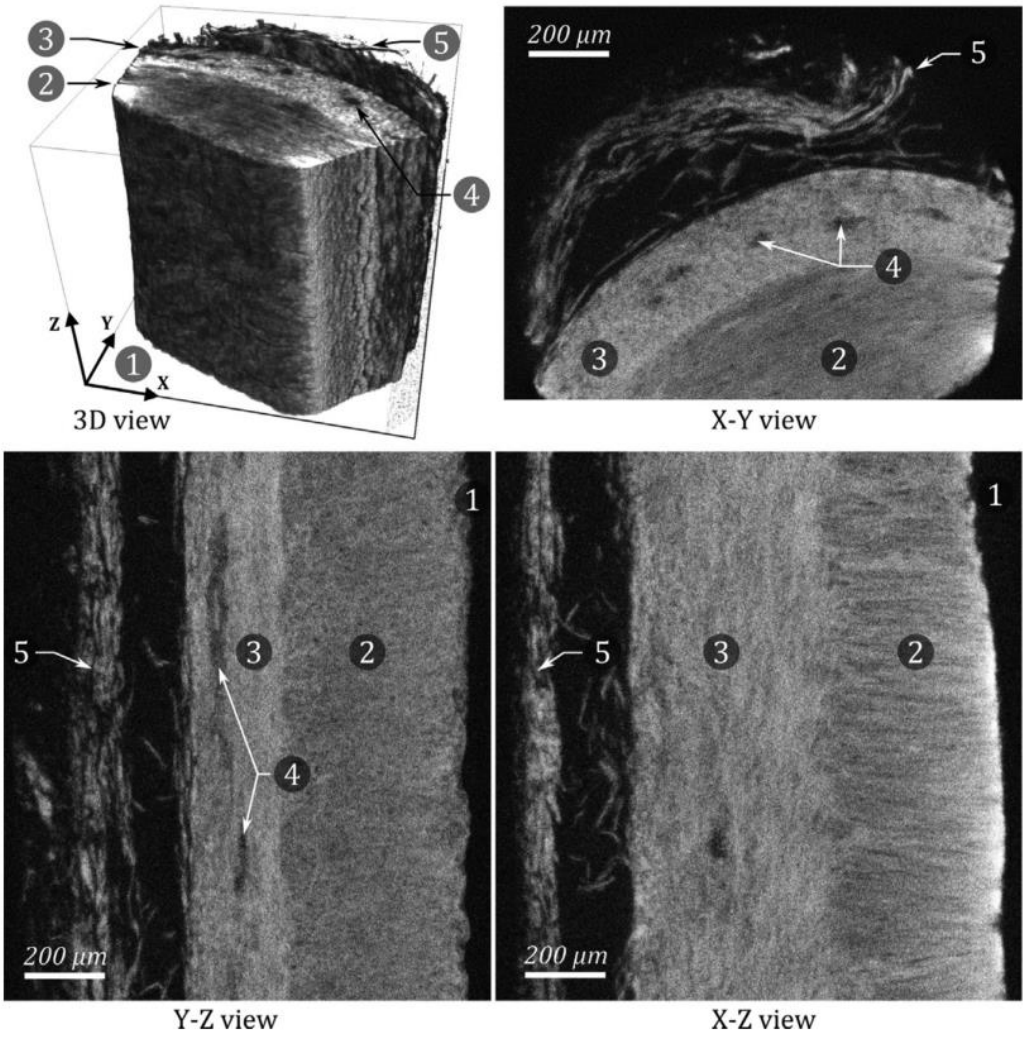

Figure 2.28 - Different views of porcine iliac vein stained with contrast agent showing clear collagen fibre orientations. 1. Vein lumen, 2. Media, 3. Adventitia, 4. Vasa vasorum, 5. Surrounding connective tissue (Nierenberger, Rémond, *et al.*, 2015).

2.6.8 Diffusion Tensor Imaging

Diffusion Tensor Imaging (DTI) is another technique which has previously been used to investigate arterial structure and elucidate the reorganisation of collagen to load (Flamini *et al.*, 2010; Ghazanfari *et al.*, 2015; Shahid *et al.*, 2017). DTI is a magnetic resonance imaging (MRI) technique whereby the diffusion of water molecules in biological samples are tracked. As with other MRI techniques, DTI is a non-invasive method of imaging biological tissue both in-vivo and ex-vivo. DTI was first developed for the study of neurological disorders, particularly in patients after incidence of stroke. In biological tissue, the diffusion of water

molecules is directed by macromolecules and fibres within the tissue. As water is more likely to diffuse along the direction of constituent fibres rather than across fibres (and other constituents), the directional anisotropy of the tissue can be determined. From this directional diffusion, a diffusion tensor and subsequently eigenvectors and eigenvalues can be determined to allow for the tissue structure to be visualised (Figure 2.29).

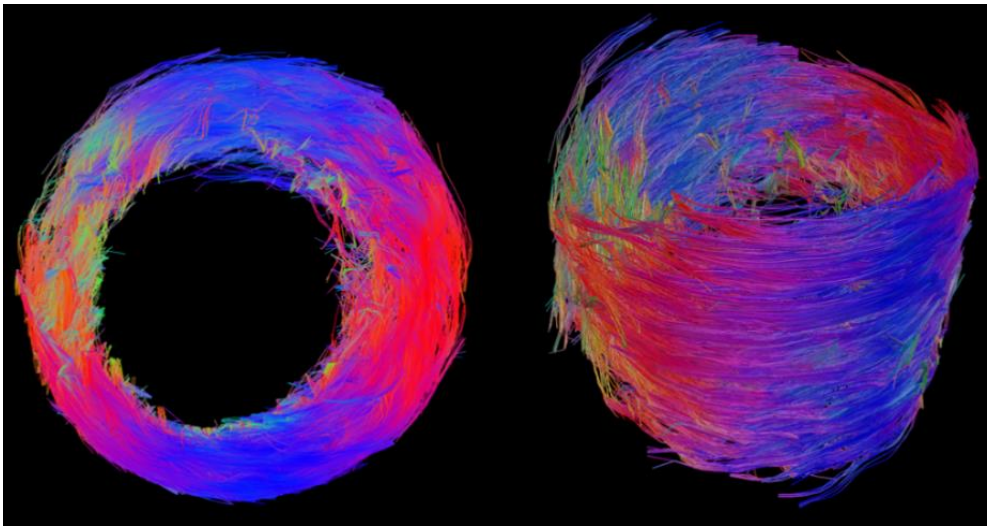

Figure 2.29 - Collagen fibre structure of the carotid artery identified using MR_DTI and fibre tractography (Shahid and Lally, 2016).

Initial DTI studies were predominantly focussed on neural tissue, however, more recently DTI has been used to study the structure of a wide range of biological tissues including bone, cartilage, cardiovascular tissue and muscle. Flamini et al. (Flamini *et al.*, 2010) were one of the first groups to consider the feasibility of DTI in determining the collagenous fibre structure of porcine aortic arteries ex-vivo. This study looked to determine the feasibility of DTI in parallel with fibre tractography as a means of ultimately characterising collagen fibre orientation in-vivo. Ghazanfari et al. (Ghazanfari *et al.*, 2012) also detailed the fibrous structure of the wall of porcine carotid arteries through DTI and tractography. The predominantly circumferential orientation of the fibres as determined by DTI were compared and showed strong agreement with results obtained using SHG imaging. A further study by Ghazanfari et al. (Ghazanfari *et al.*, 2015) also used DTI to study the reorientation of collagen fibres within cultured uniaxially constrained tissue engineered constructs over time. CLSM and histology were

used as a means of validating the results obtained from DTI and again suggest DTI is a promising means of non-invasively characterising collagen fibre orientation in biological tissue. More recently, motivated by the circumferential nature of arterial collagen reported in the literature, 2D DTI has been carried out *in vivo* to determine in-plane fibre orientations in healthy volunteers (Opriessnig *et al.*, 2016). DTI has also been employed to investigate fibre patterns occurring in human carotid plaque tissue *ex vivo*, finding increased proportions of longitudinally orientated fibres occurring in concentric plaques in comparison to eccentric plaques (Akyildiz *et al.*, 2017). Given the structural significance of collagen fibres in the mechanical response, these findings may have implications on plaque vulnerability.

DTI shows promise as a fibre mapping tool as it is non-invasive, fast relative to other techniques such as CLSM and can be conducted safely in-vivo. Consequently, the time consuming and histological tissue processing, sectioning and staining steps can be neglected which can have untold effects on the structure of the tissue. To date, limited *in vivo* analysis of arterial fibre orientation has been carried out (Opriessnig *et al.*, 2016) due to difficulties in acquiring high-resolution data, the pulsatile nature of arterial tissue and the need for patients to remain still for extended periods of time. Another major disadvantage of DTI as an imaging modality is the high associated setup and running costs which limit the amount of testing that can be carried out. DTI also has limited spatial resolution capabilities when compared to other imaging methods such as CLSM and SHG which becomes an issue at locations where large variations in fibre orientation occur. Despite this, DTI has the potential to greatly improve our understanding of fibre structure and remodelling *in vivo* and one day be used as a clinical tool capable of detecting arteries at risk of rupture. Just as with techniques such as SHG and SALS, DTI has the potential to determine load-induced changes in arterial tissue *in vivo* which may aid in our understanding of vascular remodelling and vascular disease. A comparison of the imaging techniques discussed here can be found in Table 2.1. Unfortunately, a direct comparison of the resolutions achievable with the various techniques mentioned is not straight forward and depends on many factors including the imaging setup, the quality of the lenses and cameras used and the method of sample preparation.

Table 2.1 - Summary of commonly used imaging techniques for collagen visualisation in soft tissues

Technique	Method of imaging	Sample preparation	Key finding	Analysis scale
Brightfield microscopy	White light	Histological fixing, sectioning and staining	Circumferential fibre and cell orientation (Rhodin, 1980)	Local
PLM	Polarised light	Histological fixing, sectioning and staining	Identification of collagen fibre families (Schriefl *et al.*, 2012; Sáez *et al.*, 2016)	Local
Confocal microscopy	Single laser light source	Fluorescent probes required	Adventitial collagen fibre reorientation and straightening with increasing pressure (Schrauwen *et al.*, 2012)	Local
Multiphoton microscopy	Two lasers light sources	Minimal	Adventitial and medial collagen and elastin fibre reorientation under various uniaxial loading regimes (Krasny *et al.*, 2017)	Local
Electron microscopy	Beam of electrons	Tissue fixation and conductive coating	Three-dimensional micro and nanostructure of rat aorta (O'Connell *et al.*, 2008)	Local
SALS	Laser	Minimal	Real-time structural changes in corneal tissue due to strain-dependent collagen degradation (Robitaille *et al.*, 2011). Not optimised for artery.	Global
SAXS/µCT	X-rays	Minimal/contrast agent incubation	Three-dimensional analysis of intact artery and vein (Nierenberger, Rémond, *et al.*, 2015; Walton *et al.*, 2015)	Local/ Global
DTI	Magnetic fields	Minimal	*In vivo* collagen fibre orientation in human carotid artery (Opriessnig *et al.*, 2016)	Global

2.7 Strain and load mediated collagen degradation

As living tissues, arteries sense and adapt to their environment (Rachev, 2003). This is achieved in part, through remodelling of the structurally significant collagen fibre architecture, which continually remodels over the course of a person's life. Collagen fibre remodelling *in vivo* incorporates not only the

reorientation of fibres, but also the production of new collagen and degradation of existing collagen (Chang and Buehler, 2014). These processes have been found to be load dependent and inter-linked, with degradation particularly critical for the mechanical stability of tissues (Thompson, Geraghty and Lee, 2002). In addition to cell-mediated active responses, collagen possesses an innate structural ability to respond to mechanical stimuli, thus self-regulating its susceptibility to degradation (Perumal, Antipova and Orgel, 2008; Chang *et al.*, 2012; Chang and Buehler, 2014).

Changes in the rates of protein production and degradation can be seen by the net increase in proteins that occurs after exercise (Figure 2.30) (Magnusson, Langberg and Kjaer, 2010; Chang and Buehler, 2014). This process can be seen in everyday life with increases in the size and strength of loaded bone (Andreoli and Monteleone, 2001), muscle (Andreoli and Monteleone, 2001; Ying *et al.*, 2003) and tendon (Ying *et al.*, 2003) in highly trained athletes. Mechanical overload, however, has been linked to accelerated degradation (Willett, Labow and Lee, 2008) and damage which can lead to injury (Khan and Maffulli, 1998; Maffulli, Khan and Puddu, 1998). Similarly, changes in the mechanical environment due to disease have been shown to alter tissue remodelling, while maladaptive

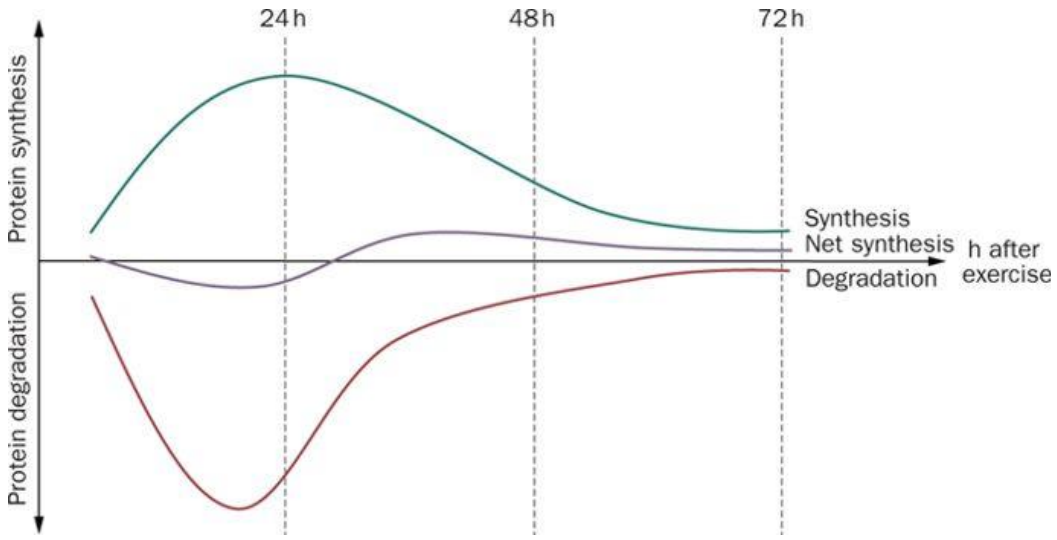

Figure 2.30 - Schematic representation of collagen remodelling occurring after exercise with increased collagen degradation and production leading to a net increase in collagen content after 72 hours (Magnusson, Langberg and Kjaer, 2010).

remodelling is hypothesised to play a role in accelerated disease progression (Thompson, Geraghty and Lee, 2002; Hahn and Schwartz, 2009; Gasser *et al.*, 2012). Although changes in collagen production are also known to depend on the strain environment (O'Callaghan and Williams, 2000; Ferdous, Jo and Nerem, 2011), load-dependent degradation will be the primary focus in this review as it has been strongly linked with arterial disease (Thompson, Geraghty and Lee, 2002; Aikawa, 2004; Daemen *et al.*, 2016; Bersi *et al.*, 2018). Load and strain-dependent changes in collagen degradation rates have also been linked to diseases such as emphysema in the lung (Yi *et al.*, 2016), lamina cribrosa thickening in early glaucoma (Grytz, Meschke and Jonas, 2011) and intervertebral disc degeneration (Lotz *et al.*, 2008). In response to these observations, many studies have sought to determine the direct relationship between collagen strain and its rate of degradation by subjecting loaded samples to collagenase; an enzyme that breaks down collagen (Chang and Buehler, 2014). Both bacterial and mammalian collagenases, known as matrix metalloproteinases (MMPs), have been used in these investigations, a comparison of which is outlined in Section 2.7.3 below. Despite these investigations, there are still conflicting findings as to whether strain accelerates collagen fibre degradation (Ellsmere, Khanna and Michael Lee, 1999; Willett, Labow and Lee, 2008; Adhikari, Chai and Dunn, 2011; Adhikari, Glassey and Dunn, 2012), or protects it from enzymatic degradation (Nabeshima *et al.*, 1996; Ruberti and Hallab, 2005; Lotz *et al.*, 2008; Bhole *et al.*, 2009; Wyatt, Bourne and Torzilli, 2009; Zareian *et al.*, 2010; Flynn *et al.*, 2010; Han *et al.*, 2010; Camp *et al.*, 2011; Robitaille *et al.*, 2011; Chang *et al.*, 2012; Grytz *et al.*, 2012; Flynn, Tilburey and Ruberti, 2013; Gyoneva *et al.*, 2016) (Table 2.2, page 66). Studies at the molecular (Chung *et al.*, 2004; Han *et al.*, 2010; Adhikari, Chai and Dunn, 2011; Camp *et al.*, 2011; Adhikari, Glassey and Dunn, 2012; Adhikari, Mekhdjian and Dunn, 2012; Chang *et al.*, 2012), fibril/fibre (Huang and Yannas, 1977; Bhole *et al.*, 2009; Wyatt, Bourne and Torzilli, 2009; Flynn *et al.*, 2010; Chang *et al.*, 2012; Flynn, Tilburey and Ruberti, 2013) and tissue (Nabeshima *et al.*, 1996; Ellsmere, Khanna and Michael Lee, 1999; Ruberti and Hallab, 2005; Lotz *et al.*, 2008; Willett, Labow and Lee, 2008; Zareian *et al.*, 2010; Robitaille *et al.*, 2011; Ghazanfari, A. Driessen-Mol, *et al.*, 2016; Yi *et al.*, 2016) scale have attempted to

explain these differences with limited success. Furthermore, complementary numerical models have been developed to aid in the understanding of the complex degradation response at these differing scales (Chang *et al.*, 2012; Grytz *et al.*, 2012; Hadi *et al.*, 2012; Loerakker, Obbink-Huizer and Baaijens, 2013; Heck *et al.*, 2015; Tonge, Ruberti and Nguyen, 2015; Gyoneva *et al.*, 2016; Loerakker, Ristori and Baaijens, 2016; Yi *et al.*, 2016). The following review of collagen degradation will look at strain and load dependent responses occurring at the molecular, fibrillar and finally tissue scales. In each category, studies will be grouped together based on whether they identified increased collagen protection, accelerated degradation or a combination of both.

2.7.1 Molecular, fibril and fibre level degradation

To explain the role that load plays in tissue degradation, a number of studies have explored the cleavage rate of single collagen molecules, called trimers, in response to load (Adhikari, Chai and Dunn, 2011; Camp *et al.*, 2011; Adhikari, Glassey and Dunn, 2012; Chang *et al.*, 2012). In all of these studies, changes in degradation are explained by conformational changes in the collagen molecule, i.e. increasing or decreasing its stability and consequently, its rate of cleavage. These studies have focussed on both naturally occurring collagen 'heterotrimers' (2 α1 chains, 1 α2 chain) (Camp *et al.*, 2011; Adhikari, Glassey and Dunn, 2012; Chang *et al.*, 2012) as well as less common collagen 'homotrimers' (3 α1 chains) (Adhikari, Chai and Dunn, 2011; Adhikari, Glassey and Dunn, 2012). These homotrimers are found in foetal, fibrotic and cancerous tissues and are known to be more thermally stable and consequently, more resistant to enzymatic cleavage (Han *et al.*, 2010; Chang *et al.*, 2012). Camp et al. identified a load-induced protection mechanism occurring in normal type I collagen heterotrimers by using a magnetic tweezers assay, to apply 3 different loads in crude bacterial collagenase (BC) (Camp *et al.*, 2011). It was hypothesised that this protection mechanism occurs as the partially unwound and enzymatically susceptible triple helix of the collagen heterotrimer refolds in response to load, increasing its stability shown in Figure 2.31A (Camp *et al.*, 2011; Chang *et al.*, 2012).

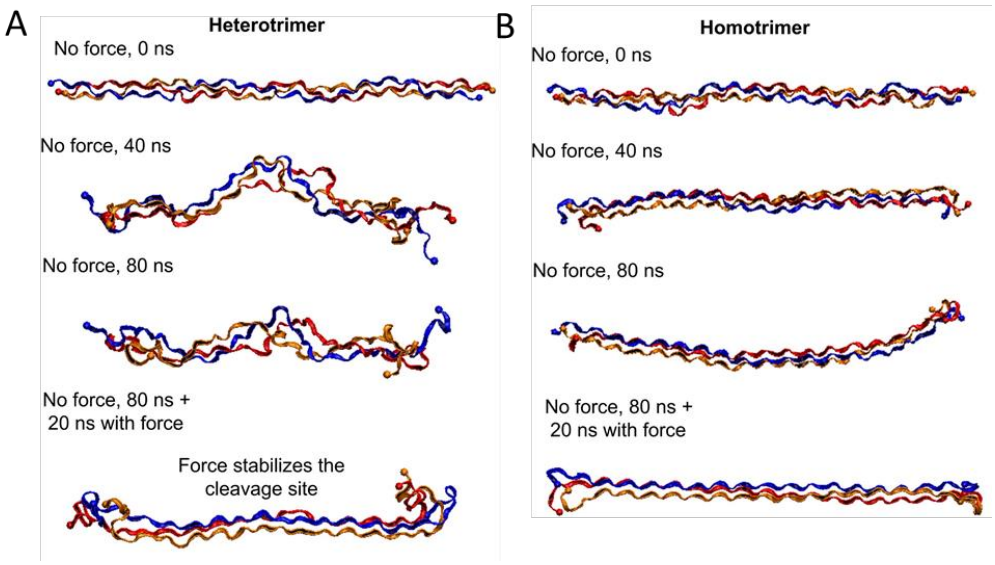

Figure 2.31 - A molecular model showing A) how the application of load stabilises the thermally unfolded collagen heterotrimer while B) load has minimal influence on the thermally stable collagen homotrimer. [Adapted from (Chang *et al.*, 2012)*]*

In contrast to Camp et al., Adhikari et al. found the opposite response, with mechanical load inducing a 100-fold increase in degradation, despite using a near identical setup (Adhikari, Chai and Dunn, 2011). These differences may be attributed to the use of more stable collagen homotrimers rather than heterotrimers, the use of MMP-1 as opposed to crude BC and the slightly higher loads applied. However, a follow-up study by the same group also found a similar load induced degradation response in collagen heterotrimers to MMP-1, ruling out the choice of trimer as the reason for the conflicting finding (Adhikari, Glassey and Dunn, 2012).

Many studies have also investigated the strain induced degradation response of collagen at the fibril (Huang and Yannas, 1977; Bhole *et al.*, 2009; Flynn *et al.*, 2010; Chang *et al.*, 2012; Flynn, Tilburey and Ruberti, 2013) and fibre levels (Wyatt, Bourne and Torzilli, 2009), with the majority of these identifying a reduction in degradation with load (Bhole *et al.*, 2009; Wyatt, Bourne and Torzilli, 2009; Flynn *et al.*, 2010; Chang *et al.*, 2012; Flynn, Tilburey and Ruberti, 2013). Bhole et al. demonstrated that reconstituted collagen fibril networks experiencing strains of up to 50% showed reduced rates of degradation (Bhole *et al.*, 2009). To achieve this, collagen fibril networks were placed between micropipettes and

strained close to their failure point in the presence of crude BC or MMP-8. Differential interference contrast microscopy with edge detection analysis was used to plot fibril diameter over time. Although fibril strain was not explicitly known in these experiments, displacement was shown to maintain the fibril network diameter for a longer period of time than that of the unstrained networks suggesting a strain protection response (Figure 2.32). Two follow up studies investigating the strain protection response of collagen in the presence of MMP-8 and BC came to a similar conclusion; strain increases the survivability of collagen fibrils in the presence of collagenase (Flynn *et al.*, 2010; Flynn, Tilburey and Ruberti, 2013). The second of these studies identified strain induced protection in fibrils extracted from bovine sclera by means of force-strain experiments (Flynn, Tilburey and Ruberti, 2013). By calculating the force per monomer in the fibril based on the fibril cross-sectional area, the authors also determined that packing of monomers intro fibrils had no influence on the rate of proteolysis. This is in contrast to other studies which suggest that packing of collagen molecules into fibrils increases the stability of the collagen molecule by restricting molecular motion (Miles and Ghelashvili, 1999; Willett, Labow and Lee, 2008).

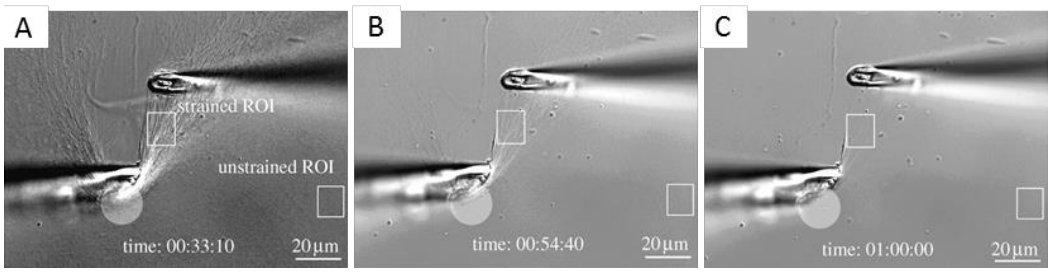

Figure 2.32 – a) Differential interference contrast images of collagen fibrils strained between micropipettes and adjacent unstrained fibrils (labelled squares) at the beginning of the experiment and b, c) accelerated degradation of unstrained fibres at further time points while strained fibrils are maintained. [Adapted from (Bhole *et al.*, 2009)*].*

These studies contrast the unique V-shaped degradation response identified by Huang and Yannas in their early study of reconstituted collagen tapes (Figure 2.33) (Huang and Yannas, 1977). This work found a strain level dependent degradation response, whereby the application of strain initially reduces the rate

of degradation before degradation begins to increase as strain increases above approximately 4%. Using a series of stress relaxation experiments, a degradation rate constant was determined by calculating the rate of force decay after BC was added. Furthermore, purified BC was chosen, reducing the potentially destructive influence of non-specific proteases present in crude collagenase.

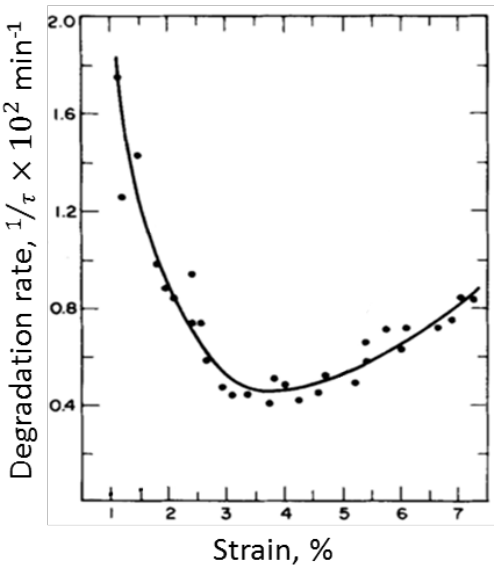

Figure 2.33 - Degradation rate of reconstituted collagen tapes in response to strain showing regions of protection and accelerated degradation. [Adapted from (Huang and Yannas, 1977)*].*

This unique response may potentially be explained by expanding on theories put forward to explain degradation differences in collagen heterotrimers and homotrimers by Chang et al. (Chang *et al.*, 2012). They hypothesised that strain results in a refolding of the enzymatically susceptible collagen heterotrimer which is partially unwound in equilibrium. In contrast, Chang *et al.* suggested that strain may instead unwind the enzymatically stable collagen homotrimer. If a similar process were to also occur in highly strained heterotrimers by first inducing a protection through molecular folding before unfolding the molecule as strain increases further, it may lead to an initial decrease in degradation before increasing above a strain threshold (Figure 2.34). Although Willet et al. suggested that there is no mechanical basis for triple helix unfolding to occur with strain, micro unfolding and molecular sliding may still explain this response by increasing enzymatic susceptibility (Willett, Labow and Lee, 2008). Additionally,

no study is yet to specifically investigate the strain-dependent degradation response of different collagen types and whether this may influence the degradation outcome; however, the underlying molecular structure and consequently, the degradation response is likely to hold regardless of collagen type.

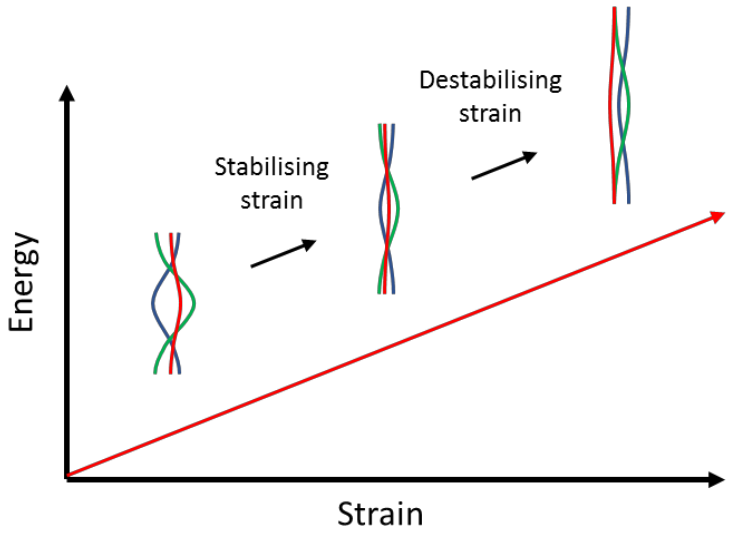

Figure 2.34 - Schematic showing the stabilising effect of strain initially as the triple helix tightens as suggested in the literature for heterotrimers (Camp *et al.*, 2011; Chang *et al.*, 2012). *Further strain may destabilise the heterotrimer as has been suggested for collagen homotrimers under load* (Chang *et al.*, 2012).

2.7.2 Tissue level degradation

Although the previous studies have offered valuable insight into the strain and load degradation response at the molecular, fibril and fibre level, remodelling at the tissue scale dictates the ultimate response of tissues such as arteries in diseases such as atherosclerosis (Tsamis, Krawiec and Vorp, 2013) and aneurysm (Thompson, Geraghty and Lee, 2002), as well as the response to load inducing medical devices such as stents (Ghazanfari, Anita Driessen-Mol, *et al.*, 2016). In accordance with many previous fibril studies, the first study to look at strain mediated collagen degradation at the tissue scale found strain induced protection to be the dominant mechanism (Nabeshima *et al.*, 1996). Using radiolabelled collagenase, the authors also determined that the application of strain did not reduce the diffusion of the collagenase through the rabbit patellar tendon, and therefore, could not be the reason for a degradation decrease. Motivated by this

work, Ruberti and Hallab (Ruberti and Hallab, 2005) carried out polarised microscopy and TEM studies identifying preferential degradation of unstrained fibres in the unique crosshatched structure of bovine corneal tissue, which led to many of the studies discussed thus far (Bhole *et al.*, 2009; Flynn *et al.*, 2010; Zareian *et al.*, 2010; Camp *et al.*, 2011; Robitaille *et al.*, 2011; Flynn, Tilburey and Ruberti, 2013). The studies of Zareian et al. (Zareian *et al.*, 2010) and Robitaille et al. (Robitaille *et al.*, 2011) also investigated the degradation response of corneal tissue, finding protection of strained fibrils and preferential degradation of unstrained fibrils.

As with the studies at the molecular, fibril and fibre level discussed in Section 2.7.1 above, relatively fewer tissue level studies have identified strain induced degradation (Ellsmere, Khanna and Michael Lee, 1999; Willett, Labow and Lee, 2008). Based on observations of increased levels of proteolytic enzymes in failed heart valves (Simionescu, Simionescu and Deac, 1993, 1996), Ellsmere et al. (Ellsmere, Khanna and Michael Lee, 1999) investigated the rate of degradation in bovine pericardium by means of time to failure creep-degradation experiments, under static and dynamic loading. Here, samples experiencing high loads (60 g) failed significantly quicker than samples experiencing low loads (1 g), leading the

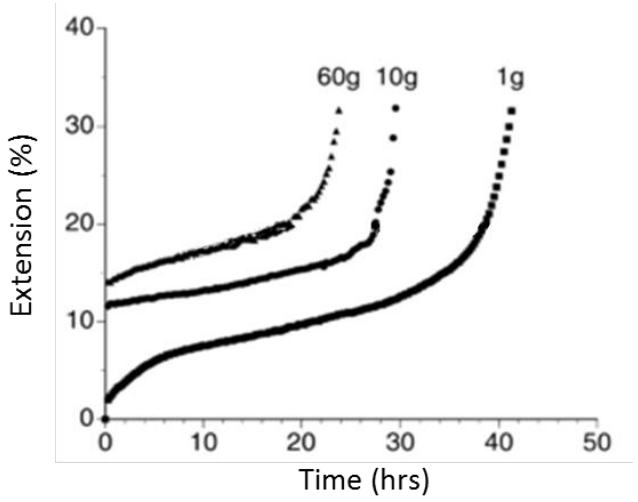

Figure 2.35 – Typical extension-time curve for statically loaded bovine pericardium incubated in BC showing accelerated time to failure for samples experiencing higher loads. Note the high initial rate of extension for samples subject to 1g loads potentially suggesting accelerated degradation at low initial strain levels. [Adapated from (Ellsmere, Khanna and Michael Lee, 1999)*].*

authors to conclude that load accelerates degradation (Figure 2.35). However, the data presented also suggests that the low load (and consequently low initial strain) samples may experience accelerated degradation initially (Figure 2.35). Investigations into overloaded bovine tail tendon also found increased susceptibility to collagenase (Willett, Labow and Lee, 2008). This study only compared unloaded and samples loaded to failure, however, potentially missing a possible strain induced protection mechanism at intermediary strains. Interestingly, both these studies also note accelerated degradation in cyclically loaded samples despite experiencing the same mean strain as their static counterparts. This finding is particularly relevant to many physiological environments, including the pulsatile blood flow experienced by arteries.

Tissue level studies (Ghazanfari, A. Driessen-Mol, *et al.*, 2016; Yi *et al.*, 2016) have also identified a similar strain level-dependent response to that of Huang and Yannas (Huang and Yannas, 1977) on reconstituted collagen tapes where degradation initially reduces with strain before increasing above a protective strain threshold, resembling a V-shaped curve. Using a similar methodology to Huang and Yannas, Ghazanfari et al. observed a V-shaped degradation response in bovine pericardium which was supported using SHG imaging (Figure 2.36)

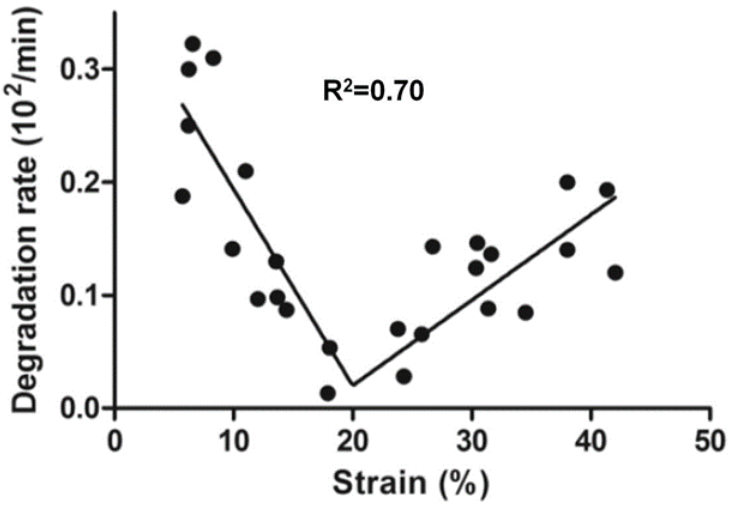

Figure 2.36 - Degradation rate of bovine pericardium in response to strain showing regions of protection and accelerated degradation resulting in a V-shaped response similar to that found in reconstituted collagen tapes (Huang and Yannas, 1977). *[Adapted from* (Ghazanfari, A. Driessen-Mol, *et al.*, 2016)*].*

(Ghazanfari, A. Driessen-Mol, *et al.*, 2016). This contradicts the conclusions drawn by Ellsmere et al. who found strain to accelerate degradation in bovine pericardium although it may explain the early creep response of their low load samples which appear to show high initial creep (Ellsmere, Khanna and Michael Lee, 1999). A strain induced protection region, flanked by regions of high degradation was also found in lung alveolar collagen. Dynamic loading was also found to accelerate the degradation process, paralleling findings in bovine pericardium (Ellsmere, Khanna and Michael Lee, 1999) and bovine tail tendon (Willett, Labow and Lee, 2008). Interestingly, the strain at which protection was found to occur in both of these studies (approximately 20%) was substantially higher than the approximately 4% strain identified in reconstituted collagen tapes. Molecular and fibril sliding that occurs at different scales may explain these differences in strain magnitude by reducing the molecular strain experienced at the cleavage site for a given tissue strain (Sherman, Yang and Meyers, 2015). Reorientation and straightening of crimped fibres may also delay the onset of strain protection found in these tissue level studies. A summary of the strain-dependent degradation studies discussed can be found in Table 2.2.

Table 2.2 - Summary of existing studies looking at load mediated collagen degradation. BC = bacterial collagenase.

Author	Sample type	Enzyme type	Loading condition
Load induced degradation			
Ellsmere et al. 1999 (Ellsmere, Khanna and Michael Lee, 1999)	Bovine pericardium	BC	1 g, 10 g, 60 g load, 40-80 g cyclic load
Willet et al. 2008 (Willett, Labow and Lee, 2008)	Bovine tail tendons	Acetyltrypsin, α-chymotrypsin	Tensile to failure
Adhikari et al. 2011 (Adhikari, Chai and Dunn, 2011)	Collagen homotrimer	MMP-1	1.0 pN, 4.0 pN, 6.2 pN, 8.6 pN, 10.1 pN, 11.5 pN, 13 pN
Adhikari et al. 2012 (Adhikari, Glassey and Dunn, 2012)	Collagen heterotrimer	MMP-1	0.25 pN, 10.7 pN, 16.7 pN

continued next page

Author	Sample type	Enzyme type	Loading condition
Load-induced protection			
Nabeshima et al. 1996 (Nabeshima *et al.*, 1996)	Rabbit patella-patellar tendon	Purified BC	0% strain, 4% strain
Ruberti and Hallab, 2005 (Ruberti and Hallab, 2005)	Bovine cornea	BC	1-2 N (approximately 15-30 pN/monomer)
Lotz et al. 2008 (Lotz *et al.*, 2008)	Mouse anulus fibrosus	MMP-1	Approximately 33% disc strain
Wyatt et al. 2009 (Wyatt, Bourne and Torzilli, 2009)	Rat tail tendon fibres	BC	0-4% grip to grip strain
Bhole et al. 2009 (Bhole *et al.*, 2009)	Reconstituted bovine collagen fibril networks	BC, MMP-8	Up to 50% strain on network (not fibril)
Zareian et al. 2010 (Zareian *et al.*, 2010)	Bovine cornea	BC	0.1 N, 0.25 N, 0.5 N
Flynn et al. 2010 (Flynn *et al.*, 2010)	Reconstituted bovine collagen fibril networks	MMP-8	Up to 50% network strain (not fibril)
Camp et al. 2011 (Camp *et al.*, 2011)	Collagen heterotrimer	BC	0.06 pN, 3.6±1.1 pN, 9.4±1.3 pN
Robitaille et al. 2011 (Robitaille *et al.*, 2011)	Bovine cornea	BC	0% strain, 6% strain
Chang et al. 2012 (Chang *et al.*, 2012)	Individual bovine sclera fibrils	MMP-8	0 pN/monomer, 0.7 pN/monomer, 70 pN/monomer
Flynn et al. 2013 (Flynn, Tilburey and Ruberti, 2013)	Individual bovine sclera fibrils	BC	2 pN/monomer, 24 pN/monomer, 40 pN/monomer
Strain level dependent response			
Huang and Yannas, 1977 (Huang and Yannas, 1977)	Reconstituted collagen fibril tapes	Purified BC	1-7% strain
Yi et al. 2016 (Yi *et al.*, 2016)	Lung alveoli	BC	0%, 20%, 40%, 80% static strain, 40±10% (1 Hz, 0.1 Hz), 40±20% (1 Hz, 0.1 Hz) cyclic strain
Ghazanfari et al. 2016 (Ghazanfari, A. Driessen-Mol, *et al.*, 2016)	Bovine pericardium	BC	5-40% strain

2.7.3 Mammalian versus bacterial collagenases

Aside from the degradation and protection mechanisms proposed in these previous studies, one possible explanation for the conflicting profiles identified could be the choice of collagenase used. A range of different collagenases have been trialled, most notably mammalian collagenases including MMP-1 (Lotz *et al.*, 2008; Adhikari, Chai and Dunn, 2011; Adhikari, Glassey and Dunn, 2012) and MMP-8 (Bhole *et al.*, 2009; Flynn *et al.*, 2010; Chang *et al.*, 2012) as well as crude BC (Ellsmere, Khanna and Michael Lee, 1999; Ruberti and Hallab, 2005; Bhole *et al.*, 2009; Wyatt, Bourne and Torzilli, 2009; Zareian *et al.*, 2010; Camp *et al.*, 2011; Robitaille *et al.*, 2011; Flynn, Tilburey and Ruberti, 2013; Ghazanfari, A. Driessen-Mol, *et al.*, 2016; Yi *et al.*, 2016) which are known to contain other non-specific proteases (Adhikari, Glassey and Dunn, 2012). These crude collagenases often contain different blends of non-specific proteases such as neutral protease and clostridipain, which may influence the outcome of a study. Consequently, some studies have used highly purified BC to remove the potentially negative influence of other non-specific proteases (Huang and Yannas, 1977; Nabeshima *et al.*, 1996). BCs, most typically, Clostridium histolyticum, function differently to mammalian collagenases, cutting the collagen molecule into multiple smaller amino acid sequences (Figure 2.37A). Consequently, they are known to be more aggressive in nature compared to their mammalian counterparts. In contrast, mammalian collagenases which are present *in vivo* are known to be extremely specific, cleaving the collagen molecule at a specific amino acid sequence located approximately ¼ along the length of the molecule (Figure

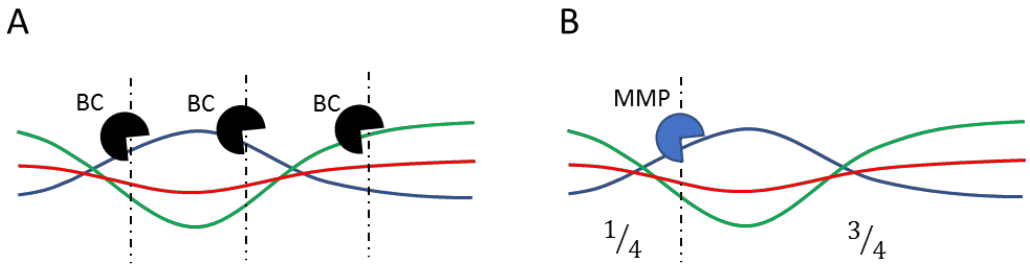

Figure 2.37 - Schematic showing cleavage of a collagen molecule by A) BC which cleaves the collagen at multiple locations along the trimer and by B) MMP at a specific amino acid sequence located 1/4 along the collagen trimer.

2.37B). The resulting ¼, ¾ chains, which are characteristic of MMP degradation, are then degraded further by other gelatinous collagenases.

Interestingly, Adhikari et al. found no load induced degradation response occurring in collagen molecules cleaved by BC in comparison to molecules cleaved by MMP-1 using a single-molecule magnetic tweezers assay (Adhikari, Glassey and Dunn, 2012). However, a near identical study using BC did find a strain induced protection mechanism (Camp *et al.*, 2011). Despite these findings by Adhikari et al. (Adhikari, Glassey and Dunn, 2012), the vast majority of studies have also identified strain dependent degradation responses using bacterial collagenases (Table 2.2), suggesting the underlying changes in structural stability of collagen and subsequent influence on degradation should hold, regardless of the collagenase type.

2.7.4 Computational modelling

As we have seen, arteries are complex in both structure and function. This complexity can make it difficult to understand, explain and predict the biomechanical response of arteries through experimental observations alone. Computational modelling of soft tissues permits the isolation of individual biomechanical factors contributing to the global tissue response, providing greater insight into tissue mechanics. Numerous strain energy functions have been developed to capture the mechanical response of soft tissues, including artery. Differentiating these strain-energy functions with respect to their corresponding strain components provides one with the associated stress arising in the model (Humphrey, 2002). Many early models describing soft tissues were phenomenological in nature, with no structural relevance to the tissue in question. More recently, structural models have increased in popularity, allowing for structurally relevant components to be incorporated such as collagen fibre orientation (Holzapfel, Gasser and Ogden, 2000; Balzani, Schröder and Gross, 2006). Further model developments have led to the incorporation of fibre dispersion (Gasser, Ogden and Holzapfel, 2006), remodelling (Driessen, Bouten and Baaijens, 2005; Hariton, DeBotton, T.C. Gasser, *et al.*, 2007; Creane *et al.*, 2011; Loerakker, Obbink-Huizer and Baaijens, 2013; Loerakker, Ristori and Baaijens, 2016) and damage (Ghasemi, Nolan and Lally, 2018). Many of these

models have been shown to fit experimental mechanical data well; however, there is a clear need for experimentally informed remodelling models, particularly those incorporating the fundamental process of degradation. This unmet need is unsurprising, given the lack of experimental data of arterial degradation.

2.7.4.1 Degradation models

A variety of models have been developed for other tissues to explain the degradation behaviour seen experimentally as well as to predict the tissue level response, with a view to ultimately aiding in the prediction of disease development and progression (Table 2.3, page 73). These models have looked at both the molecular (Chang *et al.*, 2012; Malaspina, Szleifer and Dhaher, 2017) and tissue scales (Grytz *et al.*, 2012; Hadi *et al.*, 2012; Loerakker, Obbink-Huizer and Baaijens, 2013; Heck *et al.*, 2015; Tonge, Ruberti and Nguyen, 2015; Loerakker, Ristori and Baaijens, 2016; Yi *et al.*, 2016), with the latter, often incorporating collagen production in addition to degradation.

Molecular simulations of collagen heterotrimers under load support the theory of strain induced protection by forming a tighter triple helix geometry and thus increased stability at the cleavage site as shown in Figure 2.31 (Chang *et al.*, 2012). These simulations also suggest that large forces applied to stable homotrimers may lead to molecular unfolding and destabilisation of the homotrimer, which may explain the 100-fold increase in degradation found by Adhikari et al. (Adhikari, Chai and Dunn, 2011).

Based on the experimental findings in reconstituted collagen fibrils (Bhole *et al.*, 2009), Hadi *et al.* incorporated a strain induced protective mechanism into their multiscale model of collagenous tissue (Hadi *et al.*, 2012). In their model, collagen degradation was controlled via the radius of collagen fibres within representative volume elements (RVEs) whereby collagen degradation leads to a reduction in fibre radius. RVEs experiencing low strain led to a reduction in fibre radius thus weakening the tissue while RVEs experiencing high strain maintained their fibre radius and consequently, their mechanical strength. The model also incorporated a constant collagen growth rate by increasing fibre radius to ensure that their model would be in a state of net growth during the simulation. It's worth noting that their degradation function was not able to accurately capture the

experimental response of reconstituted collagen fibrils (Bhole *et al.*, 2009) and as a result, the simulation outcome may be significantly different if a more accurate model were to be used. Gyoneva et al. further developed this degradation model by investigating three additional cases of collagen growth which are orientation and load dependent (Gyoneva *et al.*, 2016). Despite these developments, their model was not able to fully reach tensional homeostasis suggesting that further work is required which may include incorporating more complex biochemical processes. Similarly, Loerakker et al. investigated a number of different production and degradation laws to understand and predict the collagen architecture observed experimentally under different loading conditions (Loerakker, Obbink-Huizer and Baaijens, 2013). Their model, which incorporates isotropic matrix, collagen fibres and actin stress fibres, was able to successfully predict the remodelling response observed experimentally in 4 different loading scenarios. To fully understand the remodelling response, 2 different collagen production and degradation laws were investigated. In degradation, strain was assumed to either 1) induce collagen protection as proposed by Wyatt et al. (Wyatt, Bourne and Torzilli, 2009) or 2) result in a V-shaped degradation response as identified by Huang and Yannas (Figure 2.33) (Huang and Yannas, 1977). Using this second degradation law, Loerakker et al. were able to predict the helical 2 collagen fibre family architecture reported for numerous arterial tissues in the literature (Schriefl *et al.*, 2012). This model was further developed to predict the remodelling response of tissue engineered heart valves showing an increased likelihood of valvular insufficiency when valves are implanted in the low-pressure pulmonary position in comparison to the aortic position (Loerakker, Ristori and Baaijens, 2016). Degradation models have also been used to predict thickening of lamina cribrosa, a connective tissue structure supporting axons exiting the eye, which occurs in early glaucoma and has been associated with maladaptive remodelling (Grytz *et al.*, 2012). Using a growth and remodelling formulation which incorporates a collagen fibre crimp and residual stretch to achieve mechanical homeostasis, the authors were able to predict changes in collagen fibril volume with little change in volume fraction, as observed in the literature (Roberts *et al.*, 2009). However, the model also predicted inward migration of collagen fibres which is not seen clinically in lamina cribrosa

thickening in early-stage glaucoma. Unlike the previously discussed growth and remodelling formulations which have used a fibre stretch or strain based approached, Tonge et al. (Tonge, Ruberti and Nguyen, 2015) modelled mechanical inhibition of degradation using an energy-based approach (Huang and Yannas, 1977; Chang *et al.*, 2012). Degradation was implemented by reducing the radius of unloaded collagen fibres which were initially crimped in the undeformed configuration. By fitting to degradation diameter data on collagen fibril networks (Flynn *et al.*, 2010), the model was able to reproduce the degradation response identified in uniaxially loaded corneal tissue (Zareian *et al.*, 2010) and bovine pericardium (Ellsmere, Khanna and Michael Lee, 1999). The creep-degradation response of bovine pericardium under increasing loads presented by Ellsmere et al. (Ellsmere, Khanna and Michael Lee, 1999) was also modelled by Heck et al. (Heck *et al.*, 2015). Unlike Tonge et al. (Tonge, Ruberti and Nguyen, 2015) who modelled the initial degradation response over the first 1 hour period, Heck et al. were able to explain the reduced time to failure in samples experiencing higher initial loads across the 40-hour experiment despite incorporating a load protection mechanism. This was only achievable however by including mechanical rupture of highly strained fibres in addition to load-induced protection.

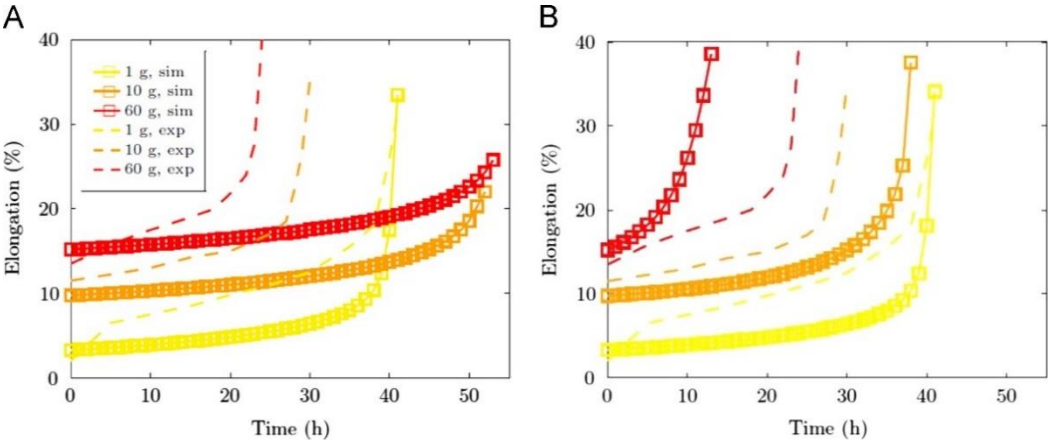

Figure 2.38 – Predicted extension-time degradation curves of statically loaded pericardium strips exposed to collagenase A) with and B) without collagen rupture, loaded with 1, 10 and 60 g (Heck *et al.*, 2015). *Predicted model response (squares) are overlaid on experimental data (dotted) presented by Ellsmere et al.* (Ellsmere, Khanna and Michael Lee, 1999) *and also presented in Figure 2.35.*

Table 2.3 - Summary of recent models incorporating load-mediated collagen degradation.

Author	Load-induced degradation response	Method of degradation	Additional	Simulation
Chang et al. 2012 (Chang *et al.*, 2012)	N/A	N/A	N/A	Molecular configuration changes with load
Hadi et al. 2012 (Hadi *et al.*, 2012)	Protective	Radius reduction	Constant collagen production	Axial dogbone and biaxial cruciform models
Grytz et al. 2012 (Grytz *et al.*, 2012)	Protective	Change in volume fraction	Collagen production to maintain homeostatic stretch. Collagen crimp and residual stretch function.	Lamina cribrosa thickening in vivo
Loerakker et al. 2013 (Loerakker, Obbink-Huizer and Baaijens, 2013)	Protective, strain level dependent	Change in volume fraction	Actin stress fibres and collagen production modelled. Collagen crimp/prestretch function.	Strip, cruciform and vessel models
Tonge et al. 2015 (Tonge, Ruberti and Nguyen, 2015)	Protective	Radius reduction	Energy based approach. Collagen crimp function.	Experimental findings in cornea (Zareian *et al.*, 2010) and bovine pericardium (Ellsmere, Khanna and Michael Lee, 1999)
Heck et al. 2015 (Heck *et al.*, 2015)	Protective	Change in volume fraction	Collagen production and rupture	Bovine pericardium creep (Ellsmere, Khanna and Michael Lee, 1999) and additional loading cases in literature.
Loerakker et al. 2016 (Loerakker, Ristori and Baaijens, 2016)	Protective	Change in volume fraction	Actin stress fibres and collagen production modelled. Collagen crimp/prestretch function.	Tissue-engineered heart valve compaction in aortic and pulmonary deployment
Gyoneva et al. 2016 (Gyoneva *et al.*, 2016)	Protective	Radius reduction	4 cases of collagen production	Uniaxial stretch of RVE

The studies outlined above highlight the importance of developing models which can aid in understanding the underlying mechanisms influencing strain mediated degradation (Chang *et al.*, 2012), explaining the degradation response in tissues *ex vivo* (Hadi *et al.*, 2012; Loerakker, Obbink-Huizer and Baaijens, 2013; Heck *et al.*, 2015; Tonge, Ruberti and Nguyen, 2015; Gyoneva *et al.*, 2016) and potentially predicting disease development *in vivo* (Grytz, Meschke and Jonas, 2011; Loerakker, Ristori and Baaijens, 2016). The different approaches used and the limitations of many of these models outline the need for further investigation into this complex strain mediated process, and particularly in arteries at the macroscale level.

2.8 Summary

Extensive research has been carried out to investigate the structure and function of the arterial wall and its components. Collagen fibre architecture has been the primary focus of much of this work, as it is the primary load-bearing constituent of the vessel wall. Remodelling of this architecture, which includes reorientation, production and degradation of collagen, is critical for both healthy and diseased arterial function. Collagen degradation, in particular, is central to the mechanical stability of collagenous tissues, with excessive degradation linked to atherosclerotic plaque cap rupture as well as aneurysm progression. Many techniques have been utilised to characterise collagen fibre organisation in the vessel wall, each with their associated advantages and disadvantages (see Section 2.6 and Table 2.1). SALS is one such technique which offers an inexpensive means of quickly and efficiently characterising fibre structure across intact tissue; potentially providing insights into arterial remodelling and degradation.

Molecular, fibril and tissue-scale studies have identified collagen degradation as a strain-dependent process. However, a distinct degradation response has not yet been determined in literature, as the findings are largely conflicting. The majority of previous studies have identified an underlying load induced protection mechanism, whereby mechanical loading and straightening of collagen increases its thermal stability and subsequent resistance to enzymatic cleavage. However, a smaller number of studies have also identified accelerated collagen degradation

in response to strain. Finally, even fewer have determined a strain level dependent mechanism whereby regions of both strain-induced degradation and protection exist. It is possible that many of the studies which solely found either increases or decreases in degradation, did not investigate a sufficiently large load or strain range. Potentially, these studies capture only part of the bilinear, V-shaped degradation curve found by others (see Section 2.7.2). Additionally, tissue level studies have observed this protective strain region occurring at a far greater strain magnitude to that found in reconstituted collagen. This highlights the importance of considering collagen and tissue hierarchy when relating findings to physiologically relevant events. It is also possible that load dependent degradation is a tissue-specific response, which illustrates the importance of investigating this process in tissues such as arteries, which are yet to be explored. Numerous computational models have also been developed in an effort to explain and implement these experimental findings with varying degrees of success (see Section 2.7.4). Despite the advent of these models, there is still a clear need for experimentally informed models capable of definitively elucidating the strain-dependent remodelling response of arterial tissue *in vivo*. A greater understanding of this strain-driven remodelling response may provide fundamental insights into arterial disease progression and the biomechanical responses following medical device deployment. To achieve this, multiple complementary techniques, including structural, mechanical and computational analysis, are required for a more comprehensive understanding of the degradation response.

Chapter 3 Collagen Fibre Characterisation in Arterial Tissue under Load using Small Angle Light Scattering

3.1 Introduction

The collagen fibre architecture of arterial tissue is known to play a key role in its resultant mechanical behaviour, while maladaptive remodelling of this architecture has also been linked to arterial diseases such as aneurysm development (Gasser et al., 2012; Niestrawska et al., 2016) and atherosclerosis (Tsamis et al., 2013). Information on the detailed fibre architecture of arterial tissues and how this architecture is influenced by load is therefore central to understanding the aetiology of vascular disease (Creane et al., 2011; Ghazanfari et al., 2012).

Techniques such as polarised light microscopy (Canham et al., 1989; Sáez et al., 2016; Schriefl et al., 2012) and electron microscopy (Dahl et al., 2007; Wolinsky and Glagov, 1964) are often used for structural assessment of these tissues; however, they often require time-consuming tissue preparation steps and are destructive in nature. Consequently, non-destructive techniques such as confocal microscopy (O'Connell et al., 2008; Rezakhaniha et al., 2012) and multiphoton microscopy (Cicchi et al., 2010; Zoumi et al., 2004) are growing in popularity as they allow tissues to remain intact during imaging (Keyes et al., 2011; Watson et al., 2016). Despite this, these techniques are generally subject to depth limitations (< 100 μm), can be time-consuming when characterising large areas and require expensive setup costs.

Small angle light scattering (SALS) analysis may offer an alternative means of measuring fibre orientations ex vivo across large regions of tissue, without the need for time-consuming preparation steps (Appendix A). SALS also offers the potential to determine real-time structural changes in intact tissue in response

to load (Robitaille et al., 2011; Sacks et al., 1997; Williams et al., 2009). Most of the work published on SALS to date has looked at thin, highly organised tissue structures, such as bovine pericardium (Sacks et al., 1994) and porcine aortic valve tissue (Billiar and Sacks, 1997; Sacks et al., 1997); whereas, SALS has seen very limited use in characterising arterial tissue, predominantly due to thickness limitations. In fact, only two studies have been identified by the authors where SALS has been used for arterial fibre characterisation, namely Williams et al. (Williams et al., 2009) and Haskett et al. (Haskett et al., 2010). Both of these studies carried out tissue extensive pre-processing by clearing vessels with glycerol (Williams et al., 2009) or cryo-sectioning vessels (Haskett et al., 2010). It remains to be seen whether SALS can be successfully employed for intact arterial tissue characterisation which may allow future remodelling studies to be carried out using SALS.

The overall objective of this study is to explore SALS as a means of measuring fibre architecture in arterial tissue. Specifically, it is yet to be established whether SALS can be used as a non-destructive or semi-destructive method to decipher load-induced changes in fibre structure.

3.2 Methods

3.2.1 Tissue harvesting

Fresh porcine common carotid arteries were excised from 15 Large White pigs aged 6 months and weighing approximately 80 kg at the time of slaughter. Porcine tissue was used due to its ready availability, its similarities to human vasculature and no ethical approval was required for use. Carotid arteries were transported on ice and processing began within 2 hours of slaughter. The excised vessels were washed with PBS to remove residual blood, and excess connective tissue was removed. The vessels were cut into 2 adjacent tube-like sections 8 mm in length from the proximal end of the vessel. The tubes were cut open longitudinally to obtain 2 flat rectangular strips.

This dissection process removes the residual stresses present within the vessel *in vivo* and consequently, may result in a more undulated collagen fibre architecture. To reduce the risk of recording fibre undulation rather than

orientation in later analysis, specimens were gently squeezed between two slides consistent with other studies on such tissue (Gasser *et al.*, 2012; Sáez *et al.*, 2016).

In the present study full intact intimal, medial, and adventitial layers are analysed. To obtain intact vessel layers, an incision was first made in the vessel cross section at the layer boundary under a microscope. Next, the vessel layers were carefully separated using a rolling and peeling technique with a forceps (Holzapfel *et al.*, 2007). Only vessels with medial layers with a thickness below 600 μm (545 ± 45 μm) were chosen to ensure sample consistency. Additionally, thin histological sections of each layer were analysed.

3.2.2 Histological processing

All histological samples were fixed in 4% paraformaldehyde overnight, dehydrated in a graded series of ethanol baths (EtOH), cleared in xylene before being embedded in paraffin wax. The resulting paraffin-embedded samples were sectioned at 8 μm using a microtome (RM-2125RT, LEICA, Germany) and affixed to microscope slides. A minimum of 2 sections were obtained from each of the 3 vessel layers for staining (108 slices in total).

The resulting sections were stained with picrosirius red to assess collagen fibre distribution. Although collagen fibres are naturally birefringent, picrosirius red significantly enhances this property without negatively impacting perceived fibre orientation under polarised light.

3.2.3 Loading

To identify changes in fibre orientations due to loading, a nominal strain of 20% was applied to one sample arising from each vessel. For histological sections, samples were strained and pinned to a mounting plate before being fixed in 4% paraformaldehyde overnight; this allowed further histological processing of the sample in its loaded state (Figure 3.1). Once fixed, the mounting pins were removed and the tissue dehydrated, cleared and wax embedded as outlined in Section 3.2.2 above. For intact layer samples, the strain was applied using a custom device mounted inside the SALS system.

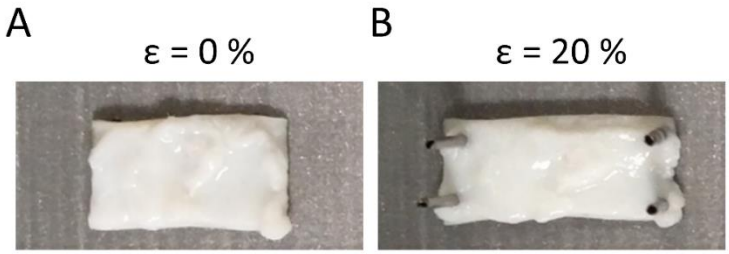

Figure 3.1 - Planar section of carotid artery in (A) the unloaded configuration and (B) the loaded pinned configuration.

3.2.4 SALS system setup

An in-house SALS system was built, based on an existing system described in the literature (Sacks, Smith and Hiester, 1997). This set-up consists of: an unpolarised 5 mW HeNe laser (λ = 632.8 nm; JDSU, Newbury, UK), focussing lenses (various focal lengths; Edmund Optics Ltd, York, UK), automated sample positioner, projection screen and a CMOS USB camera. Each component is mounted on a guide rail, to enable fine linear positional adjustments (Figure 3.2A).

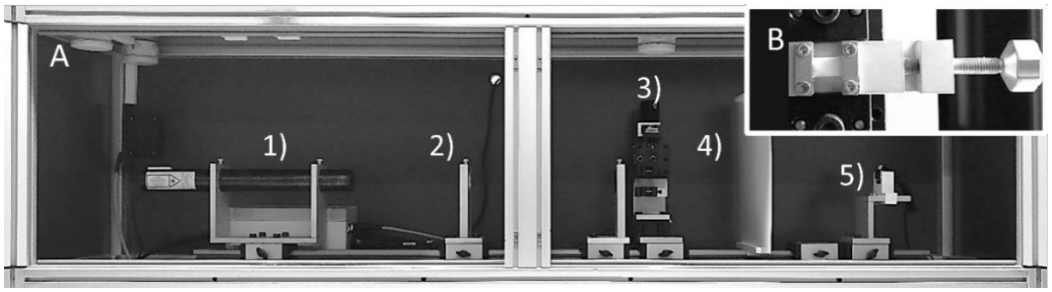

Figure 3.2 - (A) SALS setup consisting of 1) an unpolarised 5mW HeNe laser, 2) focusing lens, 3) automated sample positioner, 4) scatter plate and 5) CMOS camera, with (B) custom stretching device inset.

In order to obtain the desired beam diameter, the antagonising laser light is passed through different lens configurations before encountering the specimen, which is held in an automated positioning and stretching device (Figure 3.2B). A camera records the resulting scattered light pattern as it is projected onto a semi-transparent HDPE projection screen.

The specimen positioning device consists of 2 linear traverses, allowing travel in both x and y directions. Each linear traverse is coupled to a stepper motor (200

steps/revolution; Pololu Corporation, Las Vegas, NV, USA), providing a linear movement resolution of 5 µm across the system's 30 mm range. Stepper motor control and image acquisition are controlled through a custom LabVIEW programme (National Instruments, Berkshire, UK), which allows the user to specify the region of interest in a sample and the interrogation point spacing (see Figure 3.3A). An image of the scattered light pattern is taken and saved at each interrogation point as a sample is raster scanned. The fibre orientation at each of these points is subsequently determined by post-processing these recorded images. Whilst SALS measurement speed is influenced by the user-defined parameters used, in this study, each test specimen imaged included 192 interrogation points across a 4 x 3 mm region of interest which takes approximately 4 minutes to scan.

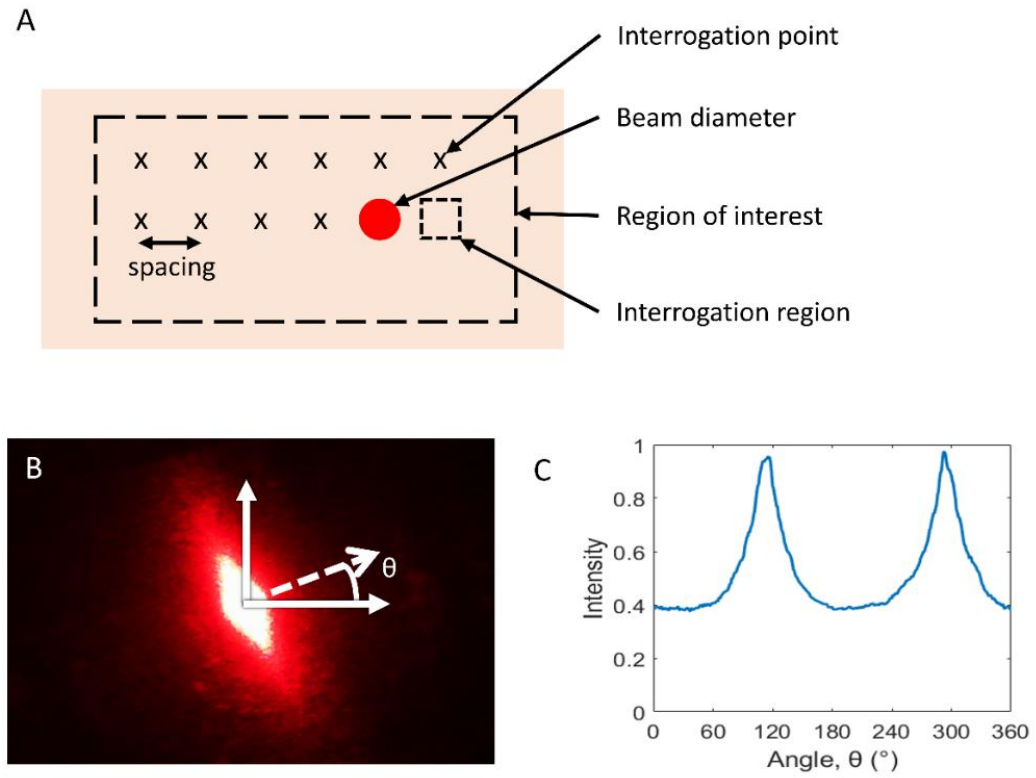

Figure 3.3 - (A) Schematic of a sample illustrating the key parameters in SALS analysis, (B) SALS pattern for single carotid artery location showing mean fibre direction overlaid which occurs orthogonally to the angle of greatest light intensity shown in (C).

3.2.5 Orientation analyses

3.2.5.1 Histological orientation analysis (HOA)

Images of histological sections were taken under crossed polarisers at two polarising angle configurations, 45° apart, using an Olympus BX-41 microscope equipped with a QImaging MicroPublisher 5.0 RTV camera. The resulting images are overlaid to achieve a complete picture of collagen fibre orientation in a sample (Figure 3.4).

Histological orientation analysis (HOA) was carried out in the same interrogation region as SALS measurements across several thin histological sections. Fibre distributions are determined by identifying pixel gradients in each image using the OrientationJ plugin (Rezakhaniha *et al.*, 2012) for ImageJ (Schneider, Rasband and Eliceiri, 2012a). Mean fibre orientation and fibre distributions were determined and compared to those determined using SALS, allowing the identification of the most suitable SALS system configuration for arterial tissue.

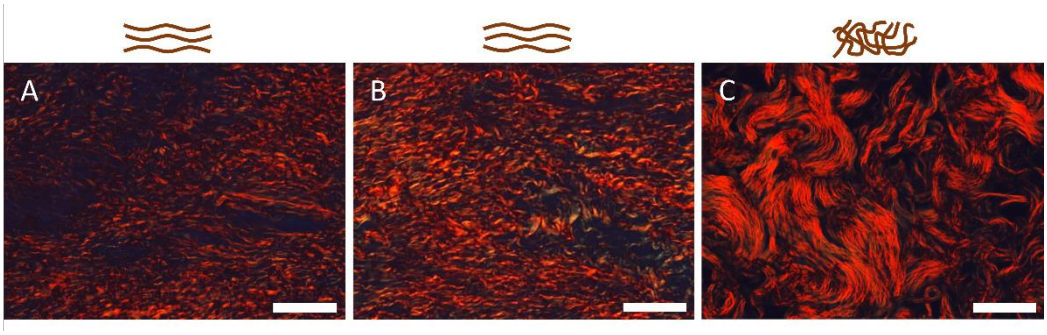

Figure 3.4 - Polarised light images of picrosirius red stained histological slices of (A) intima, (B) media and (C) adventitia showing layer specific fibre architecture. Representative schematics of the structure are shown above each vessel layer image. Scale bar: 50 μm.

3.2.5.2 SALS analysis

The scattering pattern was automatically analysed using a purpose-built Matlab (MathWorks, Cambridge, UK) code allowing for predominant collagen fibre orientations to be determined. The code determines the centroid of the scattered light pattern before systematically cycling through all angles from 1° to 360°, computing the light intensity at each angle (Figure 3.3 B-C). Light scatters orthogonally to a fibre's axis, hence the dominant fibre orientation at a specific

location can be calculated. Each sample is raster scanned over the region of interest and the fibre direction at each point is calculated.

The scattered light forms an elliptical shape with eccentricity, E, which indicates the distribution of fibres at a given interrogation point. Eccentricity is based on the ratio of major and minor axes and is given as,

$$E = \frac{\sqrt{r_{maj}{}^2 - r_{min}{}^2}}{r_{maj}}, \qquad 3.1$$

where r_{maj} and r_{min} are the major and minor radius of the SALS scattered light ellipse respectively. An eccentricity of 1 corresponds to perfect fibre alignment in one direction only, while a value of 0 corresponds to an isotropic distribution of fibres. Using both fibre orientation and alignment, structural differences and responses to load can be identified.

3.2.5.3 Statistics

Statistical analysis of fibre distributions for both SALS and HOA was carried out using a circular statistics toolbox for Matlab (Berens, 2009) and GraphPad Prism 6.0 (GraphPad Software, CA, USA). Normality of distributions was tested using D'Agostino-Pearson normality test. Correlation coefficients were calculated based on the difference in normalised orientation distributions between SALS and HOA at each angle across each sample. Fibre families in adventitial samples were determined using k-means clustering for circular data (Berens, 2009). Changes in eccentricity in response to strain for the three distinct layers of the artery were analysed using unpaired t-tests, while unbalanced one-way ANOVA was used for all other comparisons. Differences were considered significant when $P < 0.05$. All HOA and SALS measurements were measured relative to the circumferential direction ($\theta = 0°$). Results are expressed as mean±standard error (standard deviation).

3.2.6 SALS optimization

One of the primary objectives of the current study was to determine the optimum SALS system configuration for analysing arterial tissue. HOA was first performed using different interrogation region areas to determine whether there is important small-scale fibre distribution detail that SALS may be insensitive to.

Next, SALS was performed on thin histological samples using three different beam diameters and three different interrogation point spacings. Results were compared with fibre orientations found using HOA at the same interrogation points to identify the most accurate configuration. To investigate whether fibre distributions change at different scales, interrogation region areas of 600 μm^2, 150 μm^2 and 75 μm^2 were chosen, corresponding to the SALS beam diameters investigated. Furthermore, an interrogation region of 35 μm^2 was used to detect any small-scale fibre distributions. A laser beam diameter of 600 μm was previously used for bovine tendon (Sacks, Smith and Hiester, 1997) and is used here, additionally beam diameters of 150 μm and 75 μm were also tested. Interrogation point spacings of 75 μm, 125 μm and 250 μm were investigated.

3.3 Results

3.3.1 SALS system optimisation

3.3.1.1 Small Scale fibre distributions determined from histology

HOA results showed no important small-scale fibre orientation or distribution differences for the intima and media layers (Figure 3.5A). However, the fibre angle distribution tended to narrow and become noisier as the interrogation region reduced in size. In contrast, in the adventitial layer, there was greater variation in fibre distribution observed as interrogation region varied in size (Figure 3.5B).

These results show that in the intima and medial layers there is little loss of information if a large interrogation region is utilised. The fibre orientation distribution measured in the adventitial layer does change in response to a change in the interrogation region size. The fibre distribution is seen to shift depending on the interrogation region size (Figure 3.5C), which is most likely attributed to the extremely undulated fibre structure of the adventitia observed histologically in Figure 3.4C.

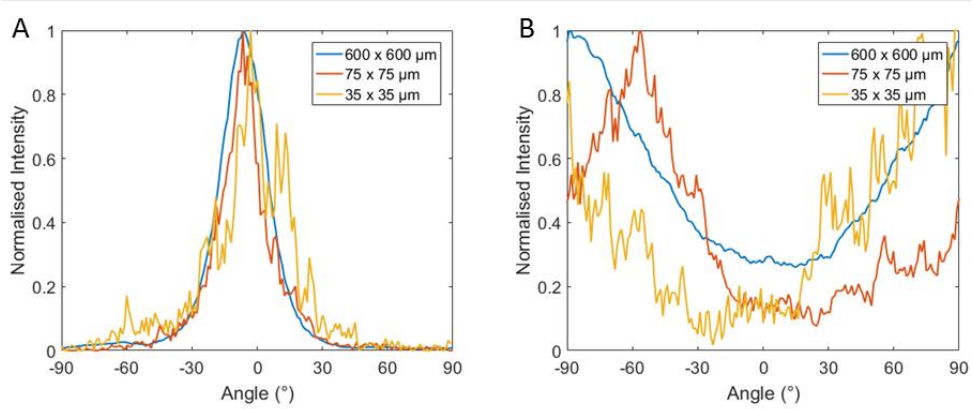

Figure 3.5 - HOA fibre orientation results for interrogation region area of 35 x 35 µm, 75 x 75 µm and 600 x 600 µm for (A) media and (B) adventitia showing the effect of interrogation area for specific layers.

3.3.1.2 Optimum SALS beam diameter

The mean fibre orientation measured using SALS for 3 different beam diameters is compared to that measured using HOA at the same interrogation point. Figure 3.6A plots the error in degrees between SALS and HOA and shows that a beam diameter 150 µm results in the lowest error across all 3 vessel layers (I: 2.6±0.5° (1.6°), M: 3.3±0.5° (1.6°), A: 9.5±2.7° (8.5°)). Circular statistics based on the results of HOA demonstrate significant differences between the adventitial layer and the medial and intimal layers (Figure 3.6B). In addition to closely identifying mean fibre orientation, similar fibre distributions were determined using SALS and HOA at the same interrogation region (Figure 3.7A). This observation was seen quantitatively through the high correlation between fibre distributions across each layer (Figure 3.7B).

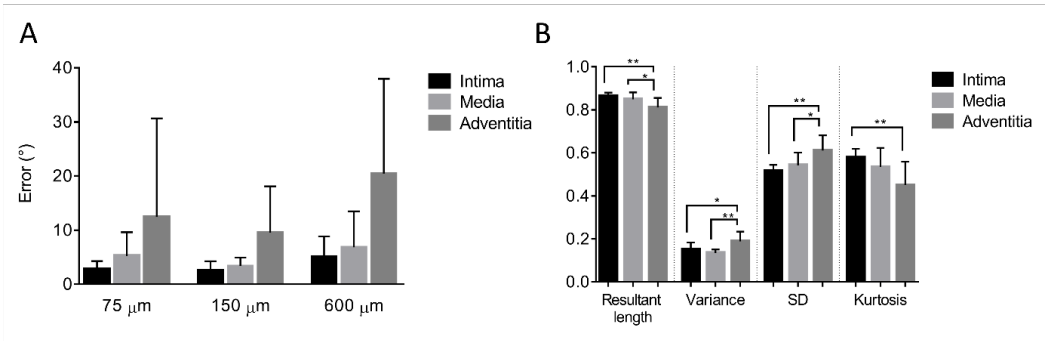

*Figure 3.6 - (A) Angular error between SALS and HOA results for different beam diameters. (B) circular statistical analysis highlighting the different architecture of the adventitia with a 150 µm interrogation region. n=10, *p<0.05, **p<0.01.*

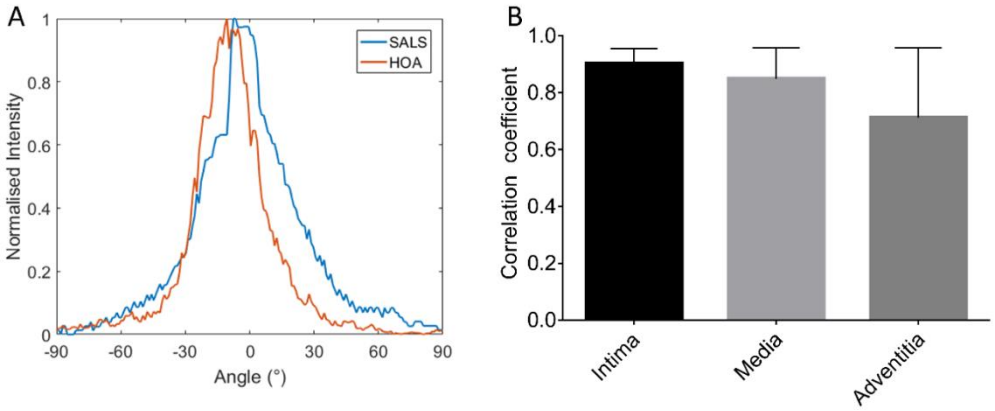

Figure 3.7 - (A) Medial fibre distribution determined using SALS and HOA for the same location, (B) Correlation coefficients between SALS and HOA for each layer. n=10.

3.3.1.3 Optimum SALS interrogation spacing

Moving forward with a beam diameter of 150 µm, the effect of interrogation point spacing for each arterial layer was analysed. Figure 3.8 shows that spacing has little effect on the mean orientation of a sample, for both the intimal and medial layers.

No statistical difference was found in mean fibre orientation for interrogation spacings of 75 µm, 125 µm and 250 µm (Figure 3.8). However, mean orientation showed greater variation based on the interrogation spacing chosen for the adventitia.

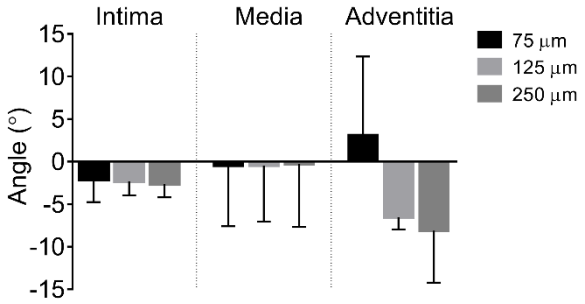

Figure 3.8 - Mean fibre angle measured using SALS across each layer using different interrogation spacing sizes. For interrogation point spacings of 75 µm, 125 µm, 250 µm, the total number of interrogation points are 600, 288 and 72 respectively.

3.3.1.4 Recommended Experimental Setup

Given the results from Sections 3.3.1.1 - 3.3.1.4, a beam diameter of 150 µm was chosen to provide suitably high spatial resolution while minimising the error in the recorded measurements. A scanning resolution of 250 µm was deemed sufficient in locations with minimal changes in architecture while a scanning resolution of 125 µm is recommended for locations of high structural variability such as is the case in complex loading scenarios. The resulting setup resulted in an approximate scan time of 2 seconds per measurement and approximately 192 measurements taken per sample.

3.3.2 Analysis of thin sections

Figure 3.9A and B plot the results of a SALS analysis on a full sample, showing the mean fibre orientation at multiple interrogation points in the region of interest. The eccentricity in the plots qualitatively indicates fibre distribution in the sample. SALS was also capable of measuring regions of considerable fibre reorganisation observed in loaded tissues occurring around the pins (Figure 3.9C). This reorganisation was also observed in a histological image, and was quantified using HOA (Fomovsky and Holmes, 2010) (Figure 3.9D).

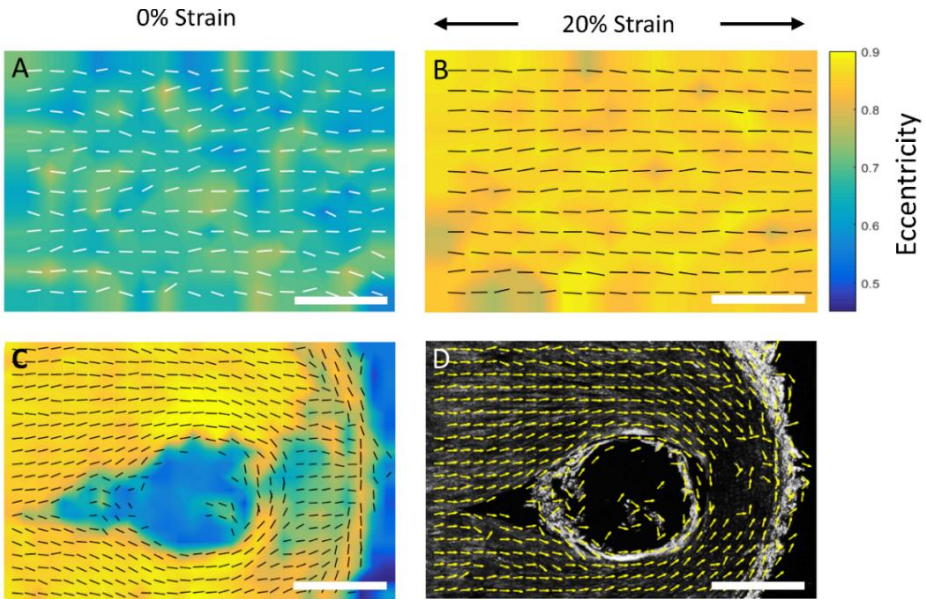

Figure 3.9 - Representative vector map of fibre directions overlaid on a contour plot of scattered light eccentricity produced using SALS for (A) unstretched media, (B) stretched media,(C) around the pinned region of tissue and(D) vector map of the same pinned location showing similar fibre patterns produced using HOA. Scale bar: 1000 µm.

3.3.2.1 Unloaded tissue

Polar histogram plots of all data show a single circumferential (0°) fibre distribution for unstrained intima (-0.1±1.4° (5.5°)) and media (-1.7±1.9° (4.7°)) thin sections (Figure 3.10A i-ii). In contrast, a more complex multi-directional structure was identified in the adventitial layer with single and multiple fibre populations. Two fibre populations were identified using k-means clustering for circular data, with mean angles of -6.4±0.7° (37.7°) and 118.3±2.7 (39.9°) (Figure 3.10A iii)

3.3.2.2 Loaded tissue

Circumferential strain had minimal influence on mean fibre orientation due to the existing circumferential orientation of fibres (Figure 3.10A iv-vi). While small changes occur in mean fibre orientations due to strain (Figure 3.9A-B), a 7.4% and 5.7% increase in eccentricity was seen for intimal and medial tissue respectively (Figure 3.10B).

3.3.3 Analysis of intact vessel layers

Having analysed thin histological sections of arterial wall, SALS analysis was applied to intact vessel layers. Polar histogram plots of fibre distribution show similar distributions to the thin slice results for intima (-2.3±1.9° (4.7°)), media (-2.7±1.2° (3.2°)) and adventitia (-1.4±3.5° (8.5°)), see Figure 3.10C. However, analysis of intact layers did not identify a second axial population of adventitial fibres as seen previously. The mean fibre orientations measured using SALS were also observed using SHG imaging (see Appendix B). Similar increases in eccentricity were also observed in intact intimal and medial layers in comparison to SALS of histological sections in response to a 20% strain (Figure 3.10B).

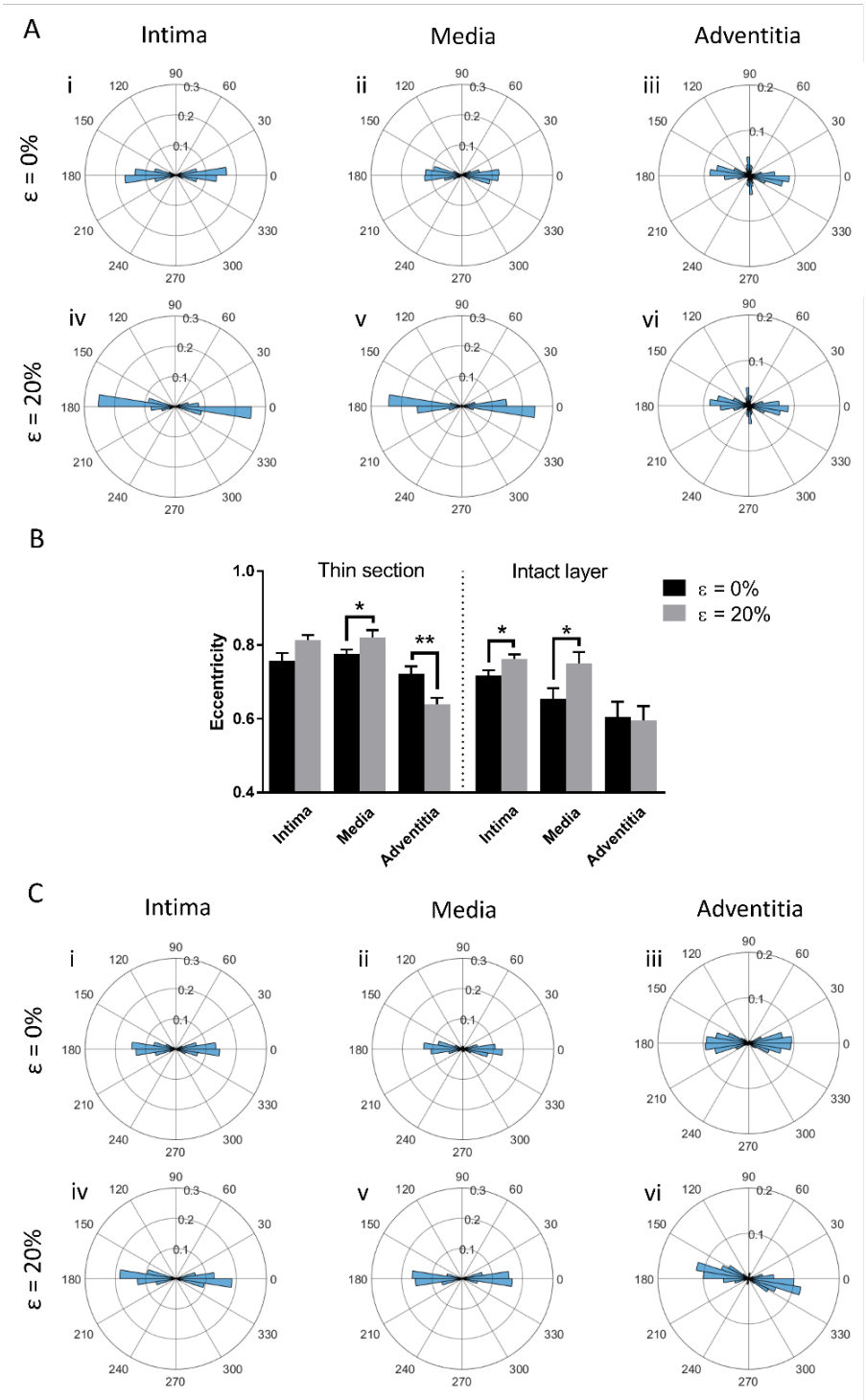

*Figure 3.10 - (A) Polar histogram plot of fibre distribution of histological sections (n = 9) under i-iii) 0% strain and iv-vi) 20% strain. (B) Eccentricity results for histological sections (n = 9) and intact layers (n = 6) in the unloaded and loaded configuration. (C) Polar histogram plot of fibre distribution of intact layers (n = 6) under i-iii) 0% strain and iv-vi) 20% strain. Each sample is made up of 1152 interrogation points. *p<0.05, **p<0.01.*

3.4 Discussion

The goal of this study was to establish whether SALS is capable of repeatedly and reproducibly characterising collagen fibre orientation in arterial tissue and how this architecture changes in response to load. To achieve this, the SALS system was first optimised for use with arterial tissue before an analysis of thin arterial sections and intact vessel walls was performed. A predominant circumferential fibre orientation was found in both thin vessel slices and intact vessel layers, while a second less dominant axial fibre family was identified in the adventitia. SALS was also capable of identifying decreased fibre dispersion in response to vessel loading, through an increase in eccentricity. These results indicate that SALS is a quick and objective alternative to histology for fibre orientation analysis of arterial tissue, with the potential to offer insights into fibre remodelling in intact tissue.

3.4.1 Beam Diameter

A beam diameter of 150 µm was chosen as the optimum for arterial tissue based on quantitative comparisons made with accepted histological results (Figure 3.6A). This is the first instance in which beam diameter has been optimised for arterial tissue. Reducing the beam diameter further to 75 µm resulted in an increase in system noise caused by self-interference of the scattered light, as noted elsewhere (Sacks, Smith and Hiester, 1997). The relatively higher angular error found for adventitial measurements was attributed to the more complex, undulated fibre structure observed histologically (Figure 3.4C).

3.4.2 Interrogation Point Spacing

Due to the high alignment, low dispersion fibre structure of the intimal and medial layers, interrogation point spacing has little effect on the mean fibre angle measured. In contrast, in adventitial samples, there is a considerable difference in the mean fibre angle measured at a spacing of 250 µm. For this spacing distance, the beam diameters do not overlap, unlike the two lower spacing distances. The non-contribution of these unmeasured regions to the mean angle may account for this difference. The interrogation point spacing should ultimately be chosen based on which layer is to be examined, the size of the region of interest, and the level of detail required (Figure 3.9A-C).

3.4.3 Fibre orientation

A single family of circumferentially orientated collagen fibres was identified in the intima and media of porcine carotid artery (Figure 3.10A). This result is in keeping with previous studies of the carotid artery using PLM (Sáez *et al.*, 2016) and DTI (Shahid *et al.*, 2016), however it differs from the typical multifamily structure observed in human aortic vessels (Gasser *et al.*, 2012; Schriefl *et al.*, 2012). This study has considered layer specific fibre orientations and found there is a different fibre structure in the adventitia, with two fibre families identified. This contrasts results from Saez *et al.* (Sáez *et al.*, 2016) who concluded there was a single fibre family in the carotid artery. That study used PLM of 3 histological slices taken at non-specified depths through the carotid artery wall and may have omitted the adventitial layer completely. Previous studies on the common iliac artery using layer-specific PLM have determined a single family of fibres in the intima and media, and two families in the adventitia (Schriefl *et al.*, 2012). It is possible that the multiple fibre families identified elsewhere may also have arisen due to an artefact of the PLM technique, whereby two or more images are required at a single location to characterise the full fibre architecture as discussed in the final paragraph in Section 2.6.2. It has been suggested that the relatively low level of axial strain in common iliac arteries is one reason for this single family fibre structure in the media (Qi *et al.*, 2015). These fibre architecture differences underscore the necessity of investigating specific vessel layers, locations and mechanics.

Collagen orientation under loading was calculated to determine whether SALS has the sensitivity to identify structural changes in intact layers, an important consideration if further remodelling analysis is to be carried out (Gaul and Lally, 2017). Circumferential strain applied to the vessel resulted in a slight shift in mean fibre orientation of the already near circumferentially aligned fibres (Figure 3.10A). Circumferential strain also led to increased fibre alignment, identified by SALS through an increase in scatted light eccentricity in intimal and medial layers. The unexpected reduction in eccentricity seen in adventitial tissue may be attributed to increased disorganisation in its multi-family fibre architecture. These changes in eccentricity highlight SALS ability to capture dispersion information of collagen fibres, something which is often incorporated into

mathematical models of the arterial wall (Sacks, 2003; Gasser, Ogden and Holzapfel, 2006).

SALS was also capable of measuring a similar predominant circumferential fibre distribution in intact vessel layers (Figure 3.10C). This study is the first to analyse intact arterial tissue using SALS without glycerol clearing to increase transparency (Williams *et al.*, 2009). While glycerol treatment allows the entire vessel wall to remain intact, the chemical treatment prevents reorganisation or remodelling of collagen fibres to be analysed in a realistic way. The argument to separate a vessel into distinct layers before SALS testing is strengthened by the confirmation that a different fibre architecture exists in the adventitia, which may obscure results were the vessel to be kept fully intact. Indeed, preliminary SALS testing of glycerol treated full vessel arteries exhibited different scattered light patterns depending on whether the adventitia faced toward or away from the incoming laser light (see Appendix B). These differences arose in response to bias imposed by the layer which the light passes through last, which has the greatest influence on the light scattering. Moreover, layer separation allows one to analyse layer specific reorientation and remodelling under load. SALS fibre measurements made on intact layers agree with SALS results for thin histological sections of the intima and media. However, the more complex multi-family fibre structure observed in thin histological sections of the adventitia using SALS was not observed in intact layers. It is plausible that the dominant circumferential fibre family seen in the adventitia may mask the less dominant second axial fibre family when intact layers are analysed using SALS.

3.4.4 Benefits of SALS

SALS offers many advantages over existing techniques used in characterising fibre orientations of soft tissues with its ability to quickly and objectively measure fibre orientations over large regions with minimal pre-processing. SALS can effectively analyse large tissue regions in a number of minutes, compared to hours for SHG imaging, and days for histological imaging of similar size regions. SALS greatest strength, however, is its potential to look at reorganisation and remodelling of intact tissue which until now has yet to be investigated in arterial tissue. The existence of a load-sensitive protective mechanism for collagen fibres

has previously been identified in corneal tissue (Robitaille *et al.*, 2011), bovine pericardium (Ellsmere, Khanna and Michael Lee, 1999; Ghazanfari, A. Driessen-Mol, *et al.*, 2016) and rat tail tendon (Wyatt, Bourne and Torzilli, 2009), yet it remains to be seen whether this mechanism exists in arteries. SALS ability to non-destructively assess structural changes in intact arterial layers can aid in deciphering whether a load-dependent degradation mechanism exists, and how this mechanism may influence healthy and diseased vessel remodelling.

3.4.5 Study limitations

It is worth noting that SALS is limited by the transparency of the sample to be interrogated. With this, thin, histological slices of tissue are not an issue; however, issues may arise as sample thicknesses increase. Additionally, as sample thickness increases, multiple scattering of light by fibres through a sample's thickness may obscure results. As layer thickness increased, the signal to noise ratio reduced and the predominate fibre directions were difficult to ascertain from the light scattering pattern resulting in a drop in eccentricity (Appendix B). Accordingly, it is best to separate samples into distinct layers to reduce the risk of incorrectly measuring fibre orientations. Although there is no specific optimal thickness for use with SALS, above 800 µm, the fibre angles determined had very low eccentricity values, increasing the likelihood of extracting an incorrect mean angle. As a result, medial layer thicknesses below 600 µm were selected for testing in this study. Although layer separation was not carried out on previous arterial characterisation studies using SALS (Williams *et al.*, 2009), the present study has identified it as an important consideration, particularly for larger mammalian arteries. Arterial samples were also gently squeezed between microscope slides using elastic bands for a 5-minute period which induces a mechanical deformation on the flat vessel sample. This squeezing was carried out as recommended elsewhere (Gasser *et al.*, 2012; Sáez *et al.*, 2016) to reduce the waviness of constituent collagen fibres while minimising disruption to the mean fibre orientation. Despite this near uniform applied deformation, it is possible that this process further disrupts vessel architecture. Additionally, collagen crimp which can be incorporated into constitutive models of collagenous tissues, for example (Tonge, Ruberti and Nguyen, 2015), is not explicitly recorded by SALS unlike techniques such as SHG (Chen *et al.*, 2011; Schrauwen *et al.*,

2012; Haskett *et al.*, 2013). Axial residual stretch which is present in arteries *in vivo* was also not present in the current study. The addition of an axial stretch may increase the likelihood of multiple fibre families emerging with a low pitch angle relative to the circumferential direction.

Finally, this study has used SALS to identify fibre orientation in the circumferential-axial plane and is not well-suited for imaging radially orientated collagen fibres. While radial fibres are not an important determinant for the pressure-diameter relationship of arteries, their number and density have been shown to be important in resisting delamination of arterial layers (Pal *et al.*, 2014). The highly undulated nature of adventitial fibres also reduces the suitability of SALS for characterising the adventitia which was found to produce different fibre distributions depending on the interrogation size and scanning resolution.

3.4.6 Conclusion

By comparing with accepted histological image processing results, this study has identified the optimum SALS setup for analysing the fibre architecture of large mammalian arteries and this same set-up can now be used for future studies on a range of similar sized vessels. SALS has been found to be a quick and easy method of accurately characterising collagen fibre orientation, particularly for intimal and medial arterial tissue, even when intact. Although SALS is less accurate in analysing the outer adventitial layer, the media is the most mechanically relevant layer in normal physiological vessel environments. SALS offers the unique ability to investigate load-induced reorganisation and remodelling of intact intima and media of arteries, thereby, offering a means to gain crucial insights into arterial disease.

Chapter 4 The use of Small Angle Light Scattering in assessing Strain-Induced Collagen Degradation in Arterial Tissue *ex vivo*

4.1 Introduction

Collagen is the most abundant protein in mammals and is responsible for providing much of the load bearing capacity in connective tissue. Remodelling of this collagen network, which is strongly influenced by degradation (Magnusson et al., 2010), is therefore crucial for the integrity of soft tissues, such as arteries.

Existing literature has established that collagen fibres exhibit a strain-dependent degradation response where the rate of degradation is governed by the magnitude of strain applied along the fibre axis. A number of techniques have been utilised to identify these degradation responses across a range of tissues including stress relaxation experiments (Huang and Yannas, 1977; Wyatt et al., 2009), creep experiments (Ellsmere et al., 1999), imaging of single collagen fibres (Wyatt et al., 2009) and tissue alignment analysis using small angle light scattering (SALS) (Robitaille et al., 2011). SALS, in particular, shows a lot of promise in evaluating strain induced degradation responses by providing quantitative measures of tissue structure quickly and non-destructively, indicated by degradation studies on corneal tissue (Robitaille et al., 2011). However, it remains to be seen whether arterial tissue exhibits a strain-dependent degradation response and if so, whether SALS can be used to quantitatively determine this response in arterial tissue.

The aim of this study was to 1) investigate the feasibility of SALS to observe changes in collagen fibre distributions in arterial tissue ex vivo, subjected to different magnitudes of strain whilst in a collagenase solution and 2) determine

whether a strain induced protection or degradation mechanism can be identified. If successfully applied to arterial tissue ex vivo, SALS offers a valuable technique for quickly and objectively assessing strain induced fibre degradation of arterial collagen.

4.2 Methods

4.2.1 Tissue preparation and collagenase treatment

Fresh common carotid arteries were excised from 6-month-old Large White pigs (n = 10) and transported on ice before undergoing cryopreservation in the presence of a cryoprotectant to maintain vessel structural properties (Müller-Schweinitzer, 2009). Prior to testing, samples were thawed in a water bath at 37°C, cut open longitudinally and opened out flat. Circumferential strips were next cut using a 4 mm wide punch for experimental testing. The intima and adventitia were then carefully removed; the media consists of predominantly circumferentially orientated fibres, and the reduction in thickness ensured light transmission through the sample for SALS analysis (Gaul, Nolan and Lally, 2017). Samples were then clamped in a custom stretching jig before being placed under a nominal circumferential strain of 0% (n = 6), 5% (n = 8) or 25% (n = 7). Strained samples were allowed to relax for approximately 30 minutes in PBS and placed in bacterial collagenase while maintaining a constant strain (Type I, 87.5 U/ml; Sigma-Aldrich, Ireland) at 37°C for a period of 4 hours before post degradation analysis. Controls (n = 6) for each strain condition were incubated at 37°C for 4 hours in PBS.

4.2.2 Histology

Samples chosen for histological analysis were fixed in 4% paraformaldehyde overnight, dehydrated in increasing concentrations of ethanol, cleared in xylene and embedded in paraffin wax. Embedded samples were sectioned at 8 μm using a microtome (RM- 2125RT, LEICA, Germany), affixed to microscope slides and mounted with a coverslip using DPX (Sigma-Aldrich, Ireland). The resulting sections were stained with picrosirius red to assess collagen fibre alignment after the degradation process. Picrosirius red significantly enhances collagen fibre birefringence when viewed under polarised light without negatively impacting

perceived fibre orientation (Junqueira, Bignolas and Brentani, 1979). Histological images were taken under crossed polarisers at two polarising angle configurations, 45° apart, using an Olympus BX-41 microscope equipped with a QImaging MicroPublisher 5.0 RTV camera. The resulting images were merged to create a complete picture of the fibre architecture, showing diagonal and off-diagonal fibres.

4.2.3 Second Harmonic Generation

Second harmonic generation (SHG) imaging was conducted with a Carl Zeiss LSM 710 NLO multiphoton microscope (Carl Zeiss, Germany) and Coherent Chameleon tuneable laser (Coherent, USA) to identify differences in fibre architecture due to strain mediated degradation. Samples were excited at 840 nm and the resulting collagen SHG signal collected using non-descanned detectors with a 485 nm short pass emission filters for the 420 nm SHG signal. Tiled image stacks (4 tiles, 12 sections, 6 µm spacing) were taken of the intimal side of the sample at 20X magnification to assess fibre architecture to a depth of 72 µm. Changes in fibre distribution due to degradation were determined in both histological and SHG images by identifying pixel gradients using the OrientationJ plugin (Rezakhaniha *et al.*, 2012) for ImageJ (Schneider, Rasband and Eliceiri, 2012b).

4.2.4 SALS

Changes in fibre alignment due to strain controlled degradation were analysed using an in-house SALS system optimised for arterial tissue in Chapter 3 (Gaul, Nolan and Lally, 2017). The system consists of an unpolarised 5 mW HeNe (λ = 632.8 nm; JDSU, Newbury, UK), focusing lens (f_l = 150 mm; Edmund Optics Ltd, York, UK), automated sample positioner, projection screen and a CMOS USB camera. In SALS, a laser is passed through a fibrous sample and the incident light is scattered orthogonally to the central axis of the constituent fibres to form an ellipse. Samples were interrogated pre- and post-degradation using a 150 µm beam diameter at 64 interrogation regions using a scanning grid size of 125 x 125 µm, informed by previous work (Gaul, Nolan and Lally, 2017). The results from the 64 interrogation regions were then averaged to get a single measurement per sample. The eccentricity of the scattered beam is a measure of alignment (Gaul,

Nolan and Lally, 2017), and was recorded pre- and post- degradation for each strain condition. The relative change in SALS eccentricity, ΔE, was calculated by determining the percentage change in eccentricity, E, from the 0 hour time point when no degradation had occurred using Equation 3.1 (page 82) and Equation 4.1.

$$\Delta E_t = \frac{E_t - E_{t_0}}{E_{t_0}} \times 100 \qquad 4.1$$

where E_{t_0} and E_t are the eccentricity at 0 and t hours respectively.

4.3 Results

4.3.1 Histological analysis of strain-dependent degradation

Distinctly different fibre architectures were identified across each strain group using orientation analysis of picrosirius red stained histology samples, viewed under polarised light. This was also observed visually (Figure 4.1). The greatest degree of collagen fibre alignment is observed at 5% when the sample is strained

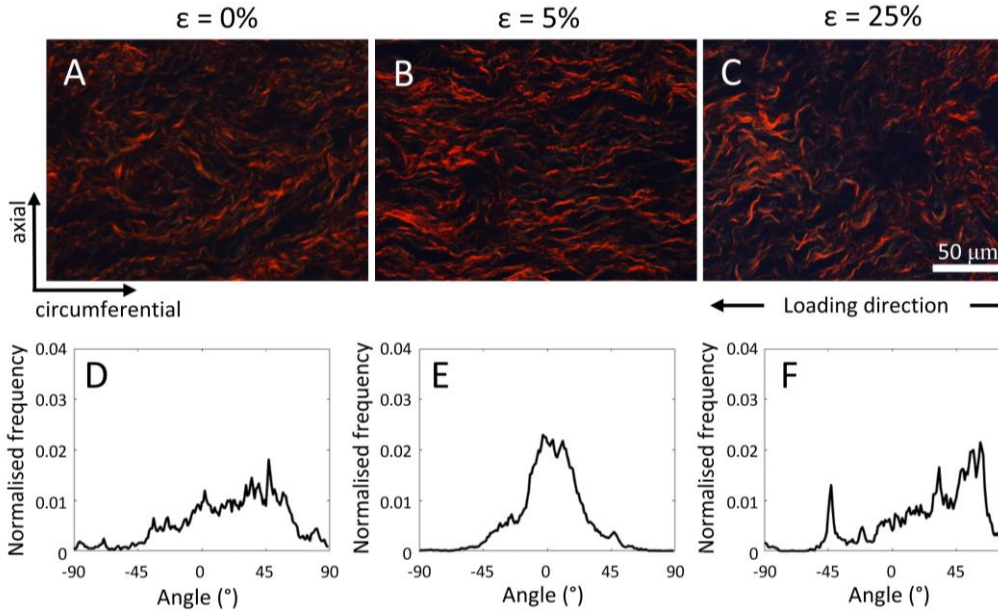

Figure 4.1 - Top panel: Representative histology images of picrosirius red stained artery wall after 4 hours of collagenase treatment, showing collagen in red viewed at 40x under polarised light for A) 0%, B) 5% and C) 25% circumferential strain. Bottom panel: Corresponding normalised frequency distribution plots of fibre angle (D, E, F) for the histological images presented in the top panel.

at 5% circumferential strain. Orientation frequency data was recorded in 1° bins across 180° and normalised so that the summation of all bins equals 1. The structure of native samples, untreated with bacterial collagenase is illustrated in Figure 3.4 in Chapter 3.

4.3.2 SHG analysis of strain-dependent degradation

Orientation analysis of collagen in intact samples identified a similar alignment response to that seen histologically with the greatest alignment occurring at 5% strain (Figure 4.2). Greater fibre dispersion is observed at higher and lower strain conditions. The structure of native, undigested samples viewed by SHG is illustrated in Appendix B, Figure B.1.

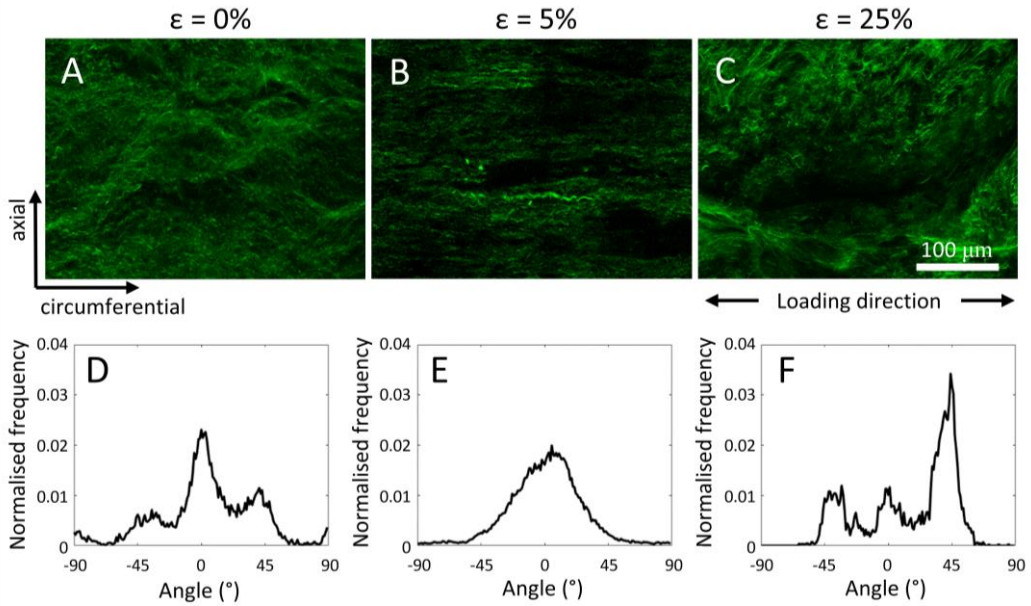

Figure 4.2 - Top panel: Representative SHG images of intact artery wall after 4 hours of collagenase treatment, showing collagen in green viewed at 20x for A) 0%, B) 5% and C) 25% circumferential strain. Bottom panel: Corresponding normalised frequency distribution plots of fibre angle (D, E, F) for the SHG images presented in the top panel.

4.3.3 SALS analysis of strain mediated degradation

SALS analysis also identified different scattered light distributions occurring in each strain group after 4 hours incubation in bacterial collagenase (Figure 4.3). Quantitative assessment of relative change in sample eccentricity at a given strain over time, a marker of alignment, showed a statistically significant 24%

increase in eccentricity at 5% strain compared to 0% and 25% strain (Figure 4.4). Conversely, 25% circumferential strain led to an 8% reduction in collagen fibre alignment over 4 hours in the presence of bacterial collagenase. Unpaired t-tests confirmed that the eccentricity changes identified in collagenase treated samples were statistically significantly different to the control condition where no collagenase was present for each strain condition.

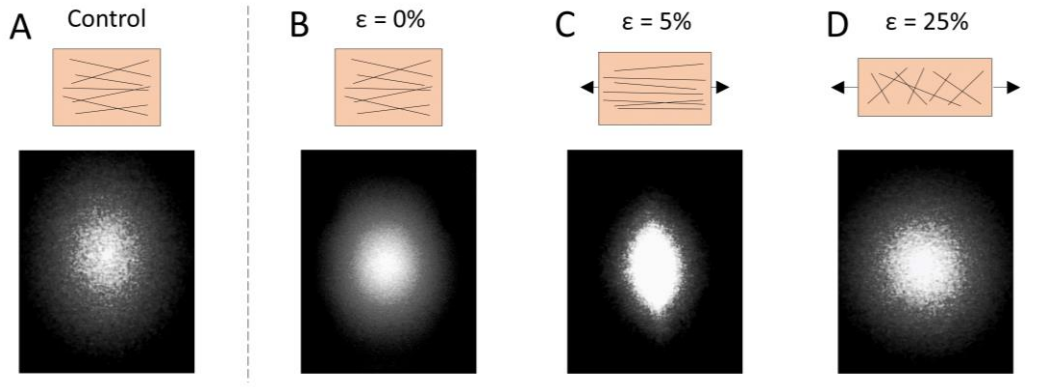

Figure 4.3 – Representative scattered light images at a single location after 4 hours incubation for A) 0% control, B) 0%, C) 5% and D) 25% circumferential strain showing greater or less fibre alignment determined by the eccentricity of the scattered light distribution. Control samples were incubated in PBS while test samples were incubated in crude bacterial collagenase.

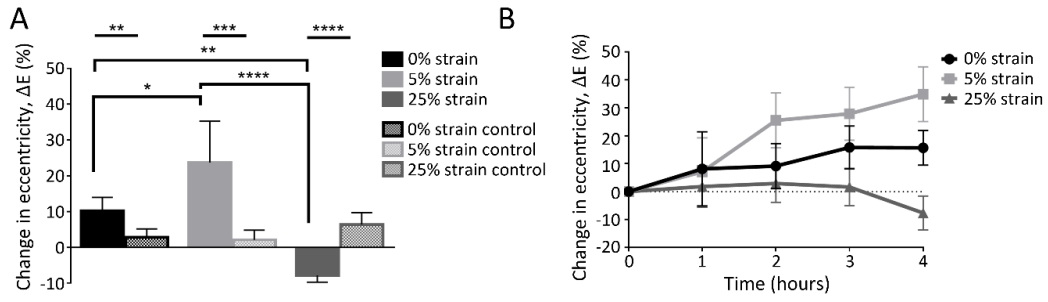

*Figure 4.4 - A) Relative change in SALS eccentricity in the presence of collagenase after 4 hours for each strain case including their untreated control. * $P \leq 0.05$, ** $P \leq 0.01$, *** $P \leq 0.001$, **** $P \leq 0.0001$. B) Relative change in eccentricity over time for a single sample at 0%, 5% and 25% strain showing mean and SD.*

4.4 Discussion

The objective of this study was to investigate whether SALS could be utilised to determine strain induced degradation in arterial tissue *ex vivo* and if so,

determine whether a strain induced degradation or protection mechanism exists for arterial tissue. It has been demonstrated for the first time that SALS is capable of identifying changes in arterial tissue architecture due to strain induced degradation. These findings also suggest that a 'V' shaped degradation response occurs in arterial tissue whereby accelerated degradation occurs either side of a region of strain-dependent protection.

Histological and SHG analysis of degraded arterial tissue show different collagen fibre distributions depending on the strain condition applied (Figure 4.1 and Figure 4.2). Highly aligned fibres were identified in samples experiencing intermediate (5%) circumferential strain, while greater disruption to the native network was observed at low (0%) and high (25%) circumferential strain. Differences can be observed between the orientation distribution plots for both PLM and SHG images for a given strain (see Figure 4.1D and Figure 4.2D). These differences likely emerge due sample variability and the time-consuming sample preparation steps required for histology and PLM. It is also likely that they could be location specific differences and neighbouring sample locations may appear more similar, resulting in more similar frequency distribution plots for a given strain. This subjectivity pertaining to location selection further strengthens the use of SALS for a quantitative and objective analysis tool for characterising collagen fibre orientation.

SALS analysis of samples experiencing these same strain conditions showed statistically significant differences in sample eccentricity, an indicator of alignment, with the greatest eccentricity change occurring in samples experiencing 5% circumferential strain (Figure 4.4). It is hypothesised that the slight increase in eccentricity identified at 0% strain may arise due to a sample thinning and clearing effect as collagen is degraded over time, increasing the signal-to-noise ratio. Interestingly, eccentricity or alignment was found to reduce across samples undergoing 25% strain, suggesting preferential degradation of these highly strained fibres. This strain induced protection mechanism was previously identified in corneal tissue using SALS; however, no higher strain magnitude was investigated to identify whether degradation once again increased with strain (Robitaille *et al.*, 2011). Similar findings, showing both strain-induced

protection and degradation have been identified through mechanical testing, with a minimum degradation rate occurring at approximately 3% strain in reconstituted collagen tapes (Huang and Yannas, 1977) and closer to 20% in bovine pericardium (Ghazanfari, A. Driessen-Mol, *et al.*, 2016). It is hypothesised that the minor increases in eccentricity identified in control samples after 4 hours incubation in PBS at 37°C may be due to fibres reorienting during viscoelastic stress relaxation, as well as a tissue clearing effect over time, resulting in a greater signal-to-noise ratio (Figure 4.4). No similar trends were identified in angular results. This is likely due to the highly organised single circumferential collagen fibre family previously identified in porcine carotid tissue (Sáez *et al.*, 2016; Gaul, Nolan and Lally, 2017) which is unlikely to vary greatly with degradation. No multiple fibre populations were identified using SALS which is consistent with previous investigations of porcine carotid media (Gaul, Nolan and Lally, 2017).

SALS offers a valuable technique for quickly and objectively assessing strain induced collagen fibre degradation across large regions, removing much of the subjectivity associated with histological analysis and the depth limitations associated with SHG analysis. Diffusion tensor imaging (DTI) may offer a potential alternative for looking at similar processes *in vivo* (Flamini *et al.*, 2010, 2013; Shahid *et al.*, 2017), however expensive and time-consuming post-processing has thus far limited such applications. The versatility of SALS enables it to be used for analysis of tissues in static and dynamic loading environments which is far more challenging with SHG imaging and other high magnification systems due to field of view and depth of field issues. SALS analysis can also be carried out in a number of minutes in comparison to hours for similar size regions in SHG imaging. SALS analysis is particularly suited to imaging thin fibrous tissues and can also be applied to other tissues such as bovine pericardium and dura mater to assess the load induced degradation response of collagen. Although the current study has only considered the medial arterial layer, SALS analysis can also be performed on other arterial layers (Gaul, Nolan and Lally, 2017).

It is important to note that the nominal strains were applied to arterial tissue strips rather than dogbone samples which may lead to a non-uniform strain

distribution across the sample. Although force data during degradation was not recorded in the current study, a thorough investigation of the mechanical degradation response of arterial tissue can be found elsewhere (Gaul *et al.*, 2018). The study also only considered a small number of strain conditions and further testing is required to find the precise strain magnitude corresponding to a minimum collagen degradation rate in arterial tissue. It's should be noted that collagenase diffusion kinetics through the tissue are likely to influence the degradation response identified (Zareian *et al.*, 2010). This, however, has less influence on results from SALS whereby collagen fibres on the light emitting surface of the vessel, which are in contact with the collagenase, have the greatest influence on the resulting signal. Additionally, the crude bacterial collagenase used in this study was found to also degrade non-collagenous material in the vessel wall which may contribute to fibre reorganisation over time when loaded. Although arterial tissue is known to have an out-of-plane, elevation angle, this has been found to be very minor in the case of porcine carotid artery and assumed to have negligible influence here (Sáez *et al.*, 2016). The reduced alignment recorded by SALS may also be attributed to an increase in collagen fibre crimp rather than removal of highly strained fibres in the direction of loading, however it is unlikely that these fibres would become more crimped while strained.

Despite these limitations, significant differences in the structural response of arterial tissue have been identified using SALS due to strain induced degradation in an intact arterial layer. These findings suggest that collagen fibres at intermediary strain magnitudes are protected from collagen degradation while higher and lower strains lead to preferential collagen fibre degradation. These preliminary findings may have implications for the onset and progression of arterial disease, such as aneurysms, where strain directed degradation may lead to maladaptive remodelling of the surrounding arterial tissue. Accelerated degradation due to strain directed remodelling may ultimately play a key role in aneurysm and plaque cap rupture.

Chapter 5 Strain-Mediated Enzymatic Degradation of Arterial Tissue: Insights into the Role of the Non-Collagenous Tissue Matrix and Collagen Fibre Crimp

5.1 Introduction

As discussed in Section 2.7, studies on soft tissues, such as tendon, corneal tissue and bovine pericardium, have shown apparently conflicting results on whether strain inhibits (Nabeshima *et al.*, 1996; Ruberti and Hallab, 2005; Bhole *et al.*, 2009; Wyatt, Bourne and Torzilli, 2009; Flynn *et al.*, 2010; Robitaille *et al.*, 2011) or enhances (Ellsmere, Khanna and Michael Lee, 1999; Adhikari, Glassey and Dunn, 2012) enzymatic collagen degradation.

These different degradation responses may be explained by a study by Huang and Yannas (Huang and Yannas, 1977) on reconstituted collagen in the form of collagen tapes. Huang and Yannas experimentally measured the level of enzymatic collagen degradation of these tapes at known strains, ranging from 1-7%. It was concluded that accelerated collagen degradation occurred at both high and low strain levels, while an intermediary strain induced protective region was found close to 4% strain. More recently, Ghazanfari *et al.* (Ghazanfari, A. Driessen-Mol, *et al.*, 2016) and Yi *et al.* (Yi *et al.*, 2016) also identified a similar strain dependent degradation response in fresh decellularised bovine pericardium and lung alveoli respectively. In contrast to Huang and Yannas (Huang and Yannas, 1977), both these studies identified a marked increase in the tissue strain at which degradation is at minimum was identified, which may be explained by the initial reorientation and straightening of constituent mature fibres with applied strain. Whilst these previous studies have investigated the strain- and load-mediated degradation of collagen fibres in structurally simple

collagenous tissues, they have overlooked collagen in its native state within more complex, organised soft tissues.

Arterial tissue, in contrast to pure collagen or bovine pericardium, can be considered as structurally more heterogeneous with circumferentially orientated collagen fibres (Gaul, Nolan and Lally, 2017) embedded in a complex network of cells and other extracellular material. In arterial tissue, matrix stiffness and collagen fibre crimp, present through the wall thickness (Rezakhaniha *et al.*, 2012; Schrauwen *et al.*, 2012; Krasny *et al.*, 2017), may play a significant role in collagen degradation and tissue remodelling but this has yet to be determined. Furthermore, previous studies have only focussed on small strain ranges, potentially missing critical information across larger strain ranges which may be the case in existing studies of collagenous tissues (Ellsmere, Khanna and Michael Lee, 1999; Wyatt, Bourne and Torzilli, 2009; Robitaille *et al.*, 2011). These strain environments may manifest themselves in arterial tissue through atherosclerosis induced stiffening, aneurysm development and vessel expansion due to stenting. It has yet to be established which, if any, of these strain dependent degradation profiles exist in arterial tissue. If established, these responses may play a pivotal role in the understanding of disease development, progression and treatment.

Given the complexity and structural heterogeneity of the arterial tissue, fully understanding the strain-dependent mechanisms influencing collagen degradation is extremely difficult. Mathematical and computational models can help to unravel these mechanisms, due to their versatility and the potential to isolate single parameters. A number of numerical studies have been developed to explore remodelling of arterial tissue (Hariton, DeBotton, T. C. Gasser, *et al.*, 2007; Creane *et al.*, 2011) and other soft collagenous tissues (Driessen *et al.*, 2003; Loerakker, Obbink-Huizer and Baaijens, 2013; Heck *et al.*, 2015; Tonge, Ruberti and Nguyen, 2015; Loerakker, Ristori and Baaijens, 2016), and many of these include explicit formulations for the degradation of collagen (Loerakker, Obbink-Huizer and Baaijens, 2013; Heck *et al.*, 2015; Tonge, Ruberti and Nguyen, 2015; Loerakker, Ristori and Baaijens, 2016). Although these computational models are based on experimental data (Loerakker, Obbink-Huizer and Baaijens, 2013; Heck *et al.*, 2015; Tonge, Ruberti and Nguyen, 2015), no model to-date has compared *in*

silico predictions, incorporating collagen degradation, to experimentally obtained strain- or load-induced degradation of intact arterial tissue.

The overall objective of this study was to determine the strain-dependent degradation response of arterial tissue, and in particular, that of the load-bearing collagen fibres within the tissue. To achieve this, the study had the following specific aims; 1) to directly investigate changes in collagen fibre distributions in loaded tissues enzymatically treated with collagenase, 2) to investigate the degradation rate of arterial tissue *ex vivo* subject to increasing strains through a series of uniaxial stress relaxation experiments, in the presence of crude and purified bacterial collagenase, and 3) to develop a theoretical model of arterial degradation to elucidate the influence of non-collagenous matrix and collagen crimp in the overall degradation response of the arterial tissue.

5.2 Tissue preparation

Fresh porcine common carotid arteries were excised from 6-month-old Large White pigs (n = 38) weighing approximately 80 kg at the time of slaughter. Carotid arteries were transported on ice and frozen to -80°C at a controlled rate of -1°C/min in the presence of a cryoprotectant to maintain mechanical and structural properties (Müller-Schweinitzer, 2009). Samples were preserved for a period of 2-3 weeks prior to mechanical and structural analysis of the tissue. Upon thawing in a water bath at 37°C (Pegg, Wusteman and Boylan, 1997), vessels were cut longitudinally and opened flat removing residual strains (Figure 5.1A) before circumferential (crude: n = 13; purified: n = 16) and axial (crude: n = 13) dogbone specimens were cut for mechanical analysis. Crude collagenase contains a mixture of collagenase and other non-specific proteases which results in the degradation of collagenous and non-collagenous tissue (Figure 5.1B). In contrast, purified collagenase has been treated to contain minimal secondary proteolytic activity, allowing for more selective collagen degradation (Figure 5.1B) (Schriefl *et al.*, 2015). Circumferential strips (crude: n = 17) of width 4 mm were also cut for structural analysis using SALS. Arterial strips were required for SALS assessment due to their larger surface area, which reduced after collagenase treatment. The intima and adventitia were then carefully removed as carried out

elsewhere (Holzapfel *et al.*, 2007; Gaul, Nolan and Lally, 2017), to ensure a consistent circumferential collagen fibre architecture (Gaul, Nolan and Lally, 2017) and to focus on the most mechanically relevant, medial layer within the vessel wall (Holzapfel *et al.*, 2007). Removing the intima and adventitia also allowed transmission of laser light through the sample, a prerequisite of SALS analysis. Sample thickness after layer separation was recorded using a measuring microscope with a micrometre controlled stage for dogbone specimen: 0.711 ± 0.017 (0.112) mm, and strip specimen: 0.646 ± 0.056 (0.144) mm. Dimensions are expressed as mean ± SEM (SD).

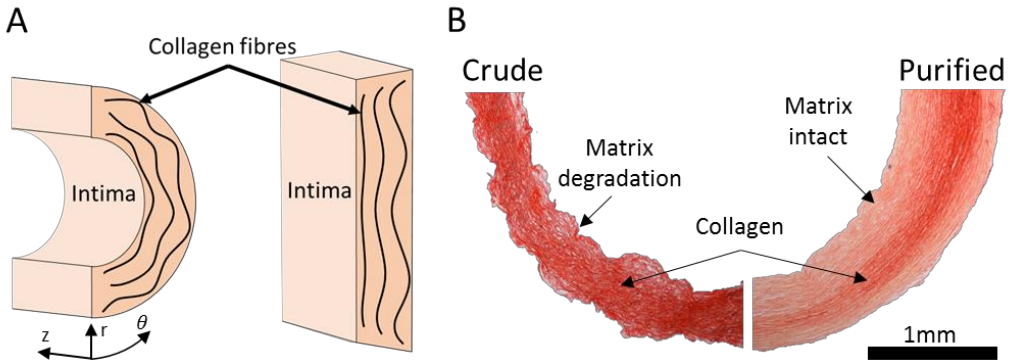

Figure 5.1 - A) Schematic showing gradient of collagen fibre crimp which is exaggerated once residual strains are removed and B) histological images of picrosirius red stained artery cross sections showing matrix and collagen degradation in the presence of crude collagenase in comparison to selective collagen degradation in the presence of purified collagenase. Collagen shows as dark red.

5.3 Structural response

5.3.1 SALS analysis

An in-house SALS system was used to assess changes in fibre architecture due to strain-dependent degradation. The system consists of an unpolarised 5mW HeNe laser (λ = 632.8 nm; JDSU, Newbury, UK), focusing lens (f_l = 75 mm; Edmund Optics Ltd, York, UK), automated sample positioner, projection screen and a CMOS USB camera as described in Chapter 3 (Gaul, Nolan and Lally, 2017). In SALS, laser light is passed through a fibrous test sample and scattered orthogonally to the central axis of the samples constituent fibres. From this scattered light pattern, orientation and alignment information may be determined.

SALS structural analysis was carried out on circumferential strip specimens which were uniaxially strained and placed in crude bacterial collagenase at 37°C for 4 hours. Specimen were analysed by SALS before and after crude collagenase treatment to identify relative changes in fibre alignment (Figure 5.2A). Specimens were interrogated over a 2 mm x 1.5 mm region at the centre of each sample at 192 interrogation regions using a 150 µm beam diameter and a 125 µm scanning resolution.

The scattered light distribution recorded using SALS was used to identify relative changes in fibre eccentricity, E, a measure of fibre distribution as carried out in Section 4.2.4. Relative changes in eccentricity were determined by evaluating the ratio of major to minor axis of the scattered light ellipse shown in Figure 5.2B using Equation 3.1 (page 82) and 4.1 (page 97). An eccentricity of 1 represents perfect fibre alignment in one direction while an eccentricity of 0 corresponds to an isotropic distribution of fibres. Eccentricity results across the 192 interrogation regions were averaged for each sample.

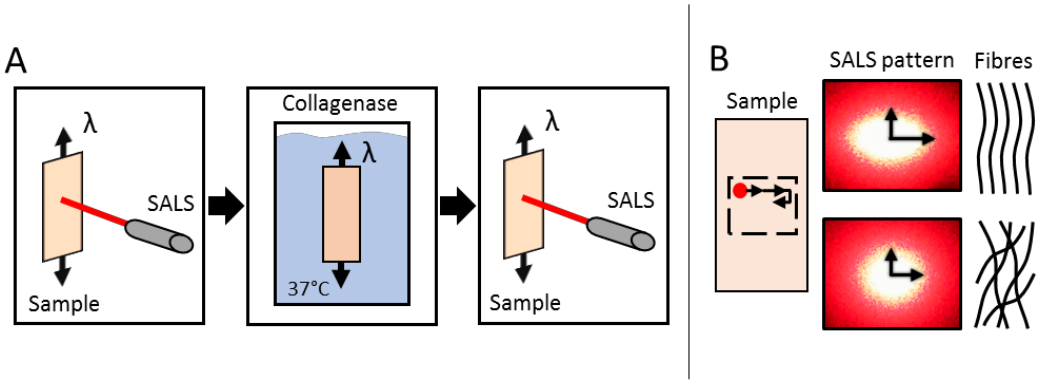

Figure 5.2 - A) Flow diagram showing SALS analysis to determine relative changes in eccentricity and B) SALS images showing a high ratio (high alignment) and low ratio (low alignment) of major to minor axis.

5.3.2 Results: SALS fibre analysis

SALS analysis of arterial strips subjected to crude collagenase showed strain-dependent structural changes (Figure 5.3). High relative increases in eccentricity, representing alignment, can be seen at low strain levels (<5%), before a sharp reduction in eccentricity is observed with increasing strain level (>5%). Eccentricity is next seen to plateau (>10%) before a large drop off at high strain

levels (>40%). This complex strain induced response may be interpreted as follows: 1) At low strains, there is still relatively high dispersion of collagen fibres due to collagen fibre crimp or a lack of reorientation. Consequently, these fibres are preferentially removed, leaving only fibres strained in the direction of loading, resulting in an increase in eccentricity. 2) At intermediary strains, all fibres are in the direction of loading so that, regardless of collagen fibre removal, the eccentricity remains relatively constant. 3) At high strains, the degradation rate has increased, leading to complete degradation of all constituent collagen fibres, resulting in little or no sample anisotropy or alignment at the end timepoint.

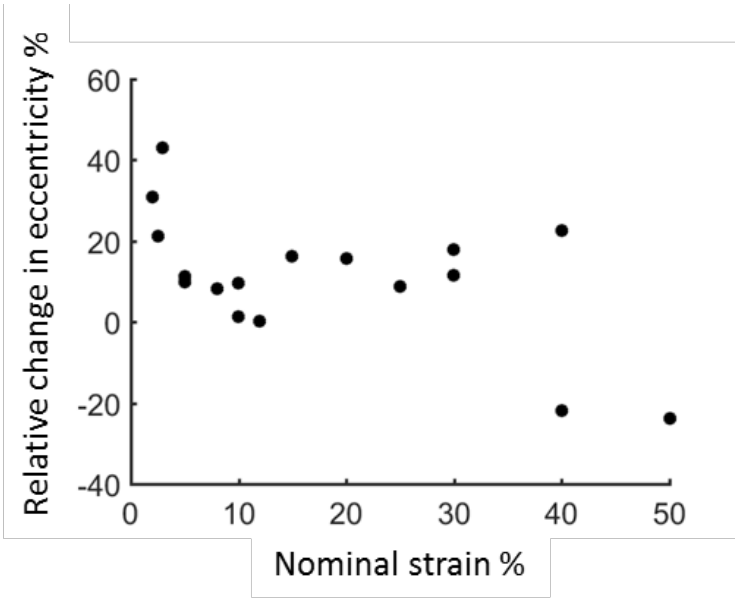

Figure 5.3 - Relative change in eccentricity for circumferential arterial strip samples following 4 hours held at a constant nominal strain in crude bacterial collagenase for a range of strains. n=17.

5.4 Mechanical testing of enzymatically digested tissue

5.4.1 Experimental setup

To assess the tissue level mechanical response to collagen degradation, uniaxial stress relaxation tests were also carried out on circumferential and axial dogbone specimens to determine tissue and collagen degradation rates using a Zwick/Roell Z005 material testing machine (Zwick/Roell, Germany) with a 20 N load cell. Each specimen was instantaneously strained to a predefined strain level and held at this strain level in a PID temperature controlled PBS bath at 37°C (Figure 5.4A).

The specimens were allowed to relax for 60 minutes before the PBS was replaced with an equal volume of either crude (Type I, 87.5 U/ml; Sigma-Aldrich, Ireland) or purified (400 U/ml; Worthington Biochemical, USA) bacterial collagenase in PBS supplemented with calcium and magnesium (D8662; Sigma-Aldrich, Ireland). The force decay due to degradation was monitored for a further 3 hours for samples treated with crude collagenase and 7 hours for those treated with the slower acting purified collagenase, resulting in a total test time of 4 hours and 8 hours respectively (Figure 5.4B). Purified collagenase was used to more selectively digest collagen, allowing for the isolation of the collagen degradation response from that of collagen and matrix degradation which was observed with crude collagenase (Figure 5.1B). Tissue strain was determined by recording the displacement of 3 black markers, which were placed along the gauge length, using ImageJ (Schneider, Rasband and Eliceiri, 2012b). Buoyancy forces are significant in this experiment, and were accounted for by subtracting the force measured with no sample present from the experimental results.

The degradation part of the force relaxation response was fit to Equation 5.1 to determine the degradation rate constant, $1/\tau$ for a given instantaneous strain level (Huang and Yannas, 1977; Ghazanfari, A. Driessen-Mol, *et al.*, 2016):

$$\sigma = \sigma_0 e^{-\frac{t}{\tau}} \tag{5.1}$$

$$\frac{1}{\tau} = -\frac{\ln\left(\frac{\sigma}{\sigma_0}\right)}{t} \tag{5.2}$$

where σ_0 is the relaxed nominal stress at the beginning of degradation calculated from the initial cross-sectional area. The degradation rate constant was calculated from the slope of a plot of the log of normalised stress against time, as shown in Equation 5.2.

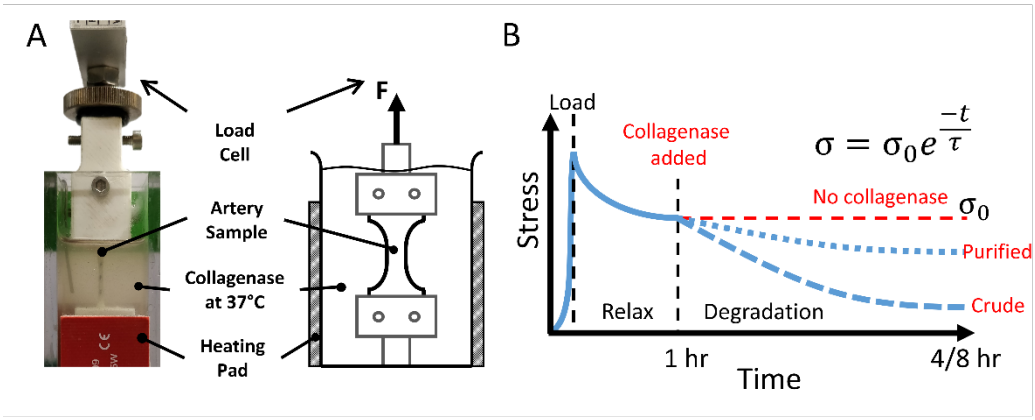

Figure 5.4 - A) Experimental setup showing temperature-controlled testing chamber and B) schematic of the experimental protocol for determining degradation rate, 1/τ, showing the stress response to an instantaneous strain, subsequent stress relaxation for 1 hour and final stress decay for a period of 3 and 7 hours respectively after either purified or bacterial collagenase is added. A greater rate of degradation is observed in the presence of crude collagenase due to degradation of non-collagenous matrix and its increased cleavage rate. If no collagenase is added the stress reaches an equilibrium stress σ_0 by 1 hour.

5.4.2 Results: Crude collagenase

A near linear increase in tissue degradation rate was found with increasing strain in circumferentially (linear fit: R^2 = 0.912) and axially (linear fit: R^2 = 0.942) strained dogbone specimens which were subjected to crude collagenase, see Figure 5.5A. Lower degradation rates were observed in axial specimens compared to circumferential specimens for equivalent strain levels. Representative force relaxation curves are shown in Appendix C for crude and bacterial collagenase.

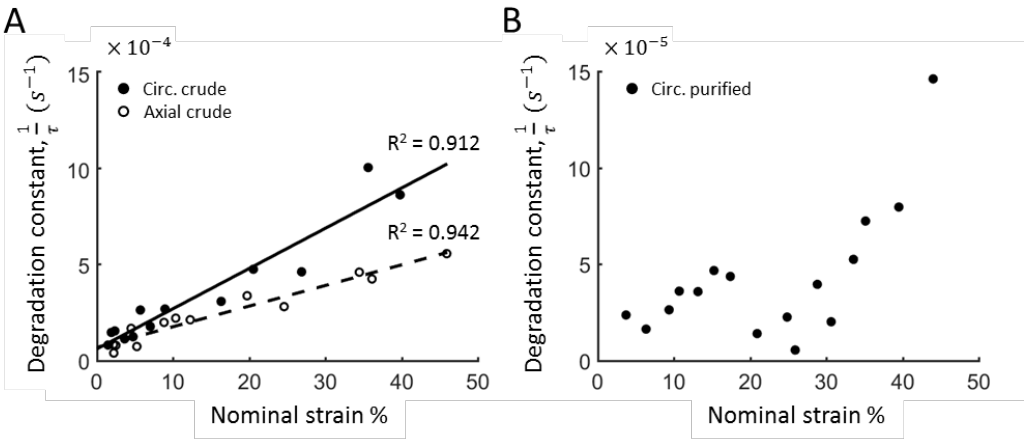

Figure 5.5 - Degradation rate with applied strain for circumferentially (closed circles) and axially (open circles) stretched arterial dogbone samples immersed in A) crude

(n=13) and B) purified (n=16) bacterial collagenase. Solid and dashed lines represent the linear fit for circumferential ($R^2 = 0.912$) and axial ($R^2 = 0.942$) crude experimental data respectively. Each data point represents a single sample. Note y-axis scale changes.

5.4.3 Results: Purified collagenase

To isolate the contribution of collagen in the degradation response of arterial tissue, additional stress degradation experiments were performed substituting the crude collagenase with a purified collagenase. A markedly different degradation response was found experimentally in circumferential dogbone samples treated with purified collagenase (Figure 5.5B). A multi-phase response can be seen with an initial increase in the degradation rate followed by a second more dramatic increase.

5.5 Numerical Modelling

5.5.1 The Fibre-Matrix Unit

A theoretical model of arterial collagen degradation was developed to elucidate the complex interplay between collagenous and non-collagenous matrix components in the net mechanical response of the arterial tissue identified experimentally. This model is a one-dimensional model, named the fibre-matrix (FM) unit. A schematic of a FM unit is shown in Figure 5.7A. The model consists of two elements in parallel; the left element represents the stress due to collagen fibres stretching σ_f, and the right element represents the stress in the non-collagenous matrix σ_m. The total stress, σ_{FMU} in the FM unit is given by the sum of stresses in these two elements; $\sigma_{\mathrm{FMU}} = \sigma_f + \sigma_m$. The contribution of fibres and matrix is weighted by their volume fractions ϕ_f and ϕ_m respectively, which sum to unity.

To represent the crimping of collagen fibres that occurs in arterial tissue when there is zero internal pressure and no residual stress, a prestretch, λ_p, is introduced to the collagen fibres in the FM unit. This is achieved through a multiplicative split of the total stretch in the FM unit λ_t into a collagen fibre stretch part λ_f, and a prestretch part λ_p (Loerakker, Obbink-Huizer and Baaijens, 2013).

$$\lambda_t = \lambda_f \lambda_p. \tag{5.3}$$

Prestretch is represented by the position of the red link in Figure 5.7A and can be used to introduce either tensile or compressive strain to the collagen fibre element. For a given FM unit configuration, λ_p is a prescribed constant which does not change as load is applied. In the initial configuration $\lambda_t = 1$. Prestretch, λ_p is a measure of the degree of crimp in an individual collagen fibre. To set collagen fibres to be crimped in the initial configuration one must prescribe a $\lambda_p > 1$, such that a $\lambda_f < 1$ emerges from Equation 5.3. It is assumed that collagen fibres do not support loads in compression, thus, the collagen fibre element contributes no stress until the chain-type link in Figure 5.7A is fully straightened; i.e. $\sigma_f = 0$ until $\lambda_f > 1$. Collagen fibres have a non-linear elastic response defined by a smoothed bilinear function with three strain domains; low, transition, and high strain (O'Connor *et al.*, 2017). The low and high strain regions are linear, while a quadratic function is used in the transition region to continuously connect the two linear regions together. The stress in a fibre is given by the continuous stepwise function,

$$\sigma_f = \phi_f \times \begin{cases} E_l \varepsilon_f, & \varepsilon_f < \varepsilon_{t1}^{\sigma} \\ T_1^{\sigma} \varepsilon_f^2 + T_2^{\sigma} \varepsilon_f + T_3^{\sigma}, & \varepsilon_{t1}^{\sigma} \le \varepsilon_f \le \varepsilon_{t2}^{\sigma} \\ E_h\left(\varepsilon_f - \varepsilon_{t2}^{\sigma}\right) + T_1^{\sigma} {\varepsilon_{t2}^{\sigma}}^2 + T_2^{\sigma} \varepsilon_{t2}^{\sigma} + T_3^{\sigma}, & \varepsilon_f > \varepsilon_{t2}^{\sigma} \end{cases} \tag{5.4}$$

where E_l and E_h are the moduli of the low strain and high strain regions respectively, $\varepsilon_f = \left(\lambda_f^2 - 1\right)/2$ is the Green strain of the fibre, $\varepsilon_{t1}^{\sigma}$ is the strain at which the low strain region switches to the transition region; $\varepsilon_{t2}^{\sigma}$ is the strain at which the transition region switches to the high strain region; and the parameters T_1^{σ}, T_2^{σ}, and T_3^{σ} ensure continuity between the three strain regions and are defined as,

$$\begin{aligned} T_1^{\sigma} &= (E_l - E_h)/\left(2(\varepsilon_{t1}^{\sigma} - \varepsilon_{t2}^{\sigma})\right) \\ T_2^{\sigma} &= E_l - \varepsilon_{t1}^{\sigma}(E_l - E_h)/(\varepsilon_{t1}^{\sigma} - \varepsilon_{t2}^{\sigma}) \\ T_3^{\sigma} &= E_l \varepsilon_{t1}^{\sigma} - T_1 {\varepsilon_{t1}^{\sigma}}^2 - T_2 \varepsilon_{t1}^{\sigma} \end{aligned} \tag{5.5}$$

To fully define Equation 5.4 four parameters are required; E_l, E_h, $\varepsilon_{t1}^{\sigma}$, and $\varepsilon_{t2}^{\sigma}$.

A simple linear elastic relationship, dependent on the Green strain corresponding to λ_t, was established for the non-collagenous matrix stress; $\sigma_m = \phi_m E_m(\lambda_t^2 - 1)/2$ where E_m is the matrix stiffness. The stress-strain response of the material is illustrated in Figure 5.6 below. Material parameters for collagen and matrix can be found in Table 5.1.

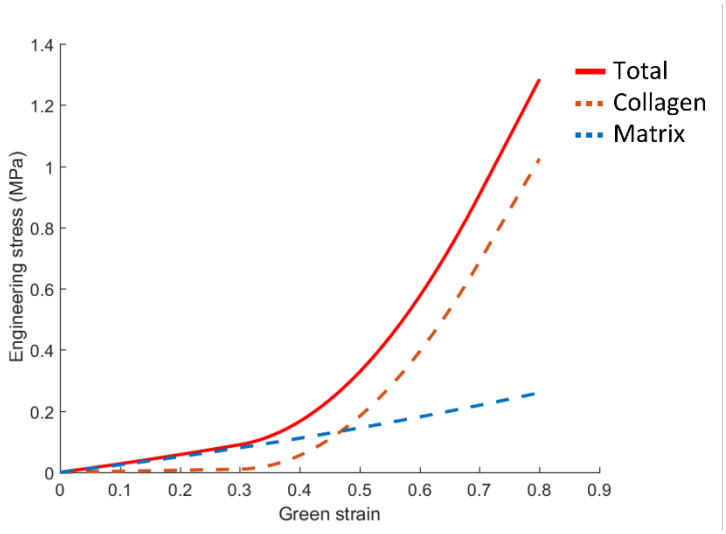

Figure 5.6 - Stress-strain response after calibration showing the matrix, collagen and total response of the tissue using the transition model outlined in Equation 5.4.

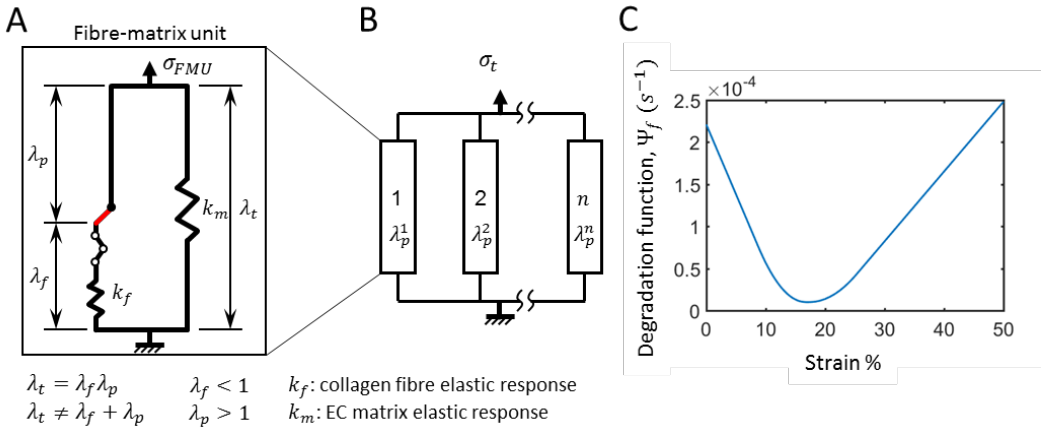

Figure 5.7 - A) Schematic showing a fibre-matrix unit which experiences a total stretch λ_t, made up of a fibre stretch λ_f and prestretch, λ_p term. The red link introduces an initial tensile or compressive strain. Only matrix stiffness k_m, and not fibre stiffness, k_f, contributes to the total stress response until the red link is fully straightened. Note: $\lambda_t \neq \lambda_f + \lambda_p$. B) Fibre-matrix units placed in parallel to make up a transmural gradient of crimp. C) Underlying V-shaped degradation response, Ψ_f for a single

collagen fibre used in this study which was motivated by SALS analysis and literature (Huang and Yannas, 1977; Ghazanfari, A. Driessen-Mol, *et al.*, 2016).

5.5.2 Stress Degradation of Fibre-Matrix Unit

Stress degradation behaviour was modelled through reduction of the fibre and matrix volume fractions over time. This was governed by a first-order rate equation,

$$\frac{d\phi_i}{dt} = -\Psi_i \phi_i, \tag{5.6}$$

where $i = \{f, m\}$, and Ψ_i is the degradation rate constant function, which is conceptually equivalent to $1/\tau$ in Equation 5.1. Equation 5.6 was solved using a forward Euler method over a period of 4×10^4 s using increments of 20 s.

Importantly, motivated by the SALS structural analysis and the studies of Huang and Yannas (Huang and Yannas, 1977) and Ghazanfari *et al.* (Ghazanfari, A. Driessen-Mol, *et al.*, 2016), Ψ_f is assumed to be dependent on the collagen fibre stretch λ_f and is described with a V-shaped degradation response defined by a smoothed bilinear function, similar to that used for the collagen stress response, with three strain domains; low, transition, and high strain (Figure 5.7C). The low and high strain regions are linear with negative and positive slopes respectively, while a quadratic function is used in the transition region to continuously connect the two linear regions together. The degradation rate in a fibre, Ψ_f, is then given by the continuous stepwise function,

$$\Psi_f = D_c + \begin{cases} D_l \varepsilon_f, & \varepsilon_f < \varepsilon_{t1}^D \\ T_1^D \varepsilon_f^2 + T_2^D \varepsilon_f + T_3^D, & \varepsilon_{t1}^D \le \varepsilon_f \le \varepsilon_{t2}^D \\ D_h\left(\varepsilon_f - \varepsilon_{t2}^D\right) + T_1^D {\varepsilon_{t2}^D}^2 + T_2^D \varepsilon_{t2}^D + T_3^D, & \varepsilon_f > \varepsilon_{t2}^D \end{cases} \tag{5.7}$$

where D_l and D_h are the degradation moduli of the low strain and high strain regions respectively, the Green strain of the fibre, $\varepsilon_f = \left(\lambda_f^2 - 1\right)/2$; ε_{t1}^D is the strain at which the low strain region switches to the transition region; $\varepsilon_{t2}^D$is the strain at which the transition region switches to the high strain region; and D_c is a constant or baseline degradation rate which translates the bilinear curve along

the y-axis. The parameters T_1^D, T_2^D, and T_3^D ensure continuity between the three regions and are defined as,

$$\begin{aligned} T_1^D &= (D_l - D_h)/\left(2(\varepsilon_{t1}^D - \varepsilon_{t2}^D)\right) \\ T_2^D &= D_l - \varepsilon_{t1}^D\,(D_l - D_h)/(\varepsilon_{t1}^D - \varepsilon_{t2}^D) \\ T_3^D &= D_l\varepsilon_{t1}^D - T_1{\varepsilon_{t1}^D}^2 - T_2\varepsilon_{t1}^D \end{aligned} \qquad 5.8$$

To fully define Equation 5.7 four parameters are required; D_l, D_h, ε_{t1}^D and ε_{t2}^D

The matrix degradation rate constant Ψ_m is assumed to be a linear function of the total green strain,

$$\Psi_m = k_m(\lambda_t^2 - 1)/2 \qquad 5.9$$

where k_m is a degradation rate constant.

As the volume fractions ϕ_f and ϕ_m decrease so too do their respective stresses,

$$\sigma_f = \phi_f\sigma_f^{t=0}, \qquad 5.10$$

where $\sigma_f^{t=0}$ is the collagen fibre stress at time $t = 0$. The matrix stress σ_m is reduced in the same manner.

5.5.3 Prestretch Gradient

The ability to incorporate a prestretch λ_p into the FM unit was introduced in Section 5.5.1. In the zero pressure, zero residual stress, planar configuration in which experiments are conducted it is assumed that there is a gradient of collagen fibre crimp through the radial thickness of the artery wall. This transmural crimp was modelled by placing 20 FM units in parallel; each FM unit had a unique fibre prestretch. This is shown schematically in Figure 5.7B. Thus the total stress $\sigma_t = \sum_{n=1}^{20}\sigma_{\mathrm{FMU}}^n$.

5.5.4 Model Calibration

A collagen fibre volume fraction, ϕ_f, of 42% was used based on experimental data on collagen content for porcine arterial tissue obtained through image processing (see Appendix C) and is supported by literature (Fischer and Llaurado, 1966; de Figueiredo Borges *et al.*, 2008; Tsamis, Krawiec and Vorp, 2013). Sensitivity to the ratio of collagen and matrix can be found in Figure 5.8. To model the axial

experimental data, a collagen volume fraction, ϕ_f, of 5% was used which was supported by experimental data showing minimal axial collagen fibres in the porcine carotid artery (Gaul, Nolan and Lally, 2017). This ensures that collagen fibres have a much lower contribution to the stress response of the axial test case, as in native tissue.

The material properties used as an input for the model (Figure 5.10) were calibrated from experimental data published previously (Ghasemi, Nolan and Lally, 2018). The matrix modulus, E_m was calibrated from the initial linear stress-strain experimental response of porcine arterial tissue (de Figueiredo Borges *et al.*, 2008; Ghasemi, Nolan and Lally, 2018). To ensure that the initial mechanical response was attributed solely to the matrix, the initial response was compared to that of the vessels treated with collagenase to degrade all collagen (see Appendix C) (Ghasemi, Nolan and Lally, 2018). The bi-linear stress-strain response for collagen fibres shown in Figure 5.6, was calibrated from the same data set as that for the matrix modulus (see Appendix C) (Ghasemi, Nolan and Lally, 2018). The V-shape degradation response was defined using the stepwise smoothed bilinear function outlined in Section 5.5.2. The initial negative slope, D_l, was chosen to be double that of the final positive slope, D_h, as approximately found by Huang & Yannas (Huang and Yannas, 1977) and Ghazanfari *et al.* (Ghazanfari, A. Driessen-Mol, *et al.*, 2016). The magnitude of this function was iteratively determined from the experimental results for pure collagenase (Figure 5.10). A minimum degradation rate was chosen at a strain of approximately 17% after an iterative process, corresponding closely to data from Ghazanfari *et al.* (Ghazanfari, A. Driessen-Mol, *et al.*, 2016). The constant, D_c, which simply shifts the bilinear curve along the y-axis, was set such that a minimum degradation rate irrespective of strain exists, as seen experimentally (Huang and Yannas, 1977; Ghazanfari, A. Driessen-Mol, *et al.*, 2016). This constant, D_c was chosen so that the V-shaped degradation response shifted an order of magnitude higher for the crude collagenase case, while keeping the same degradation profile, mimicking what was seen experimentally. This scaling process is illustrated through the flowchart in Figure 5.10. By increasing the collagen volume fraction of the tissue, the re-emergence of the underlying V-shaped degradation curve for pure collagen can be seen (Figure 5.8A). Increasing the collagen volume to 100%, leads to

complete re-emergence of a V-shaped curve (Figure 5.9) and may explain the V-shaped response found in bovine pericardium, a much more collagenous tissue (Ghazanfari, A. Driessen-Mol, *et al.*, 2016). Similarly, reducing the stiffness of the matrix material, results in a similar response as collagen begins to dominate the mechanical degradation response of the tissue (Figure 5.8B). A reduction factor for degraded material, R, of 0.0001 was chosen through a sensitivity test, such that the degraded matrix and collagen had no mechanical contribution. The matrix degradation rate k_m was assumed to be a linear function of strain, as observed in the crude experimental results in the axial direction where it was assumed that very few collagen fibres contributed to the stress decay (Figure 5.10). The matrix degradation rate k_m was subsequently calibrated from these crude collagenase results. Sensitivity to this parameter can be found in Appendix C. The prestretch gradient parameters, $\lambda_p^{\min}$ and $\lambda_p^{\max}$, were determined iteratively. An initial $\lambda_p^{\min}$ of 1.03 was chosen as it is the parameter that controls the strain at which degradation begins and coincided with the experimental findings. Increasing $\lambda_p^{\min}$ delays the degradation response of the tissue as collagen does not contribute to load bearing until higher strains are reached (Figure 5.8C). The gradient was determined iteratively to ensure that the degradation behaviour was captured over a similar range to the purified collagenase results and such that all fibres are fully straightened at the start of the transition region of the stress strain curve, i.e. $\lambda_p^i > 1$ for all $i = \{1 \rightarrow n\}$. Sensitivity to the magnitude and gradient of prestretch can be found in Figure 5.8 below. Increasing the collagen crimp gradient in the tissue leads to a smoothing of the degradation curve as some fibres are protected from degradation while others experience accelerated degradation (Figure 5.8D). Inversely, reducing the gradient of crimp results in a sharper, more distinct response as all fibres experience a similar degradation rate at a given tissue strain. The list of parameters used for degradation of the FM unit can be found in Table 5.2. The calibration process is described schematically in Figure 5.10. To assess the accuracy of the model, a non-parametric Spearman correlation coefficient was calculated for both the crude and purified data.

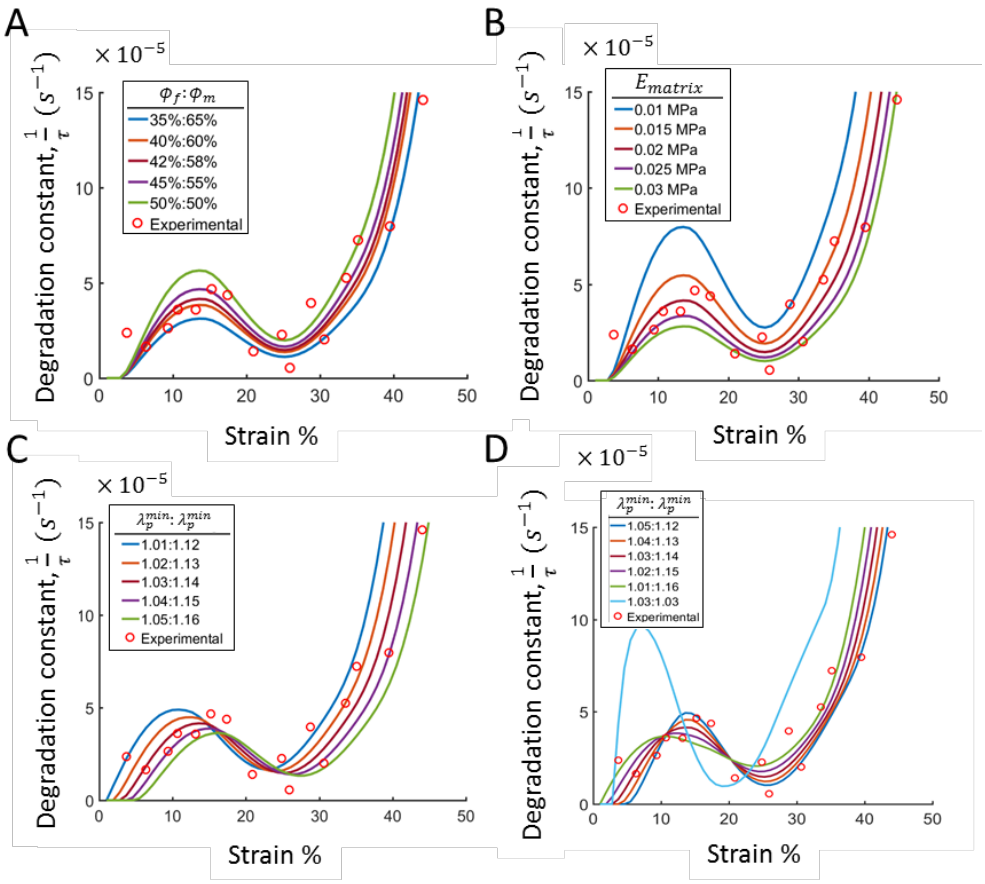

Figure 5.8 - Model sensitivity to A) Collagen content, B) Matrix stiffness, C) Pre-stretch origin and D) gradient of pre-stretch.

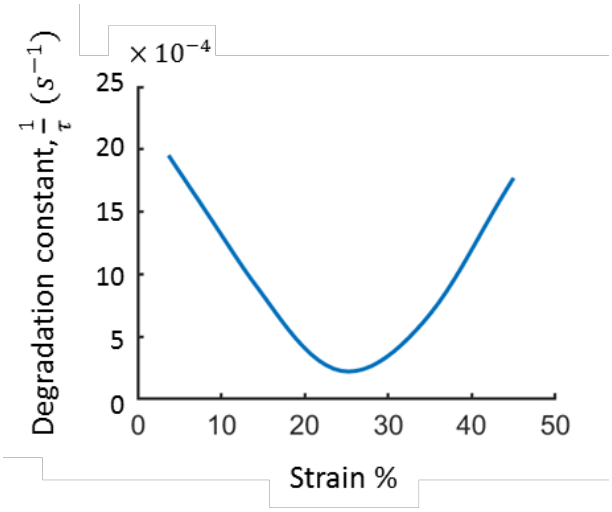

Figure 5.9 - Degradation response of artery with no matrix contribution while maintaining a crimp gradient, showing the re-emergence of the V-shaped strain dependent degradation response of pure collagen.

Table 5.1 - Material parameters for single fibre-matrix unit calibrated from experimental data.

E_l (MPa)	E_h (MPa)	$\varepsilon_{t1}^{\sigma}$	$\varepsilon_{t2}^{\sigma}$	E_m (MPa)
0.004	0.4	0.3	0.7	0.02

Table 5.2 - Model parameters calibrated and derived for crude and purified degradation models. Note that the only difference between the parameters for the crude and purified circumferential models is the magnitude of D_c and the presence of matrix degradation, k_m.

	Defined model parameters				Calibrated model parameters						
	ϕ_f	ϕ_m	D_l ms^{-1}	D_h ms^{-1}	$\lambda_p^{\min}$	$\lambda_p^{\max}$	ε_{t1}^D	ε_{t2}^D	D_c ms^{-1}	k_m (10^{-4})	R (10^{-4})
Crude											
Circumferential	0.42	0.58	-1.50	0.75	1.03	1.14	0.08	0.23	1.21	1.2	1
Axial	0.05	0.95	-1.50	0.75	1.03	1.14	0.08	0.23	1.21	1.2	1
Purified											
Circumferential	0.42	0.58	-1.50	0.75	1.03	1.14	0.08	0.23	0.21	0	1

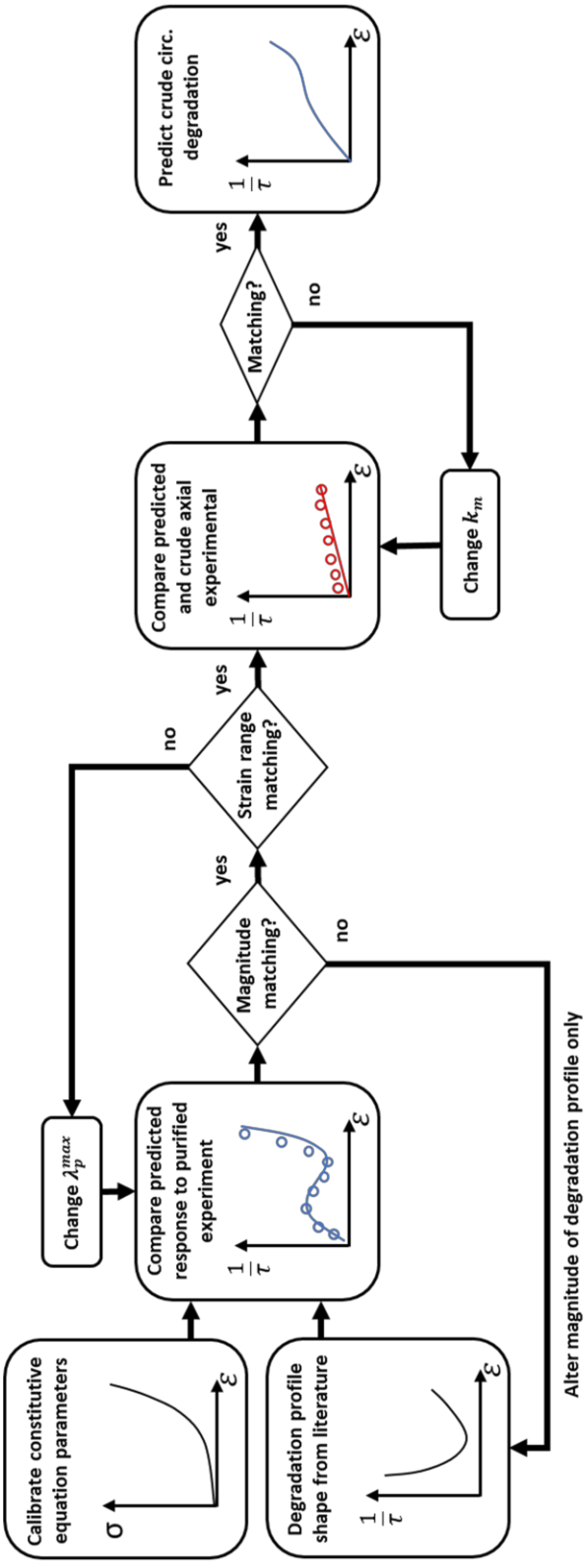

Figure 5.10 - Flowchart showing the calibration process of the numerical model to capture and predict the experimental degradation behaviour.

5.5.5 Model results: Crude collagenase

Incorporation of matrix degradation in the model allowed the prediction of a similar continuously increasing degradation response to that found experimentally. The model was also capable of identifying the experimentally observed differences in degradation rate for circumferentially and axially stretched samples where fibres were parallel and perpendicular to the direction of applied strain respectively (Figure 5.11A). A high correlation was seen between numerical and experimental results for both circumferential ($r = 0.940, p < 0.001$) and axial ($r = 0.808, p < 0.005$) data.

5.5.6 Model results: Purified collagenase

The numerical model was capable of accurately capturing the experimental response found in purified collagenase where no matrix degradation occurs. The model captured the initial degradation increase followed by a dip and subsequent increase in degradation which was observed experimentally (Figure 5.11B). A high correlation ($r = 0.835$, $p < 0.001$) was also found between the experimental and numerical results for purified data.

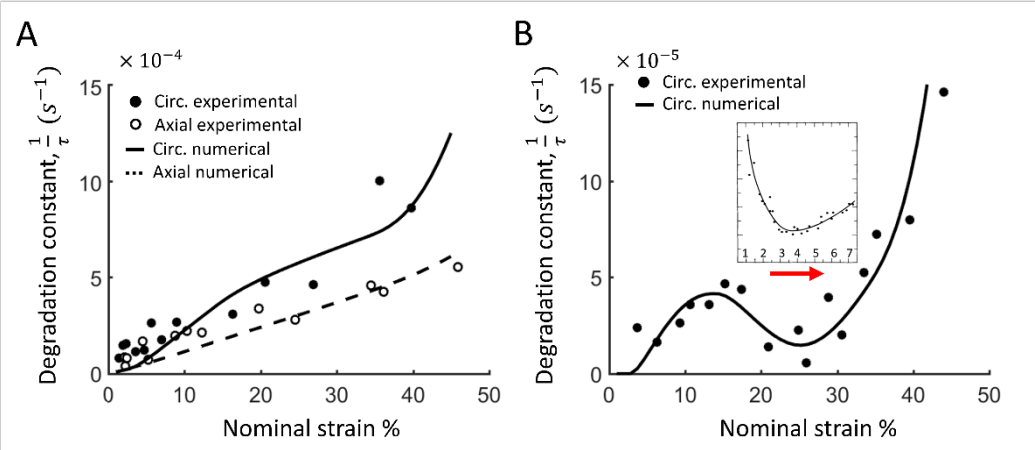

Figure 5.11 - Numerical degradation rate with applied strain for circumferentially (solid lines) and axially (dashed line) stretched arterial dogbone samples immersed in A) crude and B) purified bacterial collagenase overlaid on experimental data (circles) after calibration. Inset: V-shaped degradation found for pure collagen [Adapted from (Huang and Yannas, 1977)*], showing how scaling of the x-axis is required to produce the degradation response at the tissue scale. This scaling process is further illustrated in Figure 5.10.*

5.6 Discussion

Collagen degradation is a driving force in collagen remodelling in arterial tissue, which may be critical in the progression and development of vascular disease and determining the long-term success of interventional medical devices. The goal of this study was to identify the strain-dependent degradation response of, and mechanical factors influencing collagen degradation in arterial tissue, using a combination of experimental and theoretical methods.

SALS alignment analysis identified strain mediated structural changes in arterial tissue due to enzymatic degradation, suggesting that an underlying bi-linear V-shaped degradation response may exist for arterial collagen. Interestingly, mechanical testing identified two different strain mediated degradation responses in arterial tissue depending on whether crude or purified collagenase was used to degrade the tissue. A near linear degradation profile was seen experimentally for crude collagenase while a complex multiphase response was seen in pure collagenase, both of which differed to that of pure collagen in literature (Huang and Yannas, 1977) and what was expected from the SALS analysis. These differences identified experimentally were explained through the development of a novel 1D numerical model, however, only after a gradient of collagen fibre crimp, matrix contribution and degradation of this matrix were incorporated (see Figure 5.8 and Figure 5.9). Taken together, these results identify the significance of collagen fibre crimp and matrix stiffness in strain dependent arterial degradation, improving the understanding of arterial remodelling in disease development, progression and treatment.

SALS results suggest that a strain mediated degradation response exists in arterial tissue (Figure 5.3). The initial increase in fibre eccentricity observed at low strain levels suggests the preferential degradation of unstrained collagen fibres, whilst the reduction in eccentricity at high strain levels suggests preferential degradation of highly strained fibres. A similar response was observed using SALS at low strain levels in corneal tissue, however, higher strain levels were not considered (Robitaille *et al.*, 2011). This SALS data supports the existence of a strain-dependent degradation curve for collagen fibres within

arterial tissue at the fibre level, even if a more complex degradation response exists at the tissue level.

Uniaxial stress relaxation experiments using crude bacterial collagenase identified a continuous increase in degradation rate with increasing strain for circumferential and axial specimen (Figure 5.5). This response differs significantly from the bi-linear V-shaped degradation response observed in reconstituted collagen tapes (Huang and Yannas, 1977) as well as bovine pericardium (Ghazanfari, A. Driessen-Mol, *et al.*, 2016), although it bears similarities to another study on bovine pericardium (Ellsmere, Khanna and Michael Lee, 1999). The model shows that the lack of an emerging bi-linear degradation response may be due to the gradient of collagen crimp across the vessel thickness (Figure 5.1A), the non-collagenous matrix mechanical contribution and in particular, the partial degradation of this matrix due to the use of crude collagenase (Figure 5.1B). If true, this highlights the importance of considering collagen undulation and the role of non-collagenous constituents in analysing collagen degradation, particularly in heterogeneous tissues. The higher degradation rate in circumferential samples is believed to be associated with the higher number of load bearing collagen fibres orientated in this direction, which leads to a larger stress decay when degraded under strain. A different, more refined strain mediated degradation response was identified using purified bacterial collagenase where no matrix degradation occurs (Figure 5.7). The emergent response also differs from that seen in literature with an initial increase in degradation followed by a subsequent, more pronounced increase in degradation rate. This subsequent increase was found to begin close to the transition strain (30 %) of the tissue, something which has also been observed in other collagenous tissues (Huang and Yannas, 1977; Ghazanfari, A. Driessen-Mol, *et al.*, 2016).

The complementary numerical model helps unravel the mechanisms at play for both the crude and purified collagenase experiments. Starting with the purified case: no degradation occurs initially; as collagen fibres at low strain are crimped they bear no load and hence do not contribute to strain mediated degradation induced stress decay. Next, degradation increases as fibres begin to uncrimp and

take up the load. When all fibres are fully stretched, the V-shaped behaviour resumes. To explain the crude collagenase results; matrix degradation is incorporated into the model, whereby the degradation of mechanically relevant matrix material at lower strain levels, smooths the ultimate degradation response of the arterial tissue. To evaluate the degradation response in the axial direction, a collagen volume fraction of 5% was used, representing the low volume of axial fibres observed in earlier studies (Gaul, Nolan and Lally, 2017). Volume fractions up to 15% had minimal influence on the degradation response in the axial direction. Although a large number of parameters were required for the model, these parameters all have a physical meaning and were supported by experimental data where possible. The versatility of this model allows for the investigation of the strain-dependent degradation response of other collagenous tissues by incorporating different ratios of collagen and matrix as well as different levels of collagen fibre pre-crimp (Figure 5.8). Increasing the collagen content and reducing the gradient of crimp (Figure 5.8) results in the re-emergence of the V-shaped degradation curve of pure collagen observed in Figure 5.7C. This may explain the strain induced protection found in tendon tissue at low strain levels (Wyatt, Bourne and Torzilli, 2009) as well as the V-shaped degradation response observed in bovine pericardium across a larger strain range (Ghazanfari, A. Driessen-Mol, *et al.*, 2016). Sensitivity to these parameters can be found in Figure 5.8 and Appendix C.

The cause of the underlying V-shaped collagen degradation response, and consequently the influence on a tissue's mechanical properties, is not fully understood; however, some mechanisms have been postulated in the literature. On the one hand, a reduction in tissue porosity with stretch has been suggested as a potential reason for an initial decrease in degradation (Huang and Yannas, 1977; Wyatt, Bourne and Torzilli, 2009); while, opening up binding sites with further fibre stretching allows subsequent accelerated degradation (Huang and Yannas, 1977; Ellsmere, Khanna and Michael Lee, 1999; Chang and Buehler, 2014). On the other hand, conformational changes and increased monomer thermal stability due to collagen tension have also been proposed as a reason for reduced degradation (Nabeshima *et al.*, 1996; Miles and Ghelashvili, 1999; Bhole *et al.*, 2009; Wyatt, Bourne and Torzilli, 2009; Chang and Buehler, 2014).

Additionally, load transfer from degraded fibres to neighbouring fibres, thus increasing fibre stress has also been suggested as a potential reason for accelerated degradation (Huang and Yannas, 1977). The conflicting findings seen in literature may be influenced by this lack of understanding surrounding mechanisms of degradation as well as interpretation of results. For instance, it is unknown whether the degradation response differs when considering single collagen fibrils or thicker bundles of fibres. Collagen fibre damage which is likely to occur at the high strain levels experienced in this study is also likely to affect the degradation response and may influence the final degradation increase identified in this study. The underlying V-shaped degradation curve minimum determined in arterial tissue is also found to occur at a substantially higher strain magnitude to that found in reconstituted collagen (17% vs. 4%) (Huang and Yannas, 1977). The differences for this apparent shift are not clear, however it may be influenced by the structural hierarchy of collagen in whole tissues where collagen molecules form fibrils, in turn forming undulated, dispersed fibres within the tissue. As collagen moves from the micro to macro scale, it may permit increased levels of reorientation, straightening and sliding before the strain protection mechanism is engaged. Further details on the possible explanations behind this shift at different collagen scales can be found in Section 2.7.1 and 2.7.2. The shift found in this work is also supported by studies which have also found a V-shaped response occurring at the tissue scale in bovine pericardium (Ghazanfari, A. Driessen-Mol, *et al.*, 2016) and lung alveoli (Yi *et al.*, 2016). In addition to a shift in strain range, there are also differences in the magnitude of degradation identified in literature (Huang and Yannas, 1977; Ghazanfari, A. Driessen-Mol, *et al.*, 2016); however, these can be explained by the choice of collagenase as well as the concentration used which has been shown to vary linearly with increasing concentration (Huang and Yannas, 1977). The strain protection magnitude of 17% also corresponds approximately to healthy physiological strain ranges occurring at 100 mmHg which will be later seen in Figure 6.5 which may play a part in maintaining homeostasis. It is important to note that human arterial tissue has been found to be less compliant to that of porcine arterial tissue used in this study (Sommer and Holzapfel, 2012). Consequently, a minimum degradation strain may exist at a lower fibre strain to

that found here. Despite this difference, similar strain induced degradation trends are likely to occur in human tissue, with implications in the development and progression of disease.

One limitation of the current study is the use of bacterial collagenases to assess degradation responses to strain rather than MMPs and cysteine collagenases which are responsible for collagen degradation *in vivo* (Aikawa, 2004; Abdul-Hussien *et al.*, 2007). It is also worth noting that the effect of strain on the production of collagenase inhibitors *in vivo* has not been considered and may influence the net degradation response (Abdul-Hussien *et al.*, 2007). It is important to note that diffusion kinetics also play a role in the degradation results as shown in Figure 5.1B, where a gradient of collagen degradation can be observed in the purified degradation case. As a result, highly strained samples where pore size is reduced within the tissue may reduce the diffusion rate of the collagenase. However, this work identified an increased rate of degradation at high strains, any reduction in diffusion with increasing strain is not the dominant effect at play. In support of this, reduced porosity of rabbit patellar tendon due to strain has been shown to not affect the diffusion of radiolabelled collagenase through the tissue (Nabeshima *et al.*, 1996). However, diffusion kinetics is likely to become more important when considering other experimental setups such as pressure inflation degradation experiments where collagenase is actively being pushed through the tissue. Additionally, the stress relaxation experiments were carried out on planar specimens and in the absence of the residual strains present within an intact vessel, although this is accounted for by incorporating a gradient of fibre crimp in the model. Finally, the presence of an intimal and adventitial layer *in vivo*, not considered in this study, may also protect the vessel from experiencing the supraphysiological strain environments considered in the current study.

The results of this study have identified, for the first time, the strain-dependent degradation behaviour of arterial tissue using a combination of experimental and theoretical methods. These findings show distinctly different degradation responses when using crude or purified collagenase, highlighting the need to carefully select the appropriate enzyme when investigating tissue degradation,

particularly in tests involving highly heterogeneous tissues. A 1D numerical model has been developed with an underlying V-shaped degradation response observed for pure collagen, which is capable of predicting arterial degradation through the incorporation of matrix content and a transmural gradient of collagen crimp. By incorporating matrix degradation, it is also possible to explain the differences found experimentally in the crude and purified collagenase studies. These findings offer substantial new insights into arterial degradation, with implications for the design and development of mechanical devices which treat diseased arteries.

Chapter 6 Pressure-Induced Degradation in Arterial Tissue: Experimental and Computational Investigation

6.1 Introduction

As we have seen in Section 2.7, many studies have investigated the strain and load depended degradation of collagen, however, relatively fewer studies have investigated the tissue level degradation response, particularly at physiologically relevant loads (Section 2.7.2). It has been suggested that the degradation response of collagen may also be influenced by moving from the nanoscale to the macroscale due to molecular, fibril and fibre sliding, unfolding, reorientation and straightening (Willett, Labow and Lee, 2008; Chang *et al.*, 2012; Chang and Buehler, 2014; Gaul *et al.*, 2018). Similarly, packing of collagen molecules into fibrils and fibres may influence the degradation response further by increasing the thermal stability of the collagen (Miles and Ghelashvili, 1999; Willett, Labow and Lee, 2008). Understanding the physiologically relevant tissue scale response is critical in understanding and treating diseases, which if left unchecked, may lead to an adverse clinical event (Thompson, Geraghty and Lee, 2002).

Like existing molecular and fibril scale studies, tissue scale studies have identified conflicting findings as to whether strain enhances (Ellsmere, Khanna and Michael Lee, 1999; Willett, Labow and Lee, 2008) or inhibits (Nabeshima *et al.*, 1996; Ruberti and Hallab, 2005; Lotz *et al.*, 2008; Wyatt, Bourne and Torzilli, 2009; Zareian *et al.*, 2010; Robitaille *et al.*, 2011) collagen degradation or whether a combination of both occur (Ghazanfari, A. Driessen-Mol, *et al.*, 2016; Yi *et al.*, 2016; Gaul *et al.*, 2018). The work carried out in Chapter 5 (Gaul *et al.*, 2018), supports the existence of a V-shaped degradation response in arterial collagen which is partially masked at the tissue scale due to the mechanical contribution of the non-collagenous matrix and a gradient of collagen fibre crimp through the wall thickness. In addition, this response was supported by a 1D numerical model

capable of accurately explaining the experimental results. However, these findings were determined in excised dogbone specimen with an altered gradient of collagen fibre crimp and without the residual stresses which are present in physiologically relevant native vessel geometries. Unlike the 1D numerical model, a number of models in literature have also used a 3D computational framework, allowing them to model physiologically relevant conditions (Loerakker, Obbink-Huizer and Baaijens, 2013) and even disease development (Grytz *et al.*, 2012; Loerakker, Ristori and Baaijens, 2016).

Motivated by the findings arising from Chapters 3-5, the aim of this study is to determine the strain-dependent degradation response of intact arterial vessels at physiologically relevant blood pressures. To achieve this, the study had the following specific aims; 1) to investigate the creep response of vessels as they degrade in the presence of collagenase at constant pressures, 2) to develop a 3D finite element model based on the findings in Chapter 5 (Gaul *et al.*, 2018), to explain the experimental creep data and 3) to investigate a case study on the potential role of strain-dependent collagen degradation in aneurysm development in an idealised vessel geometry.

6.2 Methods

6.2.1 Tissue preparation

Fresh porcine common carotid arteries were excised from 6-month-old Large White pigs (n = 30) weighing approximately 80 kg at the time of slaughter. Excised carotid arteries were frozen to -80°C at a controlled rate of -1°C/min in a cryoprotectant to maintain mechanical and structural properties during storage (Müller-Schweinitzer, 2009). Prior to testing, vessels were thawed in a water bath at 37°C to minimise tissue damage (Pegg, Wusteman and Boylan, 1997), washed in PBS to remove any residual cryoprotectant and cut to approximately 30 mm in length for testing. Loose adventitial and connective tissue was carefully removed using a forceps and scalpel, facilitating accurate strain measurements and structural analysis during testing. Each specimen was then cannulated using nylon barbs and tied using nylon thread. A random speckle pattern which is required for digital image correlation (DIC) strain analysis was then applied

using black alkyd resin spray paint from a distance of approximately 70 cm. Unlike ink dots that are often applied directly to tissue for strain tracking which can dehydrate the tissue, spray paint ink is effectively dry as it lands on the tissue, minimising potential tissue dehydration which may influence mechanical results. To mitigate the risk of pattern disruption during testing, the following procedure was performed: 1) sample was blotted dry, 2) speckle pattern was applied, 3) loose paint flakes were blotted off with tissue, 4) sample was placed in PBS to wash off any other loose paint flakes, 5) sample was blotted one final time to remove any remaining loose flakes before testing.

6.2.2 Pressure inflation – degradation tests

To assess the structural response of intact vessels to collagen degradation, pressure inflation tests were carried out in the presence of purified bacterial collagenase (400 U/ml; Worthington Biochemical, USA). Briefly, one end of the cannulated vessel was connected to a PID controlled syringe pump and the other end was connected to a slider and sealed with a cap. The slider end piece, which sits into a guide rail, allowed free expansion of the vessel in the axial Z direction, minimising rigid body motion and aiding the DIC analysis. A pressure transducer was then inserted through a valve fitting allowing for pressure feedback control as the vessel degrades. Once connected, the vessel was placed in a temperature-controlled water bath at 37°C. Purified bacterial collagenase in PBS supplemented with calcium and magnesium (D8662; Sigma-Aldrich, Ireland) was added to both the syringe and the water bath. Each specimen was then pressurised to a set pressure and allowed to degrade to the point of vessel rupture or emptying of the collagenase filled syringe (16 ml). Fluid seeps through the tissue due to vessel permeability which also increases with degradation. Vessels were pressurised from 60 mmHg to 180 mmHg in 40 mmHg increments to determine vessel degradation across a large physiological pressure range. The experimental setup is depicted in Figure 6.1. Three specimens were tested at each pressure in the presence of collagenase, while one control vessel was evaluated at each pressure in the absence of collagenase to confirm vessel rupture does not occur in native tissue across the pressure range tested. Additionally, separate pressure-diameter curves were determined across 5 vessels for model calibration.

The pressure feedback system was controlled via LabVIEW (National Instruments, Berkshire, UK).

6.2.3 Pressure failure tests

To thoroughly investigate the degradation response at low pressures, where minimal expansion occurs, an additional set of pressure inflation experiments were carried out in a similar fashion to those outlined above. Vessels were first pressurised in purified bacterial collagenase to either 60 mmHg or 100 mmHg for 45 minutes to allow for collagen degradation differences to emerge. Vessel pressure was then removed before a pressure of 180 mmHg was reapplied. The time to failure was subsequently recorded. These tests allowed for experimental evaluation of whether a strain induced protection mechanism exists at a healthy physiological pressure (100 mmHg), which would lead to an increased time to failure.

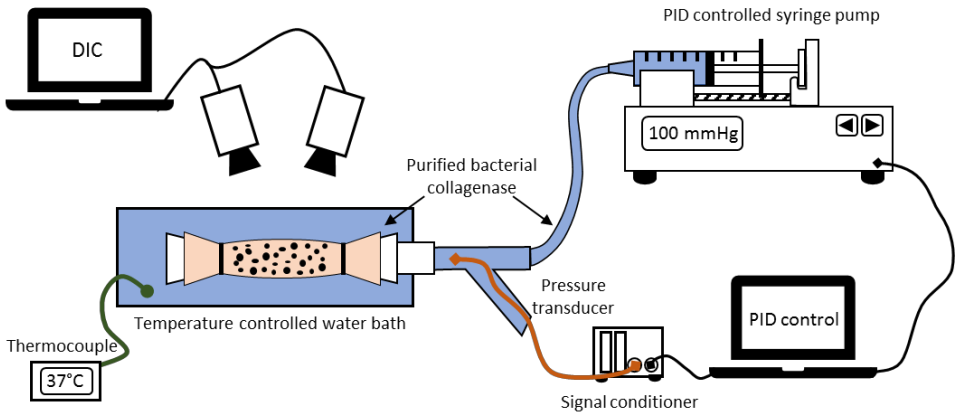

Figure 6.1 - Schematic showing experimental setup consisting of a PID controlled pressure pump to maintain constant pressure during vessel degradation. Vessel degradation is measured through DIC analysis of a speckle pattern on the artery surface throughout degradation in a temperature-controlled water bath containing purified bacterial collagenase.

6.2.4 Strain measurement

Strain was tracked throughout degradation using a commercially available 2 camera DIC system (Dantec Dynamics, Ulm, Germany), allowing for 3D strain displacement mapping (Figure 6.2). Prior to testing, the system was calibrated in a water bath at the correct focal distances to mimic testing conditions. Calibration was achieved through the successive tilting and rotation of a commercially

supplied checkerboard pattern to determine the distances and angles between both cameras as well as the cameras and the sample. Once calibrated, the experimental setup was placed beneath the camera setup for final adjustment. Fine tune adjustments were made to the camera through the aperture and focal rings on the camera lenses. Once tuned, a recording procedure was set up to take images at a frequency 5 Hz to capture the initial rapid vessel expansion. The recording frequency was incrementally reduced over the course of the experiment until reaching 0.0166 Hz, corresponding to the acquisition of an image every 1 minute to reduce the amount of data acquired. Circumferential strain was calculated within the software with a cubic spline smoothing filter applied using recommended values supplied by the company (Grid Reduction = 2, Smoothing Factor = 0). After testing, circumferential strain data was exported and post-processed in Matlab (MathWorks, Cambridge, UK) to determine the mean rate of change in circumference as the vessel degrades at a given pressure. A selection of DIC results were compared with vessel diameter measurements as well as speckle displacement results in ImageJ to validate the DIC results obtained. The wall thickness of all vessels was recorded using a measuring microscope with a micrometre stage pre- (918.7 ± 26.4 (111.8) μm) and post-degradation (672.7 ± 31.2 (132.5) μm). Dimensions are expressed as mean ± SEM (SD).

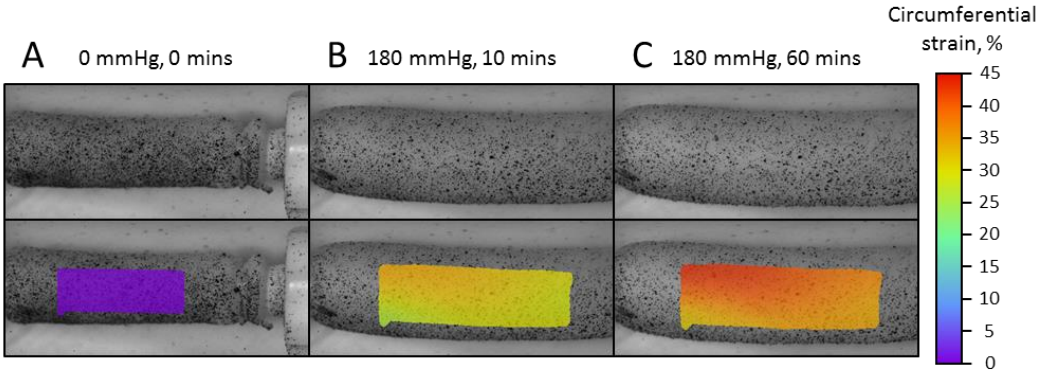

Figure 6.2 - Representative images of DIC analysis carried out on vessels in purified bacterial collagenase A) unpressurised at 0 minutes, B) pressurised to 180 mmHg at 10 minutes and C) pressurised to 180mmHg at 60 minutes. Top panel shows raw data images, bottom panel shows DIC measured circumferential strain overlaid.

6.2.5 Histological processing

Degraded vessel sections and undegraded adjacent sections of the vessel were processed for histology to confirm collagen degradation. All samples were fixed in 10% formalin overnight at 4°C, dehydrated in a graded series of ethanol baths (EtOH), cleared in xylene before being embedded in paraffin wax. The resulting paraffin-embedded samples were sectioned at 8 μm using a microtome (RM-2125RT, LEICA, Germany) and affixed to microscope slides. Slides were stained with picrosirius red and viewed under polarised light to evaluate collagen degradation. Picrosirius red enhances the natural birefringence of collagen allowing one to only see collagen when viewed under polarised light (Figure 6.3) (Junqueira, Bignolas and Brentani, 1979).

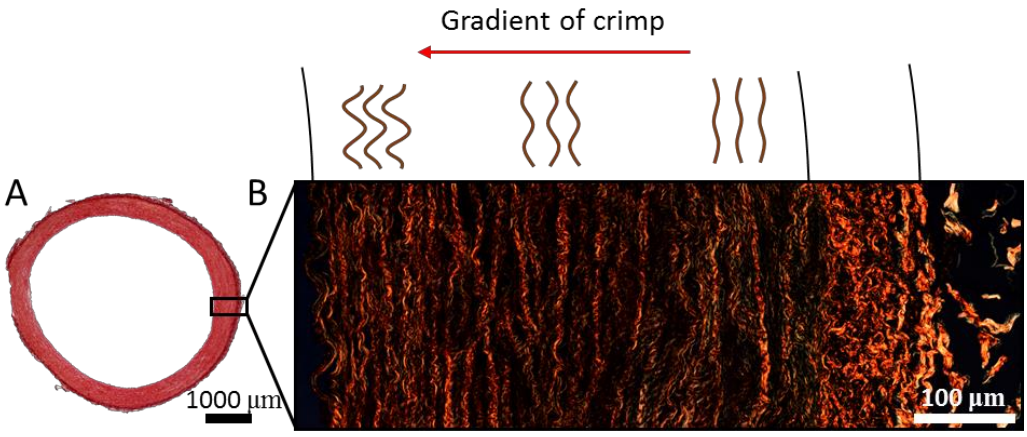

Figure 6.3 - Histological image of picrosirius red stained artery cross section viewed under A) light at 2x and B) polarised light at 40x showing a gradient of collagen fibre crimp through the thickness of an unpressurised vessel with the greatest crimp observed at the inner luminal surface. Undulation is also seen to increase in the adventitial layer which is removed during the current experiments.

6.2.6 Model development & Calibration

To model vessel degradation under constant pressure, the previously developed 1D numerical degradation model outlined in Section 5.5 was used (Gaul *et al.*, 2018) and adapted it for use in 3D finite element simulations. The model consists of an anisotropic collagen fibre component and an isotropic non-collagenous matrix component accounting for constituents such as elastin, glycosaminoglycans and the passive response of smooth muscle cells. A more thorough description of the model can be found in Section 5.5 (Gaul *et al.*, 2018).

The total stress, σ_T is given by the sum of collagen fibre stress and matrix stress which are weighted by their volume fractions ϕ_f and ϕ_m, respectively. These volume fractions sum to unity as before.

$$\sigma_t = \sigma_f + \sigma_m \tag{6.1}$$

Collagen fibre crimp which can be seen experimentally in unpressurised arteries (Figure 6.7), is modelled by a multiplicative split of the total stretch, λ_t into a collagen fibre stretch component, λ_f and a prestretch component, λ_p defined in Equation 5.3 (page 112). Like before, collagen fibres are crimped in the initial configuration if $\lambda_p > 1$, such that a $\lambda_f < 1$ emerges. Importantly, collagen fibres are assumed to only bear load in tension and thus, do not contribute to the stress until $\lambda_f > 1$.

Unlike the previous degradation model in Section 5.5 (Gaul *et al.*, 2018), and more similar to (Loerakker, Obbink-Huizer and Baaijens, 2013), collagen fibres have an exponential stress-stretch relationship as proposed by Driessen *et al.* (Driessen *et al.*, 2007) which was scaled by the collagen volume fraction:

$$\sigma_f = \phi_f \, k_1(\lambda_f)^2(e^{k_2\left((\lambda_f)^2-1\right)} - 1), \qquad \lambda_f \geq 1 \tag{6.2}$$

where ϕ_f is the collagen volume fraction, k_1 and k_2 are collagen fibre stiffness parameters calibrated to experimental data, and λ_f is the collagen fibre stretch for a given tissue stretch, λ_t, defined in Equation 5.3 (page 112).

The non-collagenous matrix contribution to the total stress was modelled using a Neo-Hookean material and scaled by its volume fraction:

$$\sigma_m = \phi_m(\kappa \frac{\ln(J)}{J} I + \frac{G}{J}(B - J^{2/3} I)), \tag{6.3}$$

where ϕ_m is the non-collagenous matrix volume fraction, $J = \det(F)$, $B = F \cdot F^T$ and κ and G are the bulk and shear modulus, respectively.

6.2.6.1 Stress degradation

Collagen degradation was modelled by reducing the collagen volume fraction over time based on the collagen fibre stretch using the first order rate equation in

Equation 5.6 (page 114). Unlike in Chapter 5, only collagen volume was reduced while matrix content was maintained here.

As the collagen volume fraction reduces, so too does the collagen stress contribution as outlined in Equation 6.2. Collagen degradation was described by a V-shaped degradation profile based on the findings in Chapter 5 (Gaul *et al.*, 2018) and findings in literature (Huang and Yannas, 1977; Ghazanfari, A. Driessen-Mol, *et al.*, 2016; Yi *et al.*, 2016), where stretch initially reduces the degradation rate before degradation once again increases above a protective stretch threshold (Figure 5.7, page 113). This V-shaped profile was captured using the smoothed bilinear function outlined in Equation 5.7 (page 114), with three domains; low strain, transition strain, and high strain (O'Connor *et al.*, 2017). As the volume fraction of collagen, ϕ_f, decreases so too does its respective stress (Equation 5.10, page 115).

6.2.6.2 Prestretch gradient

Previously in Section 5.5.3, the gradient of prestretch was iteratively determined based on experimental findings (Gaul *et al.*, 2018), however, in the current study, this gradient was set up to emerge naturally across the vessel wall. To achieve this, it was hypothesised that the gradient of collagen fibre crimp is minimised and is in a strain protection region at physiological pressure (100 mmHg/13 kPa). To determine the crimp gradient in the unpressurised state based on this hypothesis, the following process was carried out:

1. Assign arbitrary material parameters to an idealised vessel.
2. Apply a displacement boundary condition to achieve the circumferential strain experienced experimentally at 100 mmHg (i.e. 20%, see Figure 6.5).
3. Optimise the initial prestretch, λ_p across the wall thickness of the undeformed configuration to minimise the gradient of fibre stretch, λ_f around the collagen strain protection region (approximately 17%, Figure 5.7, page 113 (Gaul *et al.*, 2018)) in the deformed, pressurised configuration.
4. Calibrate the material properties from experimental pressure-strain measurements using the optimised prestretch, λ_p.

This process is shown schematically in Figure 6.4.

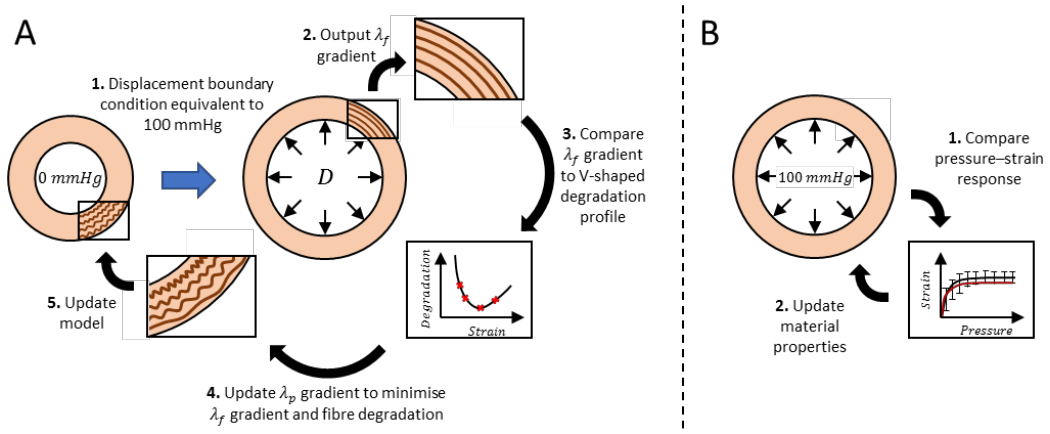

Figure 6.4 - Schematic showing A) calibration of the undeformed prestretch gradient by minimising the difference between the gradient of crimp occurring at a physiological strain magnitude and the strain at which collagen is protected from degradation (approximately 17%). Once minimised, B) material properties are calibrated based on experimental pressure inflation curves.

6.2.6.3 Model calibration

The values obtained for collagen and matrix volume fraction ($\phi_f = 42\%$, $\phi_m = 58\%$) were determined previously for Chapter 5 in Appendix C (Gaul *et al.*, 2018) and are also supported by literature (Fischer and Llaurado, 1966; de Figueiredo Borges *et al.*, 2008; Tsamis, Krawiec and Vorp, 2013). The material properties of the vessel wall were calibrated from experimental pressure diameter curves shown in Figure 6.5 after the gradient of fibre prestretch, λ_p through the vessel wall was set (Section 6.2.6.2 above). Briefly, the neo-Hookean non-collagenous matrix material was calibrated from experimental data at 60 mmHg where minimal collagen was judged to be contributing to the load. This assumption was based on experimental pressure degradation observations and histological evaluation of low pressure samples, where minimal vessel expansion was observed during collagen degradation (Figure 6.6 and Figure 6.7). Once calibrated, the anisotropic portion of the model was calibrated to experimental pressure-diameter curves by optimising k_1 and k_2, to reduce the error between the experimental and computational pressure-diameter curves, as shown in Figure 6.5. The V-shaped degradation response was defined using a stepwise smoothed bilinear function and is described in detail in Section 5.5.2 on page 114

(Gaul *et al.*, 2018). The parameters used in all simulations can be found in Table 6.1.

6.2.6.4 In-silico pressure inflation – degradation tests

To predict the pressure inflation-degradation experiments, the degradation model was applied to an idealised quarter model of a cylindrical vessel geometry of similar dimensions to experimentally tested samples (inner radius $R_i = 2\,mm$, outer radius $R_o = 3\,mm$, length $l = 0.5\,mm$, C3D20RH elements). Symmetry boundary conditions were applied to both circumferential side faces. The axial faces of the vessel were kept parallel using a constraint equation, mimicking the experimental setup described above and preventing convergence issues as the vessel degrades at different rates through its thickness. An internal luminal pressure was then applied and held constant to mimic the experimental setup. Degradation was allowed to occur only after full expansion of the vessel under pressure. Circumferential strain was exported and plotted against time during degradation for each pressure allowing for comparisons to be drawn with experimental data. The model was implemented using a user-defined subroutine (UMAT) in the commercial finite element software, Abaqus (Dassault Systèmes Simulia corporations, Vèlizy-Villacoublay, France).

6.2.6.5 Degradation case study: Aneurysm progression

Finally, the model was applied to an idealised vessel to investigate the possible role that strain-dependent collagen degradation plays in degenerative arterial disease such as aneurysm progression. To achieve this, an idealised geometry was created using a vessel with the same healthy inner and outer radius as before and with a reduced vessel thickness mid-way along the vessel segment (length $l = 20\,mm$). Vessel thickness was gradually reduced by 0.25 mm along the central 10 mm portion of the vessel to act as the site of initial aneurysm development. This reduction in thickness served as a location of increased wall strain which may arise due to a reduction in elastin content which has been linked to aneurysm formation (Thompson, Geraghty and Lee, 2002). Cyclic and axial symmetry boundary conditions allowed 1/8 of the idealised vessel to be modelled. A

Table 6.1 - Parameters used in the current model.

Model component	Parameter	Value	Source
Vessel setup	ϕ_f	0.42	(Gaul *et al.*, 2018)
	ϕ_m	0.58	(Gaul *et al.*, 2018)
	λ_p^{min}	1.01	Calibrated
	λ_p^{max}	1.19	Calibrated
	$R_i\ (mm)$	2.00	Idealised
	$R_o\ (mm)$	3.00	Idealised
	$l\ (mm)$	0.5	Idealised
Material properties	E (MPa)	0.20	Calibrated
	k_1 (kPa)	2.14	Calibrated
	k_2	7.56	Calibrated
Collagen degradation	ε_{t1}^D	0.08	(Gaul *et al.*, 2018)
	ε_{t2}^D	0.23	(Gaul *et al.*, 2018)
	$D_l\ (ms^{-1})$	-1.50	(Gaul *et al.*, 2018)
	$D_h\ (ms^{-1})$	0.75	(Gaul *et al.*, 2018)
	$D_c\ (ms^{-1})$	0.21	(Gaul *et al.*, 2018)

physiological pressure of 100 mmHg (13 Kpa) was applied to the internal luminal surface and degradation was monitored across the full vessel over time.

6.3 Results

6.3.1 Model calibration

Experimental pressure inflation experiments of vessels found a logarithmic type response with circumferential strain plateauing at approximately 25% strain with increasing pressure (Figure 6.5). A very close fit was achieved between the calibrated model and the experimental data mean with a RMSE of 0.86% strain. As anticipated with biological tissue, however, considerable sample variability is observable with circumferential strain ranging from 18.98% to 33.37% at 180 mmHg.

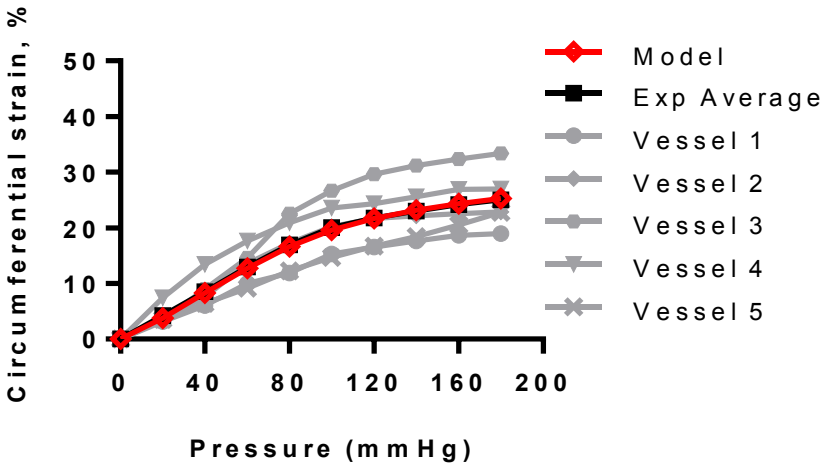

Figure 6.5 – Pressure-inflation curves for porcine carotid arteries and the calibrated FE model. Individual vessels are shown in light grey with the average for each pressure shown in black. The pressure-inflation response of the model is shown in red.

6.3.2 Experimental degradation curves

Pressure inflation-degradation experiments showed significant vessel creep with increasing pressure leading to vessel rupture at higher pressures (Figure 6.6A).

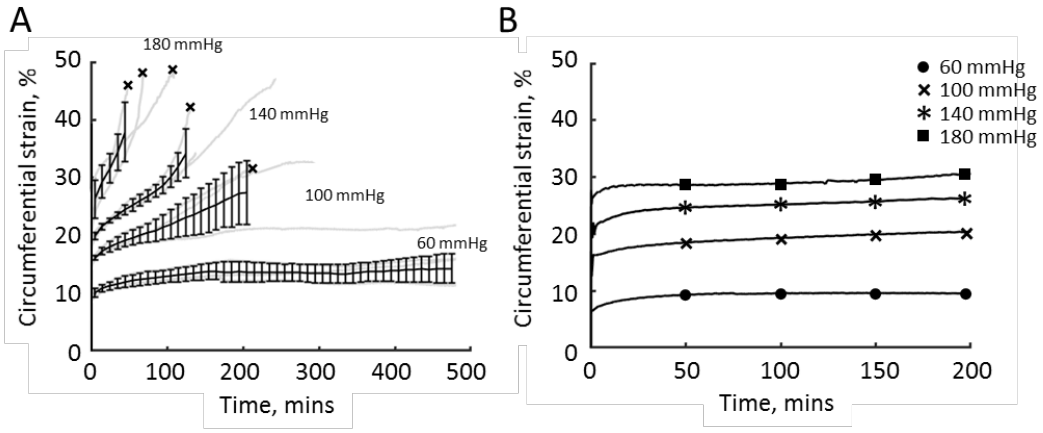

Figure 6.6 - Experimental pressure-inflation response over time of A) vessels in purified bacterial collagenase (n=3) and B) control vessels in PBS (n=1). Noticeable creep can be observed in the degradation case, particularly at high pressures. Control vessels show minimal expansion after the initial creep response within the first 20 minutes. Individual vessels are plotted in grey while the mean response per pressure is shown in black alongside error bars of SD. Vessels which failed through rupture are marked with an x.

Vessel experiencing 180 mmHg showed the highest rate of creep while no significant creep was observed in vessels experiencing 60 mmHg despite complete collagen degradation (Figure 6.7). Vessels which did not reach the 8 hours end time of the experiment failed through either vessel rupture or loss of finite pressurisation fluid (collagenase) due to increased vessel permeability during degradation. Vessels which failed through rupture are indicated symbolically in Figure 6.6A. Significant reductions in vessel thickness were also observed post degradation using a paired t-test (918.7 ± 26.4 (111.8) μm vs. 672.7 ± 31.2 (132.5) μm, $p<0.0001$).

Experimental pressure inflation experiments for undegraded control vessels show no significant creep occurring with increasing time in comparison to collagenase treated vessels (Figure 6.6B). Control vessels were found to reach approximately 90% of their final circumferential strain within 20 minutes of pressurisation. No vessel failure was observed.

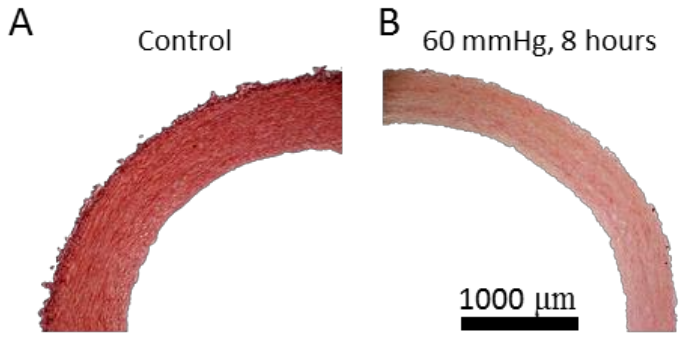

Figure 6.7 Histological images of picrosirius red stained artery cross sections at 4x magnification for A) a control vessel and B) a vessel subjected to 60 mmHg in the presence of collagenase showing complete collagen degradation. Collagen shows as dark red. Despite complete collagen degradation, no significant vessel expansion is found in Figure 6.6.

6.3.3 Pressure failure tests

Vessels experiencing 100 mmHg prior to pressurising to 180 mmHg exhibited significantly longer ($p<0.05$) failure times compared to those experiencing an initial 60 mmHg. This longer failure time suggests a strain induced protection mechanism occurs at 100 mmHg (Figure 6.8). Failure time analysis provides additional insight which is not visible in Figure 6.6. No trend was found in vessel strain across samples. One outlier as determined through a Grubbs outlier test

(alpha = 0.05) was removed from the 100/180 mmHg dataset, although this did not affect statistical significance. Complete data set including the outlier measurement is shown in Appendix D.

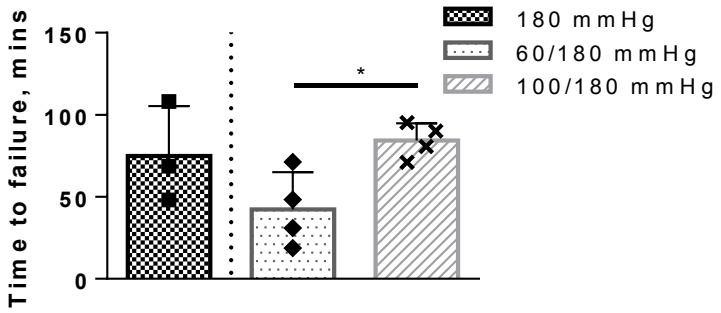

Figure 6.8 - Time to failure for specimen experiencing 180 mmHg only (n=3, Figure 6.6A) as well as those which were initially pressurised to 60 mmHg or 100 mmHg for 45 minutes before a high pressure of 180 mmHg was applied until vessel failure (n=4). Vessels initially experiencing 100 mmHg initially show increased time to failure suggesting slower initial degradation i.e. protection.

6.3.4 Model degradation

A similar degradation creep response was found through the computational model, with the highest rate of creep occurring at 180 mmHg (Figure 6.9). The

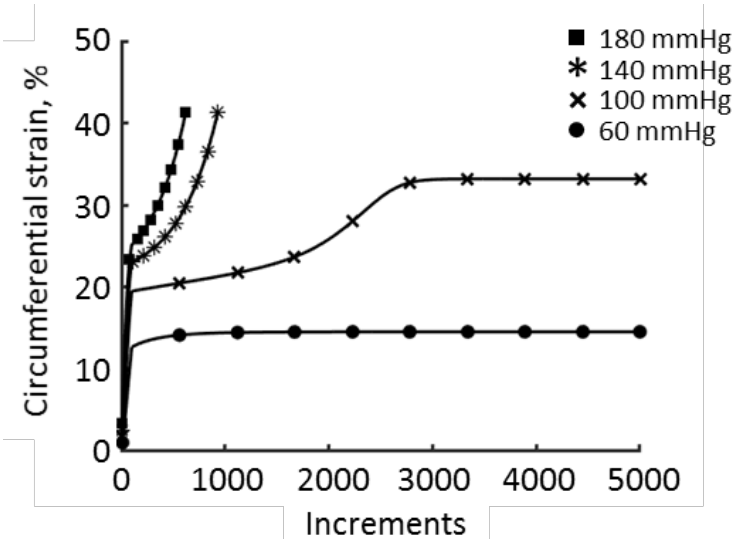

Figure 6.9 - Computational pressure-inflation response of degrading vessels at 60, 100, 140 and 180 mmHg. Noticeable creep can be observed as vessels degrade, particularly at high pressures.

model also found minimal creep occurring at 60 mmHg as observed experimentally despite a high rate of collagen degradation. Slight differences can be seen with the rate of expansion predicted by the model and that observed experimentally, which may arise due to a number of factors including the influence of diffusion at different experimental pressures. The 100 mmHg condition can be observed to level off at approximately 33% circumferential strain as the collagen volume fraction reduces to 0% and the intraluminal pressure is borne by the non-collagenous matrix alone. Representative images of these simulations are shown for 100 mmHg in Figure 6.10.

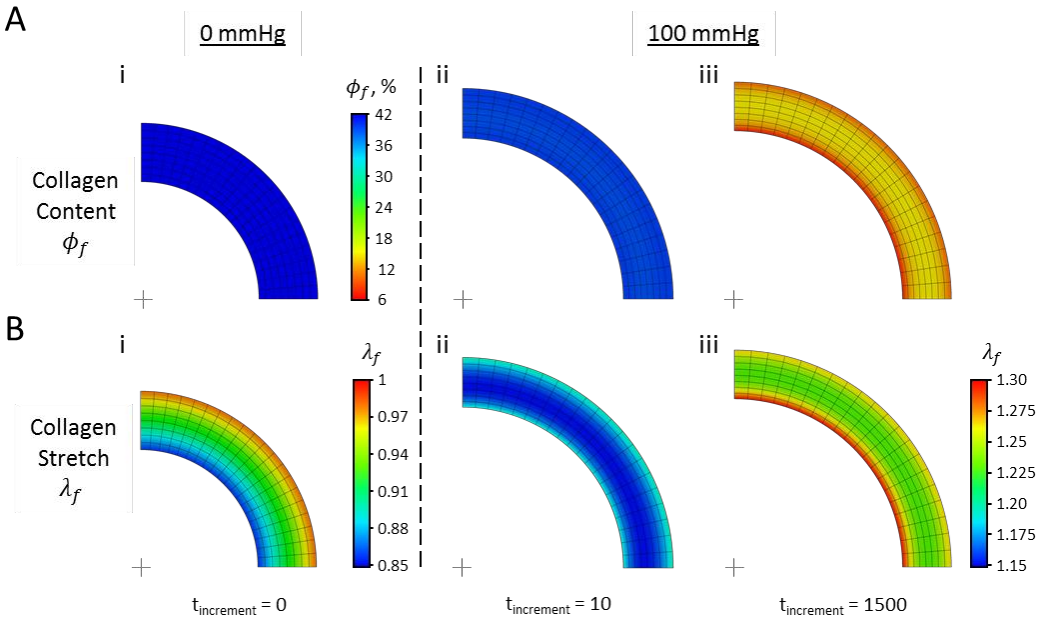

Figure 6.10 - A) collagen content and B) collagen fibre stretch are shown at i) 0 mmHg and ii) 100 mmHg prior to degradation and iii) 100 mmHg after degradation at increment 1500. At 100 mmHg before degradation, the gradient of collagen fibre stretch is minimised about the 17% protection strain. As the vessel degrades, vessel stretch and consequently fibre stretch increases leading to further degradation. Note change of legend for collagen stretch at 100 mmHg.

6.3.5 Degradation case study: Aneurysm progression

The model also predicted aneurysm growth occurring in an idealised vessel due to an initial flaw which was prescribed by a slight thinning (0.25 mm) of the vessel wall midway along the vessel's length (Figure 6.11). This thinning led to a higher initial circumferential strain, stimulating a higher rate of degradation. This increase in degradation reduces the vessel's stiffness, allowing for further

expansion and subsequent degradation through positive feedback. Consequently, the rate of degradation, resulting in vessel expansion can be observed to accelerate at a greater rate proximally to the aneurysm compared to distally (Figure 6.11B). This is further illustrated in Figure 6.11C, which shows the outer diameter of the vessel at increasing time points, with the greatest increase occurring at the site of the initial vessel flaw.

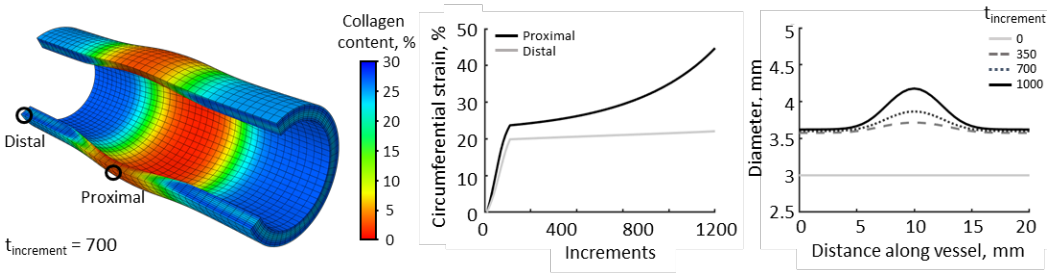

Figure 6.11 - A) Idealised vessel showing the development of an aneurysm through a reduction in collagen content at regions experiencing high strain. B) The rate of strain increase can be seen to be larger proximal to the aneurysm due to a reduction in collagen content. C) Changes in vessel outer diameter along the vessel length, showing aneurysm development over time.

6.4 Discussion

Degradation of structurally significant collagen fibres is a critical process in healthy arterial remodelling; however, excessive degradation could potentially compromise vessel integrity leading to the development of progressive, degenerative disease. The objective of this study was to investigate the degradation response of intact arterial vessels at physiologically relevant pressures using a combination of experimental and computational approaches. These findings were then applied to a simple case study investigating a potential means of aneurysm growth through strain-dependent collagen degradation.

Increasing vessel pressure resulted in an increased initial circumferential strain, an increased rate of vessel creep and a reduced time to failure across collagenase treated vessels (Figure 6.6). Ostensibly, these findings bear similarities to previous creep studies on collagenase treated bovine pericardium which found a reduced time to failure with increasing load (Ellsmere, Khanna and Michael Lee, 1999). Unlike these findings, a higher initial rate of creep is observed in bovine

pericardium experiencing low loads. These differences may be attributed to the greater influence of the non-collagenous matrix in arterial tissue which is the dominant load-bearing constituent at low-pressure (Roach and Burton, 1957). This matrix response masks the underlying degradation response of collagen. Consequently, the low pressure condition (60 mmHg) which was assumed to have a high rate of collagen degradation (Gaul *et al.*, 2018), exhibited minimal degradation induced creep and consequently, no tissue level failure. Histological analysis of these vessels also confirmed complete collagen degradation (see Figure 6.7), suggesting that the non-collagenous matrix prevents further vessel expansion at low pressures even in the absence of collagen. This hypothesis is supported by Figure 6.5 which shows a linear strain-pressure response up to 80 mmHg, suggesting that collagen doesn't contribute significantly up to this pressure. The increased rate of degradation at low pressures was also demonstrated through the pressure failure tests in Figure 6.8. The reduced time to failure in the 60-180 mmHg case compared to the 100-180 mmHg case, suggests that a higher degradation rate occurs at 60 mmHg when compared to 100 mmHg. Extending these findings to *in vivo* conditions suggests that although degradation may be elevated in low-pressure environments, tissue failure is unlikely unless high pressure and consequently increased strain conditions develop. This response may also contribute to the increased risk of adverse clinical cardiovascular events associated with hypertension (WHO, 2014).

The complementary computational model, calibrated from independent experimental data, was found to predict a similar degradation response occurring at each pressure (Figure 6.6). The model supported experimental observations that minimal vessel expansion occurs with collagen degradation at 60 mmHg due to the stiffness of the non-collagenous matrix. A similar response is also observed in the 100 mmHg model where strain plateaus as collagen is removed and pressure is borne by the non-collagenous matrix alone. This response is partially observed experimentally, with the two 100 mmHg tests found not to fail by rupture also displaying a plateauing at approximately 200 minutes. A similar non-collagenous matrix influence was reported in Chapter 5 occurring in flat dogbone specimens of arterial tissue which masked an underlying V-shaped collagen degradation response (Gaul *et al.*, 2018). Interestingly, a number of

studies have found a V-shaped degradation response occurring at the tissue level (Ghazanfari, A. Driessen-Mol, *et al.*, 2016; Yi *et al.*, 2016). This observation suggests that the non-collagenous matrix has a reduced mechanical contribution at low strains in these tissues and does not mask the underlying collagen degradation response. Although the same trend in degradation was found between the model and experimental results, the rate at which degradation occurs was found to differ slightly. These differences are likely influenced by a number of factors including sample variability which was noted in Figure 6.5. A second factor potentially influencing these results is the rate of collagenase diffusion through the artery wall at each pressure condition (Zareian *et al.*, 2010). Converting the increments on the x axis of Figure 6.9 into time results in a much slower degradation response (approximately 8 times slower) to what was found experimentally in Figure 6.6. Unfortunately, determining a diffusion scaling factor is also not straightforward as each data set experiences a different internal pressure and consequently, a different rate of diffusion. As a result, a unique and somewhat artificial scaling factor would be required for each data set with minimal experimental basis. The influence of diffusion is also highlighted histologically when comparing the timeframes required to investigate degradation with and without pressure (see Appendix D). Additional failure modes other than fibre degradation such as fibre rupture are also likely to occur at increasing pressures and may lead to further differences between experimental and computational results.

Finally, the fundamental insights into strain-dependent collagen degradation acquired here and in the proceeding studies, were applied to explore its potential role in progressive degenerative disease. Strain-dependent collagen degradation was identified as a potential cause of aneurysm development through a positive feedback loop which leads to accelerated degradation and weakening at the site of aneurysm formation (Figure 6.11). Although similar degradation models have been employed to investigate valve retraction in tissue engineered heart valves (Loerakker, Ristori and Baaijens, 2016) and lamina cribrosa thickening in glaucoma (Grytz *et al.*, 2012), this is the first use of such a model for investigating arterial disease. In order to initiate aneurysm formation, an initial flaw is required which results in increased vessel expansion. It is important to note that

thinning of vessel wall only serves as a method of introducing a location of increased wall strain and may not be representative of *in vivo* aneurysm development. *In vivo*, this process could be initiated by the gradual age-related reduction in elastin content at specific location (Thompson, Geraghty and Lee, 2002) resulting in greater vessel and collagen strain at a given pressure. Elastin degradation may also influence wall thickness through the removal of non-collagenous extracellular material. Interestingly, elastin degradation has also been found to be a strain-dependent process (Jesudason *et al.*, 2010), which would further serve to accelerate aneurysm growth. Importantly, *in vivo* collagen degradation would also be accompanied by the production of new collagen (Thompson, Geraghty and Lee, 2002), which would aid in restabilising degenerative tissue. Unfortunately, if the rate of production is surpassed by degradation or if new collagen fibres are not laid down in tension, disease progression is likely to continue. This process may explain localised changes in tissue mechanics identified thoracic aortic mice aneurysms during aneurysm progression (Bersi *et al.*, 2018). Aneurysm development is strongly linked to inflammation which is associated with increased macrophage presence and consequently MMPs including MMP-1, -8, -9 as well as cysteine collagenases such as Cathespin K, L and S (Thompson, Geraghty and Lee, 2002; Abdul-Hussien *et al.*, 2007). Additionally, a reduction in collagenase inhibitors including TIMP-1 and Cystatin C have also been linked to aneurysm progression (Abdul-Hussien *et al.*, 2007). These factors may serve to further accelerate the potential role that strain-dependent degradation plays in aneurysm progression and rupture. In addition to investigating aneurysm formation, the current model may also provide insights into other fatal degenerative arterial diseases as well as complex vessel geometries and loading environments. Applying this model to other arterial diseases such as atherosclerosis may help identify vessels at risk of plaque rupture due to excessive degradation at sites of higher or low strain. Similarly, the current model may also aid in understanding the remodelling response caused by medical devices such as stents and prosthetic heart valves, which change the local mechanical environment of arterial collagen (Ghazanfari, Anita Driessen-Mol, *et al.*, 2016).

A limitation of the current study is the use of bacterial collagenase rather than physiologically relevant MMPs and cysteine collagenases which degrade collagen *in vivo* (Aikawa, 2004; Abdul-Hussien *et al.*, 2007). Bacterial collagenases also commonly contain non-specific enzymes which can influence the experimental degradation response; however, this was mitigated through the use of purified bacterial collagenase (Gaul *et al.*, 2018). Diffusion of the collagenase solution through the vessel wall is also likely to influence the rate of degradation observed (Zareian *et al.*, 2010), with accelerated diffusion occurring at higher pressures. Unfortunately, diffusion and pressure are intrinsically linked in the current experimental setup, with pressure dictating the strain experienced in the vessel wall. Computationally, a diffusion rate could be incorporated to account for these differences, although the current predictions are suitably accurate even without accounting for diffusion. Furthermore, diffusion would only serve to increase the accuracy of the model in predicting experimental data, with diffusion less physiologically relevant due to collagenase production occurring *in situ in vivo* (Aikawa, 2004). Finally, vessel variability is likely to influence the degradation response based on factors such as vessel diameter and tissue thickness as well as collagen and elastin content.

The results of the current study have identified, for the first time, the strain-dependent degradation response of intact arterial vessels at physiologically relevant pressures. These findings have expanded on existing work on flat dogbone arterial specimen, identifying a different tissue-level response occurring in the native arterial state. Increased rates of vessel expansion were only found to occur at high intraluminal pressures, despite an increased rate of collagen degradation also occurring at low vessel pressures. These findings highlight how arterial collagen strain may contribute to accelerated collagen degradation in aneurysm growth *in vivo* and may apply to other progressive degenerative vascular diseases.

Chapter 7 Final Discussion

With the number of CVD related deaths expected to rise by more than 26% to 22.2 million by 2030, improved screening methods and treatment strategies will be central to reducing the burden of CVD (WHO, 2014). Improving our understanding of cardiovascular biomechanics and mechanobiology is one approach which offers a potential pathway to achieving this goal of advanced screening and treatment. Remodelling of the structurally significant collagen fibre architecture is particularly important as collagen dictates the mechanical stability of healthy and diseased vessels (Roach and Burton, 1957; Thompson, Geraghty and Lee, 2002). Remodelling encompasses the reorientation, production and degradation of collagen, with the latter in particular, likely to play a major role in tissue instability (Thompson, Geraghty and Lee, 2002). Despite the importance of collagen fibre remodelling, the influence of the surrounding mechanical environment on remodelling remains largely unknown. The objective of this thesis was to explore the influence of mechanical stimuli on the reorganisation and degradation of arterial collagen, to gain fundamental insights into arterial remodelling. To achieve this, a combination of experimental and computational investigations were conducted to evaluate arterial remodelling, both structurally and mechanically.

Chapter 3 outlined the development of an optimised SALS system for arterial tissue and investigated its ability to measure fibre orientation and reorientation in response to load (Gaul, Nolan and Lally, 2017). A single family of circumferentially orientated collagen fibres was identified in the intimal and medial vessel layers which was supported by both PLM imaging and by literature (Sáez *et al.*, 2016). This architecture differs from that reported in many other vessels, whereby two or more fibre families were observed (Schriefl *et al.*, 2012). Variations in fibre orientation and alignment in response to load also highlight SALS ability to determine structural changes due to mechanical stimuli. This ability to non-destructively quantify structural changes also offers a means of investigating load induced remodelling responses. The findings which arise from

this work form the foundations of the studies which follow, where fibre orientation with respect to tissue loading direction was found to be key to establishing the degradation response of arterial collagen.

The investigation into collagen degradation in loaded arterial tissue using SALS in Chapter 4, found a strain-dependent degradation response. This was concluded through structural analysis whereby alignment was found to increase at intermediary strain magnitudes and reduce at high strain magnitudes. This result agrees with strain-dependent degradation responses identified in both pure collagen (Huang and Yannas, 1977) and other collagenous tissues (Ghazanfari, A. Driessen-Mol, *et al.*, 2016; Yi *et al.*, 2016). These results indicate that strain has an important influence on arterial remodelling; both accelerating and decelerating the rate of degradation in arterial collagen. The close link between the structural organisation of collagen fibres and the tissue's mechanical properties highlight the importance of these findings in tissue stability and performance. This preliminary study is the first to investigate strain-driven collagen degradation in arterial tissue. These structural findings also serve as the motivation for the subsequent studies carried out, which investigated the degradation response mechanically and numerically.

To extend the structural findings in Chapter 4, the biomechanical response of loaded dogbone specimens during degradation was investigated in Chapter 5. The study identified a unique stress degradation response which differs from any response reported in literature to-date. This response was explored through a series of stress relaxation experiments in the presence of crude and purified bacterial collagenase, where the rate of stress decay was calculated. A complementary numerical model was also developed to elucidate the complex response observed. Here, non-collagenous matrix material and a gradient of collagen fibre crimp were found to mask an underlying V-shaped collagen degradation response which was suggested in Chapter 4. This V-shaped degradation response, reported elsewhere (Huang and Yannas, 1977; Ghazanfari, A. Driessen-Mol, *et al.*, 2016; Yi *et al.*, 2016), may also serve to explain the seemingly conflicting findings reported in literature which suggest that strain increases (Ellsmere, Khanna and Michael Lee, 1999; Willett, Labow and Lee,

2008) or decreases (Bhole *et al.*, 2009; Wyatt, Bourne and Torzilli, 2009) collagen susceptibility to degradation. If an underlying V-shaped degradation exists for collagen, the application of strain initially slows degradation before increasing above a strain protective threshold. Consequently, testing across a large strain range is paramount to comprehensively investigate a tissue's degradation response. This V-shaped response was found to occur at similar strain magnitudes to those reported in other collagenous tissue (Ghazanfari, A. Driessen-Mol, *et al.*, 2016; Yi *et al.*, 2016), but much higher strains than those reported for pure collagen (Huang and Yannas, 1977). This observation also highlights the importance of considering the organisational hierarchy of collagen and collagenous tissues when evaluating remodelling responses. The underlying V-shaped degradation response may be one of the many biomechanical mechanisms employed to maintain equilibrium or homeostasis in collagenous tissues in vivo.

Having established that a strain-dependent degradation mechanism exists in arterial collagen, Chapter 6 extended this degradation investigation to a more physiologically relevant environment. Through a series of pressure inflation creep experiments at physiological pressures, the rate of vessel expansion due to degradation was calculated. As with Chapter 5, the findings arising from these experiments were not intuitive. Interestingly, a low rate of expansion occurred at low pressures, where degradation was expected to be elevated. These findings were explained by a complementary computational model, which identified that the non-collagenous matrix was capable of withstanding the low-pressure environment even in the absence of collagen. These findings were supported through a set of pressure-failure tests where vessels experiencing an initial low preload pressure failed earlier than those experiencing a healthy physiological preload pressure. This work further highlights the importance of computational models in explaining experimental results through the isolation of individual biomechanical factors. The clinical relevance of this work is illustrated through a simulation of aneurysm development due to collagen degradation. Vessels experiencing increased strain experience accelerated degradation of structurally significant collagen, resulting in further increases in strain. Unfortunately, this may lead to a runaway process through positive feedback, potentially explaining

late stage aneurysm progression (Thompson, Geraghty and Lee, 2002; Tsamis, Krawiec and Vorp, 2013). Likewise, accelerated degradation may also play a role in plaque weakening at locations experiencing hypo- or hyper-physiological strain. It's important to note that increased strain has also been linked with increased levels of collagen production which may offset collagen degradation (O'Callaghan and Williams, 2000; Ferdous, Jo and Nerem, 2011). However, if collagen production is unable to match the rate degradation, or if new collagen is not laid down in tension (i.e. uncrimped), it would permit further tissue expansion and potential tissue failure. This process would also facilitate aneurysm growth where no net change in collagen volume occurs, as also observed in the literature (Tsamis, Krawiec and Vorp, 2013).

To thoroughly evaluate strain-driven collagen remodelling in arterial tissue, this thesis combined structural, mechanical and computational analysis of arterial organisation and degradation. To achieve this, a SALS system was developed and optimised for arterial tissue, providing insights into the native vessel architecture. This system was then employed to investigate if a strain-dependent degradation response occurs in arterial tissue. To more comprehensively explore the response observed using SALS, extensive mechanical testing was carried out to characterise the tissue and collagen degradation response. A complementary numerical model was developed in parallel, informed by both literature and experimental structural results. This model was able to explain the unique mechanical response observed. Finally, this work was translated to a more physiologically relevant environment, where intact vessel geometries were investigated experimentally and computationally. The computational model was also employed to highlight how these findings may be implicated in disease development and progression. Applying this model to realistic vessel geometries and loading environments may also allow a greater understanding of arterial remodelling in vivo, and in particular, the development of other progressive degenerative diseases. The understanding arising from this work should now facilitate the development of new and improved screening techniques; where patients at risk of accelerated tissue degeneration could be identified and interventional measures taken at an early stage. This work can also assist in the design and development of new and existing medical devices such as stents.

Understanding the degradation response, due to changes in the mechanical environment, may facilitate the design of devices capable of slowing or even reversing maladaptive remodelling associated with disease. It is clear that extensive work is required to offset the expected rise in CVD over the coming years, however, a greater understanding of the role that biomechanics and mechanobiology play in disease development and treatment may provide a means to achieve this.

Chapter 8 Concluding Remarks

8.1 Summary of Key Findings

The objective of this thesis was to explore the influence of mechanical stimuli on arterial remodelling which was achieved through structural, mechanical and computational analysis. The key contributions to the field of biomechanics emanating from the research presented in this thesis are summarised below.

- An optimised SALS system was developed which was capable of non-destructively characterising collagen fibre architecture in intact layers of arterial tissue, highlighting it as a powerful method for elucidating collagen fibre remodelling.
- A strain-dependent structural degradation response was identified in arterial tissue using SALS. SALS identified increased fibre alignment occurring at intermediary tissue strains suggesting the existence of a collagen fibre protection mechanism.
- A unique strain-dependent degradation response was also identified in arterial tissue mechanically, through a series of stress relaxation experiments in bacterial collagenase. Markedly different degradation responses were observed depending on the collagenase type chosen, highlighting the importance of collagenase choice for future studies of strain-dependent collagen degradation.
- The development of a novel numerical degradation model identified an underlying V-shaped degradation response in arterial collagen which is masked at the tissue scale by a gradient of collagen fibre crimp and the mechanical contribution of the non-collagenous matrix.

- Further insights into arterial collagen degradation were determined in physiologically relevant intact arterial vessels under pressure. Vessels experiencing super-physiological pressure and consequently, strain, experienced an increased rate of vessel expansion and reduced time to failure. Despite experiencing elevated degradation at low pressure, the non-collagenous matrix was capable of withstanding vessel expansion at these low-pressure conditions. This low-pressure response may play a role in the reduced risk of adverse clinical events in hypotensive patients.
- Tthe strain protection mechanism identified was found to occur at approximately 17% fibre strain, corresponding to values found in other collagenous tissues but substantially higher than that found in pure collagen. This observation highlights the importance of considering collagen fibre hierarchy when investigating strain mediated degradation responses.
- Finally, the model highlighted how vessels experiencing elevated strain may be more susceptible to aneurysm development and progression through a positive feedback loop, potentially leading to a major adverse clinical event. This response may also play a role in other degenerative arterial diseases and in the biomechanical response to medical device deployment.

8.2 Future perspectives

The studies outlined in this thesis provide insight into the strain-driven remodelling response of arterial tissue through a combination of experimental and computational investigations. Motivated by these insights, the following recommendations are proposed for future investigations:

- The volume fraction of collagen during degradation could be assessed using a hydroxyproline assay or histological analysis at specific time points. This would provide additional support to the mechanical rate of degradation data. Furthermore, it could be used to assess the critical collagen volume fraction required, below which, rupture occurs.
- Future studies should also investigate the strain-dependent degradation response during dynamic loading, which has been shown to accelerate degradation in other tissues. This study would provide physiologically relevant data for incorporation into future degradation models.
- The current degradation model could also be applied to real vessel geometries to investigate remodelling in healthy, atherosclerotic and aneurysmal tissue. If this were to be coupled with a critical collagen volume criterion, it may also show promise as a future preclinical tool for identifying vessels at risk of rupture.
- The degradation model may also be expanded to incorporate more complex remodelling algorithms which include fibre reorientation and damage.
- As collagen fibre remodelling also incorporates production of new collagen which was beyond the scope of the current thesis, future work should investigate strain mediated collagen production. The findings of this work could provide critical information in the tissue remodelling process which could also be incorporated into the existing degradation model.

- The work completed to date could also be extended to diseased tissue such as atherosclerotic plaque acquired through carotid endarterectomy procedures. These results would help establish whether a similar degradation response is found in diseased atherosclerotic human tissue.
- Finally, a limitation of the current work is the use of bacterial collagenase as opposed to more physiologically relevant MMPs. Purified bacterial collagenase was used during this work to mitigate some of the potential issues with bacterial collagenase such as the lack of specificity outlined in Section 2.7.3. Despite this, it may be worth confirming whether a similar strain dependent degradation response occurs using these mammalian collagenases.

References

Abdul-Hussien, H., Soekhoe, R. G. V., Weber, E., von der Thüsen, J. H., Kleemann, R., Mulder, A., van Bockel, J. H., Hanemaaijer, R. and Lindeman, J. H. N. (2007) 'Collagen Degradation in the Abdominal Aneurysm', *The American Journal of Pathology*, 170(3), pp. 809–817. doi: 10.2353/ajpath.2007.060522.

Adhikari, A. S., Chai, J. and Dunn, A. R. (2011) 'Mechanical load induces a 100-fold increase in the rate of collagen proteolysis by MMP-1', *Journal of the American Chemical Society*, 133(6), pp. 1686–1689. doi: 10.1021/ja109972p.

Adhikari, A. S., Glassey, E. and Dunn, A. R. (2012) 'Conformational dynamics accompanying the proteolytic degradation of trimeric collagen I by collagenases', *Journal of the American Chemical Society*, 134(32), pp. 13259–13265. doi: 10.1021/ja212170b.

Adhikari, A. S., Mekhdjian, A. H. and Dunn, A. R. (2012) 'Strain tunes proteolytic degradation and diffusive transport in fibrin networks', *Biomacromolecules*, 13(2), pp. 499–506. doi: 10.1021/bm2015619.

Aikawa, M. (2004) 'Vascular biology of collagenases in vulnerable atherosclerotic plaques', *International Congress Series*, 1262, pp. 67–70. doi: 10.1016/j.ics.2003.12.056.

Aird, W. C. (2011) 'Discovery of the cardiovascular system: from Galen to William Harvey.', *Journal of thrombosis and haemostasis : JTH*, 9 Suppl 1, pp. 118–29. doi: 10.1111/j.1538-7836.2011.04312.x.

Akyildiz, A. C., Chai, C. K., Oomens, C. W. J., van der Lugt, A., Baaijens, F. P. T., Strijkers, G. J. and Gijsen, F. J. H. (2017) '3D Fiber Orientation in Atherosclerotic Carotid Plaques', *Journal of Structural Biology*. Elsevier, 200(1), pp. 28–35. doi: 10.1016/j.jsb.2017.08.003.

Andreoli, A. and Monteleone, M. (2001) 'Effects of different sports on bone density and muscle mass in highly trained athletes', *Medicine & Science in Sports & Exercise*, 33, pp. 507–511. Available at: http://digilander.libero.it/andreoli1/Densita ossea massa muscolare in atleti.pdf.

Balzani, D., Schröder, J. and Gross, D. (2006) 'Simulation of discontinuous damage incorporating residual stresses in circumferentially overstretched atherosclerotic arteries', *Acta Biomaterialia*, 2(6), pp. 609–618. doi: 10.1016/j.actbio.2006.06.005.

Bangalore, S., Kumar, S., Wetterslev, J., Bavry, A. A., Gluud, C., Cutlip, D. E. and Bhatt, D. L. (2011) 'Carotid Artery Stenting vs Carotid Endarterectomy', *Archives of Neurology*, 68(2), pp. 172–184. doi: 10.1001/archneurol.2010.262.

Baskin, R., Roos, K. and Yeh, Y. (1979) 'Light diffraction study of single skeletal muscle fibres', *Biophysical journal*, 28(1), pp. 45–64. doi: 10.1016/S0006-3495(79)85158-9.

Berens, P. (2009) 'CircStat : A MATLAB Toolbox for Circular Statistics', *Journal of Statistical Software*, 31(10), pp. 1–21. doi: 10.18637/jss.v031.i10.

Bersi, M. R., Bellini, C., Humphrey, J. D. and Avril, S. (2018) 'Local variations in material and structural properties characterize murine thoracic aortic aneurysm

mechanics', *Biomechanics and Modeling in Mechanobiology*. Springer Berlin Heidelberg. doi: 10.1007/s10237-018-1077-9.

Bhole, A. P., Flynn, B. P., Liles, M., Saeidi, N., Dimarzio, C. A. and Ruberti, J. W. (2009) 'Mechanical strain enhances survivability of collagen micronetworks in the presence of collagenase: implications for load-bearing matrix growth and stability', *Philosophical Transactions of the Royal Society A: Mathematical, Physical and Engineering Sciences*, 367(1902), pp. 3339–3362. doi: 10.1098/rsta.2009.0093.

Bickerstaff, L. K., Pairolero, P. C., Hollier, L. H., Melton, L. J., Van Peenen, H. J., Cherry, K. J., Joyce, J. W. and Lie, J. T. (1982) 'Thoracic aortic aneurysms: a population-based study', *Surgery*, 92(6), pp. 1103–1108. doi: 0039-6060(82)90174-X [pii].

Billiar, K. L. and Sacks, M. S. (2000) 'Biaxial mechanical properties of the native and glutaraldehyde-treated aortic valve cusp: Part II--A structural constitutive model.', *Journal of biomechanical engineering*, 122(4), pp. 327–335. doi: 10.1115/1.1287158.

Billiar, K. and Sacks, M. (1997) 'A method to quantify the fiber kinematics of planar tissues under biaxial stretch', *Journal of biomechanics*, 30(1), pp. 753–756. Available at: http://www.sciencedirect.com/science/article/pii/S0021929097000195 (Accessed: 17 September 2014).

Bouxsein, M. L., Boyd, S. K., Christiansen, B. A., Guldberg, R. E., Jepsen, K. J. and Müller, R. (2010) 'Guidelines for assessment of bone microstructure in rodents using micro-computed tomography', *Journal of Bone and Mineral Research*, 25(7), pp. 1468–1486. doi: 10.1002/jbmr.141.

Burke, A. P. (2002) 'Morphological Predictors of Arterial Remodeling in Coronary Atherosclerosis', *Circulation*, 105(3), pp. 297–303. doi: 10.1161/hc0302.102610.

Burton, A. (1962) 'Physical principles of circulatory phenomena: the physical equilibria of the heart and blood vessels', in *Handbook of physiology; a critical, comprehensive presentation of physiological knowledge and concepts*. Baltimore, pp. 85–106. Available at: http://scholar.google.com/scholar?hl=en&btnG=Search&q=intitle:physical+principles+of+circulatory+phenomena:+the+physical+equilibria+of+the+heart+and+blood+vessels#0 (Accessed: 22 October 2014).

Camp, R. J., Liles, M., Beale, J., Saeidi, N., Flynn, B. P., Moore, E., Murthy, S. K. and Ruberti, J. W. (2011) 'Molecular mechanochemistry: Low force switch slows enzymatic cleavage of human type I collagen monomer', *Journal of the American Chemical Society*, 133(11), pp. 4073–4078. doi: 10.1021/ja110098b.

Campbell, E. M., Cahill, P. A. and Lally, C. (2012) 'Investigation of a small-diameter decellularised artery as a potential scaffold for vascular tissue engineering; biomechanical evaluation and preliminary cell seeding', *Journal of the Mechanical Behavior of Biomedical Materials*. Elsevier, 14, pp. 130–142. doi: 10.1016/j.jmbbm.2012.06.001.

Campbell, G. M. and Sophocleous, A. (2014) 'Quantitative analysis of bone and soft tissue by micro-computed tomography: applications to ex vivo and in vivo studies', *BoneKEy Reports*. Nature Publishing Group, 3(February), pp. 1–12. doi: 10.1038/bonekey.2014.59.

Canham, P. B., Finlay, H. M., Dixon, J. G., Boughner, D. R. and Chen, A. (1989) 'Measurements from light and polarised light microscopy of human coronary arteries fixed at distending pressure', *Cardiovascular Research*, 23(11), pp. 973–982. doi:

10.1093/cvr/23.11.973.

Cavinato, C., Helfenstein-Didier, C., Olivier, T., du Roscoat, S. R., Laroche, N. and Badel, P. (2017) 'Biaxial loading of arterial tissues with 3D in situ observations of adventitia fibrous microstructure: A method coupling multi-photon confocal microscopy and bulge inflation test', *Journal of the Mechanical Behavior of Biomedical Materials*. Elsevier Ltd, 74(May), pp. 488–498. doi: 10.1016/j.jmbbm.2017.07.022.

Chaikof, E. L., Brewster, D. C., Dalman, R. L., Makaroun, M. S., Illig, K. A., Sicard, G. A., Timaran, C. H., Upchurch, G. R. and Veith, F. J. (2009) 'The care of patients with an abdominal aortic aneurysm: The Society for Vascular Surgery practice guidelines', *Journal of Vascular Surgery*. Elsevier Inc., 50(4), pp. S2–S49. doi: 10.1016/j.jvs.2009.07.002.

Chakhtoura, E. Y., Hobson, R. W., Goldstein, J., Simonian, G. T., Lal, B. K., Haser, P. B., Silva, M. B., Padberg, F. T., Pappas, P. J. and Jamil, Z. (2001) 'In-stent restenosis after carotid angioplasty-stenting: Incidence and management', *Journal of Vascular Surgery*, 33(2), pp. 220–226. doi: 10.1067/mva.2001.111880.

Chambless, L. E., Heiss, G., Folsom, A. R., Rosamond, W., Szklo, M., Sharrett, A. R. and Clegg, L. X. (1997) 'Association of Coronary Heart Disease Incidence with Carotid Arterial Wall Thickness and Major Risk Factors: The Atherosclerosis Risk in Communities (ARIC) Study, 1987-1993', *American Journal of Epidemiology*, 146(6), pp. 483–494. doi: 10.1093/oxfordjournals.aje.a009302.

Chang, S.-W. and Buehler, M. J. (2014) 'Molecular biomechanics of collagen molecules', *Materials Today*. Elsevier Ltd., 17(2), pp. 70–76. doi: 10.1016/j.mattod.2014.01.019.

Chang, S.-W., Flynn, B. P., Ruberti, J. W. and Buehler, M. J. (2012) 'Molecular mechanism of force induced stabilization of collagen against enzymatic breakdown', *Biomaterials*, 33(15), pp. 3852–3859. doi: 10.1016/j.biomaterials.2012.02.001.

Chen, H., Liu, Y., Slipchenko, M. N., Zhao, X., Cheng, J.-X. and Kassab, G. S. (2011) 'The layered structure of coronary adventitia under mechanical load.', *Biophysical journal*. Biophysical Society, 101(11), pp. 2555–62. doi: 10.1016/j.bpj.2011.10.043.

Chien, J. C. W. and Chang, E. P. (1972) 'Small-Angle Light Scattering of Reconstituted Collagen', *Macromolecules*, 5(5), pp. 610–617. doi: 10.1021/ma60029a016.

Chung, L., Dinakarpandian, D., Yoshida, N., Layer-Fields, J. L., Fields, G. B., Visse, R. and Nagase, H. (2004) 'Collagenase unwinds triple-helical collagen prior to peptide bond hydrolysis', *EMBO Journal*, 23(15), pp. 3020–3030. doi: 10.1038/sj.emboj.7600318.

Cicchi, R., Kapsokalyvas, D., De Giorgi, V., Maio, V., Van Wiechen, A., Massi, D., Lotti, T. and Pavone, F. S. (2010) 'Scoring of collagen organization in healthy and diseased human dermis by multiphoton microscopy.', *Journal of biophotonics*, 3(1–2), pp. 34–43. doi: 10.1002/jbio.200910062.

Clair, D. G. (2008) 'Carotid Stenting: New Devices on the Horizon and Beyond', *Seminars in Vascular Surgery*, 21(2), pp. 88–94. doi: 10.1053/j.semvascsurg.2008.03.004.

Cochran, R. and Kunzelman, K. (1991) 'Nondestructive analysis of mitral valve collagen fiber orientation', *ASAIO …*, 37(3), pp. M447-8. Available at:

http://journals.lww.com/asaiojournal/Abstract/1991/07000/Nondestructive_Analysis_of_Mitral_Valve_Collagen.167.aspx (Accessed: 10 October 2014).

Colombo, A., Stankovic, G. and Moses, J. W. (2002) 'Selection of coronary stents', *Journal of the American College of Cardiology*, 40(6), pp. 1021–1033. doi: 10.1016/S0735-1097(02)02123-X.

Converse, M. I., Walther, R. G., Ingram, J. T., Li, Y., Yu, S. M. and Monson, K. L. (2018) 'Detection and characterization of molecular-level collagen damage in overstretched cerebral arteries', *Acta Biomaterialia*, 67, pp. 307–318. doi: 10.1016/j.actbio.2017.11.052.

Creane, A., Maher, E., Sultan, S., Hynes, N., Kelly, D. J. and Lally, C. (2011) 'Prediction of fibre architecture and adaptation in diseased carotid bifurcations', *Biomechanics and Modeling in Mechanobiology*, 10(6), pp. 831–843. doi: 10.1007/s10237-010-0277-8.

Crisby, M., Nordin-Fredriksson, G., Shah, P. K., Yano, J., Zhu, J. and Nilsson, J. (2001) 'Pravastatin treatment increases collagen content and decreases lipid content, inflammation, metalloproteinases, and cell death in human carotid plaques: Implications for plaque stabilization', *Circulation*, 103(7), pp. 926–933. doi: 10.1161/01.CIR.103.7.926.

Crowther, M. A. (2005) 'Pathogenesis of Atherosclerosis', *Hematology*, 2005(1), pp. 436–441. doi: 10.1182/asheducation-2005.1.436.

Daemen, M. J., Ferguson, M. S., Gijsen, F. J., Hippe, D. S., Kooi, M. E., Demarco, K., van der Wal, A. C., Yuan, C. and Hatsukami, T. S. (2016) 'Carotid plaque fissure: An underestimated source of intraplaque hemorrhage', *Atherosclerosis*. Elsevier Ltd, 254, pp. 102–108. doi: 10.1016/j.atherosclerosis.2016.09.069.

Dahl, S., Vaughn, M. and Niklason, L. (2007) 'An ultrastructural analysis of collagen in tissue engineered arteries', *Annals of biomedical engineering*, 35(10), pp. 1749–55. doi: 10.1007/s10439-007-9340-8.

Dahlgren, E. D. (2002) *Small Angle Light Scattering Analysis of Tissue*. Worcester Polytechnic Institute.

Dangas, G. D., Claessen, B. E., Caixeta, A., Sanidas, E. a., Mintz, G. S. and Mehran, R. (2010) 'In-stent restenosis in the drug-eluting stent era', *Journal of the American College of Cardiology*. Elsevier Inc., pp. 1897–1907. doi: 10.1016/j.jacc.2010.07.028.

Davis, L. A., Stewart, S. E., Carsten, C. G., Snyder, B. A., Sutton, M. A. and Lessner, S. M. (2016) 'Characterization of fracture behavior of human atherosclerotic fibrous caps using a miniature single edge notched tensile test', *Acta Biomaterialia*. Acta Materialia Inc., 43, pp. 101–111. doi: 10.1016/j.actbio.2016.07.027.

Daxer, A. and Fratzl, P. (1997) 'Collagen fibril orientation in the human corneal stroma and its implication in keratoconus.', *Investigative ophthalmology & visual science*, 38(1), pp. 121–9. Available at: http://www.iovs.org/content/38/1/121.short (Accessed: 17 October 2014).

Debye, P. (1947) 'Molecular-weight determination by light scattering.', *The Journal of Physical Chemistry*, 18(8), pp. 18–32. Available at: http://pubs.acs.org/doi/abs/10.1021/j150451a002 (Accessed: 10 October 2014).

Delfino, a, Stergiopulos, N., Moore, J. E. and Meister, J. J. (1997) 'Residual strain effects on the stress field in a thick wall finite element model of the human carotid bifurcation.', *Journal of biomechanics*, 30(8), pp. 777–786. doi: Doi: 10.1016/s0021-

9290(97)00025-0.

Driessen, N. J. B., Bouten, C. V. C. and Baaijens, F. P. T. (2005) 'A Structural Constitutive Model For Collagenous Cardiovascular Tissues Incorporating the Angular Fiber Distribution', *Journal of Biomechanical Engineering*, 127(3), p. 494. doi: 10.1115/1.1894373.

Driessen, N. J. B., Mol, A., Bouten, C. V. C. and Baaijens, F. P. T. (2007) 'Modeling the mechanics of tissue-engineered human heart valve leaflets', *Journal of Biomechanics*, 40(2), pp. 325–334. doi: 10.1016/j.jbiomech.2006.01.009.

Driessen, N. J., Boerboom, R. A., Huyghe, J. M., Bouten, C. V and Baaijens, F. P. (2003) 'Computational analyses of mechanically induced collagen fiber remodeling in the aortic heart valve.', *Journal of biomechanical engineering*, 125(4), pp. 549–57. doi: 10.1115/1.1590361.

Duca, L., Blaise, S., Romier, B., Laffargue, M., Gayral, S., El Btaouri, H., Kawecki, C., Guillot, A., Martiny, L., Debelle, L. and Maurice, P. (2016) 'Matrix ageing and vascular impacts: Focus on elastin fragmentation', *Cardiovascular Research*, 110(3), pp. 298–308. doi: 10.1093/cvr/cvw061.

Ellsmere, J. C., Khanna, R. A. and Michael Lee, J. (1999) 'Mechanical loading of bovine pericardium accelerates enzymatic degradation', *Biomaterials*, 20(12), pp. 1143–1150. doi: 10.1016/S0142-9612(99)00013-7.

Engelmayr, G. C., Papworth, G. D., Watkins, S. C., Mayer, J. E. and Sacks, M. S. (2006) 'Guidance of engineered tissue collagen orientation by large-scale scaffold microstructures.', *Journal of biomechanics*, 39(10), pp. 1819–31. doi: 10.1016/j.jbiomech.2005.05.020.

Falk, E. (2006) 'Pathogenesis of Atherosclerosis', *Journal of the American College of Cardiology*, 47(8 SUPPL.), pp. 0–5. doi: 10.1016/j.jacc.2005.09.068.

Ferdman, A. (1987) *The Measurement of Collagen Fiber Orientation in Tissue by Small-Angle Light Scattering*. Massachusetts Institute of Technology.

Ferdman, A. and Yannas, I. (1993) 'Scattering of light from histologic sections: a new method for the analysis of connective tissue', *Journal of investigative dermatology*, 100(5), pp. 710–6. Available at: http://www.nature.com/jid/journal/v100/n5/abs/5611649a.html (Accessed: 10 October 2014).

Ferdous, Z., Jo, H. and Nerem, R. M. (2011) 'Differences in valvular and vascular cell responses to strain in osteogenic media', *Biomaterials*. Elsevier Ltd, 32(11), pp. 2885–2893. doi: 10.1016/j.biomaterials.2011.01.030.

de Figueiredo Borges, L., Jaldin, R. G., Dias, R. R., Stolf, N. A. G., Michel, J. B. and Gutierrez, P. S. (2008) 'Collagen is reduced and disrupted in human aneurysms and dissections of ascending aorta', *Human Pathology*. Elsevier Inc., 39(3), pp. 437–443. doi: 10.1016/j.humpath.2007.08.003.

Fischer, G. M. and Llaurado, J. G. (1966) 'Collagen and Elastin Content in Canine Arteries Selected from Functionally Different Vascular Beds', *Circulation Research*, 19(2), pp. 394–399. doi: 10.1161/01.RES.19.2.394.

Flamini, V., Kerskens, C., Moerman, K. M., Simms, C. K. and Lally, C. (2010) 'Imaging Arterial Fibres Using Diffusion Tensor Imaging—Feasibility Study and Preliminary Results', *EURASIP Journal on Advances in Signal Processing*, 2010, pp. 1–14. doi: 10.1155/2010/904091.

Flamini, V., Kerskens, C., Simms, C. and Lally, C. (2013) 'Fibre orientation of fresh and frozen porcine aorta determined non-invasively using diffusion tensor imaging', *Medical Engineering and Physics*. Institute of Physics and Engineering in Medicine, 35(6), pp. 765–776. doi: 10.1016/j.medengphy.2012.08.008.

Flynn, B. P., Bhole, A. P., Saeidi, N., Liles, M., DiMarzio, C. A. and Ruberti, J. W. (2010) 'Mechanical Strain Stabilizes Reconstituted Collagen Fibrils against Enzymatic Degradation by Mammalian Collagenase Matrix Metalloproteinase 8 (MMP-8)', *PLoS ONE*. Edited by J. P. R. O. Orgel, 5(8), p. e12337. doi: 10.1371/journal.pone.0012337.

Flynn, B. P., Tilburey, G. E. and Ruberti, J. W. (2013) 'Highly sensitive single-fibril erosion assay demonstrates mechanochemical switch in native collagen fibrils', *Biomechanics and Modeling in Mechanobiology*, 12(2), pp. 291–300. doi: 10.1007/s10237-012-0399-2.

Fomovsky, G. M. and Holmes, J. W. (2010) 'Evolution of scar structure, mechanics, and ventricular function after myocardial infarction in the rat', *AJP: Heart and Circulatory Physiology*, 298(1), pp. H221–H228. doi: 10.1152/ajpheart.00495.2009.

Friedman, M., Deters, O., Mark, F., Brent Bargeron, C. and Hutchins, G. (1983) 'Arterial geometry affects hemodynamics *1A potential risk factor for atherosclerosis', *Atherosclerosis*, 46(2), pp. 225–231. doi: 10.1016/0021-9150(83)90113-2.

García, a., Peña, E., Laborda, A., Lostalé, F., De Gregorio, M. A., Doblaré, M. and Martínez, M. A. (2011) 'Experimental study and constitutive modelling of the passive mechanical properties of the porcine carotid artery and its relation to histological analysis: Implications in animal cardiovascular device trials', *Medical Engineering & Physics*, 33(6), pp. 665–676. doi: 10.1016/j.medengphy.2011.01.016.

Gasser, T. C., Gallinetti, S., Xing, X., Forsell, C., Swedenborg, J. and Roy, J. (2012) 'Spatial orientation of collagen fibers in the abdominal aortic aneurysm's wall and its relation to wall mechanics', *Acta Biomaterialia*. Acta Materialia Inc., 8(8), pp. 3091–3103. doi: 10.1016/j.actbio.2012.04.044.

Gasser, T. C., Ogden, R. W. and Holzapfel, G. A. (2006) 'Hyperelastic modelling of arterial layers with distributed collagen fibre orientations.', *Journal of the Royal Society, Interface / the Royal Society*, 3(6), pp. 15–35. doi: 10.1098/rsif.2005.0073.

Gaul, R. and Lally, C. (2017) 'Strain Mediated Enzyme Degradation of Arterial Tissue; Implications in Disease and Medical Device Design', in *Summer Biomechanics, Bioengineering and Biotransport Conference 2017*. Tucson.

Gaul, R. T., Nolan, D. R. and Lally, C. (2017) 'Collagen fibre characterisation in arterial tissue under load using SALS', *Journal of the Mechanical Behavior of Biomedical Materials*. Elsevier Ltd, 75(November), pp. 359–368. doi: 10.1016/j.jmbbm.2017.07.036.

Gaul, R. T., Nolan, D. R., Ristori, T., Bouten, C. V. C., Loerakker, S. and Lally, C. (2018) 'Strain mediated enzymatic degradation of arterial tissue: Insights into the role of the non-collagenous tissue matrix and collagen crimp', *Acta Biomaterialia*. Acta Materialia Inc., 77, pp. 301–310. doi: 10.1016/j.actbio.2018.06.037.

Ghasemi, M., Nolan, D. R. and Lally, C. (2018) 'An investigation into the role of different constituents in damage accumulation in arterial tissue and constitutive model development', *Biomechanics and Modeling in Mechanobiology*. doi: 10.1007/s10237-018-1054-3.

Ghazanfari, S., Driessen-Mol, a., Strijkers, G. J., Kanters, F. M. W., Baaijens, F. P. T. and Bouten, C. V. C. (2012) 'A comparative analysis of the collagen architecture in the carotid artery: Second harmonic generation versus diffusion tensor imaging', *Biochemical and Biophysical Research Communications*. Elsevier Inc., 426(1), pp. 54–58. doi: 10.1016/j.bbrc.2012.08.031.

Ghazanfari, S., Driessen-Mol, A., Bouten, C. V. C. and Baaijens, F. P. T. (2016) 'Modulation of collagen fiber orientation by strain-controlled enzymatic degradation', *Acta Biomaterialia*, 35, pp. 118–126. doi: 10.1016/j.actbio.2016.02.033.

Ghazanfari, S., Driessen-Mol, A., Hoerstrup, S. P., Baaijens, F. P. T. and Bouten, C. V. C. (2016) 'Collagen Matrix Remodeling in Stented Pulmonary Arteries after Transapical Heart Valve Replacement', *Cells Tissues Organs*, 201(3), pp. 159–169. doi: 10.1159/000442521.

Ghazanfari, S., Driessen-Mol, A., Strijkers, G. J., Baaijens, F. P. T. and Bouten, C. V. C. (2015) 'The Evolution of Collagen Fiber Orientation in Engineered Cardiovascular Tissues Visualized by Diffusion Tensor Imaging', *PLOS ONE*. Edited by J. S. Burns, 10(5), p. e0127847. doi: 10.1371/journal.pone.0127847.

Gijsen, F. J. H., Migliavacca, F., Schievano, S., Socci, L., Petrini, L., Thury, A., Wentzel, J. J., van der Steen, A. F. W., Serruys, P. W. S. and Dubini, G. (2008) 'Simulation of stent deployment in a realistic human coronary artery', *BioMedical Engineering Online*, 7, pp. 1–11. doi: 10.1186/1475-925X-7-23.

Gray, H. (1853) *The internal carotid and vertebral arteries. Right side.*, *Anatomy of the Human Body*. Available at: https://commons.wikimedia.org/wiki/File:Gray513.png (Accessed: 8 June 2016).

Gray, H. (1858) *Anatomy of the heart*, *Anatomy of the Human Body*.

Groen, H. C., Gijsen, F. J. H., Lugt, A. Van Der, Ferguson, M. S., Hatsukami, T. S., Yuan, C., Steen, A. F. W. Van Der and Wentzel, J. J. (2008) 'High shear stress influences plaque vulnerability', 16(7), pp. 280–283.

Grytz, R., Meschke, G. and Jonas, J. B. (2011) 'The collagen fibril architecture in the lamina cribrosa and peripapillary sclera predicted by a computational remodeling approach', *Biomechanics and Modeling in Mechanobiology*, 10(3), pp. 371–382. doi: 10.1007/s10237-010-0240-8.

Grytz, R., Sigal, I. A., Ruberti, J. W., Meschke, G. and Crawford Downs, J. (2012) 'Lamina cribrosa thickening in early glaucoma predicted by a microstructure motivated growth and remodeling approach', *Mechanics of Materials*, 44, pp. 99–109. doi: 10.1016/j.mechmat.2011.07.004.

Gyoneva, L., Hovell, C. B., Pewowaruk, R. J., Dorfman, K. D., Segal, Y. and Barocas, V. H. (2016) 'Cell–matrix interaction during strain-dependent remodelling of simulated collagen networks', *Interface Focus*, 6(1), p. 20150069. doi: 10.1098/rsfs.2015.0069.

Hadi, M. F., Sander, E. A., Ruberti, J. W. and Barocas, V. H. (2012) 'Simulated remodeling of loaded collagen networks via strain-dependent enzymatic degradation and constant-rate fiber growth', *Mechanics of Materials*, 44(2), pp. 72–82. doi: 10.1016/j.mechmat.2011.07.003.

Hahn, C. and Schwartz, M. A. (2009) 'Mechanotransduction in vascular physiology and atherogenesis', *Nature Reviews Molecular Cell Biology*, 10(1), pp. 53–62. doi: 10.1038/nrm2596.

Hamann, M. C., Sacks, M. S. and Malinin, T. I. (1998) 'Quantification of the collagen fibre architecture of human cranial dura mater.', *Journal of anatomy*, 192 (Pt 1(1), pp. 99–106. doi: 10.1046/j.1469-7580.1998.19210099.x.

Han, H.-C. and Fung, Y.-C. (1995) 'Longitudinal strain of canine and porcine aortas', *Journal of Biomechanics*, 28(5), pp. 637–641. doi: 10.1016/0021-9290(94)00091-H.

Han, S., Makareeva, E., Kuznetsova, N. V., DeRidder, A. M., Sutter, M. B., Losert, W., Phillips, C. L., Visse, R., Nagase, H. and Leikin, S. (2010) 'Molecular mechanism of type I collagen homotrimer resistance to mammalian collagenases', *Journal of Biological Chemistry*, 285(29), pp. 22276–22281. doi: 10.1074/jbc.M110.102079.

Hariton, I., DeBotton, G., Gasser, T. C. and Holzapfel, G. a. (2007) 'Stress-driven collagen fiber remodeling in arterial walls', *Biomechanics and Modeling in Mechanobiology*, 6(3), pp. 163–175. doi: 10.1007/s10237-006-0049-7.

Hariton, I., DeBotton, G., Gasser, T. C. and Holzapfel, G. a. (2007) 'Stress-modulated collagen fiber remodeling in a human carotid bifurcation', *Journal of Theoretical Biology*, 248(3), pp. 460–470. doi: 10.1016/j.jtbi.2007.05.037.

Hart, J. P., Peeters, P., Verbist, J., Deloose, K. and Bosiers, M. (2006) 'Do device characteristics impact outcome in carotid artery stenting?', *Journal of Vascular Surgery*, 44(4), pp. 725–730. doi: 10.1016/j.jvs.2006.06.029.

Haskett, D., Azhar, M., Utzinger, U. and Vande Geest, J. P. (2013) 'Progressive alterations in microstructural organization and biomechanical response in the ApoE mouse model of aneurysm', *Biomatter*, 3(3), p. e24648. doi: 10.4161/biom.24648.

Haskett, D., Johnson, G., Zhou, A., Utzinger, U. and Vande Geest, J. (2010) 'Microstructural and biomechanical alterations of the human aorta as a function of age and location', *Biomechanics and Modeling in Mechanobiology*, 9(6), pp. 725–736. doi: 10.1007/s10237-010-0209-7.

Heck, T. A. M., Wilson, W., Foolen, J., Cilingir, A. C., Ito, K. and van Donkelaar, C. C. (2015) 'A tissue adaptation model based on strain-dependent collagen degradation and contact-guided cell traction', *Journal of Biomechanics*. Elsevier, 48(5), pp. 823–831. doi: 10.1016/j.jbiomech.2014.12.023.

Helfenstein-Didier, C., Taïnoff, D., Viville, J., Adrien, J., Maire, É. and Badel, P. (2018) 'Tensile rupture of medial arterial tissue studied by X-ray micro-tomography on stained samples', *Journal of the Mechanical Behavior of Biomedical Materials*, 78(July 2017), pp. 362–368. doi: 10.1016/j.jmbbm.2017.11.032.

Hilbert, S. L., Sword, L. C., Batchelder, K. F., Barrick, M. K. and Ferrans, V. J. (1996) 'Simultaneous assessment of bioprosthetic heart valve biomechanical properties and collagen crimp length.', *Journal of biomedical materials research*, 31(4), pp. 503–9. doi: 10.1002/(SICI)1097-4636(199608)31:4<503::AID-JBM10>3.0.CO;2-H.

Holzapfel, G. A. (2008) 'Collagen in Arterial Walls: Biomechanical Aspects', in Fratzl, P. (ed.) *Collagen*. Boston, MA: Springer US, pp. 285–324. doi: 10.1007/978-0-387-73906-9.

Holzapfel, G. a., Gasser, T. C. and Stadler, M. (2002) 'A structural model for the viscoelastic behavior of arterial walls: Continuum formulation and finite element analysis', *European Journal of Mechanics, A/Solids*, 21(3), pp. 441–463. doi: 10.1016/S0997-7538(01)01206-2.

Holzapfel, G. A., Sommer, G., Auer, M., Regitnig, P. and Ogden, R. W. (2007) 'Layer-Specific 3D Residual Deformations of Human Aortas with Non-Atherosclerotic

Intimal Thickening', *Annals of Biomedical Engineering*, 35(4), pp. 530–545. doi: 10.1007/s10439-006-9252-z.

Holzapfel, G. a., Stadler, M. and Schulze-Bauer, C. a J. (2002) 'A layer-specific three-dimensional model for the simulation of balloon angioplasty using magnetic resonance imaging and mechanical testing', *Annals of Biomedical Engineering*, 30(6), pp. 753–767. doi: 10.1114/1.1492812.

Holzapfel, G. a, Gasser, T. C. and Ogden, R. W. (2000) 'A new constitutive framework for arterial wall mechanics and a comperative study of material models', *J. Elasticity*, 61, pp. 1–48.

Holzapfel, G. a, Sommer, G., Gasser, T. C. and Regitnig, P. (2005) 'Determination of layer-specific mechanical properties of human coronary arteries with nonatherosclerotic intimal thickening and related constitutive modeling', *AJP: Heart and Circulatory Physiology*, 289(5), pp. H2048–H2058. doi: 10.1152/ajpheart.00934.2004.

Hu, J., Humphrey, J. D. and Yeh, A. T. (2009) 'Characterization of engineered tissue development under biaxial stretch using nonlinear optical microscopy.', *Tissue engineering. Part A*, 15(7), pp. 1553–64. doi: 10.1089/ten.tea.2008.0287.

Huang, C. and Yannas, I. V (1977) 'Mechanochemical studies of enzymatic degradation of insoluble collagen fibers', *Journal of Biomedical Materials Research*, 11(1), pp. 137–154. doi: 10.1002/jbm.820110113.

Humphrey, J. D. (2002) *Cardiovascular Solid Mechanics: Cells, Tissues, and Organs*. Springer Science & Business Media. Available at: https://books.google.ie/books/about/Cardiovascular_Solid_Mechanics.html?id=DBglTvXRtGcC&pgis=1 (Accessed: 7 May 2016).

Humphrey, J. D. and Delange, S. L. (2004) *An Introduction to Biomechanics*. New York, NY: Springer New York. doi: 10.1007/978-1-4899-0325-9.

Jesudason, R., Sato, S., Parameswaran, H., Araujo, A. D., Majumdar, A., Allen, P. G., Bartolák-Suki, E. and Suki, B. (2010) 'Mechanical forces regulate elastase activity and binding site availability in lung elastin', *Biophysical Journal*, 99(9), pp. 3076–3083. doi: 10.1016/j.bpj.2010.09.018.

Junqueira, L. C. U., Bignolas, G. and Brentani, R. R. (1979) 'Picrosirius staining plus polarization microscopy, a specific method for collagen detection in tissue sections', *The Histochemical Journal*, 11(4), pp. 447–455. doi: 10.1007/BF01002772.

Kawai, M. and Kuntz, I. D. (1973) 'Optical diffraction studies of muscle fibers.', *Biophysical journal*, 13(9), pp. 857–76. doi: 10.1016/S0006-3495(73)86031-X.

Keyes, J. T., Haskett, D. G., Utzinger, U., Azhar, M. and Vande Geest, J. P. (2011) 'Adaptation of a Planar Microbiaxial Optomechanical Device for the Tubular Biaxial Microstructural and Macroscopic Characterization of Small Vascular Tissues', *Journal of Biomechanical Engineering*, 133(7), p. 075001. doi: 10.1115/1.4004495.

Khan, K. M. and Maffulli, N. (1998) 'Tendinopathy: An Achilles' heel for athletes and clinicians', *Clinical Journal of Sport Medicine*, pp. 151–154. doi: 10.1097/00042752-199807000-00001.

Kok, A. M., van der Lugt, A., Verhagen, H. J. M., van der Steen, A. F. W., Wentzel, J. J. and Gijsen, F. J. H. (2017) 'Model-based cap thickness and peak cap stress prediction for carotid MRI', *Journal of Biomechanics*. The Author(s), 60, pp. 175–180. doi: 10.1016/j.jbiomech.2017.06.034.

König, K., Schenke-Layland, K., Riemann, I. and Stock, U. a (2005) 'Multiphoton autofluorescence imaging of intratissue elastic fibers.', *Biomaterials*, 26(5), pp. 495–500. doi: 10.1016/j.biomaterials.2004.02.059.

Krasny, W., Morin, C., Magoariec, H. and Avril, S. (2017) 'A comprehensive study of layer-specific morphological changes in the microstructure of carotid arteries under uniaxial load', *Acta Biomaterialia*. Acta Materialia Inc., 57, pp. 342–351. doi: 10.1016/j.actbio.2017.04.033.

Kronick, P. and Buechler, P. (1986) 'Fiber orientation in calfskin by laser light scattering or X-ray diffraction and quantitative relation to mechanical properties', *The Journal of the American Leather …*, 81(7), pp. 221–230. Available at: http://agris.fao.org/agris-search/search.do?recordID=US8702841 (Accessed: 20 November 2014).

Kunzelman, K. S., Cochran, R. P., Chuong, C., Ring, W. S., Verrier, E. D. and Eberhart, R. D. (1993) 'Finite element analysis of the mitral valve.', *The Journal of heart valve disease*, 2(3), pp. 326–40. Available at: http://www.ncbi.nlm.nih.gov/pubmed/8269128 (Accessed: 24 May 2016).

Labrosse, M. R., Beller, C. J., Mesana, T. and Veinot, J. P. (2009) 'Mechanical behavior of human aortas: Experiments, material constants and 3-D finite element modeling including residual stress', *Journal of Biomechanics*, 42(8), pp. 996–1004. doi: 10.1016/j.jbiomech.2009.02.009.

Lal, B. K., Hobson, R. W., Goldstein, J., Geohagan, M., Chakhtoura, E., Pappas, P. J., Jamil, Z., Haser, P. B., Varma, S., Padberg, F. T., Cerveira, J. J., Clair, D., AbuRahma, A. F., Perler, B., Queral, L. A., Harris, L. and Ouriel, K. (2003) 'In-stent recurrent stenosis after carotid artery stenting: Life table analysis and clinical relevance', *Journal of Vascular Surgery*, 38(6), pp. 1162–1169. doi: 10.1016/j.jvs.2003.08.021.

Lally, C., Dolan, F. and Prendergast, P. J. (2005) 'Cardiovascular stent design and vessel stresses: A finite element analysis', *Journal of Biomechanics*, 38(8), pp. 1574–1581. doi: 10.1016/j.jbiomech.2004.07.022.

Learoyd, B. M. and Taylor, M. G. (1966) 'Alterations with age in the viscoelastic properties of human arterial walls.', *Circulation research*, 18(March 1966), pp. 278–292. doi: 10.1161/01.RES.18.3.278.

Lee, S.-W., Antiga, L., Spence, J. D. and Steinman, D. A. (2008) 'Geometry of the Carotid Bifurcation Predicts Its Exposure to Disturbed Flow', *Stroke*, 39(8), pp. 2341–2347. doi: 10.1161/STROKEAHA.107.510644.

Liao, J., Yang, L., Grashow, J. and Sacks, M. S. (2005) 'Molecular orientation of collagen in intact planar connective tissues under biaxial stretch.', *Acta biomaterialia*, 1(1), pp. 45–54. doi: 10.1016/j.actbio.2004.09.007.

Loerakker, S., Obbink-Huizer, C. and Baaijens, F. P. T. (2013) 'A physically motivated constitutive model for cell-mediated compaction and collagen remodeling in soft tissues', *Biomechanics and Modeling in Mechanobiology*, 13(5), pp. 985–1001. doi: 10.1007/s10237-013-0549-1.

Loerakker, S., Ristori, T. and Baaijens, F. P. T. (2016) 'A computational analysis of cell-mediated compaction and collagen remodeling in tissue-engineered heart valves', *Journal of the Mechanical Behavior of Biomedical Materials*. Elsevier, 58, pp. 173–187. doi: 10.1016/j.jmbbm.2015.10.001.

Lotz, J. C., Hadi, T., Bratton, C., Reiser, K. M. and Hsieh, A. H. (2008) 'Anulus

fibrosus tension inhibits degenerative structural changes in lamellar collagen', *European Spine Journal*, 17(9), pp. 1149–1159. doi: 10.1007/s00586-008-0721-y.

Macrae, R. A., Miller, K. and Doyle, B. J. (2016) 'Methods in Mechanical Testing of Arterial Tissue: A Review', *Strain*, 52(5), pp. 380–399. doi: 10.1111/str.12183.

Maffulli, N., Khan, K. M. and Puddu, G. (1998) 'Overuse tendon conditions: time to change a confusing terminology.', *Arthroscopy: the journal of arthroscopic & related surgery: official publication of the Arthroscopy Association of North America and the International Arthroscopy Association*, 14(8), pp. 840–3. doi: 10.1016/S0749-8063(98)70021-0.

Magnusson, S. P., Langberg, H. and Kjaer, M. (2010) 'The pathogenesis of tendinopathy: balancing the response to loading', *Nature Reviews Rheumatology*. Nature Publishing Group, 6(5), pp. 262–268. doi: 10.1038/nrrheum.2010.43.

Malaspina, D. C., Szleifer, I. and Dhaher, Y. (2017) 'Mechanical properties of a collagen fibril under simulated degradation', *Journal of the Mechanical Behavior of Biomedical Materials*. Elsevier Ltd, 75(March), pp. 549–557. doi: 10.1016/j.jmbbm.2017.08.020.

Mantese, V. a., Timaran, C. H., Chiu, D., Begg, R. J. and Brott, T. G. (2010) 'The Carotid Revascularization Endarterectomy Versus Stenting Trial (CREST): Stenting Versus Carotid Endarterectomy for Carotid Disease', *Stroke*, 41(10, Supplement 1), pp. S31–S34. doi: 10.1161/STROKEAHA.110.595330.

Martini, F. H., Nath, J. L. and Bartholomew, E. F. (2011) *Fundamentals of Anatomy & Physiology*. Benjamin-Cummings Publishing Company. Available at: http://books.google.ie/books/about/Fundamentals_of_Anatomy_Physiology_With.html?id=2XVntQAACAAJ&pgis=1 (Accessed: 27 October 2014).

Mathers, C. D. and Loncar, D. (2006) 'Projections of global mortality and burden of disease from 2002 to 2030.', *PLoS medicine*, 3(11), p. e442. doi: 10.1371/journal.pmed.0030442.

Miehe, C. (1995) 'Discontinuous and Continuous Damage Evolution in {O}gden-Type Large Strain Elastic Materials', *European Journal of Mechanics - A/Solids*. Elsevier, 14(5), pp. 697–720. Available at: http://cat.inist.fr/?aModele=afficheN&cpsidt=3692484 (Accessed: 24 May 2016).

Miles, C. A. and Ghelashvili, M. (1999) 'Polymer-in-a-Box Mechanism for the Thermal Stabilization of Collagen Molecules in Fibers', *Biophysical Journal*. Elsevier, 76(6), pp. 3243–3252. doi: 10.1016/S0006-3495(99)77476-X.

Misof, K., Rapp, G. and Fratzl, P. (1997) 'A new molecular model for collagen elasticity based on synchrotron X-ray scattering evidence.', *Biophysical journal*, 72(3), pp. 1376–81. doi: 10.1016/S0006-3495(97)78783-6.

Moneta, G. L., Edwards, J. M., Chitwood, R. W., Taylor, L. M., Lee, R. W., Cummings, C. A. and Porter, J. M. (1993) 'Correlation of North American Symptomatic Carotid Endarterectomy Trial (NASCET) angiographic definition of 70% to 99% internal carotid artery stenosis with duplex scanning', *Journal of Vascular Surgery*, 17(1), pp. 152–159. doi: 10.1016/0741-5214(93)90019-I.

Mozaffarian, D., Benjamin, E. J., Go, A. S., Arnett, D. K., Blaha, M. J., Cushman, M., de Ferranti, S., Després, J.-P., Fullerton, H. J., Howard, V. J., Huffman, M. D., Judd, S. E., Kissela, B. M., Lackland, D. T., Lichtman, J. H., Lisabeth, L. D., Liu, S., Mackey, R. H., Matchar, D. B., McGuire, D. K., Mohler, E. R., Moy, C. S., Muntner, P.,

Mussolino, M. E., Nasir, K., Neumar, R. W., Nichol, G., Palaniappan, L., Pandey, D. K., Reeves, M. J., Rodriguez, C. J., Sorlie, P. D., Stein, J., Towfighi, A., Turan, T. N., Virani, S. S., Willey, J. Z., Woo, D., Yeh, R. W. and Turner, M. B. (2015) 'Heart Disease and Stroke Statistics—2015 Update', *Circulation*, 131(4), pp. e29–e322. doi: 10.1161/CIR.0000000000000152.

'MRC European Carotid Surgery Trial: interim results for symptomatic patients with severe (70-99%) or with mild (0-29%) carotid stenosis. European Carotid Surgery Trialists' Collaborative Group.' (1991) *Lancet (London, England)*, 337(8752), pp. 1235–43. Available at: http://www.ncbi.nlm.nih.gov/pubmed/1674060 (Accessed: 27 May 2016).

Müller-Schweinitzer, E. (2009) 'Cryopreservation of vascular tissues', *Organogenesis*, 5(3), pp. 97–104. doi: 10.4161/org.5.3.9495.

Nabeshima, Y., Grood, E. S., Sakurai, A. and Herman, J. H. (1996) 'Uniaxial tension inhibits tendon collagen degradation by collagenase in vitro', *Journal of Orthopaedic Research*, 14(1), pp. 123–130. doi: 10.1002/jor.1100140120.

Naghavi, M. (2003a) 'From Vulnerable Plaque to Vulnerable Patient: A Call for New Definitions and Risk Assessment Strategies: Part I', *Circulation*, 108(14), pp. 1664–1672. doi: 10.1161/01.CIR.0000087480.94275.97.

Naghavi, M. (2003b) 'From Vulnerable Plaque to Vulnerable Patient: A Call for New Definitions and Risk Assessment Strategies: Part II', *Circulation*, 108(15), pp. 1772–1778. doi: 10.1161/01.CIR.0000087481.55887.C9.

Nair, A. (2002) 'Coronary Plaque Classification With Intravascular Ultrasound Radiofrequency Data Analysis', *Circulation*, 106(17), pp. 2200–2206. doi: 10.1161/01.CIR.0000035654.18341.5E.

National Heart Lung and Blood Insitute (NIH) (2010) *Diagram of aortic aneurysm*. Available at: https://commons.wikimedia.org/wiki/File:Aortic_aneurysm.jpg (Accessed: 13 September 2018).

National Heart Lung and Blood Insitute (NIH) (2013a) *Carotid endarterectomy illustration*. Available at: https://commons.wikimedia.org/wiki/File:Cad_endarterectomy.jpg?uselang=en-gb (Accessed: 8 June 2016).

National Heart Lung and Blood Insitute (NIH) (2013b) *Carotid stenting illustration*. Available at: https://commons.wikimedia.org/wiki/File:Cad_stentplacement.jpg?uselang=en-gb (Accessed: 8 June 2016).

National Heart Lung and Blood Insitute (NIH) (2013c) *Healthy and diseased carotid artery*. Available at: https://commons.wikimedia.org/wiki/File:Cad_anatomy.jpg?uselang=en-gb (Accessed: 8 June 2016).

Nicholls, S. C., Gardner, J. B., Meissner, M. H. and Johansen, K. H. (1998) 'Rupture in small abdominal aortic aneurysms', *Journal of Vascular Surgery*, 28(5), pp. 884–888. doi: 10.1016/S0741-5214(98)70065-5.

Nierenberger, M., Fargier, G., Ahzi, S. and R??mond, Y. (2015) 'Evolution of the three-dimensional collagen structure in vascular walls during deformation: An in situ mechanical testing under multiphoton microscopy observation', *Biomechanics and Modeling in Mechanobiology*. Springer Berlin Heidelberg, 14(4), pp. 693–702. doi:

10.1007/s10237-014-0630-4.

Nierenberger, M., Rémond, Y., Ahzi, S. and Choquet, P. (2015) 'Assessing the three-dimensional collagen network in soft tissues using contrast agents and high resolution micro-CT: Application to porcine iliac veins', *Comptes Rendus Biologies*, 338(7), pp. 425–433. doi: 10.1016/j.crvi.2015.04.009.

Niestrawska, J. A., Viertler, C., Regitnig, P., Cohnert, T. U., Sommer, G. and Holzapfel, G. A. (2016) 'Microstructure and mechanics of healthy and aneurysmatic abdominal aortas: experimental analysis and modelling', *Journal of The Royal Society Interface*, 13(124), p. 20160620. doi: 10.1098/rsif.2016.0620.

Nieuwstadt, H. A., Fekkes, S., Hansen, H. H. G., de Korte, C. L., van der Lugt, A., Wentzel, J. J., van der Steen, A. F. W. and Gijsen, F. J. H. (2015) 'Carotid plaque elasticity estimation using ultrasound elastography, MRI, and inverse FEA - A numerical feasibility study', *Medical Engineering and Physics*. Elsevier Ltd., 37(8), pp. 801–807. doi: 10.1016/j.medengphy.2015.06.003.

Nishida, K., Ogawa, H. and Matsuba, G. (2008) 'A high-resolution small-angle light scattering instrument for soft matter studies', *Journal of Applied …*, 41(4), pp. 723–728. doi: 10.1107/S002188980801265X.

Nowrozani, F. R. and Zareiyan, B. (2011) 'A microscopic study of the external carotid artery transitional zone of the adult male dog', *Journal of Applied Animal Research*, 39(4), pp. 406–411. doi: 10.1080/09712119.2011.622928.

O'Callaghan, C. J. and Williams, B. (2000) 'Mechanical strain-induced extracellular matrix production by human vascular smooth muscle cells: Role of TGF-ß1', *Hypertension*, 36(3), pp. 319–324. doi: 10.1161/01.HYP.36.3.319.

O'Connell, M. K., Murthy, S., Phan, S., Xu, C., Buchanan, J., Spilker, R., Dalman, R. L., Zarins, C. K., Denk, W. and Taylor, C. A. (2008) 'The three-dimensional micro- and nanostructure of the aortic medial lamellar unit measured using 3D confocal and electron microscopy imaging.', *Matrix biology : journal of the International Society for Matrix Biology*, 27(3), pp. 171–81. doi: 10.1016/j.matbio.2007.10.008.

O'Connor, C. A., Nolan, D. R., McEvoy, E. and McGarry, J. P. (2017) 'A three part hyperelastic law for anisotropic aortic tissue: Model developement and experimental validation', in *Summer Biomechanics, Bioengineering and Biotransport Conference*. Arizona.

Opriessnig, P., Mangge, H., Stollberger, R., Deutschmann, H. and Reishofer, G. (2016) 'In vivo cardiovascular magnetic resonance of 2D vessel wall diffusion anisotropy in carotid arteries', *Journal of Cardiovascular Magnetic Resonance*. Journal of Cardiovascular Magnetic Resonance, 18(1), pp. 1–9. doi: 10.1186/s12968-016-0304-8.

Ozolanta, I., Tetere, G., Purinya, B. and Kasyanov, V. (1998) 'Changes in the mechanical properties, biochemical contents and wall structure of the human coronary arteries with age and sex', *Medical Engineering & Physics*, 20(7), pp. 523–533. doi: 10.1016/S1350-4533(98)00050-2.

Pal, S., Tsamis, A., Pasta, S., D'Amore, A., Gleason, T. G., Vorp, D. A. and Maiti, S. (2014) 'A mechanistic model on the role of "radially-running" collagen fibers on dissection properties of human ascending thoracic aorta', *Journal of Biomechanics*. Elsevier, 47(5), pp. 981–988. doi: 10.1016/j.jbiomech.2014.01.005.

Pawley, J. B. (ed.) (2006) *Handbook Of Biological Confocal Microscopy*. Boston, MA: Springer US. doi: 10.1007/978-0-387-45524-2.

Peeters, W., Hellings, W. E., de Kleijn, D. P. V., de Vries, J. P. P. M., Moll, F. L., Vink, A. and Pasterkamp, G. (2009) 'Carotid Atherosclerotic Plaques Stabilize After Stroke: Insights Into the Natural Process of Atherosclerotic Plaque Stabilization', *Arteriosclerosis, Thrombosis, and Vascular Biology*, 29(1), pp. 128–133. doi: 10.1161/ATVBAHA.108.173658.

Pegg, D. E., Wusteman, M. C. and Boylan, S. (1997) 'Fractures in Cryopreserved Elastic Arteries', *Cryobiology*, 34(2), pp. 183–192. doi: 10.1006/cryo.1996.1997.

Perumal, S., Antipova, O. and Orgel, J. P. R. O. (2008) 'Collagen fibril architecture, domain organization, and triple-helical conformation govern its proteolysis', *Proceedings of the National Academy of Sciences*, 105(8), pp. 2824–2829. doi: 10.1073/pnas.0710588105.

Qi, N., Gao, H., Ogden, R. W., Hill, N. A., Holzapfel, G. A., Han, H.-C. and Luo, X. (2015) 'Investigation of the optimal collagen fibre orientation in human iliac arteries', *Journal of the Mechanical Behavior of Biomedical Materials*. Elsevier, 52, pp. 108–119. doi: 10.1016/j.jmbbm.2015.06.011.

Rachev, A. (2003) 'Remodeling of Arteries in Response to Changes in their Mechanical Environment', in *Biomechanics of Soft Tissue in Cardiovascular Systems*. Vienna: Springer Vienna, pp. 221–271. doi: 10.1007/978-3-7091-2736-0_6.

Raub, C. B., Suresh, V., Krasieva, T., Lyubovitsky, J., Mih, J. D., Putnam, A. J., Tromberg, B. J. and George, S. C. (2007) 'Noninvasive assessment of collagen gel microstructure and mechanics using multiphoton microscopy.', *Biophysical journal*. Elsevier, 92(6), pp. 2212–22. doi: 10.1529/biophysj.106.097998.

Rezakhaniha, R., Agianniotis, a., Schrauwen, J. T. C., Griffa, a., Sage, D., Bouten, C. V. C., Van De Vosse, F. N., Unser, M. and Stergiopulos, N. (2012) 'Experimental investigation of collagen waviness and orientation in the arterial adventitia using confocal laser scanning microscopy', *Biomechanics and Modeling in Mechanobiology*, 11(3–4), pp. 461–473. doi: 10.1007/s10237-011-0325-z.

Rhodin, J. A. G. (1980) 'Architecture of the Vessel Wall', in Terjung, R. (ed.) *Comprehensive Physiology*. Hoboken, NJ, USA: John Wiley & Sons, Inc., pp. 1–31. doi: 10.1002/cphy.cp020201.

Roach, M. R. and Burton, a C. (1957) 'The reason for the shape of the distensibility curves of arteries.', *Canadian journal of biochemistry and physiology*, 35(8), pp. 681–690. doi: 10.1139/o57-080.

Roberts, M. D., Grau, V., Grimm, J., Reynaud, J., Bellezza, A. J., Burgoyne, C. F. and Downs, J. C. (2009) 'Remodeling of the Connective Tissue Microarchitecture of the Lamina Cribrosa in Early Experimental Glaucoma', *Investigative Opthalmology & Visual Science*, 50(2), p. 681. doi: 10.1167/iovs.08-1792.

Robitaille, M. C., Zareian, R., Dimarzio, C. a, Wan, K.-T. and Ruberti, J. W. (2011) 'Small-angle light scattering to detect strain-directed collagen degradation in native tissue.', *Interface focus*, 1(5), pp. 767–76. doi: 10.1098/rsfs.2011.0039.

Roy, C. S. (1881) 'The Elastic Properties of the Arterial Wall', *The Journal of Physiology*, 3(2), pp. 125–159. doi: 10.1113/jphysiol.1881.sp000088.

Ruberti, J. W. and Hallab, N. J. (2005) 'Strain-controlled enzymatic cleavage of collagen in loaded matrix', *Biochemical and Biophysical Research Communications*, 336(2), pp. 483–489. doi: 10.1016/j.bbrc.2005.08.128.

Rüdel, R. and Zite-Ferenczy, F. (1980) 'Efficiency of light diffraction by cross-striated

muscle fibers under stretch and during isometric contraction', *Biophysical journal*, 30(3), pp. 507–16. doi: 10.1016/S0006-3495(80)85110-1.

Rutsch, W., Kiemeneij, F., Colombo, A., Macaya, C., Guermonprez, J.-L., Grip, L., Hamburger, J., Umans, V., Gotsman, M., Almagor, Y., Morice, M.-C., Garcia, E., Chevalier, B., Erbel, R., Cobaugh, M., Morel, M.-A. and Serruys, P. W. (2000) 'Clinical and angiographic results with the NIR stent: First International NIR Endovascular Stent Study (FINESS-II).', *International journal of cardiovascular interventions*, 3(3), pp. 143–151. doi: 10.1080/14628840050516055.

Sacks, M. S. (2003) 'Incorporation of Experimentally-Derived Fiber Orientation into a Structural Constitutive Model for Planar Collagenous Tissues', *Journal of Biomechanical Engineering*, 125(2), pp. 280–287. doi: 10.1115/1.1544508.

Sacks, M. S., Chuong, C. J. C. and More, R. (1994) 'Collagen Fiber Architecture of Bovine Pericardium', *ASAIO Journal*, 40(3), pp. M632–M637. doi: 10.1097/00002480-199407000-00075.

Sacks, M. S., Smith, D. B. and Hiester, E. D. (1997) 'A small angle light scattering device for planar connective tissue microstructural analysis.', *Annals of biomedical engineering*, 25(4), pp. 678–89. Available at: http://www.ncbi.nlm.nih.gov/pubmed/9236980.

Sáez, P., García, A., Peña, E., Gasser, T. C. and Martínez, M. A. (2016) 'Microstructural quantification of collagen fiber orientations and its integration in constitutive modeling of the porcine carotid artery', *Acta Biomaterialia*, 33, pp. 183–193. doi: 10.1016/j.actbio.2016.01.030.

Sasaki, N. and Odajima, S. (1996) 'Elongation mechanism of collagen fibrils and force-strain relations of tendon at each level of structural hierarchy', *Journal of Biomechanics*, 29(9), pp. 1131–1136. doi: 10.1016/0021-9290(96)00024-3.

Schaar, J., Mastik, F., Regar, E., den Uil, C., Gijsen, F., Wentzel, J., Serruys, P. and W. van der Stehen, A. (2007) 'Current Diagnostic Modalities for Vulnerable Plaque Detection', *Current Pharmaceutical Design*, 13(10), pp. 995–1001. doi: 10.2174/138161207780487511.

Schneider, C. a, Rasband, W. S. and Eliceiri, K. W. (2012a) 'NIH Image to ImageJ: 25 years of image analysis', *Nature Methods*. Nature Publishing Group, 9(7), pp. 671–675. doi: 10.1038/nmeth.2089.

Schneider, C. a, Rasband, W. S. and Eliceiri, K. W. (2012b) 'NIH Image to ImageJ: 25 years of image analysis', *Nature Methods*. Nature Publishing Group, 9(7), pp. 671–675. doi: 10.1038/nmeth.2089.

Schrauwen, J. T. C., Vilanova, A., Rezakhaniha, R., Stergiopulos, N., van de Vosse, F. N. and Bovendeerd, P. H. M. (2012) 'A method for the quantification of the pressure dependent 3D collagen configuration in the arterial adventitia.', *Journal of structural biology*. Elsevier Inc., 180(2), pp. 335–42. doi: 10.1016/j.jsb.2012.06.007.

Schriefl, A. J., Schmidt, T., Balzani, D., Sommer, G. and Holzapfel, G. A. (2015) 'Selective enzymatic removal of elastin and collagen from human abdominal aortas: Uniaxial mechanical response and constitutive modeling', *Acta Biomaterialia*. Acta Materialia Inc., 17, pp. 125–136. doi: 10.1016/j.actbio.2015.01.003.

Schriefl, A. J., Zeindlinger, G., Pierce, D. M., Regitnig, P. and Holzapfel, G. A. (2012) 'Determination of the layer-specific distributed collagen fibre orientations in human thoracic and abdominal aortas and common iliac arteries.', *Journal of the Royal*

Society, Interface / the Royal Society, 9(71), pp. 1275–86. doi: 10.1098/rsif.2011.0727.

Setacci, C., de Donato, G., Setacci, F., Pieraccini, M., Cappelli, A., Trovato, R. A. and Benevento, D. (2005) 'In-stent restenosis after carotid angioplasty and stenting: A challenge for the vascular surgeon', *European Journal of Vascular and Endovascular Surgery*, 29(6), pp. 601–607. doi: 10.1016/j.ejvs.2005.01.033.

Shahid, S. and Lally, C. (2016) 'MR-DTI fibre angles of porcine common carotid artery'.

Shahid, S. S., Gaul, R. T., Kerskens, C. M., Flamini, V. and Lally, C. (2017) 'Quantifying the ultrastructure of carotid artery using high-resolution micro-diffusion tensor imaging – comparison of intact vs. open cut tissue', *Physics in Medicine and Biology*, 62(23), pp. 8850–8868. doi: 10.1088/1361-6560/aa9159.

Shahid, S. S., Kerskens, C., Gaul, R., Flamini, V. and Lally, C. (2016) 'Ex-vivo arterial collagen fibre tractography using micro diffusion tensor imaging', in *ESMRMB 2016, 33rd Annual Scientific Meeting, Vienna, AT, September 29–October 1*. Vienna: Springer, p. 28. doi: 10.1007/s10334-016-0568-x.

Sherman, V. R., Yang, W. and Meyers, M. A. (2015) 'The materials science of collagen', *Journal of the Mechanical Behavior of Biomedical Materials*. Elsevier, 52, pp. 22–50. doi: 10.1016/j.jmbbm.2015.05.023.

Silver, F. H., Snowhill, P. B. and Foran, D. J. (2003) 'Mechanical Behavior of Vessel Wall: A Comparative Study of Aorta, Vena Cava, and Carotid Artery', *Annals of Biomedical Engineering*, 31(7), pp. 793–803. doi: 10.1114/1.1581287.

Simionescu, A., Simionescu, D. and Deac, R. (1996) 'Biochemical pathways of tissue degeneration in bioprosthetic cardiac valves. The role of matrix metalloproteinases.', *ASAIO journal (American Society for Artificial Internal Organs : 1992)*, 42(5), pp. M561-7. Available at: http://www.ncbi.nlm.nih.gov/pubmed/8944942.

Simionescu, D., Simionescu, A. and Deac, R. (1993) 'Detection of remnant proteolytic activities in unimplanted glutaraldehyde-treated bovine pericardium and explanted cardiac bioprostheses', *Journal of Biomedical Materials Research*, 27(6), pp. 821–829. doi: 10.1002/jbm.820270615.

Simo, J. C. and Ju, J. W. (1987) 'Strain- and stress-based continuum damage models-I. Formulation', *International Journal of Solids and Structures*, 23(7), pp. 821–840. doi: 10.1016/0020-7683(87)90083-7.

Singer, M. A., Henshaw, W. D. and Wang, S. L. (2009) 'Computational modeling of blood flow in the TrapEase inferior vena cava filter.', *Journal of vascular and interventional radiology : JVIR*, 20(6), pp. 799–805. doi: 10.1016/j.jvir.2009.02.015.

Slager, C. J., Wentzel, J. J., Gijsen, F. J. H., Schuurbiers, J. C. H., van der Wal, A. C., van der Steen, A. F. W. and Serruys, P. W. (2005) 'The role of shear stress in the generation of rupture-prone vulnerable plaques', *Nature Clinical Practice Cardiovascular Medicine*, 2(8), pp. 401–407. doi: 10.1038/ncpcardio0274.

Sommer, G. and Holzapfel, G. A. (2012) '3D constitutive modeling of the biaxial mechanical response of intact and layer-dissected human carotid arteries', *Journal of the Mechanical Behavior of Biomedical Materials*. Elsevier Ltd, 5(1), pp. 116–128. doi: 10.1016/j.jmbbm.2011.08.013.

Stary, H. C. (2000) 'Natural History and Histological Classification of Atherosclerotic Lesions : An Update', *Arteriosclerosis, Thrombosis, and Vascular Biology*, 20(5), pp. 1177–1178. doi: 10.1161/01.ATV.20.5.1177.

Stary, H. C., Chandler, A. B., Dinsmore, R. E., Fuster, V., Glagov, S., Insull, W., Rosenfeld, M. E., Schwartz, C. J., Wagner, W. D. and Wissler, R. W. (1995) 'A Definition of Advanced Types of Atherosclerotic Lesions and a Histological Classification of Atherosclerosis : A Report From the Committee on Vascular Lesions of the Council on Arteriosclerosis, American Heart Association', *Circulation*, 92(5), pp. 1355–1374. doi: 10.1161/01.CIR.92.5.1355.

Stary, H. C., Chandler, A. B., Glagov, S., Guyton, J. R., Insull, W., Rosenfeld, M. E., Schaffer, S. A., Schwartz, C. J., Wagner, W. D. and Wissler, R. W. (1994) 'A definition of initial, fatty streak, and intermediate lesions of atherosclerosis. A report from the Committee on Vascular Lesions of the Council on Arteriosclerosis, American Heart Association', *Circulation*, 89(5), pp. 2462–2478. doi: 10.1161/01.CIR.89.5.2462.

Steele, P. M., Chesebro, J. H., Stanson, A. W., Holmes, D. R., Dewanjee, M. K., Badimon, L. and Fuster, V. (1985) 'Balloon angioplasty. Natural history of the pathophysiological response to injury in a pig model', *Circulation Research*, 57(1), pp. 105–112. doi: 10.1161/01.RES.57.1.105.

Thompson, R. W., Geraghty, P. J. and Lee, J. K. (2002) 'Abdominal aortic aneurysms: basic mechanisms and clinical implications.', *Current problems in surgery*, 39(2), pp. 110–230. doi: 10.1067/msg.2002.121421.

Tonge, T. K., Ruberti, J. W. and Nguyen, T. D. (2015) 'Micromechanical Modeling Study of Mechanical Inhibition of Enzymatic Degradation of Collagen Tissues', *Biophysical Journal*. Biophysical Society, 109(12), pp. 2689–2700. doi: 10.1016/j.bpj.2015.10.051.

Tower, T. T., Neidert, M. R. and Tranquillo, R. T. (2002) 'Fiber Alignment Imaging During Mechanical Testing of Soft Tissues', *Annals of Biomedical Engineering*, 30(10), pp. 1221–1233. doi: 10.1114/1.1527047.

Tsamis, A., Krawiec, J. T. and Vorp, D. a (2013) 'Elastin and collagen fibre microstructure of the human aorta in ageing and disease: a review', *Journal of The Royal Society Interface*, 10(83), p. 20121004. doi: 10.1098/rsif.2012.1004.

Tsamis, A., Phillippi, J. A., Koch, R. G., Pasta, S., D'Amore, A., Watkins, S. C., Wagner, W. R., Gleason, T. G. and Vorp, D. A. (2013) 'Fiber micro-architecture in the longitudinal-radial and circumferential-radial planes of ascending thoracic aortic aneurysm media', *Journal of Biomechanics*. Elsevier, 46(16), pp. 2787–2794. doi: 10.1016/j.jbiomech.2013.09.003.

Urabe, G., Hoshina, K., Shimanuki, T., Nishimori, Y., Miyata, T. and Deguchi, J. (2016) 'Structural analysis of adventitial collagen to feature aging and aneurysm formation in human aorta', *Journal of Vascular Surgery*, 63(5), pp. 1341–1350. doi: 10.1016/j.jvs.2014.12.057.

Varnava, A. M. (2002) 'Relationship Between Coronary Artery Remodeling and Plaque Vulnerability', *Circulation*, 105(8), pp. 939–943. doi: 10.1161/hc0802.104327.

Voytik-Harbin, S. L., Roeder, B. A., Sturgis, J. E., Kokini, K. and Robinson, J. P. (2003) 'Simultaneous mechanical loading and confocal reflection microscopy for three-dimensional microbiomechanical analysis of biomaterials and tissue constructs.', *Microscopy and microanalysis : the official journal of Microscopy Society of America, Microbeam Analysis Society, Microscopical Society of Canada*, 9(1), pp. 74–85. doi: 10.1017/S1431927603030046.

Walton, L. A., Bradley, R. S., Withers, P. J., Newton, V. L., Watson, R. E. B., Austin, C. and Sherratt, M. J. (2015) 'Morphological Characterisation of Unstained and Intact

Tissue Micro-architecture by X-ray Computed Micro- and Nano-Tomography', *Scientific Reports*. Nature Publishing Group, 5(1), p. 10074. doi: 10.1038/srep10074.

Wang, R., Brewster, L. P. and Gleason, R. L. (2013) 'In-situ characterization of the uncrimping process of arterial collagen fibers using two-photon confocal microscopy and digital image correlation', *Journal of Biomechanics*. Elsevier, 46(15), pp. 2726–2729. doi: 10.1016/j.jbiomech.2013.08.001.

Watson, S. R., Liu, P., Peña, E. A., Sutton, M. A., Eberth, J. F. and Lessner, S. M. (2016) 'Comparison of Aortic Collagen Fiber Angle Distribution in Mouse Models of Atherosclerosis Using Second-Harmonic Generation (SHG) Microscopy', *Microscopy and Microanalysis*, 22(01), pp. 55–62. doi: 10.1017/S1431927615015585.

WHO (2014) *Global Status Report On Noncommunicable Diseases 2014*.

Wilkes, G. and Wilkes, P. (1974) 'Evidence for in vivo anisotropic rod structure in collagenous tissue as noted by small angle light scattering', *Biopolymers*, 13(2), pp. 411–3. doi: 10.1002/bip.1974.360130217.

Willett, T. L., Labow, R. S. and Lee, J. M. (2008) 'Mechanical overload decreases the thermal stability of collagen in an in vitro tensile overload tendon model', *Journal of Orthopaedic Research*, 26(12), pp. 1605–1610. doi: 10.1002/jor.20672.

Williams, C., Liao, J., Joyce, E. M., Wang, B., Leach, J. B., Sacks, M. S. and Wong, J. Y. (2009) 'Altered structural and mechanical properties in decellularized rabbit carotid arteries', *Acta Biomaterialia*. Acta Materialia Inc., 5(4), pp. 993–1005. doi: 10.1016/j.actbio.2008.11.028.

Wolinsky, H. and Glagov, S. (1964) 'Structural Basis for the Static Mechanical Properties of the Aortic Media.', *Circulation research*, 14(5), pp. 400–413. doi: 10.1161/01.RES.14.5.400.

Wyatt, K. E.-K., Bourne, J. W. and Torzilli, P. a (2009) 'Deformation-Dependent Enzyme Mechanokinetic Cleavage of Type I Collagen', *Journal of Biomechanical Engineering*, 131(5), p. 051004. doi: 10.1115/1.3078177.

Xiong, W., Knispel, R., MacTaggart, J., Greiner, T. C., Weiss, S. J. and Baxter, B. T. (2009) 'Membrane-type 1 matrix metalloproteinase regulates macrophage-dependent elastolytic activity and aneurysm formation in vivo', *Journal of Biological Chemistry*, 284(3), pp. 1765–1771. doi: 10.1074/jbc.M806239200.

Yi, E., Sato, S., Takahashi, A., Parameswaran, H., Blute, T. A., Bartolák-Suki, E. and Suki, B. (2016) 'Mechanical forces accelerate collagen digestion by bacterial collagenase in lung tissue strips', *Frontiers in Physiology*, 7(JUL), pp. 1–12. doi: 10.3389/fphys.2016.00287.

Ying, M., Yeung, E., Li, B., Li, W., Lui, M. and Tsoi, C.-W. (2003) 'Sonographic evaluation of the size of achilles tendon: the effect of exercise and dominance of the ankle', *Ultrasound in Medicine & Biology*, 29(5), pp. 637–642. doi: 10.1016/S0301-5629(03)00008-5.

Zahnd, G., Schrauwen, J., Karanasos, A., Regar, E., Niessen, W., van Walsum, T. and Gijsen, F. (2016) 'Fusion of fibrous cap thickness and wall shear stress to assess plaque vulnerability in coronary arteries: a pilot study', *International Journal of Computer Assisted Radiology and Surgery*, 11(10), pp. 1779–1790. doi: 10.1007/s11548-016-1422-3.

Zareian, R., Church, K. P., Saeidi, N., Flynn, B. P., Beale, J. W. and Ruberti, J. W. (2010) 'Probing collagen/enzyme mechanochemistry in native tissue with dynamic,

enzyme-induced creep', *Langmuir*, 26(12), pp. 9917–9926. doi: 10.1021/la100384e.
Appendices

A Applications of SALS

A.1 Introduction

As previously outlined in Section 2.6.6, SALS is a versatile technique for structural characterisation of fibrous soft tissues. This has led SALS to be used to evaluate a host of collagenous tissues in literature including skin (Kronick and Buechler, 1986; Ferdman and Yannas, 1993), dura mater (Hamann, Sacks and Malinin, 1998), cornea (Robitaille *et al.*, 2011), valvular tissue (Cochran and Kunzelman, 1991; Billiar and Sacks, 2000) and bovine pericardium (Sacks, Chuong and More, 1994; Sacks, Smith and Hiester, 1997). One trait which these tissues share is their relatively thin and transparent structure which is a prerequisite for SALS analysis. Given the flexibility of the system, SALS analysis has also been used to investigate the structure of a number of other soft tissues during the course of this research including, human carotid plaque sections, intact human carotid plaque cap tissue, decellularised porcine carotid artery, porcine cerebral dura mater, bovine pericardium and porcine corneal tissue. Preliminary results arising from these feasibility studies are presented below for a selection of tissues.

A.2 Methods

Briefly, the system consists of an unpolarised 5mW HeNe laser (λ = 632.8 nm; JDSU, Newbury, UK), focussing lens (f_l = 150 mm; Edmund Optics Ltd, York, UK), automated sample positioner, projection screen and a CMOS USB camera as outlined in the main body of the thesis. A 150 µm beam diameter was used to investigate regions of different sizes across the various tissues using scanning grids ranging from 125 x 125 µm to 1000 x 1000 µm. Collagen fibre alignment was determined based off the ratio of major to minor axis of the scattered light ellipse as before.

Human plaque tissue was obtained from carotid endarterectomy procedures after approval from the local ethics committee with all patients giving written informed consent. Plaque cap samples were dissected by gently separating the cap from the underlying tissue using a forceps at existing layer boundaries. Regions of calcification were avoided as they did not permit smooth layer delamination. Plaque separation is shown in Figure A.1 prior to intact plaque cap SALS analysis. Additional plaque samples were also histologically processed at 8 µm slices and stained prior to histological SALS analysis.

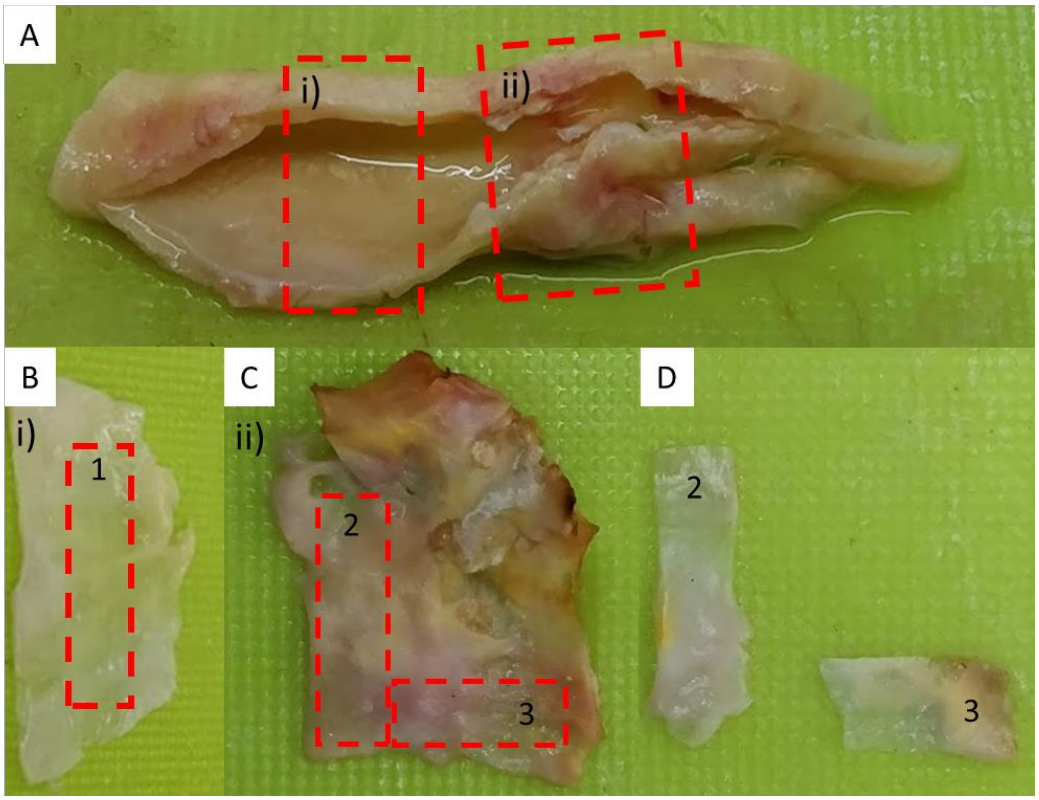

Figure A.1 - A) Human carotid plaque obtained from carotid endarterectomy procedures showing the locations of plaque sections in B) and C). Individual plaque caps dissected and subsequently analysed using SALS are shown in D).

Decellularised porcine carotid tissue was also analysed to investigate whether any structural changes in collagen occurred due to the decellularisation process. Briefly, vessels were decellularised using 0.1M sodium hydroxide solution (NaOH, S8045, Sigma-Aldrich) for 18 hours to breakdown cellular content followed by a 3-hour rinsing process with 0.9% saline (NaCl) to remove cellular

debris from the vessel wall. The decellularisation protocol was based off a protocol used for coronary artery and adapted for use on porcine carotid arteries (Campbell, Cahill and Lally, 2012). Decellularised and control vessels were then histologically processed and stained prior to histological SALS analysis.

Excised porcine dura mater was also characterised using SALS to identify whether porcine dura mater should be considered structurally isotropic or anisotropic. One half of the dura mater was cut into 6 smaller patches of approximately 25 mm x 10 mm allowing SALS interrogation.

A.3 Results

A.3.1 Histological human atherosclerotic plaque cross sections

Human atherosclerotic plaque tissue was found to exhibit structural variations across the plaque sample with regions of dense cellular and collagenous tissue as well as regions of low cell and collagen content (Figure A.2). SALS orientation plots of histological plaque samples showed regions of high alignment denoted by warm colours at regions of high collagen content and alignment as observed by strong picrosirius red birefringence in polarised light images (Figure A.3C). Likewise, regions of low collagen at the centre of the plaque burden show low alignment through SALS analysis. The circumferential fibre orientation of the artery wall is also observed with regions of transition occurring at plaque shoulders.

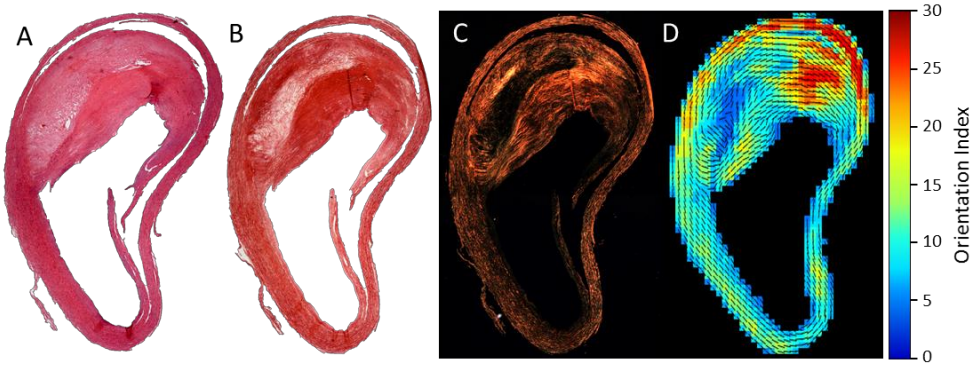

Figure A.2 - Cross section of human carotid plaque stained with A) H&E, B) picrosirius red, C) picrosirius red and viewed under polarised light and D) analysed using SALS for a single cross section.

Serial SALS analysis generated through stacking, co-registration and interpolation of sequential SALS images provides 3-dimensional visualisation of the plaque structure (Figure A.3A). This study was conducted in collaboration Professor Michael Sacks (University of Texas at Austin) using their inhouse developed serial SALS analysis technique (manuscript on serial SALS technique in preparation). Analysis of three distinct regions found clear differences in the plaque structure as seen in Figure A.3B. As a single sample case, statistical analysis was not carried out between these regions due to the associated bias of measurements being taken from neighbouring regions.

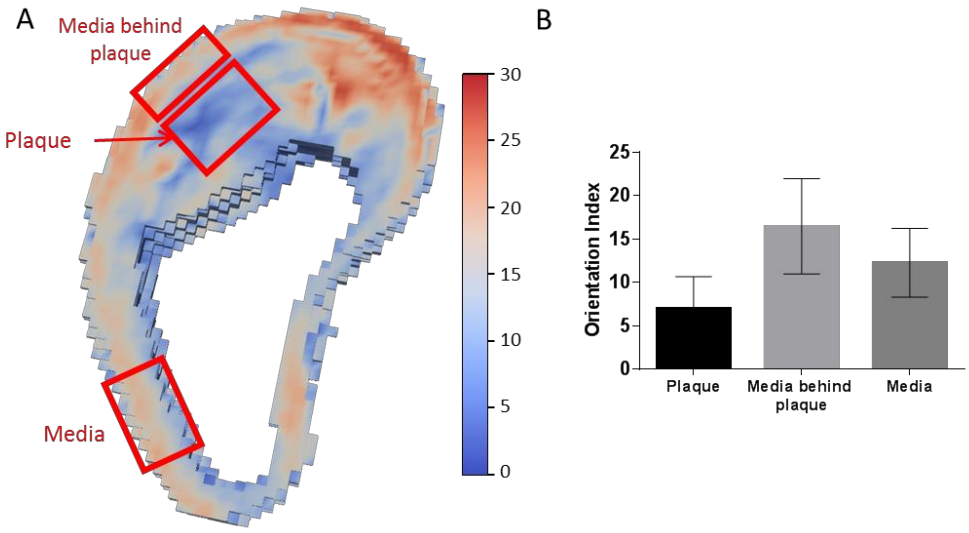

Figure A.3 - A) Reconstructed human carotid artery using serial SALS stacking of individual slices of plaque showing the alignment of collagen across the plaque. B) Alignment determined via orientation index with SD shown for each highlighted region in A) for a single plaque sample.

A.3.2 Intact human atherosclerotic plaque cap

Preliminary analysis of human plaque tissue shown in Figure A.1 found large variations in the structural organisation of collagen fibres in terms of both orientation and alignment (Figure A.4). Sample 1 shows a predominantly axial fibre orientation with low alignment while sample 2 shows strong circumferential alignment. Finally, sample 3 shows the greatest fibre dispersion with fibres orientated in multiple directions.

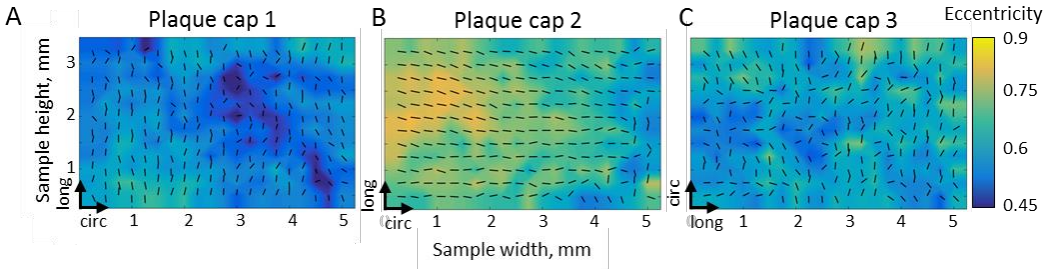

Figure A.4 - SALS plots showing plaque orientation and alignment for plaques 1, 2 and 3 dissected in Figure A.1. Plaque 1 and 2 are orientated with the long edge corresponding to the circumferential vessel direction while plaque 3 was cut along the longitudinal direction.

A.3.3 Decellularised porcine arterial tissue

SALS analysis found no significant differences between mean fibre angle for control and decellularised tissue in intimal (0.10° ± 2.52 (6.17°) vs -0.84° ± 1.98 (4.86°)) and medial tissue (-1.04° ± 9.20 (9.20°) vs 0.97° ± 2.86 (7.00°)), see Figure A.5. Angles are presented as mean ± SEM (SD).

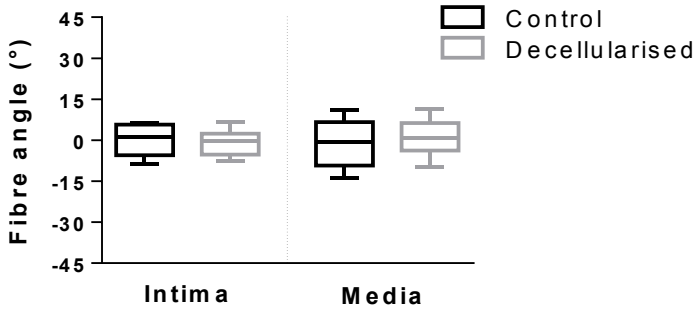

Figure A.5 - Mean fibre angle for control and decellularised porcine carotid artery showing no significant change in collagen fibre architecture. Collagen fibres are found to align circumferentially (0 degrees) with minimal dispersion in native and decellularised vessels

A.3.4 Porcine dura mater

SALS contour plots were generated for one half of the DM and the results were mirrored along the superior sagittal sinus (Figure A.6). Results indicate that there are local regions of high alignment (shown in yellow and inset), however there is no global preferred orientation as seen in Figure A.7. The lack of a

dominant angle in the frequency distribution plot in Figure A.7 indicates that dura mater is globally isotropic.

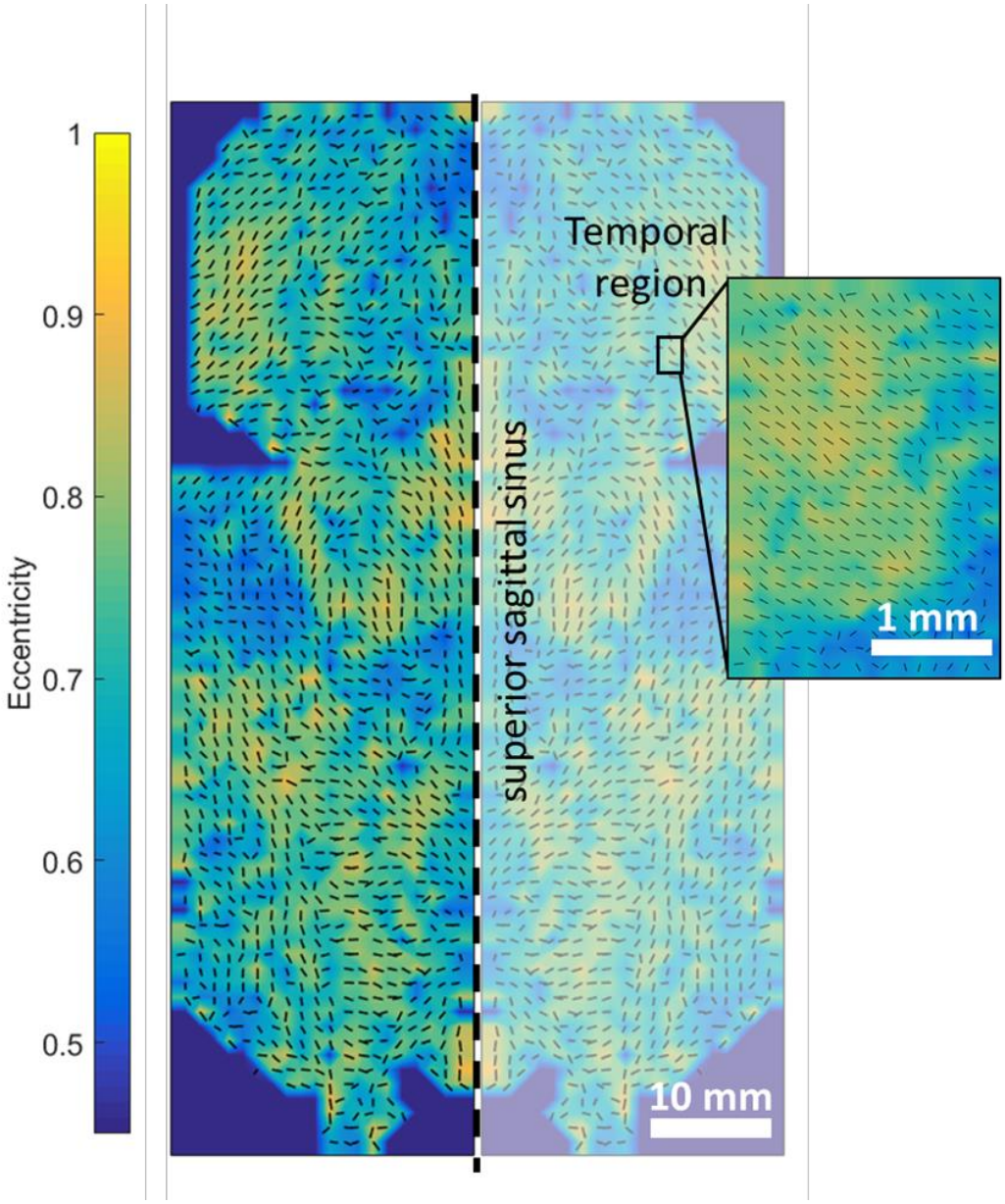

Figure A.6 - Global and local (inset) SALS contour plots of porcine dura mater showing global fibre dispersion as well as local anisotropy. Only the left hand portion of the dura mater is analysed with the right hand side generated through mirro symmetry along the superior sagittal plane.

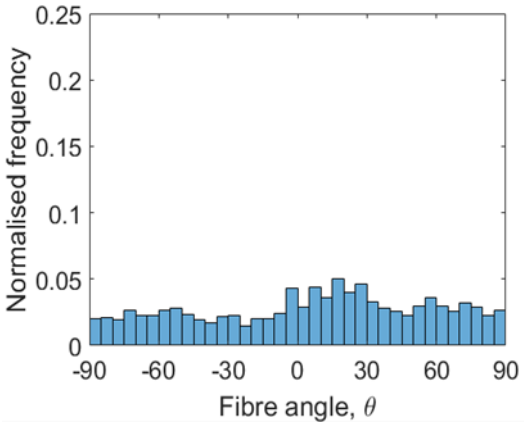

Figure A.7 - Normalised orientation distribution plot of global dura mater fibre directions showing no dominant fibre direction.

A.4 Discussion

A.4.1 Histological human atherosclerotic plaque cross sections

SALS histological analysis highlights SALS ability to distinguish different plaque regions quickly and objectively through orientation and alignment analysis (Figure A.2). Unlike traditional histological analysis, SALS does not require sample staining which was carried out here for comparison purposes. SALS also removes much of the subjectivity and bias associated with histological analysis which can occur in the absence of rigid analysis protocols. This is the first time SALS has been used for investigating human plaque tissue and supports it's use for future plaque investigations. The ability to extend 2D SALS analysis to 3D may also provide a means of incorporating 3D alignment data into future computational models.

A.4.2 Intact human atherosclerotic plaque cap

SALS analysis identified variations in fibre orientation and alignment across the three plaque cap samples investigated (Figure A.4). These findings may offer a potential technique for plaque screening prior to mechanical testing and subsequent mechanical characterisation. Non-destructive SALS analysis of plaque caps would permit categorisation of plaques according to fibre direction or explain early failure in samples with fibres aligned orthogonally to the direction

of mechanical loading. Consequently, much of the variation associated with plaque testing may be removed (Davis *et al.*, 2016).

A.4.3 Decellularised porcine arterial tissue

SALS analysis of decellularised porcine carotid arteries identified no significant changes in fibre orientation or dispersion after the decellularisation process (Figure A.5). This finding supports the use of 0.1M sodium hydroxide solution as a structure preserving decellularisation solution at the timeframe considered in the current study.

A.4.4 Porcine dura mater

SALS orientation analysis shows global isotropy in the dura mater, highlighted by the lack of a dominant direction in the orientation distribution plot shown in Figure A.7. There are, however, regions of local fibre alignment, such as the temporal region which has been reported elsewhere for human DM (Hamann *et al.*). These similarities suggest that porcine DM may be a suitable model for human tissue. The local fibre alignment observed are likely to influence subsequent mechanical testing of dura mater. SALS may also aid in preselecting samples based on fibre directions, allowing for improved material characterisation in future studies.

A.5 Summary

The results outlined above highlight the ability of SALS to interrogate a wide range of intact and histologically sectioned tissues to determine structural organisation. The use of SALS for human plaque screening is one particularly interesting application of SALS. The ability to characterise fibre architecture before mechanical evaluation may allow more detailed relationships to be drawn between plaque geometry, type, structure and mechanics.

B Study 1

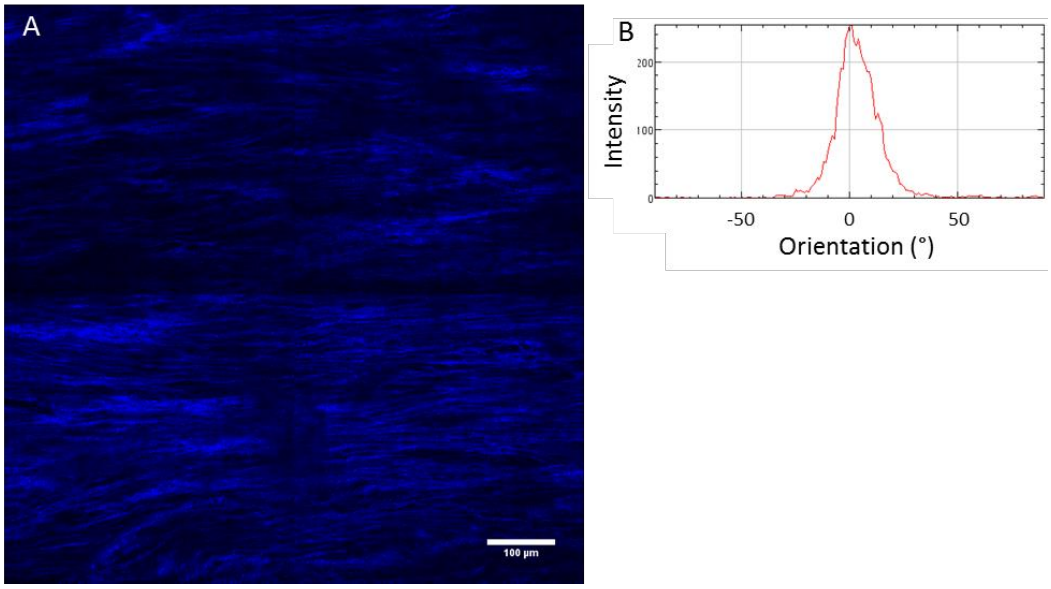

Figure B.1 - A) Tiled 20x SHG image of medial collagen fibres shown in blue showing B) a circumferential fibre distribution identified using the OrientationJ plugin for ImageJ.

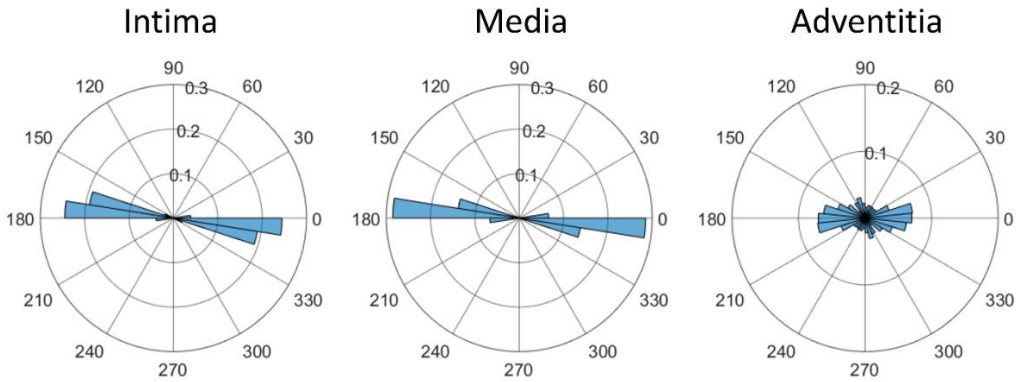

Figure B.2 – Polar histogram plot of fibre distribution of intact layers cleared using glycerol to increase transparency.

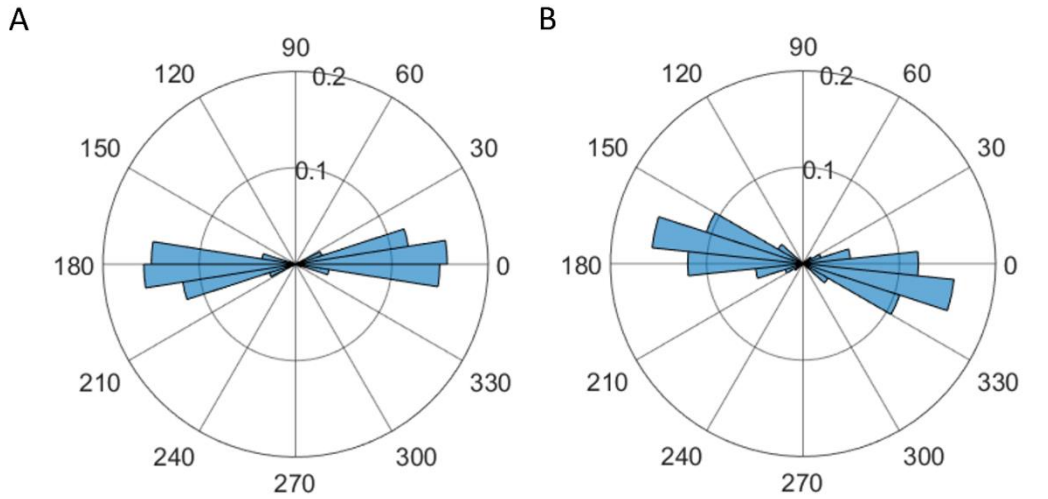

Figure B.3 – Polar histogram plot of fibre distribution of full intact vessel wall cleared using glycerol to increase transparency showing differences based on whether the adventitia faced A) toward the laser or B) away from the laser.

Table B.1 – Quantitative results of fibre distribution of full intact vessel wall cleared using glycerol showing bias imposed by the layer which the laser light passes through last.

	Adventitia facing laser (°)	Adventitia facing away from laser (°)
Mean Angle	2.953	-8.423
SD	0.5791	6.573
SEM	0.4095	4.648

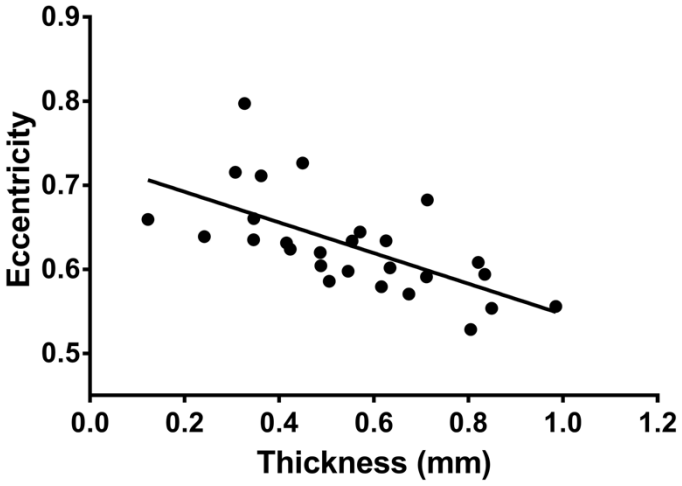

Figure B.4 – Reduction in eccentricity as sample thickness increases caused by a reduction in light transmission and subsequent drop in the signal to noise ratio.

C Study 2

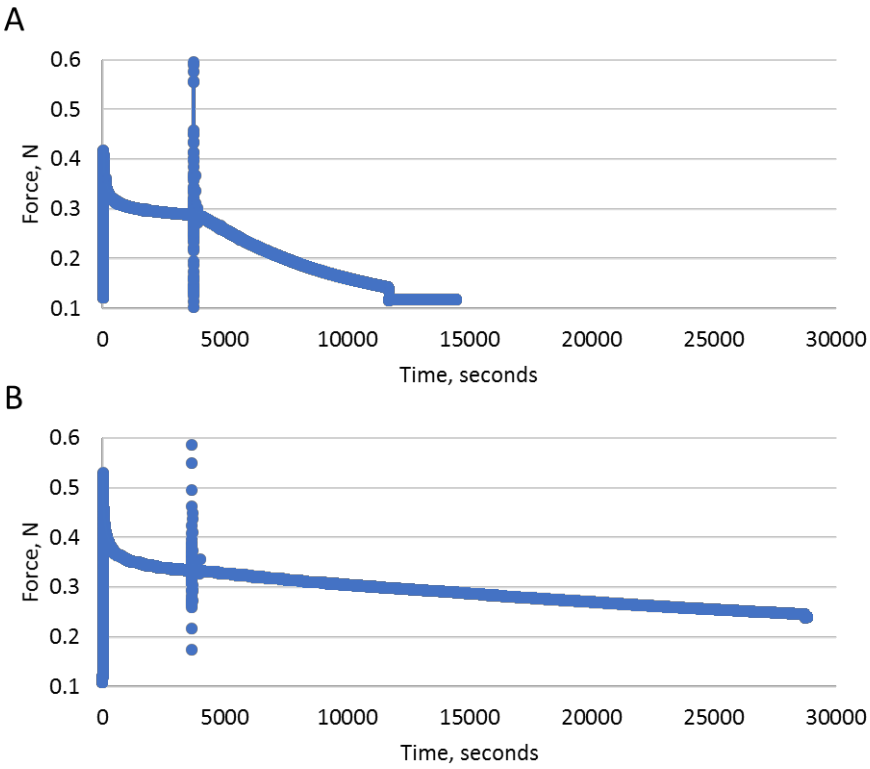

Figure C.1 – Representative force relaxation (raw data; stress not shown) curves for A) sample experiencing 40% uniaxial circumferential strain in Crude bacterial collagenase and B) 44% uniaxial circumferential strain in Purified bacterial collagenase. Note: Accelerated degradation in the crude case (A), leads to the sample breaking at approximately 12,000 seconds. Consequently, the degradation rate was calculated prior to this point.

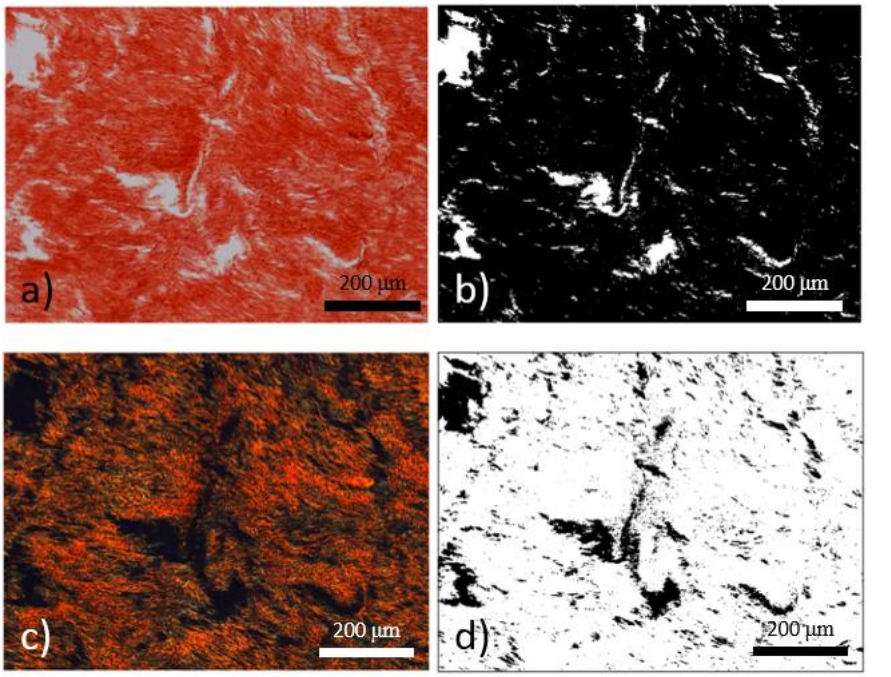

Figure C.2 - Collagen content analysis process showing A) picro-sirius red stained tissue under normal light, B) thresholded image with total tissue content in black, C) picro-sirius red stained tissue under polarised light and D) thresholded image showing collagen fibres as white. 10x magnification.

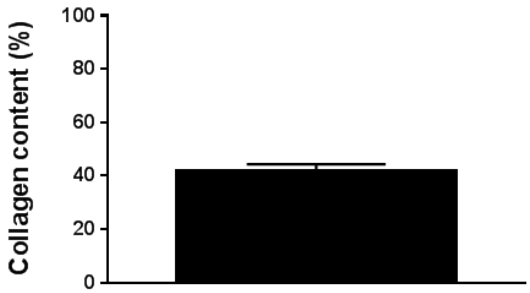

Figure C.3 - Collagen content for arterial tissue found using image processing. N=6.

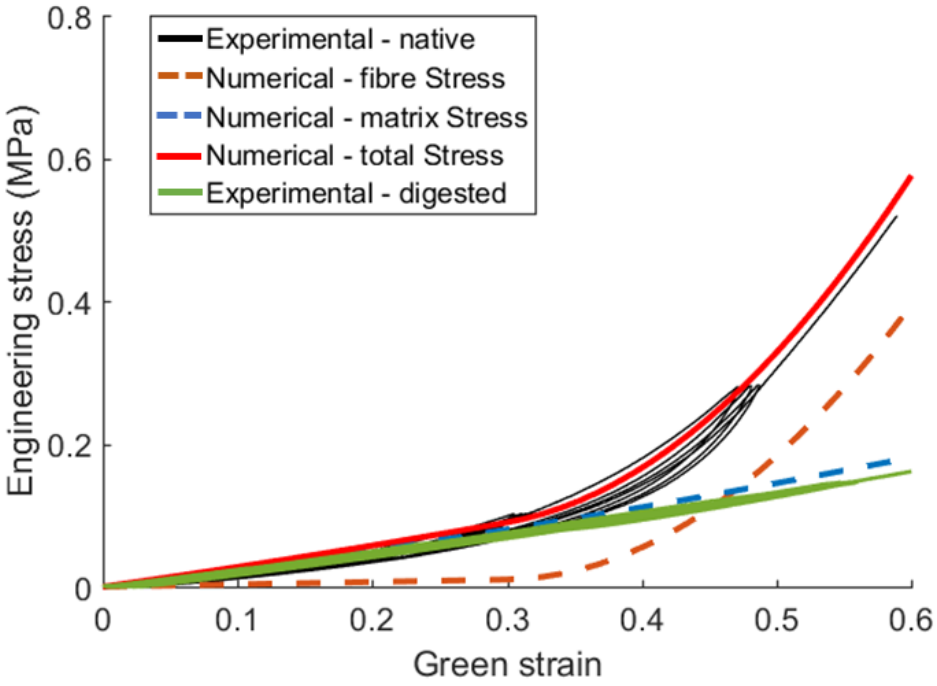

Figure C.4 - Calibration of collagen and matrix stiffness using experimental results of native and collagen digested porcine arterial tissue loaded in the circumferential direction from (Ghasemi, Nolan and Lally, 2018).

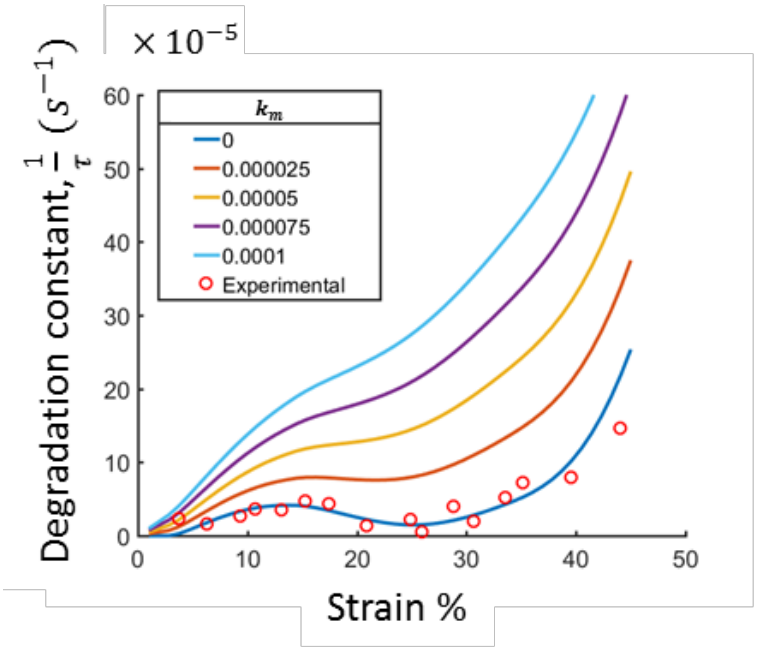

Figure C.5 - Model sensitivity to matrix degradation rate, k_m.

D Study 4

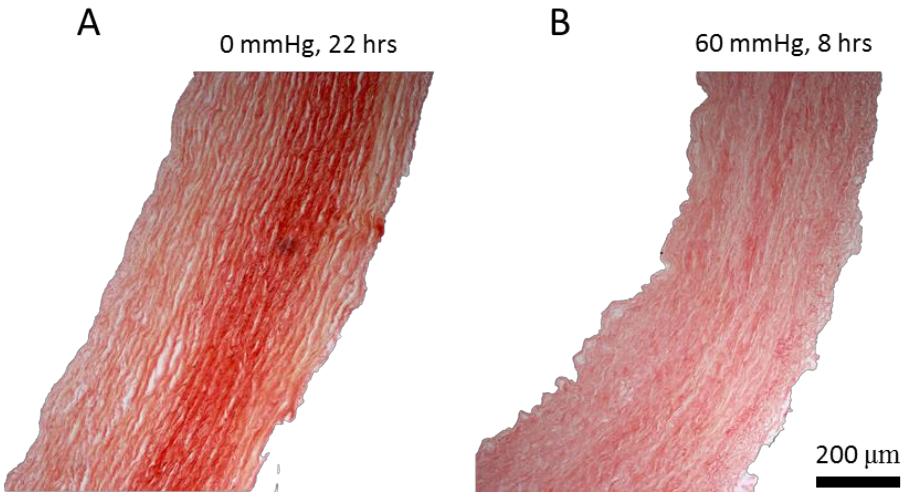

Figure D.1 - Histological images of picrosirius red stained artery cross sections at 10x magnification for A) an unpressurised vessel after 22 hours incubation in collagenase still showing collagen in dark red and B) a vessel subjected to 60 mmHg in the presence of collagenase showing complete collagen degradation after 8 hours highlighting the influence of pressure on degradation.

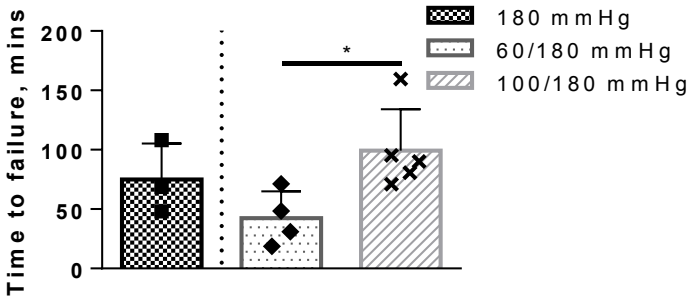

Figure D.2 - Time to failure results shown in Figure 6.7 including data point identified as an outlier for the 100/180 mmHg condition. Statistical significance is still maintained with the inclusion of the outlier. $P < 0.05$.